6-5-2023

DESIGN, CONSTRUCTION, AND TESTING OF RECOMBINANT DNA-BASED VACCINES FOR PROTECTION AGAINST SALMONELLA ENTERICA SUBSPECIES ENTERICA SEROVAR JAVIANA

Ashley Edwards

DESIGN, CONSTRUCTION, AND TESTING OF RECOMBINANT DNA-BASED VACCINES FOR PROTECTION AGAINST *SALMONELLA ENTERICA* SUBSPECIES *ENTERICA* SEROVAR JAVIANA

A Dissertation

Submitted to the Graduate Faculty of the
Louisiana State University and
Agricultural and Mechanical College
in partial fulfillment of the
requirements for the degree of
Doctor of Philosophy

in

The Department of Agriculture
School of Animal Sciences

by
Ashley Reneé Edwards
B.A., Louisiana State University, 2017
August 2023

This work is dedicated to my baby girl, Olive.
Your love knows no bounds, and I could not have done this without you.

“Young people, when informed and empowered, when they realize that what they do truly makes a difference, can indeed change the world.”
– Jane Goodall

Acknowledgments

The research within this dissertation would not have been possible without the following individuals, and I would like to sincerely thank each of them for all their help and support.

Dr. Richard K. Cooper, Chairman of my committee, for giving me the opportunity to conduct my research in his laboratory, and especially for his guidance and support.

Dr. Diana Coulon, Dr. Mark Mitchell, Dr. Philip Elzer, and Dr. Christine Lattin for serving on my committee, reviewing this document, and providing invaluable insights and advice throughout this project.

Dr. Billy Dudley for aiding me in developing my protein isolation, protein assay, antibody assay, and cytokine assay protocols.

Dr. Erin Oberhaus for aiding me in developing my ELISA assay protocols and providing guidance in the statistical analyses of the *in vivo* portion of this project.

Dr. Robert Keene for providing guidance and insight into the veterinary medicine market and common veterinary procedures.

Jacqueline M. McManus for providing guidance and mentorship in navigating cell culture experiments.

The Louisiana School of Veterinary Medicine for providing the *S. enterica* serotype Javiana isolates within this project.

Caitlin Smith, Kenneth Edwards, Benjamin Faucheux, and Alondra Torres for assisting me at various stages of this research project during their time as undergraduates.

Susan Hagius, Cassandra Rattle, Whittney Lathan, Renee Welch, and Sharon Hymel for their technical support, their advice, and keeping our laboratory and building functioning.

Dr. Xing Fu, Dr. Jerome F. La Peyre, and their graduate students for allowing me to use their laboratories and equipment for various portions of this research project.

Marilyn A. Dietrich for her enthusiastic guidance and support in the flow cytometry portions of this project.

Taylor Haynie, Alexis Nguyen, Mack Solar, Mary Hannah Cotton, Dr. Stephanie Korle, and Dr. Dorra Djebbi-Simmons for their assistance, advice, and camaraderie throughout this research project.

Jill and James Edwards for their unwavering support and enthusiasm throughout this project and for spending my lifetime instilling the work ethic necessary to complete it.

Dylan Zepeda for his endless patience, love, and support throughout our entire relationship. Thank you for being by my side.

Table of Contents

List of Abbreviations

AMB	absorbance minus background
APC	antigen-presenting cell
BCA	Bicinchoninic
BHI	Bacto Brain Heart Infusion
CB	CelLytic B Plus-harvested proteins
CBE	CelLytic B Plus-harvested proteins that were treated with the AbCam Endotoxin Removal Kit
CDC	Centers for Disease Control and Prevention
cDNA	complementary DNA
CDT	cytolethal distending toxin
CE	competitive exclusion (diet)
CMV	cytomegalovirus
CO_2	carbon dioxide
ConSS	conalbumin (ovotransferrin) signal sequence
COSTAR	Corning® 96-well EIA/RIA Clear Flat Bottom Polystyrene High Bind Microplate
CPSF	cleavage and polyadenylation specificity factor
CstF	cleavage stimulation factor
CTD	carboxyl-terminal repeat domain
CTL	cytotoxic T lymphocyte
CV	coefficient of variation
DAMP	damage-associated molecular pattern
DC	dendritic cell
DMEM	Dulbecco's Modified Eagle Medium (ATCC, cat 30-2002)

DNA	deoxyribonucleic acid
DPBS	Dulbecco's phosphate-buffered saline
EDTA	ethylenediaminetetraacetic acid
EH	HEK293 cells transfected with nothing via electroporation
EHG	HEK293 cells transfected with pGFP via electroporation
EJ	J774A.1 cells transfected with nothing via electroporation
EJG	J774A.1 cells transfected with pGFP via electroporation
ELISA	enzyme-linked immunosorbant assay
EMEM	Eagle's Minimum Essential Medium (ATCC, Cat # 30-2003)
endotoxin-free PBS	endotoxin-free 1X Dulbecco's phosphate-buffered saline without Ca++ & Mg++ (Sigma-Aldrich, TMS-012)
ERS	Economic Research Service
EU	endotoxin units
FBS	fetal bovine serum
FDA	Food and Drug Administration
FRS	free rotational spacers (flexible polypeptide linkers)
FSC	forward-scatter
GeneLab	Gene Probes and Expression Systems Laboratory/LSU BioMMED
GFP	green fluorescent protein
GLM	General Linear Model
HBA1	*Homo sapiens* hemoglobin subunit alpha 1 gene
HEK293	human embryonic kidney cells 293
HPE	hot phenol extraction
HRP	horseradish peroxidase
IDT	Integrated DNA Technologies

IEDB	Immune Epitope Database
Ig	Immunoglobulin
IL	Interleukin
iNTS	invasive nontyphoidal salmonellosis
LAL	Limulus Amebocyte Lysate
LEB	lysate extraction buffer
LH	HEK293 cells transfected with nothing via Lipofectamine3000
LHG	HEK293 cells transfected with pGFP via Lipofectamine3000
LJ	J774A.1 cells transfected with nothing via Lipofectamine3000
LJG	J774A.1 cells transfected with pGFP via Lipofectamine3000
LNP	lipid nanoparticle
LPS	Lipopolysaccharide
LRP1	Low-density lipoprotein receptor-related protein 1
MEM	Minimum Essential Medium
MHC	major histocompatibility complex
MLN	mesenteric lymph nodes
molecular grade 1X DPBS	molecular-grade 1x DPBS without calcium or magnesium (Thermofisher Scientific, Massachusetts, Catalog Number 14190144)
mRNA	messenger ribonucleic acid
NADPH	nicotinamide adenine dinucleotide phosphate
NCBI	National Center for Biotechnology Information
NEB	New England Biolabs
NH	HEK293 cells with no exposures
NIH	National Institutes of Health
NJ	J774A.1 cells with no exposures

NLR	NOD-like receptor
NUNC	Nunc™ MaxiSorp™ ELISA Plates, Uncoated
OH	HEK293 cells transfected with nothing via jetOPTIMUS
OHG	HEK293 cells transfected with pGFP via jetOPTIMUS
OJ	J774A.1 cells transfected with nothing via jetOPTIMUS
OJG	J774A.1 cells transfected with pGFP via jetOPTIMUS
ORF	open-reading frame
ORI	origin of replication
PAMAM	polyamidoamine
PAMP	pathogen-associated molecular pattern
PCR	polymerase chain reaction
PCV	packed cell volume
pDNA	plasmid DNA
pGFP	lentiviral pLKO.1-puro plasmid from SigmaAldrich (cat: SHC003)
PMSF	phenylmethylsulfonyl fluoride
poly(A)	Polyadenine
PON1	paraoxonase 1
PRR	pattern recognition receptor
RE	restriction enzyme
RNA	ribonucleic acid
RT-PCR	reverse transcription polymerase chain reaction
SCV	*Salmonella* containing vacuoles
SOD	superoxide dismutase
SPI	*Salmonella* pathogenicity island
SRP	siderophore receptor and porin

SSC	side-scatter
SV40	simian virus 40
T3SS	T3 secretion system
TCR	T cell receptor
Th	T helper
TLR	toll-like receptor
USDA	United States Department of Agriculture
USP18	ubiquitin specific peptidase
UTR	untranslated region
VBNC	viable but nonculturable state
ZNF223	zinc finger protein 223

Abstract

In the United States, *Salmonella* Javiana is among the top 5 most common nontyphoidal *Salmonella* serotypes, with a 325% increase in infection rate since 1970. Globally, nontyphoidal *Salmonella* leads to approximately 93.8 million illnesses and 155,000 deaths annually, with disproportionate impacts in developing countries. In the United States alone, these infections lead to over $4 billion in costs, the majority of which are attributed to those expenses incurred from mortalities. The zoonotic nature of nontyphoidal *Salmonellae* and their ability to survive on and within vegetation mean huge economic burden potential for various agricultural industries as well, especially since some of their products serve as the primary reservoirs for infection. Fluid therapy and antibiotics are the only available treatments for *S*. Javiana infections because this serotype is resistant to most common antibiotics. While *Salmonella* vaccines do exist, none cover this serotype, and the types of *Salmonella* vaccines commercially available are not practical for large-scale industry use or distribution to developing regions where protection is needed most. This pragmatism issue is largely because of vaccine production costs and storage requirements. Up-and-coming recombinant plasmid DNA vaccine technologies offer an opportunity to address both hurdles. This project begins exploration of this opportunity with the design, construction, assay development, and testing of 4 recombinant pDNA vaccines.

Chapter 1. Literature Review

1.1. Introduction to *Salmonella enterica* subspecies *enterica* serotype Javiana

Salmonellae are gram-negative and rod-shaped bacteria belonging to the family Enterobacteriaceae. There are 2 species of *Salmonella*, *S. bongori* and *S. enterica*, the latter of which is divided into 6 subspecies and then further divided into 2500+ serotypes or serovars. Within the *S. enterica* subspecies *enterica*, there are typhoidal and nontyphoidal serotypes (Figure 1.1) [1-3]. Typhoidal serotypes are primarily found in developing regions of the world and exclusively have humans as their reservoirs. Nontyphoidal serotypes by contrast are prevalent worldwide and are zoonotic, meaning that transmission can take place human-to-human, animal-to-animal, human-to-animal, or animal-to-human. Many consumable vegetations also serve as reservoirs for infection for nontyphoidal serotypes, as *Salmonellae* are facultative intracellular, anaerobic bacteria [1, 3]. This means that *Salmonella* can replicate inside a host cell or in the environment and can survive with or without oxygen [4, 5].

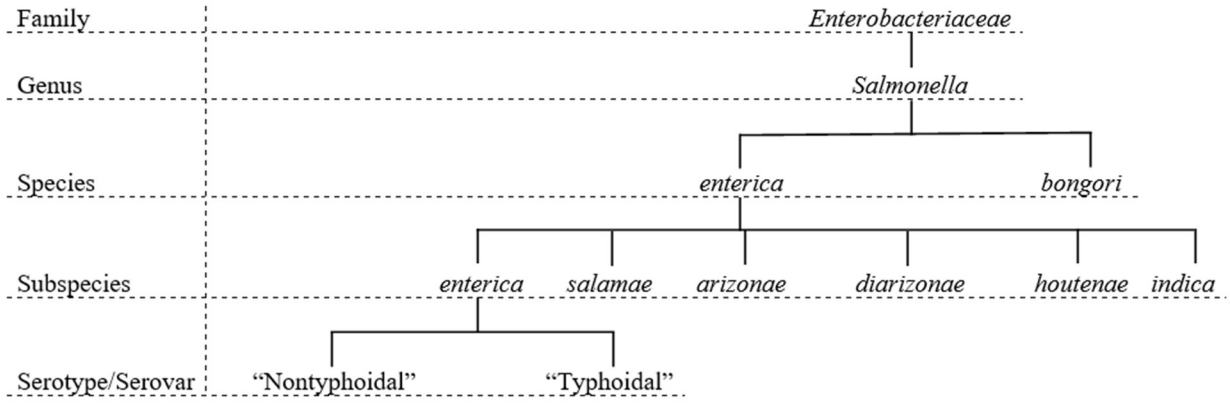

Figure 1.1. *Salmonella* taxonomy tree. *Sources:* [1-3].

The proper nomenclature for *Salmonella* serotypes is debated and has evolved over several decades. The Centers for Disease Control (CDC), as of 2000, reports the full name of the serotype of interest as *Salmonella enterica* serotype Javiana [6]. Common literature refers to this serotype in full as *S. enterica* subspecies *enterica* serotype Javiana [6, 7]. The shortened version, *S.* Javiana, is seen commonly in literature and will be used throughout this project [8-12].

S. Javiana, the serotype of interest in this project, is a nontyphoidal serotype of *S. enterica* that is resistant to a variety of antibiotics, including sulfonamides, ticarcillin, tetracycline, trimethoprim, streptomycin, amoxicillin, trimethoprim plus sulfamethoxazole, spectinomycin, and nitrofurantoin [13]. Furthermore, it is among the few nontyphoidal serotypes of *Salmonella* that are known to produce *Salmonella* cytolethal distending toxin (CDT), otherwise referred to as "typhoid toxin." This toxin leads to systemic host colonization, deoxyribonucleic acid (DNA) damage, typhoid fever-like symptoms, and in severe cases, death [8, 14].

1.2. *Salmonella* and Its Known Pathogenesis

Salmonella's primary route of invasion is via ingestion of contaminated food and water sources, and once inside the host, they can colonize the intestines and replicate in the lumen. Invasion of the intestinal epithelial cells is made possible by mannose-binding lectins, and a collection of invasion genes found on the *Salmonella* pathogenicity island-1 (SPI-1) – *sipC, sipA, sopE, sopE2, sopD,* and *sopB* are among them [1, 15-17]. SPI-1 additionally encodes a T3 secretion system (T3SS-1), otherwise known as a needle complex, for transport of the encoded invasion effector proteins into the host cell and surrounding environment (Table 1.1) [1, 18]. These effector proteins then alter actin cytoskeleton arrangement and increase membrane ruffling of epithelial cells to aid in their invasion via macropinocytosis [1, 16, 19]. Once in the epithelial

cells, *Salmonella* replicates in the cytoplasm, leading to pyroptotic cell death, ultimately resulting in gastroenteritis and an initial round of bacterial shedding (Figure 1.2) [1, 15].

During the invasion of the epithelial cells, phagocytes are recruited to the sites of infection via inflammation and vasodilation from the complement system and pattern recognition receptor (PRR) responses. PRRs, such as toll-like receptors (TLR) and NOD-like receptors (NLR), respond to the pathogen-associated molecular patterns (PAMPs) of the "free" *Salmonella* (i.e., their bacterial lipopolysaccharides (LPS)) and damage-associated molecular patterns (DAMPs) from the already invaded epithelial cells. The inflammation and vasodilation from these innate immune responses contribute to the diarrhea symptoms often observed upon infection [1, 20]. While awaiting epithelial invasion, *Salmonella* is protected from the complement system via its O-region – a protective physical barrier on the outermost region of the LPS– and the *Rck* gene, which inhibits polymerization of the complement component 9 (C9) on *Salmonella*'s surface (Figure 1.2) [21, 22]. The importance of this C9 polymerization will be explained later.

Upon phagocytosis by various immune cells either directly or via the apoptotic bodies from previous cell death, *Salmonella* can adapt to the phagocytic environment [1, 23]. The phagocytic immune cells primarily involved in *Salmonella* invasion include macrophages, dendritic cells (DC), and neutrophils [1, 23, 24].

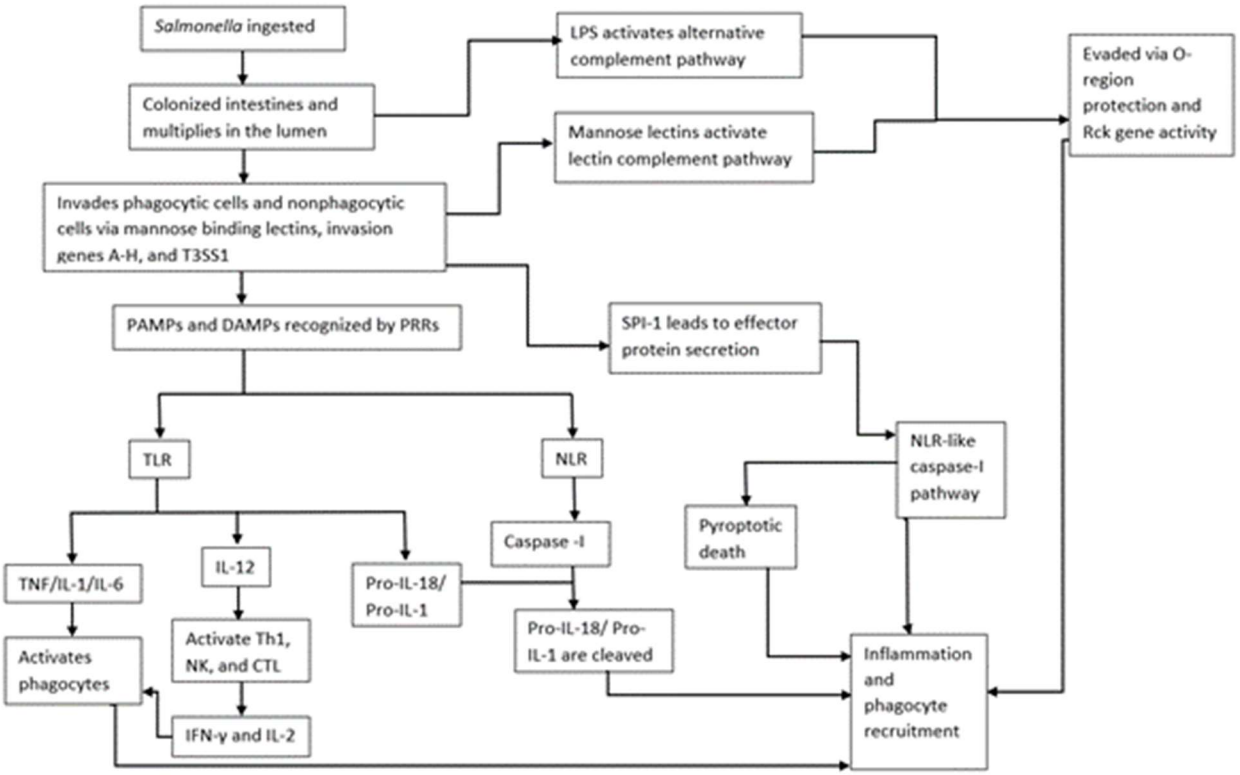

Figure 1.2. Summary diagram of *Salmonella* pathogenesis from ingestion to phagocyte recruitment.

While inside macrophages, SPI-1- and SPI-2-encoded effector proteins – SifA, SipA, SseJ, and SopB– are secreted through T3SS-1 and T3SS-2 and form *Salmonella* containing vacuoles (SCV) for *Salmonella* to replicate in, evading the various phagocytic modes of bacterial killing (Table 1.1). One of these modes of killing is the nicotinamide adenine dinucleotide phosphate (NADPH) oxidase-dependent respiratory bursts, which is further inhibited by additional SPI-2 encoded effector proteins. This inhibition protects *Salmonella* from destruction while inside the host cell. The effector proteins – SpiC, SSaJ, SsaT, SseB, & SsrA– prevent NADPH-oxidase assembly and movement to the SCV (Table 1.1) [1, 16, 23, 25-27]. In cases such as these, where phagocytic modes of killing are successfully avoided, *Salmonella* is more likely to lead to a systemic infection [1, 23, 28]. Alternatively, if *Salmonella* remains in the

cytosol without the SCV, it may be surrounded by an autophagosome-like structure and subsequently destroyed. *Salmonella* antigens are then presented on major histocompatibility complex class 1 glycoproteins (MHC-I), leading to the maturation of *Salmonella*-specific CD8+ T cells (Figure 1.3) [28]. In some cases, *Salmonella* can kill the infected macrophage via a T3SS-1-delivered SipB-mediated cell death (Figure 1.3) [16, 29]. *Salmonella*'s signaling for cell survival and cell death pathways in macrophages aids in its ability to prolong infection and allow for extended replication, but the exact determinants of these signals are still under investigation [15, 30]. Hypotheses are that *Salmonella* is reacting to host-cell environment changes [30]. However, *Salmonella*-induced host cell death plays an integral role in systemic dissemination. This is because the SipB-mediated cell death pathway employed by *Salmonella* is a pro-inflammatory version of apoptosis referred to as "pyroptosis" that recruits even more macrophages to the area for invasion (Figures 1.2 & 1.3) [31].

Dendritic cells tend to serve as an intermediary between the intestinal lumen and macrophage invasion, and upon engulfment, *Salmonella* induces the T3SS-1 delivered SipB-mediated cell death of the DC to escape and enter its preferred cell type– the macrophage. *Salmonella* can survive within DC, and DC involvement has been linked to systemic infection. However, the exact mechanisms of *Salmonella* and DCs are still being explored [16, 29]. In neutrophils, *Salmonella* is more readily eliminated than in macrophages. The hypothesis for this is that the neutrophil phagosomes are more basic than those in macrophages and contain myeloperoxidase. The higher pH and myeloperoxidase presence keep the NADPH-oxidase complex protonated, inhibiting membrane cross-over. Without the ability to disperse to other areas of the cell, the NADPH-oxidase complex can overwhelm *Salmonella's* defenses and

destroy it, leading to major histocompatibility complex class II glycoprotein (MHC-II) antigen presentation and subsequent CD4+ T cell maturation [28].

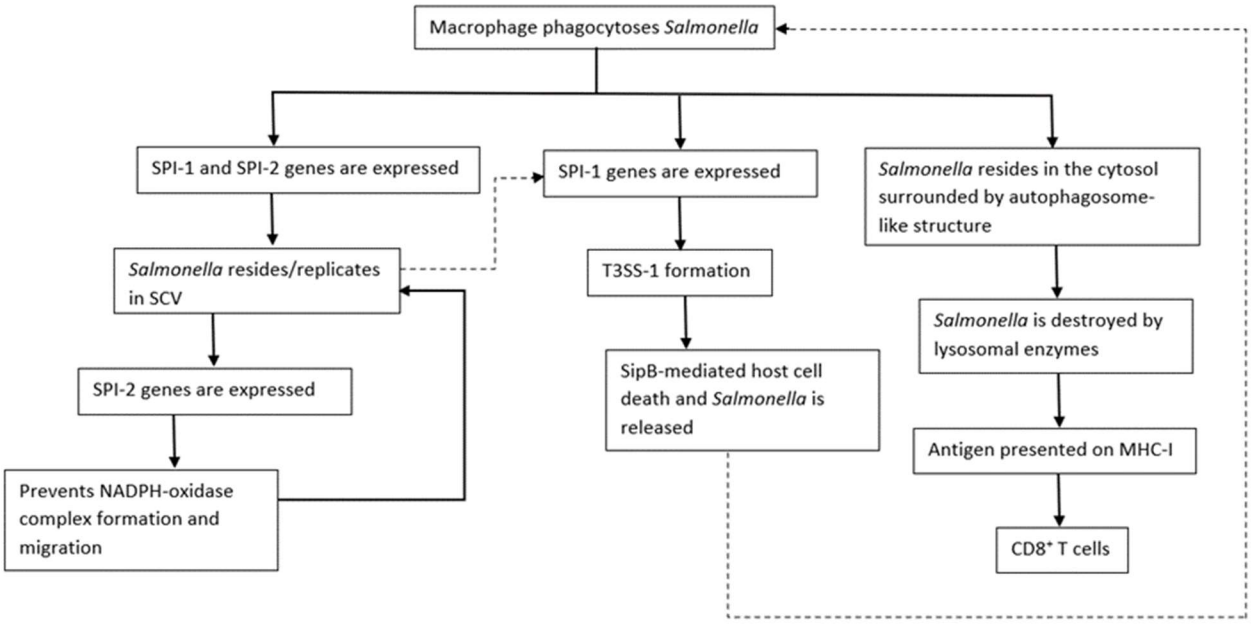

Figure 1.3. Summary diagram of *Salmonella* mechanisms once inside a macrophage.

In humans, it is known that typhoidal strains of *Salmonella* tend to infect macrophages that have been recruited to the infected Peyer's patch or solitary intestinal lymphoid tissues [23, 32, 33]. In contrast, it is also known that nontyphoidal strains are more readily recognized by macrophage PRRs and tend to recruit neutrophils and T cells to the infected distal ileum and colon via interleukin-8 (IL-8) production. The additional immune cells lead to more effective elimination of infection than with macrophages alone. The hypothesis for this cellular preference is that it is somehow linked to fimbriae structure, but investigation is still needed [1, 32, 33]. Those *Salmonellae* that are not successfully eliminated by these various phagocytes can be transported to the mesenteric lymph nodes (MLN) and then disseminated into the blood leading to systemic infection [16, 23]. The MLN is, however, where *Salmonella*-specific T cells are

activated following oral infection, and these cells can aid in protection against future systemic infections [23]. *Salmonella* does employ effector protein SteD from SPI-2 to inhibit antigen presentation and subsequent T cell activation, though (Table 1.1) [17, 27]. If systemic infection does take hold in a mammal, *Salmonella* replication can take place in the spleen, liver, and bone marrow [23].

As previously mentioned, *S.* Javiana is among the few nontyphoidal serotypes of *S. enterica* that are known to produce *Salmonella* CDT [8, 14]. Specifically, *S.* Javiana possesses the cytolethal distending toxin B (*cdtB*) gene within the CdtB-islet pathogenicity island, a virulence factor also found in *S.* Typhi, a typhoidal serotype of *Salmonella* [10, 34, 35]. CdtB in both typhoidal and nontyphoidal serotypes leads to DNase activity, arrested cell cycle progression and death of the infected, and sometimes surrounding, epithelial and immune cells [10, 34]. *Salmonella* Javiana's CdtB is hypothesized to lead to epithelial senescence instead of death, as evidenced by the release of proinflammatory cytokines by cells infected with CdtB+ *S.* Javiana (Table 1.1) [34, 36]. This inflammatory response leads to phagocytic cell recruitment as previously described and subsequent bacterial invasion of those phagocytes. In true *Salmonella* fashion, though, *S.* Javiana's CdtB also partially suppresses those innate immune responses, and *S.* Javiana creates an SCV, so the bacteria can survive long enough to disseminate beyond the intestinal lumen. The mechanism of this immunosuppression is not fully understood, but it is known CdtB plays an integral role in *S.* Javiana's ability to cause systemic infections [33, 34, 37].

Table 1.1. Known effector proteins involved in *S. enterica* pathogenesis, their functions, and their involved secretion systems.

Functional Group	**Effector Protein**	**T3SS**	**Specific Function**
Host invasion	SipC	1	Nucleates and bundles actin for membrane ruffling [17]
	SipA	1	Actin polymerization promotion [17, 38]; works with SipC for direct membrane ruffling [16]
	SopE	1	Manipulation of host cytoskeleton [17]; causes membrane ruffling through cell signaling interference [16]
	SopE2	1	Manipulation of host cytoskeleton [17]; causes membrane ruffling through cell signaling interference [16]
	SopD	1	Works with SopB to alter host membrane [17]
	SopB	1	Alters host membrane for invasion [17];causes membrane ruffling through cell signaling interference[16]
SCV Formation and Maintenance	SifA	2	Lysosomal-associated membrane protein 1 enriched membrane recruitment for SCV [17]; maintains SCV membrane integrity [16]
	SseJ	2	Works with SifA to regulate SCV membrane dynamics [17]; located on the cytoplasmic side of the SCV and esterifies cholesterol [39]
	SipA	1	Works with SifA to regulate SCV morphology [17]; not essential for SCV formation [38]
	SopB	1	Phosphatidylinositol 3-phosphate formation on SCV outer leaflet for SCV maturation [40]
NADPH oxidase evasion	SpiC	2	Inhibits endosome trafficking [17]; prevents lysosome fusion to SCV [27]
	SsaJ	2	Inhibits NADPH-oxidase trafficking to SCV [27]
	SsaT	2	Inhibits NADPH-oxidase trafficking to SCV [25, 27]
	SseB	2	Inhibits NADPH-oxidase trafficking to SCV [25, 27]
	SsrA	2	Inhibits NADPH-oxidase trafficking to SCV [27, 41]
T cell activation prevention	SteD	2	Inhibits infected cells from presenting MHC-II via MARCH8-dependent ubiquitination and subsequent T cell activation [17, 27, 42]
Host cell death	SipB	1	Activation of caspase-1 induced cell death [17, 27, 29]
	CdtB	?	DNA damage from DNase-I-like activity, leading to G2/M cell cycle arrest by the cell for DNA repair, and apoptosis from intrinsically expressed *Bax* and caspase 9 and 3 activation. Enters surrounding cells by endocytosis; senescence induction hypothesized for *S.* Javiana [14]

1.3. *Salmonella* and the Environment

Preventing infection circumvents the need for treatment, and this can be difficult with pathogens that can survive without a host. *S. enterica* are known to be able to colonize in and on common crop plants and survive in soil, in water, and on various surfaces for prolonged periods of time, given appropriate conditions – warmth, moisture, and shade [43-46]. Survival in soil can last for over a year, and it can last weeks to months in water and on/in plants [44, 47]. This environmental survival presents many issues when considering biorisk management, the only universal prevention method aside from personal hygiene currently available for several *Salmonella* serotypes, including *S.* Javiana [48].

Water is among the more problematic *Salmonella* dissemination vehicles when thinking about biorisk management. *Salmonella* can persist in water in a viable but nonculturable state (VBNC) and via residence in free-living protozoa. Mechanisms for induction of VBNC and resuscitation to a culturable state are still unknown and debated, but if *Salmonella* is replicating within a protozoa, like *Acanthamoeba*, they maintain their pathogenicity [49]. *Salmonella*'s presence in water can be traced to animal origins. Pathogens from feces and exudate of infected wildlife can be transported via rainwater runoff to larger waterways and subsequently into water reservoirs for agricultural use. In freshwater, *Salmonella* maintains viability longer than other Enterobacteriaceae, and rivers specifically are among the largest viable *Salmonella* reservoirs on earth [49, 50].

If contaminated water or excrement touches soil, then that soil can become contaminated with *Salmonella* as well. *Salmonella* Javiana has been found to persist in sand and sandy loam in temperatures ranging from 20°C to 30°C for up to 168 and 224 days respectively in a laboratory environment [51]. *Salmonella* Javiana and other studied *Salmonella* serotypes are known to be

able to survive much longer in manure-amended soils, particularly if the manure came from bovine, hog, or poultry [52, 53]. Serotypes do have soil-type preferences, though. *S.* Javiana is among the minority of investigated serotypes to survive longer in sandy-loam soils than clay-loam soils. Irrigation schedules, manure supplementation, manure source, and soil type all influence *Salmonella* survival in soil, and that interaction of influences may also be serotype-specific [53].

In close contact with water and soil are plants, and edible ones are an easy means of transport for infection. Survival on plant surfaces requires adhesion and attachment of *Salmonella* to the plant following exposure via contaminated feces, water, or soil [43, 45]. Adhesion is when bacteria are adsorbed to the phylloplane or fructoplane of the plant. This step is reversible, and strong force can dislodge the bacteria from the surface to which it is adhered. Attachment is the point at which *Salmonella* can replicate within the phylloplane or fructoplane biofilm and is protected from outside forces [45]. *Salmonella* Typhimurium, a nontyphoidal serotype of *S. enterica*, can attach to fruits such as peaches and plums in as little as thirty seconds [54] *S.* Newport, another nontyphoidal serotype of *S. enterica,* can adhere to mangoes immediately and attach within 2 minutes [45]. Both serotypes can also survive refrigeration while adhered or attached to various vegetation [45, 54]. Studies could not be found on *S.* Javiana-specific plant attachment or refrigeration survival, but outbreaks have been linked to uncooked cucumbers, onions, leafy greens, and tomatoes [55, 56]. Tomatoes, among other crops– lettuce, spinach, radishes, mustard, barley, alfalfa seeds, peanuts and thale cress– are known to become infected with nontyphoidal *Salmonella* rather than just superficially contaminated. Exposure to contaminated water through the rhizosphere, root system, leaves, fruits, or flowers can all lead to internalized *Salmonella* in edible portions of the plant. The

mechanisms of plant infection are still relatively unknown, but damaged plants are generally more susceptible than healthy ones [43, 57]. This infection means that simple cleaning or peeling of the plant will not make it safe for consumption.

Salmonellae are sensitive to common disinfectants, such as chlorine and bleach. However, cleaning and disinfection must be thorough to ensure complete elimination of the bacteria, and this is often labor-intensive and costly [47, 58]. Sanitation becomes particularly difficult if disinfection does not take place within a week's time of initial contamination, at which point sterilization capabilities on even nonporous, inorganic surfaces like glazed tiles are reduced [59]. *Salmonella*'s ability to survive in a plethora of environments for extended lengths of time, development of biofilms resistant to disinfectants, and direct linkage to human and animal activity as a mechanism of spread makes it an almost impossible pathogen to avoid on a wide-spread scale [44, 47].

1.4. *Salmonella*'s Impact on Animals

Salmonella is often transported through various types of animal shedding, with the usual route of infection being fecal-oral [60, 61]. Various serotypes have been found in the milk of bacteria-carrying cows and the feces of cattle, horses, chickens, dogs, and other animals that commonly have contact with humans [8, 62-66]. Wildlife that live in close proximity to humans have higher rates of *Salmonella* than those that live in less human-dense regions– raccoons being one common example of an urban animal found to contribute to the epidemiology of *Salmonella* in North America, with up to 27% of apparently healthy animals being carriers [44]. Shedding from many species can occur if the animal is apparently healthy or ill [47, 63, 64]. *Salmonella* Javiana has been specifically found to be a predominantly shed serotype in apparently healthy dogs in studies in Trinidad, Texas, and West Indies as well as apparently healthy cattle in South

America [65, 67-69]. Susceptibility to *Salmonella* infection and development of symptoms is hypothesized to be linked to an inability to harbor host-adapted enteric strains, but the exact reasons for the existence of silent-carriers of *Salmonella* is still unknown [66]. Shedding from otherwise healthy animals makes early detection and elimination of infection at the source extremely difficult, especially considering *Salmonella's* exceptional ability to survive in the environment. The most common animals to spread *Salmonella* to humans are various cattle, a wide range of poultry and avian species, dogs, cats, horses, reptiles, amphibians, rodents, and hedgehogs—those animals with which humans have more direct contact [23, 70]. All these species are known carriers of the serotype *S.* Javiana, with the only exception being the hedgehog [11, 12, 65, 69, 71-73].

In the dairy and beef cattle industries, *Salmonella* can have significant health, and therefore economic, impacts as it can lead to abortions, death of cattle at any age, and a decrease in milk production. Additional costs are added when infection is diagnosed because of the labor to treat and contain an infection or outbreak, loss of cattle to culling, loss of product to waiting out antibiotic clearance, recalls on contaminated milk, and inability to sell animals from the herd [47]. As of 2017, the most common serotype found in apparently healthy cattle in North America is *S.* Montevideo, and *S.* Javiana is the most frequently found serotype in our closely neighboring continent of South America [69].

The economic impact of *Salmonella* outbreaks is also a major concern within the poultry industry. Poultry products lead to over 1 million *Salmonella*-related illnesses each year in the United States, with nearly a quarter of those cases coming from chicken or turkey consumption. Human *Salmonella* infections from chicken alone lead to an annual economic burden of $2.8 billion in the United States, and *S.* Javiana is on the top 10 list of most common serotypes in

commercial poultry products [71, 74, 75]. Birds themselves do not typically exhibit signs of illness when infected with nontyphoidal serotypes of *Salmonella*, such as *S.* Javiana, so the veterinary concerns are limited. However, poultry-linked salmonellosis is considered a major public health concern in the U.S., and is therefore an issue heavily pressed upon poultry product companies and individuals who own their own birds [76, 77]. In fact, backyard poultry is linked to outbreaks on an annual basis in the U.S. because of the close proximity of this common *Salmonella* reservoir to a human host [78].

In addition to poultry, cats and dogs are among the list of common animals in close human contact that typically do not show signs of *Salmonella* infection, but rather act as silent carriers [65, 67, 68, 79]. Again, like in poultry, the concern with these infections is primarily public health, and *S.* Javiana specifically has been isolated from fecal samples in both species [65, 72, 79]. Cats and dogs are the two most common house pets in the world, and trends in pets being treated more like family than just companion animals puts them in even closer contact with people than many other species, increasing opportunities for transmission [80-88].

Among the list of companion animals are also horses, which have their own contributions to human outbreaks due to *Salmonella*'s zoonotic nature [63, 89]. In adult horses, salmonellosis is among the most common diagnoses for infectious causes of diarrhea, and *S.* Javiana is among the leading strains in equine infections [73, 79]. While *Salmonella* infections in horses may be asymptomatic, symptoms often do occur and can range in severity from signs of depression to death [79, 90]. Fatal cases mostly occur in horses that are otherwise ill or stressed or if they consumed a large dose of the bacteria at once [63, 79, 90].

Reptiles and amphibians are asymptomatic carriers of *Salmonella,* including *S.* Javiana. Reptiles and amphibians are considered risk factors for *S.* Javiana infections in the southeastern

United States, with several outbreaks linked to close contact with these animals [11, 12, 91]. This close association between reptiles, amphibians, and *S.* Javiana is hypothesized to be at least partially due to the similar environmental preferences of this serovar and these species– water and warmth [11, 12].

Exact economic impacts of *Salmonella* in animals are hard to determine, as there are few-to-no available reports. However, one should consider costs to include those of veterinary care as well as costs of cleaning, animal death, product loss, product recalls, and any possible lawsuits resulting from human infection. Knowing that *S.* Javiana is zoonotic, human infections arguably should also be considered when thinking about economic burden, especially since the primary reservoir for the nontyphoidal serotypes of *Salmonella* is production animal intestinal tracts [44].

1.5. *Salmonella* and *S.* Javiana, Human and Economic Impact

Salmonellosis cases in humans in the United States as of 2011 have cost approximately $4.7 billion annually just in combined cases related to poultry and pork, the bulk of those costs being because of related deaths [75, 92]. Foodborne illnesses specifically in the United States caused by nontyphoidal *Salmonella* serotypes led to $3.67 billion in costs in 2013, ranking it in the number one spot for economic burden from a foodborne pathogen ten years ago [93, 94]. That year, there was a mean incidence number of 1,027,561 cases of nontyphoidal *Salmonella* infections, 19,339 hospitalizations, and 378 deaths [94]. The U.S. Department of Agriculture (USDA) Economic Research Service (ERS) further estimates that in 2018, the most recent data set of *Salmonella*'s economic impact, the cost of nontyphoidal *Salmonella* infections from food was $4.14 billion, again the bulk of which was from costs related to deaths from infection [95-97].

While it is not a leading cause of death in the United States, *S.* Javiana is the fourth most common serotype associated with *Salmonellosis* and is among the leading causes of food-borne illness [7, 8, 98, 99]. National infection rates of *S.* Javiana have increased by 325% since 1970 and 136% between 2001 and 2016, and it currently accounts for approximately 5% of salmonellosis cases in the United States [7, 8]. In Louisiana, *S.* Javiana was the fifth most common serotype as of 2017, with 1332 total confirmed cases between 1987 and 2017 [100]. In 2019, the most recent available report for the state, there were 25.5 new cases of general nontyphoidal *Salmonella* infections per 100,000 population, ranking Louisiana the fifth worst state for human *Salmonella* infections, but specific serotype information was not available for that year [101].

S. Javiana has been identified in several countries beyond the U.S., such as Germany, Canada, Trinidad, West Indies, Australia, Thailand, and Malawi [8, 9, 65, 68, 69, 102-105]. However, exact infection rates and economic impact information have not been released in relation to this specific serotype on a global scale. It is known, however, that outbreaks are largely associated with consumption of contaminated foods, drinking from exposed water sources, and animal contact, regardless of where they occur (Table 1.2) [8, 9]. Human-to-human transmissions can also take place if the infection is systemic [23].

Table 1.2. Recorded outbreaks of *S.* Javiana globally between 1942 and 2022.

Date of Outbreak	**Source of Infection**	**Location(s)**	**Number of Cases**	**Number of Hospitalizations**	**Citation**
Nov-Dec 2021	Unknown	Not disclosed	42 confirmed	Unknown	[106]
Nov 2019 - Feb 2020	Cut fruit	CA, CO, CT, DE, FL, GA, IL, MA, MN, NJ, NY, VA, and WA, USA	165 confirmed	73	[107]
Aug 2018	Unknown	CO, USA	31 confirmed	5	[108]
Jan 2017 - Apr 2018	Kratom	CA, AZ, NY, MN, WI, OR, UT, CO, IA, WA, MD, MI, NC, OH, PA, VA, WV, AK, ID, ND, KS, MA, AL, DE, FL, GA, IL, IN, KY, LA, MS, MO, NV, OK, SC, TN, and TX, USA	15 confirmed	38*	[109]
Oct 2017	Clam chowder	NY, MD, NC, PA, VA, WV, DE, and NJ, USA	172 probable	18	[110]
Jan 2017	Shredded coconut	CA, NY, CO, WA, PA, NJ, and OK, USA	29 total salmonellosis cases*	6*	[111]
2016	Peppered shrimp	AZ, USA	40 confirmed, 10 probable	14	[112]
October 2008	Watermelon	Multisite daycare center in CA, USA	594 probable	31	[113]
August 2008	Barbeque pork	NC, USA	71 probable	17	[114]
August 2008	Striped bass consumption	VA	45 probable	1	[115]
Nov 2006	Iceberg lettuce	TN, USA	16 probable	7	[116]
Aug - Oct 2004	Well water consumption; reptile and amphibian contact	GA and TN, USA	117 confirmed	Unknown	[8, 11]

Notes: Recorded outbreaks of *Salmonella enterica* serotype Javiana globally between 1942 and 2022.
*Did not distinguish the number between *S.* Javiana and other serotypes involved in the outbreak, but *S.* Javiana was among the known serotypes involved.
(table cont'd.)

Date of Outbreak	Source of Infection	Location(s)	Number of Cases	Number of Hospitalizations	Citation
July 2004	Tomatoes	MD, MI, MO, NC, NH, OH, PA, VA, and WV, USA; Ontario, Canada	383 in the US; 7 in Canada	30% of cases for the states*; 14% of all confirmed and probable cases in Canada	[117]
May - Jun 2003	Cafeteria food	Children's hospital in MO, USA	101 confirmed, 540 probable	Unknown	[118, 119]
Jun - July 2002	Tomatoes	Orlando, FL, USA	141 probable	3	[120, 121]
Aug - Sep 2001	Contact with snakes, turtles, frogs, & toads (pet or wild); visiting a lake/pond	MS, USA	164 confirmed	Unknown	[8, 12]
Apr - July 1993	Paprika	Germany	1000 probable	Unknown	[8, 122]
Jun 1991	Watermelon	Elementary school in MI, USA	39 confirmed, 11 probable	Unknown	[123, 124]
May - Jun 1990	Tomatoes	MN, MI, IL, and WI, USA	176 confirmed	Unknown	[8, 56]
May - Jun 1989	Cheese	MN, USA	136 confirmed	Unknown	[8, 125]
July 1942	Cheese	NM, USA	40 confirmed	Unknown	[8]

Notes: Recorded outbreaks of *Salmonella enterica* serotype Javiana globally between 1942 and 2022.
*Did not distinguish the number between *S.* Javiana and other serotypes involved in the outbreak, but *S.* Javiana was among the known serotypes involved.

Systemic infections are when *Salmonella* does the most damage. Those infection types with nontyphoidal *S. enterica* serotypes, such as *S.* Javiana, can lead to a disease called invasive nontyphoidal salmonellosis (iNTS). The disease presents with fever, respiratory symptoms, hepatosplenomegaly, and even death if left untreated [126-128]. *Salmonella* Javiana iNTS has been recorded to also cause liver abscess, cholecystitis with gallbladder perforation, and

meningitis [8]. Typically, the development of iNTS is a result of failed immunological control of the bacterial infection, which historically could be avoided with proper antibiotic treatment [129]. However, antibiotics have been found in the last two to three decades to not decrease the longevity of the infection's symptoms nor the presence of the bacteria in the feces of the patients, and antibiotic resistance is a growing issue [130-132].

An estimated 93.8 million cases of *Salmonella*-induced gastroenteritis, a potential precursor to iNTS, occur globally each year, and just those gastroenteritis cases result in approximately 155,000 deaths without development of systemic infection [133, 134]. Globally, iNTS is considered among the major causes of death and illness, disproportionately impacting developing countries. As an example, the continent of Africa has an estimated annual iNTS case rate of 3.4 million, and the annual case-fatality ratio is over 20% [135]. Within the African country of Malawi, one of the poorest countries in the world, *S.* Javiana-linked iNTS has estimated fatality rates of 47% in adults and 38% in children [8, 136, 137].

1.6. Existing *Salmonella* Vaccines and Treatments

The two main types of traditional vaccines are live-attenuated and inactivated or killed vaccines, both of which fall under the umbrella of "whole-pathogen" vaccines [138]. Live-attenuated vaccines are those that contain a weakened version of a living pathogen with reduced virulence. The benefit of these vaccines is that they are similar enough to the virulent pathogen that protection is induced similarly to that of a true infection, leading to long-lasting and effective immunity. However, because they are living, patients with weakened immune systems are at risk of falling ill to the attenuated version, and there is a possibility of virulence being regained. Additionally, these vaccines need to be refrigerated, making distribution difficult, particularly for developing countries [138-140]. Inactivated or killed vaccines are those that

contain pathogens that are no longer living. These do not pose the same risks as the live-attenuated vaccines. The pathogen has no opportunity to revert to a virulent state or otherwise cause harm if the inactivation/killing process was successful. However, the inactivation process can damage the immunogenic portions of a pathogen, leading to shorter and weakened immune responses [138, 139, 141]. In the case of *Salmonella* vaccines, live-attenuated versions are generally used instead of the inactivated vaccines because of this pitfall [142].

Subunit vaccines were later designed to be easier to produce and safer than their whole-pathogen counterparts, but they typically require an adjuvant to be co-administered to get a strong, long-term immune response [138]. For *Salmonella*, the subunit vaccine for veterinary use is composed of the siderophore receptor and porin (SRP) proteins found on the exterior surfaces of the bacterial cells [143]. These vaccines function by leading to antibody production and antibody binding to the SRP, which blocks iron transport and ultimately leads to *Salmonella* cell death [144]. For humans, a subunit vaccine exists that contains the Vi polysaccharide antigen, which leads to antibody development and recognition of this exterior *S.* Typhi antigen and subsequent pathogen elimination [145, 146]. While considered safer than live-attenuated or killed vaccines because of their lack of whole-pathogen, these SRP vaccines for *Salmonella* do contain adjuvants [138, 143]. Adjuvants are typically microbial components, chemicals, or mammalian proteins that enhance presentation and stability of antigens or modulate the immune system through cytokine upregulation, increasing immune cell density and activity at the site of injection. The major problem with adjuvants is their potential to do harm, adding a risk component to these vaccines. An increase in immune response means that there is potential for amplified adverse effects typically seen with a standard vaccination, such as fever, lethargy, soreness, granulomas, and abscesses, among others. In more significant instances, side effects

can include autoimmune reactions or sarcoma development, particularly in veterinary medicine [147, 148].

Currently, *Salmonella* vaccines exist for use in poultry, cattle, pigs, and even humans. However, they have a list of issues that need to be addressed: the majority of these vaccines are live-attenuated, so they have potential to cause infection or illness and often are costly; the remaining few vaccines are subunit/extract vaccines, which typically require the addition of an adjuvant to get a strong immune response and therefore pose health threats as well; they are each specific to only one or two serotypes; and they are not designed for practical large-scale use in agricultural production or impoverished communities [149-163]. Despite these pitfalls, however, live-attenuated and inactivated vaccines are continuing to be developed and tested [164-166].

With *Salmonella*'s heavy impact in the developing world, where iNTS and enteric fever can have fatality rates of up to 25%, distribution to those countries and multi-serotype protection are ideals when discussing *Salmonella* vaccine design [162, 163]. Live-attenuated vaccines and subunit vaccines both require refrigeration for storage to maintain their efficacy, making this distribution difficult as these countries do not have wide-scale refrigeration access [139, 143, 167]. Even if those vaccines could be distributed, in the cases of the 2 vaccines in existence for humans, protection rates are only 50% and only cover *S.* Typhi (Table 1.3) [162, 163, 168]. Coverage in animal *Salmonella* vaccines are also serotype limited, meaning multiple vaccinations may need to be given to get protection against multiple serovars, and vaccines that are commercially available are only for protection against a tiny fraction of the over 2500 nontyphoidal serotypes [149-161]. Those vaccines currently on the market only cover *S.* Typhimurium, *S.* Choleraesuis, *S.* Dublin, *S.* Typhi, *S.* Enteritidis, and *S.* Heidelberg, and this list is missing several major serotypes for animal-linked human outbreaks, including *S.* Javiana and

S. Agona (Table 1.3) [145, 150-153, 155, 156, 158-160, 169-175]. Additionally, other heavily impacted/impactful species, such as horses, reptiles, and amphibians, do not currently have vaccines commercially available [176].

Aside from vaccinations, the only other *Salmonellae* preventative that can be administered to animals is competitive exclusive diets (CE) [177]. CE is a probiotic strategy that uses non-pathogenic bacterial culture to colonize the gastrointestinal tract of a given animal. Those "good" bacteria then leave little room and resources for the pathogenic bacteria to colonize [177, 178]. CE is known to be effective at reducing *Salmonellae* populations in poultry, pigs, and ruminants [177, 179, 180]. The major drawback of CE is that antibiotic use can negate the effects of CE by reducing the presence of the beneficial bacteria [177]. Additionally, administration must be at a young age, which can be difficult depending on the species and housing situation. Administration of CE as an animal ages has less consistent results for *Salmonella* colonization, and this is hypothesized to be because of the older animals possessing a more established GI population [177, 181].

If prevention is not achieved, infections are left to be treated. The increase in antibiotic resistance within a variety of pathogens, including *S*. Javiana, means that antibiotic use may not be the most ecological or effective remedy. The treatment of symptoms– which includes pain management methods, fluid therapy, and antidiarrheals– are the preferred treatment methods among medical professionals in the event of an infection that is not life-threatening. In the more severe cases of infection where iNTS has taken hold, symptom management becomes more difficult and antibiotics are typically attempted without guaranty of success [61, 162, 163, 182, 183].

Table 1.3. Commercially available vaccines for protection against *Salmonellae* as of January 2023, their classifications, their specified serotypes for protection, and their host species.

Vaccine Name	**Vaccine Type**	**Serotype(s) Covered**	**Recipient Species**	**Sources**
Endovac-Beef® with ImmunePlus Cattle Vaccine	Core-antigen killed vaccine	*S.* Typhimurium-induced endotoxemia	Beef cattle	[150, 158]
Endovac-Dairy® with ImmunePlus Cattle Vaccine	Core-antigen killed vaccine	*S.* Typhimurium- induced endotoxemia	Dairy cows and heifers in third trimester	[151, 156, 159]
Endovac-Porci® with ImmunePlus Swine Vaccine	Core-antigen killed vaccine	*S.* Typhimurium- or *S.* Choleraesuis- induced endotoxemia	Swine	[152]
Vaxxon SRP Salmonella Cattle Vaccine	Subunit	*S.* Newport	Healthy cattle, 6+ months	[153]
EnterVene® -d	Live	*S.* Dulbin	Cattle	[155]
Enterisol® Salmonella T/C	Avirulent live	*S.* Choleraesuis, *S.* Typhimurium	Swine	[160]
Vivotif®	Live attenuated	*S.* Typhi strain Ty2	Human	[170-172]
TYPHIM VI- salmonella typhi ty2 vi polysaccharide antigen injection, solution	Subunit	*S.* Typhi	Humans	[145]
Equivac® EST	Live attenuated	*S.* Typhimurium	<10 weeks, foal	[173, 174]
Poulvac® ST	Live attenuated	*S.* Enteritidis, *S.* Heidelberg, *S.* Typhimurium	Poultry	[175]

1.7. Comparing Existing *Salmonella* Vaccines and pDNA-based Vaccines

Recombinant plasmid deoxyribonucleic acid (pDNA) vaccines are a potential avenue to get the immunological impact of a live-attenuated or subunit vaccine while being safer than even the inactivated vaccines [184]. They are also less expensive to produce than the current vaccine types for protection against *Salmonella*, possess multi-serotype protection potential, and have easier storage requirements than existing *Salmonella* vaccines [184-187]. Low costs and easier storage have huge implications for vaccine equity for developing nations as well as commercial

use in large-scale agriculture. No nucleic acid-based vaccines, including recombinant pDNA, could be found for protection against any *Salmonella*, and the only research towards this endeavor that could be found used only a singular whole-protein from a particular serotype with each vaccination [188]. However, the research for pDNA vaccines in general is extensive, and there is now even one in commercial circulation for protection against the SARs-cov-2 virus that started the COVID-19 pandemic [189].

Existing research from clinical trials in humans and animals have shown that pDNA-based vaccines are capable of inducing both arms of the immune system, much like an actual *Salmonella* infection or live-attenuated vaccination, and provide protection against infection if the vaccine is well-designed [190, 191]. Unlike an actual *Salmonella* exposure or existing vaccinations, however, the immune system is not exposed to the actual pathogen or even a whole protein of the actual pathogen. Rather, the pDNA vaccine utilizes the host's cells to create portions of immunogenic proteins called "epitopes" from a genetic sequence which are then presented to the immune system. For vaccination to be successful, these epitopes must successfully mimic those found on and within the pathogen of interest, but they are not functional and therefore do not pose the same threats as the proteins from which they are modeled [192].

Direct safety comparisons between pDNA vaccines and traditional vaccines have not been made, and this may be because of the lack of variety of vaccine types for a specific pathogen. However, a big point in favor of pDNA vaccine safety is its lack of a whole pathogen, as compared to live-attenuated and killed vaccines. There is no risk of reversion to a virulent state, and the lack of whole pathogens means reduced risks to the immunologically compromised [184]. When comparing pDNA vaccines to subunit vaccines, implications for safety are less

clear. The presence of an adjuvant has been shown to aid in pDNA vaccine immune responses, and adjuvants are a main point of concern when considering safety of subunit vaccines [147, 148, 193, 194]. However, the presence of an adjuvant has not been shown to be necessary to achieve an adequate immune response in the case of pDNA vaccine useage [195-197].

Lacking a whole pathogen or protein in its native form makes pDNA-based vaccines not only potentially safer but easier and quicker to produce than traditional vaccines, which stands to translate to lowered costs [192]. The ease of quick producibility is because their production is synthetic [186, 198]. The pDNA itself is made by adding nucleotide monomers together via phosphoramidite chemistry followed by polymerase chain assembly, and larger-scale production is achieved through propagation of that pDNA through a bacterial cell line [199]. Materials costs are incredibly low, with some claims putting the resulting pDNA vaccines at as low as $1 per dose [185, 186].

In addition to cost benefits, the synthetic creation of these vaccines means that their design is flexible. Sequences responsible for protection against any given pathogen can be altered without changing the physio-chemical characteristics of the vaccines and without significant adjustments to the production line, allowing for quick and inexpensive expansion into vaccines for protection against new pathogens or adjustments to an existing vaccine [187]. Additionally, because of the vaccine's synthetic nature, multiple epitope codes can be combined from different pathogens to aid in cross-protection, meaning one vaccine could prevent infection from multiple *Salmonella* serotypes [200-202]. Multi-serotype protection means fewer necessary vaccines, and again, aid in cost and subsequent accessibility.

Low cost is one of two milestones necessary for accessibility of these vaccines. The other is storage. Storage conditions not only contribute to cost evaluation for vaccination but can also

determine if a vaccine will be efficacious following distribution. DNA is a highly stable molecule, and it has less need for refrigeration than all 3 existing *Salmonella* vaccine types as well as its other nucleic-acid-based vaccine counterpart –messenger ribonucleic acid (mRNA) [192]. Lacking the need for cold storage means that these vaccines can be distributed to the more remote parts of the world, where access to such amenities is limited or unheard-of.

1.8. Summary, Overall Hypotheses, and Overall Aims

There is a need for an efficacious and economical vaccine design for various *Salmonella* serotypes, given their global impacts in public health and economic burdens. *Salmonella* Javiana, among the more common *Salmonella* serotypes, needs particular focus because of the lack of vaccines commercially available. Plasmid DNA-based vaccines could be the solution to this gap in *Salmonella* protection: they pose no threat of causing an inadvertent infection because they do not contain any actual pathogen, epitopes of various antigens can be included in a single vaccine to allow for cross-protection rather than protection against a single serotype, their entire production process is considerably more cost-effective than traditional modes of vaccine production, and vaccines in general are more ecologically responsible than the available antibiotic treatments [203].

Within this project, four pDNA vaccines have been designed for protection against *S.* Javiana, with cross-protection potential in mind. The first three vaccines are identical aside from the presence and length of a genetic adjuvant, a known immunogenic epitope encoded with the intent to aid in immune stimulation. The fourth vaccine is a modified version of one of the first three vaccines. The overall aim of this project is to begin development of a pDNA vaccine platform for protection against *S.* Javiana. The overall hypothesis of this project is that at least

one of the pDNA vaccines will lead to detectable protein and/or antibody production specific to *S.* Javiana.

It is important to note that this project was started because of an outbreak of *S.* Javiana in thoroughbred horses in Louisiana, as communicated by the Louisiana State University (LSU) Veterinary School. The original design of the vaccines will reflect this project's inception, but further chapters will explore other potential recipients (i.e., poultry) for these vaccines because of research practicality as well as the potential markets for these vaccines outside of the equine industry.

Chapter 2. Bioinformatic Approach to Epitope Selection

2.1. Introduction

2.1.1. How DNA Vaccines Work

The immune system consists of innate and adaptive systems. The innate immune system is immediate and antigen-independent, so it is rapidly involved in the elimination of foreign bodies. This system also plays a role in the recruitment of cells involved in adaptive immunity. The adaptive immune system by contrast is not immediate, and it is antigen-specific and capable of developing memory [204]. This memory development is one of the goals of vaccination, and the other goal is making sure that the memory is sufficient to prevent future infections. Recombinant pDNA vaccines, if well-designed, utilize both the innate and adaptive immune systems and have the potential to produce long-term humoral and/or cellular immunity [205, 206].

Plasmid DNA vaccines are intended to enter antigen-presenting cells (APCs) such as DC and macrophages when administered, but they can also enter other nearby cells. Once inside a cell, the foreign double-stranded DNA is recognized by sensors of the innate immune system, such as AIM2, STING/TBK1, and TLR9, which activate cytokine production (Table 2.1). These cytokines lead to immune cell recruitment to the injection site and subsequent migration of the APCs to local lymphoid tissues (Table 2.1) [207, 208]. If they make it to the lymphoid tissues, the APCs with the presented antigens from the DNA code can then activate naive T cells. The type of T cells that are activated by the APCs is dependent upon how the antigen is presented, and presentation is determined by how the vaccine is processed once proteins are produced [204, 209].

Table 2.1. Sensors of the innate immune system that recognize foreign DNA

Innate immune system sensor	What is being recognized	Resulting cytokines	Immune cells recruited	Sources
TLR9	Recognition of bacterial and viral DNA rich in unmethylated CpG-DNA motifs	type-I interferon or NF-kB	Polymorphonuclear lymphocytes and natural killer cells	[204, 210, 211]
AIM2	Recognition of dsDNA in the cytoplasm	IL-1beta	Macrophages, DC	[212, 213]
STING/TBK1	Cyclic dinucleotides of bacteria	NF-kB or type-I interferon	Polymorphonuclear lymphocytes and natural killer cells	[204, 211, 214, 215]

Notes: Sensors of the innate immune system that recognize foreign DNA, the components of DNA that are being recognized by each sensor, their resulting cytokine production, and the specific immune cells recruited by each reaction.

If the pDNA vaccine's resulting proteins are processed like an endogenous pathogen, then they are presented via the major histocompatibility complex I (MHC-I). Endogenous proteins are degraded within the proteasome into epitopes and further processed within the endoplasmic reticulum, where MHC-I is initially created and bound to the epitopes. The MHC-I-epitope complex is transported from the ER and through the Golgi apparatus. An endosome then takes the MHC-I-epitope complex from the Golgi apparatus to the cell surface [204]. MHC-I is involved in the activation of CD8+ cytotoxic T lymphocytes (CTL), also referred to as killer T cells, which are an important part of cellular immunity [209, 216]. When the T cell receptor (TCR) on the naive CD8+ cells interacts with the MHC-I molecule of a target cell and the T cell CD28 molecule interacts with CD80 or 86 of the APC, the CD8+ cell is activated and differentiates into a CTL [217]. The antigen-specific CTL then recognizes and kills infected cells via perforin and granzyme secretion [209].

If the proteins are secreted and engulfed by another APC, then they are treated like an exogenous pathogen. Exogenous pathogen proteins are presented via MHC-II. When the proteins are engulfed, they are within a phagosome which eventually fuses with a lysosome for protein digestion. An endosome containing the newly made MHC-II fuses with the phagolysosome, and the epitopes from the proteins within the phagolysosome bind to the MHC-II cleft. The endosome then takes the MHC-II-peptide complex to the cell surface [204]. MHC-II is involved in the activation of CD4+ T cells, or T helper (Th) cells, which can then differentiate into Th1 or Th2 cells [218, 219]. Th1 cells secrete IL-2 and interferon-γ, which are involved in activating CTLs and macrophages [204, 219]. The importance of CTL activation was previously described, and the importance of macrophage activation will be described later. The Th2 cells, however, have a transmembrane CD40 ligand and secrete cytokines, which are both involved in the activation and differentiation of B cells. This activation and differentiation is necessary for subsequent antibody production and is therefore important for humoral immunity [209, 219].

The antigen-specific part of the antibody is called the paratope, which is part of the fragment antigen-binding (F(ab)) region of the antibody structure. The paratope is comprised of the variable domain (V), which has heavy (H) and light (L) chains. The remainder of the F(ab) region of the antibody consists of constant domains (C) also with H and L chains. The H chains of C domains of the F(ab) region connect to the base of the antibody via a flexible hinge. The base of the antibody consists of C domains with H chains that form the fragment crystallizable (Fc) region (Figure 2.1) [220]. The Fc region is the part of the antibody responsible for inducing effector functions, which are specific to the antibody class produced [221]. So, in a pDNA vaccination, antibody production should include paratopes specific to the epitopes encoded within the pDNA and Fc regions capable of inducing effective bacterial elimination strategies.

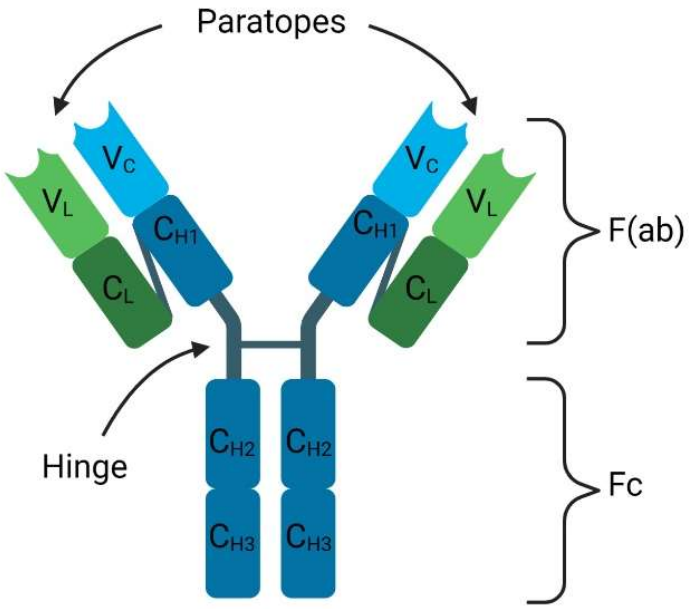

Figure 2.1. Basic antibody structure, demonstrating the F(ab) and F(c) regions, their C and/or V domains, and their H or L chains. Created with BioRender.com (Appendix D).

2.1.2. Components of a DNA Vaccine and Navigating Innate Immunity

The proteins that result from the pDNA vaccine are encoded within the open-reading frame (ORF). The ORF consists of the string of codons, or trinucleotides, that begins with the "start" code and ends just before the "stop" code, or alternatively described as the length of DNA which is both transcribed and translated [222]. As previously described though, DNA can induce an innate immune response. While beneficial for immune cell recruitment and migration of transfected cells to the lymphoid tissues, these immune responses also have the potential to eliminate the pDNA before protein production can ever take place. Therefore, a balance needs to be achieved. Current research on striking this balance involves optimizing transfection as well as the transcription and translation components of pDNA to outpace the immune system and incorporating other immune-inducing strategies [223].

Transfection efficiency has a plethora of involved components. Techniques for transfection, among the list of factors for efficiency, will be covered in Chapters 3 and 4 of this project. In terms of the pDNA vaccine itself, size has a significant role in transfection ability. Plasmids up to 10,000 bp can be transfected *in vitro* with detectable resulting protein expression, but efficiency is known to increase with decreasing plasmid size with a variety of transfection methodologies [224-227].

Adjusting plasmid size has the limitation of the number and sizes of components within the vaccine. The ORF along with all transcription and translation components are all necessary for a pDNA vaccine to be successful. Transcription and translation components will be covered in Chapter 3 of this project, and the sizes of these components are non-adjustable. Transcription and translation components are selected based on their function over their size, and therefore their incorporation can be considered a minimum base pair count for the plasmid. However, the ORF is adjustable in its size, as it is entirely customizable.

In addition to its size, the ORF can also be customized for translation efficiency via codon optimization. Codon optimization is the process through which trinucleotides are altered without altering the resulting amino acid sequence based on the host organism's codon biases [228]. Accommodating these biases aids in elongation rate and translation accuracy [229, 230]. There are several codon optimization tools available, but the host species available within each program and access to each program is limited. Integrated DNA Technologies (IDT) possesses such a program/tool to which this lab has immediate access, and their codon optimization tool additionally accounts for ease of production. So, the IDT codon optimization tool accommodates the translational preferences of the desired host while ensuring that the DNA creation is feasible [230].

An optional addition to the ORF is a co-encoded adjuvant. Adjuvants delivered separately from the antigens are known to be quickly degraded and potentially induce autoimmunity, therefore, co-encoded adjuvants are among the preferred applications if an adjuvant is included [231, 232]. The options for co-encoded adjuvants are vast, but among them are known immunogenic antigens [232]. In this context, a co-encoded genetic adjuvant is a coding sequence within the vector for the production of a known immunogenic protein to aid in immune cell recruitment for vaccination [233, 234]. The adjuvant selected for this vaccine was a known immunogenic epitope of bacterial superoxide dismutase (SOD) [234]. There is evidence suggesting that bacterial SOD is a PAMP and that co-encoded PAMPs within protein-based vaccines may increase interferon-γ and antibody production [235, 236]. Therefore, incorporation of bacterial SOD in theory should aid in inducing immune activities after translation has already taken place.

2.1.3. Vaccine Design and Its Immunogenic and Cross-Protection Potential

One of the keys to cross-protection potential for pDNA vaccines is the inclusion of multiple epitopes. Selecting epitopes that are highly conserved across multiple serotypes or combining epitopes that are specific to a multitude of serotypes allows for recognition of multiple serotypes by the immune system following vaccination. For this recognition to take place, however, the epitopes need to have a high MHC binding affinity and need to be conformationally identical to their state in the native protein [237-239].

MHC binding affinity refers to the likelihood that a given epitope will be presented by either MHC-I or MHC-II in the event of an infection. There are a variety of programs that can be used for determining MHC binding affinity [240, 241]. Among the free software is the Immune Epitope Database (IEDB) Analysis Resource, which allows for binding predictions of MHC-I

and MHC-II [240]. The program allows for the analysis of proteins for binding predictions within a handful of species and their known alleles. According to IEDB's algorithm, the lower the percentile number given for an epitope, the higher the affinity. Additionally, this affinity can be extrapolated to the affinity between antibody and epitope, and therefore, the increased immunogenic potential of the epitope [242, 243].

Ensuring native protein conformation is vital within the pDNA vaccine design process. If MHC-I or MHC-II is presenting an epitope in a non-native conformation, then resulting immunity will not recognize those epitopes on the actual pathogen. Stringing epitopes together one by one can lead to incorrect protein folding because of the amino acid charge interactions as the epitopes are being translated [244]. One technology that is used to prevent this epitope-epitope interaction is the inclusion of spacers, also referred to as "flexible polypeptide linkers" or "free rotational spacers" (FRS) [244, 245]. FRS in modern technology are typically a string of glycines with intermittent neutral-charge amino acids [246, 247]. Serine and proline are among the commonly used neutral amino acids within FRS designs [247-249]. FRS occur in nature and are rigid, but the addition of glycine-rich regions in the artificial arenas allows for flexibility. This flexibility aids in allowing the less structurally stable epitopes to maintain their weaker interactions for conformational folding [244].

2.1.4. What Makes a *Salmonella* Vaccine Work, Current Research and Hypotheses

Evidence from human case reviews and mice studies suggests that CD4+ Th1 and Th17 cells are required for adequate protective immunity in combination with antibody development, which involves Th2 cells in addition to B cells [23, 33, 127, 168, 250, 251]. CD8+ cells are also involved in the elimination of *Salmonella*, but their importance in the *Salmonella* elimination process as compared to CD4+ cells is debated [33, 188].

While *Salmonella* prefers to exist intracellularly during an infection, CD4+ Th1 cells are needed for protection in the event of intramacrophage infections, and macrophages are the preferred host cell of *Salmonella*, as previously described [162]. The infected macrophage gets activated by the Th1 cells via contact and focal interferon-γ secretion. The resulting cascade of biochemical responses causes the macrophage's antimicrobial and antigen presentation mechanisms to amplify and overpower *Salmonella's* defenses [209, 252]. Therefore, one of the goals of vaccination should be CD4+ T cell development and therefore MHC-II affinity.

Additionally supporting the notion that the vaccine design should have an emphasis on MHC-II affinity is the importance of antibody development. *Salmonella* that makes it past GI tract barriers and is free of a host cell is typically eliminated via antibody-mediated immune responses. In humans, antibodies initiate *Salmonella* killing through complement and opsonophagocytosis, and in mice, antibodies almost exclusively employ the latter [253]. Opsonophagocytosis is the phagocytosis of a pathogen that has been opsonized, and opsonization can occur via antibodies alone or via the complement system [254]. IgM, IgG, and IgA are the major antibodies found after a *Salmonella* infection. IgA and IgG can opsonize the pathogen themselves [255]. IgM binds the *Salmonella* and activates the classical complement pathway, something that IgG is also capable of doing [253, 256]. If the complement system is activated, inflammation is induced via C4a, C3a, C5a, and C5b and subsequent phagocyte recruitment via the previously mentioned C3a and C5a. Additionally, C3b is involved in opsonization, making the *Salmonella* more readily phagocytosed. Finally, C5b, C6, C7, C8, and C9 come together to form the membrane attack complex on the surface of the *Salmonella*. Once the C9 is polymerized, it can form a transmembrane ring and a subsequent pore in the target cell, allowing osmotic lysis of the target cell to take place [257]. As previously described, however,

Salmonella has several mechanisms to survive within macrophages and prevent C9 polymerization. It has been well-established that the presence of *Salmonella*-specific antibodies is essential for protection, but the exact mechanisms surrounding their effective nature against nontyphoidal *Salmonellae* are still relatively unknown [255].

Previous research points to fimbria and outer membrane proteins as ideal candidates for *Salmonella* vaccines. They are immunogenic and present on the surface of the bacteria, making them readily recognizable by the immune system regardless of whether or not *Salmonella* has yet found a host cell [127, 258]. However, the only DNA-based vaccine that has shown promise in *Salmonella* trials is an SopB whole-protein encoding plasmid. As previously explained, SopB is a secreted effector protein by *Salmonella*, and it is hypothesized to be important in CTL activation during *Salmonella* infections with shown affinity for MHC-I and MHC-II binding [188]. Therefore, fimbrial proteins, outer membrane proteins, and SopB should all be investigated for use in a multi-epitope vaccine.

2.1.5. Proteins of Interest

FimH was selected because of its location on *S*. Javiana, its efficacy in other vaccine research, its functionality in the immune response incurred by an infection, and its cross-protective potential. FimH functions in cell adhesion and is a fimbrial protein, meaning it meets the criteria of suggested focus proteins for future vaccine research [259]. It has already been shown to be an effective component in vaccines against mucosal *Escherichia coli* infections, leading to a 99 percent decrease in bacterial colonization [260]. FimH induces proinflammatory cytokine expression via the TLR4 in *Salmonella*-infected macrophages, making it extremely immunogenic and therefore, a great candidate for further analysis [261]. Additionally, FimH is a

component of Type 1 fimbriae, which most *Salmonella* possess with significant shared genetic homology [258, 262].

SopB was selected because of its conserved nature between at least *S.* Javiana, *S.* Typhimurium, and *S.* Enterica; its role in host immune response; and its efficacy in other nontyphoidal vaccine research. SopB being a highly conserved protein between multiple *Salmonella* serotypes makes it a great candidate for cross-protection potential, and therefore a good candidate for the vaccines within this project. Its role across the various serotypes is threefold: it is among the effector proteins that cause membrane ruffling for cellular invasion, it contributes to the formation of SCVs while inside host cells, and it is secreted for neutrophil recruitment [16, 20, 40, 263]. SopB's immunogenic nature and vital role in *Salmonella* colonization make it a good vaccine candidate, and while it is not an exterior protein on *Salmonella*, it is secreted, which could help recruit appropriate immune cells to the area of infection following vaccination. In one clinical trial, the entirety of SopB encoded in a DNA vaccine reduced virulent *Salmonella* loads, further demonstrating its potential as a recombinant vaccine candidate [188].

Outer membrane protein (Omp) A, like SopB, is a highly conserved protein across at least *S.* Javiana, *S.* Typhimurium, and *S.* Enterica. Additionally, it is an outer membrane protein and therefore meets the suggested criteria previously mentioned, is heavily involved in *Salmonella* survival in the host, and leads to antibody production [264]. OmpA functions in structural molecule activities [265]. Additionally, OmpA promotes evasion of phagocytosis by macrophages, promotes intracellular survival once inside the macrophage, and promotes epithelial cell invasion and intracellular survival. The intracellular survival of *Salmonella*, regardless of host cell type, is dependent on OmpA. Firstly, OmpA is directly involved in the

process of creating and maintaining the SCV, within which *Salmonella* safely replicates within the cell. Additionally, while in phagocytes, OmpA aids in protection of the *Salmonella* from nitrosative stress responses even outside of the SCV [264]. In an oral protein-based vaccine study in chickens, OmpA did not fully protect against *S.* Enterica in a challenge, but it did induce a humoral immune response with increased immunoglobulin (Ig) G levels specific to OmpA. The lack of protection was hypothesized to be because of a lack of cellular immunity development following vaccination. Cellular immunity is hypothesized to be necessary in conjunction with humoral immunity for adequate protection, and utilization of OmpA in conjunction with epitopes of other immunogenic proteins may provide such a reaction [266].

OmpC and OmpD (also known as PhoE) are proteins within various nontyphoidal serotypes including *S.* Typhimurium and *S.* Enterica, and OmpC is also in *S.* Javiana specifically. These proteins function in porin activity and ion transport, and they are outer membrane proteins located in the pore complex [267]. OmpC and OmpD were both selected because of their known locations, the fact that they are highly conserved across multiple serotypes, and their shown efficacy in both protection of the vaccinated subjects as well as the reduction of potential spreading of *Salmonella* in prior vaccine research [168, 268, 269]. In a 2013 poultry study, protein-based vaccines with recombinant OmpC produced a significant enough humoral response to protect against virulent *S.* Typhimurium strains, and the vaccine reduced the *Salmonella* found in the fecal shedding of the tested poultry as well as in the edible portions of the birds [268]. *S.* Typhimurium infections induce a B cell response that targets OmpC, D, and F, and OmpD is a crucial target of the antibodies induced by the *Salmonella* infection [269].

2.1.6. Project Description

Three recombinant pDNA vaccines have been designed and constructed with the above details in mind. These vaccines each use epitopes from five proteins found on or within *S. enterica* serovars Javiana and Typhimurium that are known to lead to MHC-I and/or MHC-II production. Stimulating both arms of the immune system, as typical *Salmonella* infections do, will allow for subsequent cellular and humoral responses to the vaccines, greatly increasing their chances of effectiveness against future infections [129]. This portion of the project details the designing of the epitope regions within the ORFs of the three vaccines.

2.2. Aims and Hypotheses

The first aim of this project was to identify *S.* Javiana epitopes with strong immunogenic potential as demonstrated through MHC affinity predictions. The hypothesis for aim one is that there will be at least one immunogenic epitope for each selected protein of interest from *S.* Javiana.

The second aim was to design pDNA ORFs with the aforementioned epitopes in a way that maintains each epitope's immunogenic potential after complete ORF design. The hypothesis for aim two is that there will be no difference in MHC binding predictions between each epitope within its origin protein versus within each ORF design.

The third aim was to determine if the ORF designs have any cross-protection potential as demonstrated through National Institutes of Health (NIH) Blastp Suite matches of each epitope. The hypothesis for aim three is that each epitope will match at least one *Salmonella* serotype in addition to *S.* Javiana.

2.3. Material and Methods

2.3.1. Selecting Target Proteins

Investigation into possible epitopes for the proposed vaccine began with the use of a fully sequenced *S.* Javiana bacteria (*Salmonella* enterica, 2016, GenBank CP004027.1) and an extensive literature review. Proteins that were from the fimbria and outer membrane were selected and investigated first, following the suggestions of previous research into nontyphoidal *Salmonella* vaccinations. Proteins from various other locations on and within *S.* Javiana, as well as proteins from other nontyphoidal *Salmonella* serotypes, were also investigated. The search produced the following proteins for further analysis: FimH, SopB, OmpA, OmpC, and OmpD.

2.3.2. Selecting Epitopes for the ORF

Amino acid sequences for each selected protein– FimH, SopB, OmpA, OmpC, and OmpD– were obtained from the National Center for Biotechnology Information (NCBI) (Table 2.2) [270]. All sequences were from *S.* Javiana strains except for the OmpD sequence. The OmpD sequence was obtained from a closely related serotype, *S.* Typhimurium, because a full OmpD sequence was not available for *S.* Javiana.

Table 2.2. Selected antigen accession numbers for *S.* Javiana pDNA-based vaccine design.

Antigen	**GenBank Accession Number**
FimH	AIH08113.1
SopB	EDZ05526.1
OmpA	OCZ83312.1
OmpC	OCZ79765.1
OmpD	NP_460531.1

The IEDB Analysis Resource [271] was used to identify immunogenic epitopes within the selected proteins' sequences previously mentioned. Protein sequences were analyzed using the T cell epitope prediction software for predictions of MHC-I binding and MHC-II binding. Predictions for MHC-I binding were produced for the six available mouse alleles (H-2-Db, H-2-Dd, H-2-Kb, H-2-Kd, H-2-Kk, H-2-Ld), and predictions for MHC-II binding were produced for the three available mouse H-2-1 alleles (H2-lAb, H2-lAd, H2-lEd). Mouse was the selected species for analysis, as this was the most relevant available species within the software at the time of design.

Peptide sequences with percentile rankings of under 5% were arbitrarily considered to have a high affinity and therefore be immunogenic. Portions of the peptide sequences that had high affinity rankings – 5% or lower – across the most alleles for both MHC-I and MHC-II were selected as the epitopes for these vaccines. MHC-II was prioritized in the event of no or little overlap between MHC-I and MHC-II predicted binding.

One epitope from each analyzed protein was selected and incorporated into the ORF design. Two FRS amino acid sequences, as outlined in Table 2.3, were inserted between each epitope sequence in alternation. FRS sequences were included to allow flanking epitopes to rotate and fold freely.

For two of the vaccines designed, a genetic adjuvant was also included in the ORF design. For each, an FRS was placed on the 3' end of the final *Salmonella* epitope while maintaining the alternating pattern of the FRS sequences. Then, the adjuvant sequence was placed on the 3' end of that FRS. The adjuvant selected for this vaccine was a bacterial SOD [272, 273]. The epitopes selected share some of an immunogenic region of SOD, but one epitope sequence was extended further than the other for hypothesized increased immunogenic potential.

Sequences for SOD are outlined in Table 2.3. "SOD extended" refers to the longer SOD epitope, and "SOD short" refers to the shorter SOD epitope.

Table 2.3. Amino acid sequences for the FRS 1, FRS 2, and both SODs.

Additional ORF Component	**Amino Acid Sequence**	**Source**
FRS 1	GPGGGPGGGPGG	[234]
FRS 2	GGGGSGGGGSGGGGS	[234]
SOD short	MAFELPALPYDYDALAPFMSRETLEYHHDKHHQAYVT	[272]
SOD extended	MAFELPALPYDYDALAPFMSRETLEYHHDKHHQAYVT NGNKLLEGSGLEGKSFEEIVKESFGKNQALFNNAGQHY NHIHFWKWMKKDGGGKKLPGKLEKAFDSDLGGYDKF RADDIAAGAGQFGSGWAWLSVKDGKLEISKTPNGENP LVHG	[234]

2.3.3. Codon Optimization of the ORF

Once the full vaccine was digitally constructed in SnapGene, the amino acid sequence was codon optimized via the IDT codon optimization tool [274]. All the codons were optimized for *Bos taurus*, as *Bos taurus* was the closest related species to equine available in the program at the time of design.

2.3.4. Immunogenicity Check

The final designs for each vaccine were analyzed in IEDB's T cell epitope prediction software for predictions of MHC-II binding. These analyses were performed exactly as they were for epitope selection and against the same alleles used for the epitope selection process.

2.3.5. Cross-Protection Potential

The amino acid sequences of the epitopes of the ORF were blasted in NIH Blastp Suite [275] against the entire available NIH database as of November 2022. Outputs were read for matches to any *Salmonella* serotypes other than *S.* Javiana.

2.4. Results and Discussion

Each investigated protein produced at least one epitope with high MHC-I and MHC-II binding potential, and one epitope for each investigated protein was selected for use within the ORF (Table 2.4). Therefore, aim 1 was achieved.

Table 2.4. Amino acid sequences of the selected epitopes for the vaccine ORFs.

Antigen	**Selected Epitope Amino Acid Sequence**
FimH	GNRPQGVTPQTKTIAIKCTNVAAQAYLSMRLEAEKASGQAMVSDNP
SopB	VLGKQDPVLTSMANQMELAKVKADRPATKQEEAAAKALKKNLIELI
OmpA	GLLSVGVSYRFGQQEAAPVVAPAPAPAPEVQTKHFT
OmpC	KVKVLSLLVPALLVAGAANAAEIYNKDGN
OmpD	KLKLVAVAVTSLLAAGVVNAAEVYNKDGN

Three vaccines were designed, all the same except for the presence and length of the SOD adjuvants added to the 3’ end of the vaccine (Figure 2.2). The S vaccine had no adjuvant, the SE vaccine had the SOD extended epitope, and the SS vaccine had the SOD short epitope. In the immunogenicity check, all the chosen epitopes maintained their MHC binding predictions within their vaccine designs from pre-epitope selection to full ORF design (Appendix C). This indicated that the codon optimization and arrangement of vaccine components did not affect the epitopes’ 3D structure and immunogenic potential. Therefore, aim 2 was achieved.

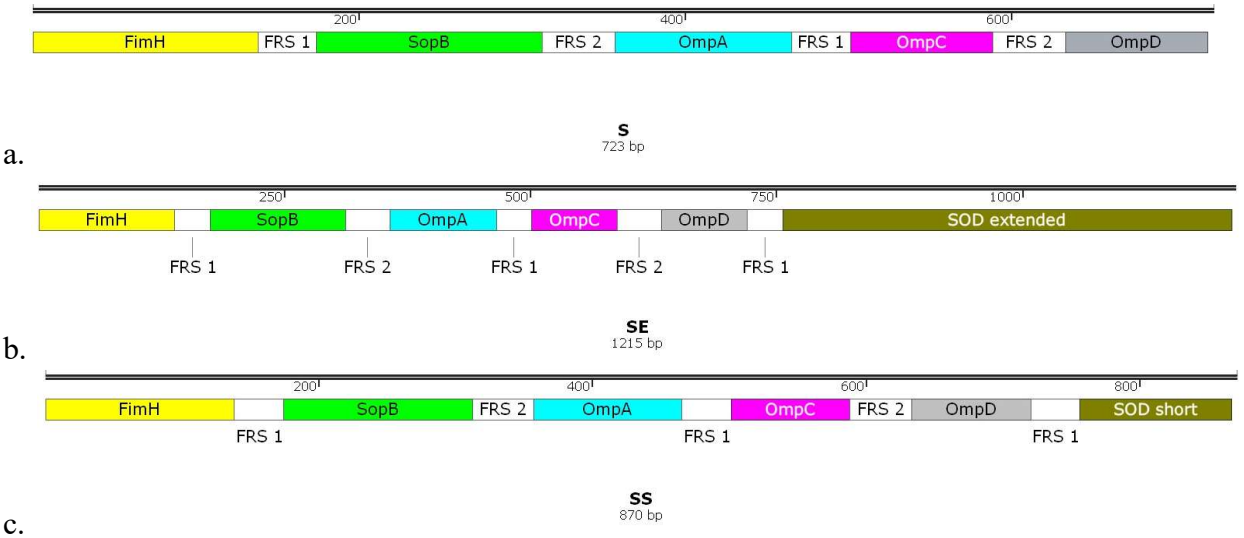

Figure 2.2. Epitope and FRS portions of the ORFs for each vaccine design. Top (a.) is the S vaccine with no adjuvant. Middle (b.) is the SE vaccine with the SOD extended adjuvant epitope. Bottom (c.) is the SS vaccine with the SOD short adjuvant epitope.

FimH, SopB, OmpA, OmpC, and OmpD all produced 100% matches to epitope regions on the same proteins within *S.* Heidelberg. FimH, SopB, OmpA, and OmpD all produced 100% matches to epitope regions on the same proteins within *Salmonella* Enterica, Infantis, Enteritidis, Kentucky, and Typhimurium. FimH, OmpA, and OmpD also all produced 100% matches to epitope regions on the same proteins within *S.* Dublin. Additionally, all epitope sequences produced a list of a total of 100 matches with 100% identity to a variety of *Salmonella* serotypes and other Enterobacteriaceae. Therefore, aim 3 was achieved, and it is hypothesized that the ORF designed in this project could produce protective immunity across a spectrum of *Salmonella* serotypes including, at a minimum, *S.* Heidelberg, Enterica, Infantis, Enteritidis, Kentucky, Typhimurium, and Dublin.

Chapter 3. Round One of Vaccine Designs and Testing

3.1. Introduction

3.1.1. Necessary pDNA Vaccine Components

Plasmids used for DNA vaccines have several functional requirements: protein production within the target host's APC cells, replication in *Escherichia coli* (*E. coli*) cells, and selection in prokaryotic and eukaryotic cells.

Protein production within target cells is the mechanism through which a plasmid functions as a vaccine, as described in Chapter 2 of this project. Plasmid DNA vaccines require several components for successful transcription and translation to occur. Sequences that specifically function in both transcription and translation – the promoter and polyadenylation codes for example – are typically selected from common viral organisms that are well-equipped for those tasks. Other important sequences include those involved in protein transport, like signal sequences, which may be derived from the known genetic sequences of naturally occurring proteins [276, 277].

Promoters are the locations within a DNA sequence, just upstream of a transcription start codon and ORF, where ribonucleic acid (RNA) polymerase binds for transcription initiation. Promoter sequences from cytomegalovirus (CMV) are known to lead to high recombinant protein yields. Additionally, CMV promoters outperform other popular promoters, such as E1A, Rouse sarcoma virus, and simian virus 40 (SV40), at driving long-term gene expression in multiple cell types and under multiple different transfection methodologies [278-282]. The CMV promoter is also consistent in providing a significant and broad immunity induction, in which it drives antigenic expression as well as DC-specific immune activities, making it an ideal candidate for vaccine expression [283, 284].

Polyadenylation is a necessary occurrence during transcription. The polyadenine (poly(A)) tail protects the mRNA from enzymatic degradation during cytoplasmic transport from the nucleus until translation takes place. Additionally, poly(A) aids in the translation process via the attachment of the poly(A) binding protein and subsequent bridging to the 5' cap via eIF4E and eIF4G to create a pseudo-circular structure. This structure aids in mRNA stability which further increases the probability of a successfully completed translation [285]. Four commonly used poly(A) signal sequence sources in nucleic acid vaccine research and mammalian expression plasmids are SV40, hGH, bGH, and rbGlob [286, 287]. SV40 poly(A) tails are among the more commonly used sequences for nucleic acid vaccine research specifically and are thought to be the more efficient sequences among those in popular use [286, 288, 289].

Once a protein is produced, transport of said protein to its desired location is vital for correct immune responses to occur. If the desired outcome of vaccination is antibody production, then transport of the protein outside of the cell may be necessary so that it can be processed as an exogenous protein. Any protein that does not successfully leave the cell would be processed as an endogenous protein, the consequences of which are previously described. Secretion signal sequences can be selected based on the intended host by identifying naturally occurring secreted proteins and those proteins' signal sequences. However, the highly secreted conalbumin, or ovotransferrin, protein's signal sequence (ConSS) has already been identified and used in previous vaccine research [272, 273, 290].

Before proteins are ever produced, the protein-encoding plasmids must first be produced in quantities sufficient for use. Replication and isolation of pDNA for manufacturing purposes begins in *E. coli*, and therefore, the backbone of the plasmid needs to be equipped for replication and selection within that host—i.e. it needs an origin of replication (ORI) and a selectable

marker [277]. Various ORIs have been investigated in existing research, with the preferred ORI being from pUC, a plasmid within the ColE1 family. Its selection is because of its lack of a *rop* gene, which is otherwise responsible for keeping copy numbers low in the replication process [291]. One issue with ORIs however is the possibility of gene transfer, specifically to other plasmid-containing organisms such as bacteria. This is of particular concern because of the issue of selection for recombinant plasmids and antibiotic resistance [292].

The most common selection marker used in pDNA-based therapies and vaccines is an antibiotic resistance marker—in the case of this project, it is against ampicillin [277, 286]. While useful in the selection of *E. coli* that only contain therapeutic plasmids, distribution of antibiotic resistance to other bacteria is already a rising issue. Removal of ORI and antibiotic resistance markers is considered a necessity for further progress within pDNA vaccine development, but if already achieved, methods for doing so have not been disclosed by those companies already commercially producing pDNA vaccines. Some methods of removing the antibiotic resistance portion of the plasmid in research involve incorporation of other genes allowing for *E. coli*'s survival in minimal medium. However, the ORI issue has been primarily tackled by the incorporation of a modified ORI sequence that only operates in specific species of bacteria, which is not considered sufficient for vaccine use [277]. Again, which methods are in current use in commercially available nucleic-acid vaccines is unclear, but the strategic inclusion of restriction enzyme (RE) sites are also often included for the easy removal of these additional components before transfection, which eliminates the possibility of antibiotic resistance development through horizontal gene transfer to other bacteria, and RE site incorporation is extremely achievable within the context of this project [203].

While not fully ready for vaccine use because of the presence of ORI and ampicillin resistance, pBluescript is a popular vector backbone that provides a good starting point for pDNA vaccine construction. There are a variety from which to select, but generally, pBluescript vectors are phagemids derived from pUC19, a plasmid found within *E. coli* [293]. They are great for production of plasmids in bacteria because they possess a bacterial ORI and because they have an ampicillin resistance gene for bacterial selection [294]. The pBluescript vectors are also popular, especially within recombinant plasmid research, because they contain a multiple cloning site with 21 to 26 unique RE sites [293-295]. This multiple cloning site allows for insertion of a variety of DNA sequences, including a custom ORF, which is ideal when discussing pDNA vaccine design [294].

3.1.2. Cell Culture: Transfection Methodologies and HEK293 Cells

Use of cell culture experimentation in pDNA vaccine testing allows the researcher to determine if two very necessary processes are taking place once the pDNA is inside the cell: transcription and translation. Transcription is the process through which a cell produces mRNA from DNA. Per the Central Dogma of Genetics, transcription is a necessary process on the road to protein production, otherwise referred to as translation [296]. Translation is necessary for a pDNA-based vaccine to be efficacious, as this is the mechanism through which the patient's immune system gets exposed to antigens and develops protective measures for future exposures.

Human embryonic kidney 293 (HEK293) cells are a commonly used heterologous expression system for recombinant protein production. This is largely because of their ability to efficiently take up plasmid DNA through transfection and their reliable translation and protein processing capabilities [297]. This cell line was selected because of its ease of use when compared to other commonly used cell lines and availability at the time of the experiment [298].

Transfection is the deliberate introduction of nucleic acids into eukaryotic cells and is the process through which HEK293 cells take up pDNA for subsequent protein expression. There are two (2) different types of transfections: stable and transient. Stable transfections are used for long-term expression through integration of the DNA into the genome, and it ensures passage to progeny over several generations [299]. Alternatively, transient transfection does not integrate the DNA into the genome and therefore, DNA is not typically passed on to progeny cells and the protein production eventually ceases. The main benefit of a transient transfection over a stable transfection is that it takes less time for experimentation and transient transfection is the goal in a vaccination [300].

Transfections can be further characterized as either viral or non-viral depending on the delivery vehicle used. While viral-based transfections are often used for stable transfections of cells, they can lead to immune responses *in vivo* that may inhibit the transfection process or lead to high levels of cytotoxicity *in vitro*. Non-viral transfections on the other hand can be used for stable or transient transfections and typically do not result in high levels of cytotoxicity or immediate immune response [301].

There are several different non-viral transfection reagents commercially available. Physical, or mechanical, transfections include sonoporation, magnetofection, electroporation, gene microinjection, and laser irradiation. All these transfection methods involve disruption or penetration of the cell membrane to aid in nucleic acid uptake. While shown to be effective for the transfection process, this membrane disruption can lead to cellular death, preventing the transcription-translation process from occurring. Chemical transfections, another type of non-viral transfection, use either liposomal- or non-liposomal-based reagents to aid in membrane passage. The liposomal-based and some non-liposomal-based reagents aid in cellular entry

through the positive charges of the aggregated lipids. This positive charge allows for attraction to and movement through the phospholipid bilayer of the host cell. Non-liposomal-based reagents include calcium phosphate, polymers, dendrimers, non-liposomal lipids, and nanoparticles, of which the most efficacious of these reagents include the latter two [301].

Lipofectamine3000 (ThermoFisher) is a lipid nanoparticle (LNP) transfection reagent with proven efficacy in various cell types, including HEK293 [302]. The positive charge on the head group of the lipid interacts with the negatively charged phosphate backbone of the nucleic acid, causing the DNA to condensate for enhanced encapsulation. Additionally, this transfection reagent includes a helper lipid that is positively charged when in water but is otherwise neutral. This shifting charge aids in fusion between the LNP and the cell membrane, ultimately leading to endocytosis of the LNP and encapsulated DNA [303]. Lysosome-endosome fusion, which occurs shortly after endocytosis, leads to a decrease in pH within the endosome, now called an endolysosome. This pH decrease causes the LNPs to become more positively charged, increasing the LNP's interaction with the negatively charged membrane of the endosome. Once the LNP crosses the membrane to the cytoplasmic side, the neutral pH leads to the dissociation of the LNP and release of the DNA into the cytoplasm [304, 305]. Once in the cytoplasm, the DNA can make its way to the nucleus [306].

Nuclear uptake is required for DNA transcription to take place. In the case of LNP use, the way to ensure nuclear uptake is having the cells actively undergoing mitosis during the transfection. Mitosis leads to a temporary break-down of the nuclear envelope, providing an opportunity for the DNA to become passively encapsulated in said envelope. One easy way to ensure mitosis is taking place is to leave room for additional growth within a flask when transfection is performed [306].

Often, once the transfection process is complete, a selection process is used to isolate the successfully transfected cells. While more commonly used for stable transfections, selection can also be used in transient transfections to eliminate the non-transfected cells and to induce plasmid maintenance by the host cells despite a lack of genome incorporation [234]. Selection is achieved, within the context of this experiment, through introduction of an antibiotic-resistance marker within the DNA used for transfection and subsequent exposure of cells to said antibiotic. For mammalian cells, puromycin is a popular choice of antibiotic, as it is a translation inhibitor for these cell types. Additionally, it kills non-transfected cells quickly at low concentrations compared to other applicable antibiotics [299, 300].

3.1.3. Assays for mRNA, Proteins, and Antibodies

Once transfection and selection are complete in cell culture, transcription and translation need to be confirmed. To verify that mRNA is produced from the introduced pDNA, reverse transcription polymerase chain reactions (RT-PCRs) can be performed. To verify that protein is produced, there are a variety of available assays, but only Indirect ELISAs were applicable given the available resources at the time of this experiment, as will be explained.

RT-PCRs use reverse transcriptases and sequence-specific primers to amplify the DNA of interest from an mRNA sequence, evidencing transcription [307]. Reverse transcriptases are enzymes found within many living organisms that create complementary DNA (cDNA) sequences from mRNA sequences. The PCR then amplifies that cDNA so that detection is more probable [296, 308]. A positive RT-PCR means that transcription has taken place, but it does not indicate if protein was produced.

Two common methods of detecting and quantifying proteins are Western blots and enzyme-linked immunosorbent assays (ELISA). The two function similarly, in that they both use

protein-specific antibodies and antibody tagging [309, 310]. However, Western Blots are limited to detection of denatured proteins, as denaturation is among the early steps in the protein preparation process. ELISAs on the other hand can be used to detect proteins in their native conformations because ELISAs lack steps that would denature the proteins of interest [311]. In the case of this project, ELISA was the chosen assay to move forward with for three reasons: 1) there were no commercially available tagged antibodies for *S.* Javiana or this vaccine; 2) available antibodies for detection and positive control are from an infected horse, meaning that they would likely be specific to native proteins; and 3) the antibodies resulting from vaccination need to be specific to native proteins for protection from infection.

There are three main types of ELISAs: Direct, Sandwich, and Indirect (Figure 3.1). All three versions use a labeled antibody that, when activated by a substrate, allows for quantitation via a colorimetric, chemiluminescence, or fluorescence plate reader [310]. This label is typically horseradish peroxidase (HRP) [312]. Antibodies that directly bind a protein or antigen are referred to as "primary" antibodies and those that bind other antibodies are referred to as "secondary" antibodies. In Direct ELISAs, there is only a primary antibody, and it is labeled. The protein or antigen of interest on a Direct ELISA is bound to an ELISA plate. In Sandwich ELISAs, the protein/antigen is captured between two primary antibodies, and a secondary labeled antibody binds one of the two antigen-bound antibodies. Sandwich ELISA requires two separate primary antibodies that recognize two different epitopes of the antigen, and one of those primary antibodies must be bound to the plate. In Indirect ELISAs, the protein or antigen is bound to the plate and then bound by an unlabeled primary antibody. The primary antibody is then bound by a labeled secondary antibody (Figure 3.1) [310]. Indirect ELISAs were chosen for this project over the other two types of ELISAs for one major reason: no known antibodies

specific to *S.* Javiana epitopes exist. In the case of a Direct ELISA, a labeled antibody specific to *S.* Javiana is required, and in the case of a Sandwich ELISA, two antibodies specific to two different *S.* Javiana epitopes are required. For the indirect ELISA, the primary antibody does not need to be labeled, so commercial availability and/or customized antibody labeling are not needed. Additionally, the labeled secondary just needs to recognize the primary antibody, which was feasible for this project.

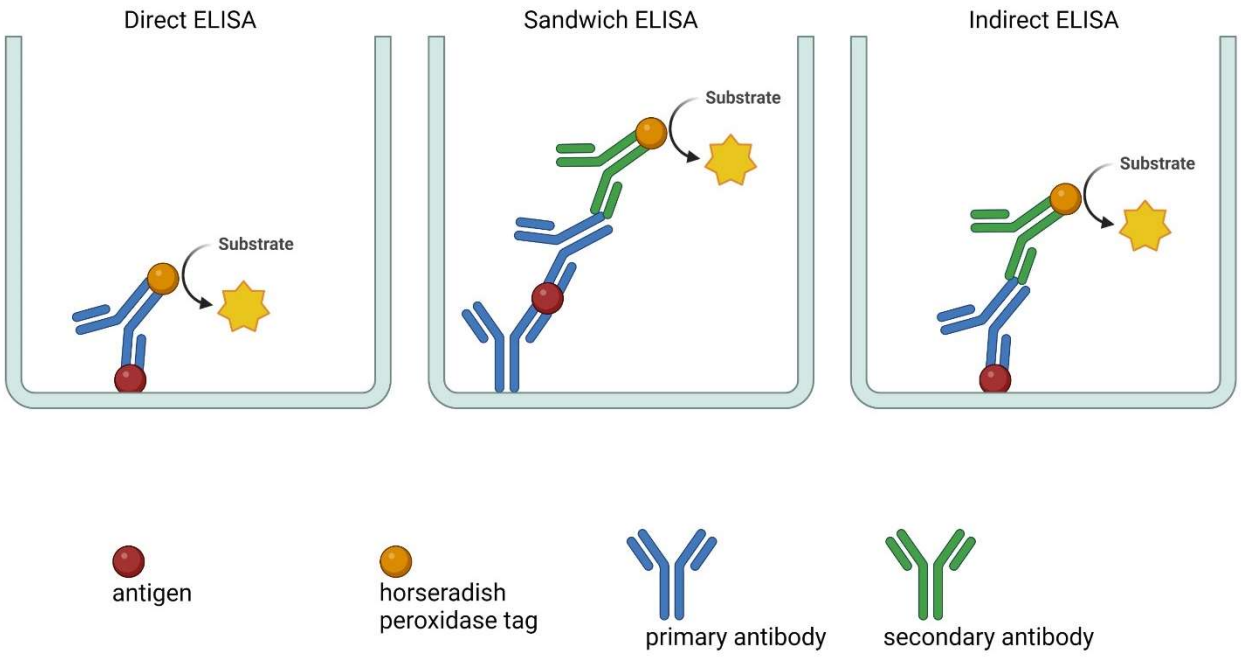

Figure 3.1. Visual explanation of the three types of ELISAs discussed: direct ELISA, sandwich ELISA, and indirect ELISA. Created with BioRender.com (Appendix D).

Secondary antibodies are created by exposing a host to an antibody from another species. As an example, anti-horse antibodies can be created by injecting purified horse antibodies into virtually any animal that is not a horse. The generated antibodies are then purified for use via affinity binding and cross-absorption [312]. The isolated antibodies from this process have a V region that now recognizes some portion of the antibodies originally injected. For example, if a

goat was injected with horse antibodies, the secondary antibody would be goat anti-horse, and the goat antibody's V region would bind and recognize horse antibodies on an ELISA. Different types of secondaries bind different regions of the target antibody, with universal secondaries being the broadest category which binds heavy and light chains in all formats and classes [313].

The goat anti-horse antibody chosen for this project is an IgG polyclonal, or universal, antibody that recognizes equine IgM and is labeled with HRP [314]. IgM is the antibody initially produced by the horse when a foreign body is introduced, and IgM lasts approximately 2 to 5 months following infection [315-317].

3.1.4. Protein Extraction, CelLytic™ B Plus

To perform ELISAs, the protein of choice needs to be acquired. The CelLytic™ B Plus Kit is a bacterial lysis and protein extraction kit from Sigma Aldrich. It involves the use of a proprietary zwitterionic detergent mixture, called CelLytic™ B, along with egg-isolated lysozyme, a protease inhibitor cocktail, and Benzonase® Nuclease [318, 319].

Given the proprietary nature of the CelLytic™ B, there is very little information on the exact functionality of the reagent. However, zwitterions are molecules that are dipolar, with a positively charged end and a negatively charged end [320, 321]. Some examples of zwitterionic detergents include 3-[(3-cholamidopropyl)dimethylammonio]-1-propanesulfonate (CHAPS) and 3-[(3-cholamidopropyl)dimethylammonio]-2-hydroxy-1-propanesulfonate (CHAPSO), which are both regarded as mild lysis agents that are good for protein extraction. They are surfactants that can disrupt the hydrophobic-hydrophilic interactions of the cell membrane, disintegrating or solubilizing them without denaturing the proteins within [322].

S. Javiana is a gram-negative bacterium, which falls within the described capabilities of the CelLytic™ B Plus Kit. Because the kit claims the ability to lyse gram-negative bacteria, that

means that it must be able to not only lyse a singular membrane, but also a cell wall and an additional outer membrane. Therefore, it is likely that the CelLytic™ B reagent contains ethylenediaminetetraacetic acid (EDTA) or another similar reagent in addition to the zwitterionic detergents. EDTA disrupts the outer membrane of gram-negative bacteria through chelation of the metal ions [323]. More specifically, EDTA removes Mg2+ and Ca2+ ions from the cell wall, both of which otherwise stabilize the LPS and lipoproteins that are part of the composition of the outer membrane [324, 325]. Once the outer membrane is gone, lysozymes are typically used to break down the cell wall [322]. Lysozymes, commonly found in egg whites, are enzymes that hydrolyze linkages in peptidoglycan, a molecule that comprises approximately 90% of the cell wall [323, 326].

Once the cell is fully lysed, proteases are free to begin protein digestion through the hydrolysis of peptide bonds [327]. In a process where the isolation of whole proteins is desired, protease inhibitors are therefore necessary. In obtaining a pure whole protein sample, the removal of nucleic acids is also necessary. The Benzonase® Nuclease is a synthetic and nonspecific endonuclease derived from *Serratia marcescens*, which digests all forms of RNA and DNA, including single- and double- stranded as well as linear and circular structures [328, 329]. Endonucleases work by cleaving the phosphodiester bonds within a nucleotide sequence, thereby separating the nucleotides and dismantling the DNA or RNA strands [330].

3.1.5. Endotoxins, Their Assays, and Their Extraction Methods

LPS is part of the outer membrane structure of gram-negative bacteria, as explained previously. The anchoring portion of LPS that connects it to the bacteria is referred to as Lipid A, also known as “endotoxin”, and it resides within the cell wall [331, 332]. Release of endotoxins occurs when the bacteria die and lyse, which is an ongoing occurrence upon infection

[332, 333]. Therefore, antibodies to endotoxins are common in natural infections, such as the one incurred by the origin horses of the primary antibodies used in this project [334].

Endotoxins are microbial pyrogens that lead to inflammatory responses within a host, which aids in bacterial clearance, but when endotoxin levels are high enough, septic shock and death can occur [332, 333]. So, there are regulations for the amounts allowable in products that would be exposed to immune systems. The Food and Drug Administration (FDA) allows up to 0.5 endotoxin units (EU) per millimeter for medical devices and inhalables [333, 335]. However, all injectables cannot have more than 0.25 EU/mL in a full dose [333].

The Limulus Amebocyte Lysate (LAL) Test is recognized as an acceptable test for measuring endotoxin levels in drugs and medical device products [333]. The chromogenic method of analyzing the LAL Test utilizes a chromogenic substrate that is released from p-nitroaniline when there is endotoxin contact. The release from p-nitroaniline is directly proportional to the amount of endotoxin within the sample, and the reaction can be measured via visual inspection of the color change or more precisely via a spectrophotometer [336]. The kit used within this project for endotoxin detection – LAL ToxinSensor^{TM} Endotoxin Detection System – is a chromogenic LAL test.

There are several protein and LPS extraction protocols in existence for bacteria, including hot phenol extraction (HPE), ultrafiltration, size-exclusion filters, two-phase micellar systems, and affinity resin spin column kits [337-339]. Each has their own set of benefits and drawbacks, depending on the goal of their use.

HPE is considered a gold standard for LPS extraction, but it is typically used for harvesting LPS, not for harvesting proteins. It also does not guarantee removal of other impurities from the protein portion of the solution, like DNA and RNA [337]. Ultrafiltration is

considered effective at removing LPS from water samples, but it is ineffective for removing LPS from proteins. Ultrafiltration is damaging to proteins because of the physical forces involved in the process, therefore limiting the ability to obtain proteins in their native conformations [339]. Size-exclusion filters are useful if the exact size of the protein of interest is known and chemical properties of the LPS within a sample. However, size-exclusion filters are not considered effective for LPS removal from "large" proteins, and some forms of LPS can aggregate, making them more difficult to filter out based on size alone [338, 339].

Two-phase micellar systems and affinity resin spin columns are the preferred methods of endotoxin removal from protein samples, primarily because they involve mild conditions that won't denature the protein product [340]. Triton X-114 is an example of a popular two-phase micellar system, in which Triton X-114 causes endotoxins to separate from proteins while in a homogenous solution [339, 341]. The solution then dissociates upon centrifugation into a detergent phase that contains the endotoxins and an aqueous phase that contains the proteins. The disadvantage to this process is that it is difficult to consistently retrieve the aqueous phase without disturbing/reintegrating the detergent phase [341]. Affinity resin spin columns, such as the one being used in this project, help eliminate this potential for procedural error. The kit used in this project is the Abcam Endotoxin Removal Kit (Rapid) (ab239707), and it uses immobilized polymyxin B (PMB) in a resin spin column for endotoxin removal [342]. The PMB binds to lipid A via hydrophobic forces and ionic forces [343, 344]. The protein sample in solution can pass through the filter, leaving behind the endotoxins within the resin. PMB filters are fast-acting compared to several of the other endotoxin removal methods, such as HPE, and they have high protein yields [342].

3.1.6. *Salmonella* in Poultry

Backyard poultry have been linked to *Salmonella* outbreaks in the United States every year since 2012, and poultry are among the largest reservoirs for *Salmonella,* especially for infections in humans [60, 77, 78, 345]. The most recent available data set for backyard poultry-linked outbreaks in the United States was in November of 2022 and encompassed 49 states, Washington D. C., and the United States territory of Puerto Rico, which cumulatively led to 1,230 illnesses, 225 hospitalizations, and 2 deaths [346]. All serotypes involved were non-typhoidal [347]. When looking at the industry level rather than domestic, eggs and poultry products were attributed to over 80% of non-typhoidal *Salmonella* infections between 1998 and 2008, the most recent available data set. *S.* Javiana specifically was linked to 10% of the overall outbreaks for those years, and 10% of those *S.* Javiana outbreaks were linked to chicken [348]. *S.* Javiana is among the 10 most common serotypes found in commercial chicken as well as turkey and ducks worldwide [71].

Most infected poultry are asymptomatic, and the exact reasons for this are unknown. *Salmonellae* are not part of the normal gut flora, but they easily colonize the upper intestines, cecum, gizzard, and proventriculus in young chicks. Infection can persist for the duration of rearing, during which time shedding can occur and infections can spread [349]. While symptoms and bird loss are not a concern in the event of contagion, contamination of poultry products is of significant public health and economic concern [76].

Various methods of controlling and preventing avian salmonellosis have been investigated including dietary antibiotics, organic alternatives, and vaccines. Antibiotics are not generally recommended for use due to the rising antimicrobial resistance occurring in bacteria, so organic alternatives to classic antimicrobials are being investigated. Organic alternatives

include probiotics, prebiotics, symbiotics, organic acids, nanotechnologies, essential oils, and chitosan. All the organic options have either shown a decrease in *Salmonella* colonization in poultry or anti-*Salmonella* effects *in vitro*, but none have been shown to completely eliminate infection or shedding or prevent colonization from taking place within a bird. Vaccines have had varied results, with the most efficacious, safe, and cost-effective option currently being subunit vaccines, the pitfalls of which are discussed in Chapter 1 [76].

3.1.7. Quail as a model organism

Quail, particularly *Coturnix japonica*, are a common model organism for research in endocrinology, reproductive biology, behavioral genetics, transgenic animal production, and immunology [350-352]. Their use as a model organism dates back to 1959, and they have many publications noting their practicality as compared to other animals [350]. Quail make good research models because they are small, inexpensive, easy to raise, and quickly maturing [353]. Their idealities for general research combined with the prevalence of *S.* Javiana in poultry make quail a good choice for *in vivo* testing of the vaccines within this project.

3.1.8. Avian Immune Systems and Their Vaccination Strategies

Birds have innate and adaptive immune systems which consist of cellular- and humoral-mediated immunity, much like that described in Chapter 2 of this project [354]. Complete elimination of *Salmonella* from an avian system requires dual efforts of the cell- and humoral-mediated immune responses, much like previously described in mammals [349].

An important cell involved in the cell-mediated elimination of *Salmonella* infection is the avian heterophil. Avian heterophils are considered first responders in an avian *Salmonella* infection and the avian counterpart to mammalian neutrophils. Much like the mammalian neutrophil, avian heterophils are well-equipped for handling *Salmonella* infections, employing

similar elimination strategies as previously described [355]. However, also like in mammalian species, *Salmonella* can survive within macrophages for systemic transport. Therefore, antibodies also need to be involved in *Salmonella* elimination [356].

IgY is the main antibody found in avian species. It consists of two heavy and two light chains, and each chain has constant and variable regions, forming a monomeric structure, as seen in Figure 2.1 [357, 358]. The constant region is responsible for the effector functions of the antibody, activating complement and opsonization, and the variable regions are responsible for antigen recognition [357, 359]. IgY is similar to IgG in humans in that they are the predominant humoral antibody and pass from mother to offspring, and therefore, they can be purified from the eggs or from the serum [359, 360].

If not given *in ovo*, poultry vaccines are traditionally given the day of hatch or two to four weeks old for the first injection [361-363]. The vaccination timeline is to account for the presence of maternal antibodies still present within the birds interfering with vaccination. Two weeks is the standard for backyard poultry, specifically chicken, but quail reach maturity in about a third the time of a chicken and therefore get vaccinated earlier [362, 364, 365]. It is important to note, however, that DNA vaccine research in a variety of animals points to their ability to drive immunity even with maternal antibodies present [191].

The investigation into pDNA efficacy as an *in ovo* vaccine has been proposed and begun, but evidence is still needed for its efficacy [366, 367]. One major issue in investigating *in ovo* vaccinations is access to equipment for these injections, and therefore, may not be realistic for researchers depending on resources available. In delivery method comparison studies for pDNA vaccines in poultry that were not *in ovo*, intramuscular (IM) vaccinations outperformed all other investigated delivery methods – intravenous, intraperitoneal, subcutaneous, intratracheal,

intrabursal, and intraorbital – with higher antibody titers and reduced signs of illness [366, 368]. Intramuscular injections work by rapid absorption of the vaccine into the bloodstream and quick delivery to nearby lymph nodes with a plethora of naïve T and B cells for activation [369].

Some post-hatch vaccinations have the capability to produce protective levels of antibodies for over 12 weeks without a booster [370]. Poultry slaughter, when talking about chicken and turkey, is typically at 6 weeks to 1.5 years of age, with times being dependent on species and meat status preferences [370-372]. Knowing that quail reach maturity two to three times faster than chickens, 6 weeks of *S.* Javiana-specific antibody response without a booster should be the goal of this project [353].

3.1.9. Superfect

The chosen transfection reagent for quail delivery in this project is Superfect. Superfect is an activated polyamidoamine (PAMAM) dendrimer transfection reagent from QIAGEN [373]. PAMAM dendrimers are synthetic, spherical molecules with branches comprised of PAMAM backbones and terminal amine groups radiating from the center. Simultaneous heat and water or butanol solvent treatment trims some of the branches away, increasing the molecule's flexibility [374]. The size and shape of the molecule do not change during the activation process, but the more flexible structure increases transfection efficiency [374, 375]. The reason increased flexibility increases transfection efficiency is because the remaining PAMAM branches can more freely move to bind and release the DNA [376].

Activated PAMAM dendrimers are nonviral transfection vectors, much like LNPs, such as Lipofectamine3000 [373, 374]. In fact, the two reagents have a strikingly similar alternating charge system that allows its uptake into cells and nucleic-acid release from the endolysosome, as previously described [373]. The key difference between Lipofectamine3000 and Superfect

however is that Superfect has been used in *in vivo* studies [234, 377]. Activated PAMAM dendrimers, like Superfect, have low *in vivo* cytotoxicity [374]. Additionally, there is some evidence that antibody development against Superfect does not occur which allows for repeated delivery, such as a booster vaccination, if ever needed [234].

3.1.10. Project Description

This portion of the project will illustrate the process of constructing three full-plasmid vaccines that incorporate the designs described in Chapter 2 of this project. The full plasmids will include the culmination of the complete ORFs, the transcription components, and the translation components. The testing of these three vaccines, *in vitro* and *in vivo*, will also be covered in this chapter. This testing process will involve the development of an *S.* Javiana protein isolation and endotoxin removal protocol as well as an indirect ELISA protocol for protein and antibody detection.

3.2. Aims and Hypotheses

3.2.1. pCP Vaccines Construction

The aim of this portion of this project is to construct three plasmids containing the epitope designs from Chapter 2 of this project, a promoter, a poly(A) signal, antibiotic resistance markers for *E. coli* and mammalian cell selection, and an ORI for *E. coli* replication. The hypothesis is that all three vaccines will be completed, as evidenced by electrophoresis size verification and sequencing with 100% match of each vaccine plasmid to the theoretical design.

3.2.2. Establishing an ELISA Protocol

The first aim of this portion of this project is to determine a protein preparation protocol that will produce an endotoxin reading below 0.25 EU/mL. Hypothesis for aim one is that at least

one of the protein isolation protocols will produce proteins with endotoxin readings less than 0.25 EU/mL (H_0:μ=0.25; H_1:μ<0.25).

The second aim of this portion of this project is to determine how much endotoxin is leached into protein samples from each potential ELISA plate for use. The hypothesis for aim two of this project is that at least one of the two ELISA plates will produce endotoxin readings less than 0.25 EU/mL (H_0:μ=0.25; H_1:μ<0.25).

The third aim of this project is to determine if proteins with the lowest EU/mL readings are detectable by the provided primary and secondary antibodies via an indirect ELISA. Hypothesis for aim three is that the proteins tested on the ELISA will produce absorbance readings higher than zero (H_0: μ=0; H_1: μ>0).

3.2.3. *In Vivo* Testing of pCP Vaccines

Aim one of this part of this project is to determine if and which of the pCP versions of the vaccines would lead to *S.* Javiana-specific antibody production, as evidenced by indirect ELISA data. The hypothesis for aim one was that all three vaccines would lead to *S.* Javiana-specific antibodies in concentrations detectable on an indirect ELISA, and that there would be a difference in antibody concentrations between at least two experimental groups (H_0:μ_{C1} =μ_{C2} = μ_S = μ_{SS} = μ_{SE}; H_1: Not H_0).

Aim two was to establish a titer timeline for each vaccine, as evidenced by indirect ELISA data. The hypothesis for aim two was that those vaccines that produced detectable *S.* Javiana antibodies would have a difference in antibody concentrations between at least 2 bleeds (H_0:μ_{1bleed} = μ_{2bleed} = μ_{3bleed} = μ_{4bleed} = μ_{5bleed}; H_1: Not H_0).

Aim three is to determine safety of the vaccines, which will be evidenced by deaths following vaccination. Hypothesis for aim three was that there would be no difference in survival

between the control and vaccine groups at any time following vaccination (H_0:$S_{C1t} = S_{C2t} = S_{St} = S_{SSt} = S_{SEt}$; H_1: $S_{C1t} \neq S_{C2t} \neq S_{St} \neq S_{St} \neq S_{SEt}$).

3.2.4. *In Vitro* Testing of pCP Vaccines

The first aim of this portion of this project was to establish which, if any, of the vaccines will be transcribed. The hypothesis for aim one was that all three vaccines will be transcribed, as evidenced by RT-PCR on electrophoresis gel images.

The second aim was to determine which, if any, of the vaccines will be translated upon transfection. The hypothesis for aim two was that all three vaccines will be translated at detectable concentrations– i.e. cell lysates from vaccine-transfected HEK293 cells will produce positive indirect ELISA results when exposed to convalescent horse serum (H_0: θ_c & $\theta_t \leq 0$; H_1: $\theta_c \leq 0$, $\theta_t > 0$).

The third aim was to determine if the translated proteins are being secreted. The hypothesis for aim three was that all three vaccines, upon translation, will lead to secretion of their encoded proteins at detectable concentrations – i.e. spent media from vaccine-transfected HEK293 cells will produce positive indirect ELISA results when exposed to convalescent horse serum (H_0: θ_c & $\theta_t \leq 0$; H_1: $\theta_c \leq 0$, $\theta_t > 0$).

"Positive" results on indirect ELISAs will be indicated by absorbance data that is high enough to be interpolated to the standard curve of the ELISA or too high to be interpolated to the standard curve of the ELISA. "Negative" results will be indicated by absorbance data that is too small to be interpolated to the standard curve of the ELISA.

The fourth aim pertains to aims two and three. Aim four is to determine what range of protein concentrations with the antibody parameters determined in section two of this chapter will produce a positive linear trend (i.e., the standard curve). The hypothesis for aim four is that

proteins serially diluted somewhere between 60ng/μL and 0ng/μL will produce a positive correlation coefficient that is significantly different from zero on an indirect ELISA (H_0: $\rho=0$; H_1: $\rho > 0$).

3.3. Materials and Methods

3.3.1. pCP Vaccines Construction

ConSS (Genbank X02009.1 base pairs 74-133) and the SV40 poly(A) signal sequence [234] were incorporated into the 5' and 3' ends, respectively, of the epitope designs from part one of this chapter. RE sites for SalI and PacI on the 5' and 3' ends respectively were also incorporated into the final ORF designs with the ConSS and poly(A) for directional cloning into the necessary vector backbones. The vaccine sequences at this point were constructed by IDT in plasmid form. The S vaccine became pS, the SE vaccine became pSE, and the SS vaccine became pSS.

Puromycin resistance gene (1408 bp) was retrieved from BV5025 [234] via a restriction digest with XhoI (ThermoFisher Scientific Inc., Cat. FD0694) and EcoRV (ThermoFisher Scientific Inc., Cat. ER0301) following the manufacturer protocol for ThermoFisher Fast Digestion (Appendix A). The 1408 bp band was excised via a 1% agarose SYBR Safe gel (Invitrogen, CA, Cat S33102) and purified via Zymoclean Gel DNA Recovery kit following the manufacturer protocol (Zymo Research Orange, CA, USA, Cat D4002; Appendix A). Then, pBluescript SXD, kindly provided by Thaya Stoufflet at Gene Probes and Expressions Laboratory, was digested with XhoI and EcoRV (ThermoFisher Scientifics Inc., Cat. FD0304) and then purified via a Zymo DNA Clean & Concentrator®-5 (Zymo Research, Cat D4014) following the manufacturer protocol (Appendix A). The purified pBluescript SXD digest and purified puromycin resistance gene were ligated together via a Quick Ligation Kit (New England

Biolabs, Cat M2200) following manufacturer instructions (Appendix A) to form the pP vector. The pP was used to transform dam-/dcm- competent *E. coli* cells (New England Biolabs, Cat C2925) following manufacturer instructions (Appendix A), and pP was purified in larger quantities via ZymoPURE™ II Plasmid Midiprep kit (Zymo Research, Cat D4200) following manufacturer instructions (Appendix A).

CMV was purchased from IDT within their pUCIDT(Amp) vector with a 5' AsiSI restriction site and 3' EheI restriction site along with SalI and PacI sites downstream of the CMV promoter with SalI being upstream of PacI. The CMV IDT vector and pP were both digested with AsiSI (Thermo Fisher Scientific, Cat ER2091) and EheI (Thermofisher Scientific, Cat FD0443) and ligated together via the New England Biolabs (NEB) Quick Ligation kit to form pCP. The pCP was used to transform dam-/dcm- competent *E. coli* cells (New England Biolabs, Cat C2925), and the DNA was purified in larger quantities for future use via ZymoPURE™ II Plasmid Midiprep kit. An ethidium bromide 1% agarose gel was used to confirm the size of pCP.

The pCP and each ORF were digested with SalI (Thermo Fisher Scientific, Massachusetts, USA, catalog no. ER0642) and PacI (Invitrogen, Cat FD2204) and were ligated together via the NEB Quick Ligation Kit. Each vaccine, now within pCP, was used to transform dam-/dcm- competent *E. coli* cells from NEB, and the plasmids were harvested and purified via ZymoPURE™ II Plasmid Midiprep kit. Vectors were tested for size via electrophoresis on an ethidium bromide 1% agarose gel. The ORF-specific primers were used to perform a PCR to verify that each ORF was successfully ligated with pCP. The pSCP ORF primers were SJ1 F and SJ1 R, pSSCP primers were SJ1S F and SJ1S R, and pSECP primers were SJ1E F and SJ1E R (Table 3.1). PCRs were conducted using the AccuPrime™ *Pfx* DNA Polymerase kit and

followed manufacturer protocols with annealing temperatures listed in Table 3.1 (ThermoFisher Scientific, Cat 12344024; Appendix A). Extension times were 43 seconds for pSCP, 52 seconds for pSSCP, and 73 seconds for pSECP. The PCRs were analyzed via an ethidium bromide 1% agarose gel.

Table 3.1. ORF primers and parameters for PCR verification of the ORF within each harvested plasmid.

Primer Name	**Vector Sequenced**	**Primer Sequence**	**Melting Temperature**	**Annealing Temperature**	**Expected Product Size**
SJ1 F	pSCP	5'- TCG GTC GAC AAC ATG AAG TGG G -3'	59.4℃	55.0℃	720bp
SJ1 R	pSCP	5'- TTA ATT CCC GTC CTT GTT GTA CAC C -3'	57.1℃		
SJ1 Short F	pSSCP	5'- GGT CGA CAA CAT GAA GCT CA -3'	55.1℃	51.5℃	867bp
SJ1 Short R	pSSCP	5'- TTA GGT AAC ATA TGC TTG GTG ATG T -3'	54.2℃		
SJ1 Ext F	pSECP	5'- GGT CGA CAA CAT GAA GCT CA -3'	55.1℃	53.0℃	1212bp
SJ1 Ext R	pSECP	5'- TTA CCC GTG AAC CAA CGG AT -3'	56.6℃		

Once the size and PCR evidence was obtained, each vector was sequence verified with primers listed in Table 3.2. The ORFs for each vaccine were also sequenced with primers specific to that ORF, as listed previously for the ORF PCRs (Table 3.1). All sequencing for this project was ABI 3130 Sanger Sequencing performed by the Gene Probes and Expression Systems Laboratory/LSU BioMMED (GeneLab).

Table 3.2. Amino acid sequences of the selected epitopes for the vaccine ORFs.

Primer Name	**Primer Sequence**	**Melting Temperature**
Excised puro REV	5'-TCT GAG GCG GAA AGA ACC AG-3'	57.0°C
Excised puro FWD	5'-AGG GCG CGC CTC AGC-3'	62.7°C
AE Reverse	5'- AAG TTG GCC GCA GTG TTA TC-3'	58.0°C
SXD Nae F	5'- GTT TTT CGG AAA GAT AGT CAC GAC GTT GTA AAA CG-3'	63.0°C
DS Forward	5'- CCG TAT TGA CGC CGG GCA-3'	61.0°C
SK Forward 2	5'- ACT TTA GAT TGA TTA AAA C-3'	44.0°C
SK Forward1	5'- TTT ATA GTC CTG TCG GGT TT-3'	53.0°C
CMV F1	5'- CCG GCA TCA GAT TGG CTA TTG GCC A-3'	65.0°C
SXD Nae R	5'- TAT AAT TTT CTT GAA AGG GAA AAC CCT GGC GTT A-3'	60.0°C
Korle Forward 1	5'- TCC GCC CCA TTG ACG CAA AT-3'	63.0°C
CMV R1	5'- CGA GAC GGT GAC TGC AGA AAA GAC CCA TGG-3'	67.0°C
Binx Forward 1	5'- GAG GTA ACT CCC GTT GCG GT -3'	61.0°C
Georgia Reverse 1	5'- CTC TGT CGA TAC CCC-3'	49.0°C
Ippo Reverse 1	5'- AGC TGG TGC AGT GTT TGC TG-3'	61.0°C

3.3.2. Establishing an ELISA Protocol

3.3.2.1. Protein Harvest and Endotoxin Removal

All *Salmonella* samples used in this project were *S.* Javiana isolate 430 that was isolated from two infected thoroughbreds from the LSU Veterinary School. This *S.* Javiana was cultured in 5mL Bacto Brain Heart Infusion (BHI) broth (BD, ref 237500) in a New Brunswick Scientific Excella E25 shaker incubator at 100 rpm for 24 hours at 37°C. CelLytic™ B Plus kit from

Sigma-Aldrich (Cat CB0050) was used for protein harvest following the manufacturer protocol for Trial Scale Extraction (Appendix A). Half of the isolated protein solution was used with the Abcam Endotoxin Removal Kit (CBE) (ab239707) and without the Abcam Endotoxin Removal Kit (CB). Endotoxin Removal Kit was used following manufacturer protocol for the CBE sample after the protein isolation (Appendix A). All extracted proteins for CB and CBE were kept in pyrogen-free copolymer tubes (USA Scientific, Item# 1415-2500).

Two-hundred microliters endotoxin-free 1X Dulbecco's phosphate-buffered saline (DPBS) without Ca++ & Mg++ (endotoxin-free PBS) (Sigma-Aldrich, TMS-012) was used to coat the two available types of ELISA plates, Corning® 96-well EIA/RIA Clear Flat Bottom Polystyrene High Bind Microplate (COSTAR) (Corning, Product Number 3590) and Nunc™ MaxiSorp™ ELISA Plates, Uncoated (NUNC) (BioLegend, Cat 423501), and these incubated at 4°C overnight to simulate an ELISA protein coat incubation. Both plates incubated while covered with an adhesive microplate film (VWR, North American catalog number 60941-120). These plates were set up to determine how much endotoxin was being leached into samples during the protein coat incubation of an ELISA setup.

All solutions and samples above were prepared and stored in pyrogen-free copolymer tubes and pipetted with endotoxin-free pipette tips (Corning, MilliporeSigma, CLS4860). Storage was less than 20 hours.

3.3.2.2. Endotoxin Testing, Pilot

Following protein extraction, samples were tested for protein concentration via the Pierce™ bicinchoninic acid (BCA) Protein Assay Kit from Thermo Scientific (REF 23227) following the manufacturer protocol (Appendix A).

Each protein sample, with a concentration of 800 ng/µL, and each ELISA plate endotoxin-free PBS sample was tested with the LAL ToxinSensor™ Endotoxin Detection System from GenScript (cat L00350) following the manufacturer protocol (Appendix A).

All LAL ToxinSensor™ Endotoxin Detection System test and control samples were analyzed via the Bio-Rad Benchmark Plus microplate spectrophotometer at 545 nm. Internal temperature of the plate reader was 21.4°C. LAL ToxinSensor™ Endotoxin Detection System standards, LAL water blank, CBE sample, CB sample, NUNC PBS sample, and COSTAR PBS sample were loaded in duplicate on the NUNC plate.

3.3.2.3. Detectability Testing, Pilot

To determine if the proteins with the lowest endotoxin levels would be detected by the available positive primary antibody, the Indirect ELISA Protocol (Appendix A) was performed on a COSTAR plate versus a NUNC plate with the following modifications:

1. CB samples were serially diluted from 60 ng/µL down to 0.8125ng/µL in endotoxin-free PBS for the protein coat. Pipet tips were swapped between each dilution. Protein coat was in duplicate, and a duplicate of endotoxin-free PBS was also loaded.

10. The primary antibody was pooled convalescent horse serum in the stock blocking buffer at a 1:10,000 ratio. All wells were exposed to this primary.

12. The secondary antibody, Goat Anti-Equine (Invitrogen PA 1-84647), was diluted to a 1:25,000 ratio in the stock blocking buffer. All wells were exposed to this secondary.

15. 1-Step Ultra TMB-ELISA incubation was 25 minutes.

17. Temperature inside the spectrophotometer was 19.6°C.

3.3.2.4. Replication for Statistical Analysis

A sample size of 5 was determined using the Sample Size tool in MedCalc for single mean testing. Previous samples were used to estimate a mean and standard deviation. The estimated mean was 0.07, standard deviation was 0.l, and null hypothesis value was 0.25. Alpha was 0.05, and beta was 0.2.

CB protein harvest protocol was replicated 5 times. Five NUNC plates were coated with a duplicate of 200µL/well endotoxin-free PBS. The NUNC plates incubated at 4°C overnight to simulate a protein coat for the ELISA protocol.

All CB samples were tested for protein concentration via the Pierce™ BCA Protein Assay Kit. Proteins were diluted to 600 ng/µL and 60 ng/µL in endotoxin-free PBS. Then, each protein and the NUNC PBS samples were tested with the LAL ToxinSensor™ Endotoxin Detection System from GenScript (cat L00350) following the manufacturer protocol (Appendix A).

All LAL ToxinSensor™ Endotoxin Detection System test and control samples were analyzed via the Bio-Rad Benchmark Plus microplate spectrophotometer at 545 nm. LAL ToxinSensor™ Endotoxin Detection System standards, LAL water blank, CB sample, and NUNC PBS sample were loaded in duplicate on a NUNC plate.

3.3.2.5. Statistics

3.3.2.5.1. Protein Harvest and Endotoxin Removal

No statistics to be performed.

3.3.2.5.2. Endotoxin Testing, Pilot

Duplicate absorbances were averaged by sample in Microsoft Excel. The average absorbance for the LAL water blank was subtracted from each standard absorbance average and the CB, CBE, NUNC PBS, and COSTAR PBS average absorbances to obtain absorbance-minus-blank (AMB) values. Experimental sample AMB values were then interpolated to the standard curve in GraphPad Prism 9.1.2.

3.3.2.5.3. Detectability Testing, Pilot

Coefficients of variation (CV) were first calculated for each duplicate of absorbance values in Microsoft Excel. All duplicate absorbances were then averaged, and the average absorbance of the endotoxin-free PBS duplicate– the background – was subtracted from each sample absorbance average to obtain AMB values. CV and AMB calculations were performed in Microsoft Excel. Samples that had a CV above 30 were repeated to account for the possibility of human or mechanical error. Samples with a CV below 30 and an absorbance reading above 0 after subtracting the background were considered "detectable" proteins.

3.3.2.5.4. Replication for Statistical Analysis

LAL water blank average absorbance was subtracted from each standard and sample average of absorbances to obtain AMB values in Microsoft Excel. Interplate CV was also calculated in Microsoft Excel. CB and NUNC PBS AMB values were interpolated to the standard curve AMB values in GraphPad Prism 9.1.2. Interpolated data for CB at each concentration and interpolated data for NUNC PBS were each statistically analyzed via a Single Sample T Test in SPSS.

3.3.3. *In Vivo* Testing of pCP Vaccines

3.3.3.1. Vaccinating Quail and Collecting Samples

All birds were purchased from Sandy Hill Quail & Hatchery in Union, Louisiana and cared for in accordance with the approved IACUC protocol A2018-19 under IBRDSC #16021. Power analysis with beta of 0, alpha of 0.5, and sigma of 0.4 was used to determine the sample size under IACUC committee advisement, and additional birds were added to each group to account for attrition. Twelve (12) birds were injected for each treatment group at 7 days old. Groups included the following: 1X DPBS/Saline control, Superfect control, pSCP, pSSCP, and pSECP. Each bird was injected with 50µL of its given treatment in the left breast muscle. The total volume for the vaccine treatment group consisted of the following for each individual bird: 5µg DNA, 15µL Superfect, and QS to the 50µL with molecular grade 1X DPBS without calcium or magnesium (molecular grade 1X DPBS) (Thermofisher Scientific, Massachusetts, Catalog Number 14190144). The Superfect control group injections consisted of the same formula, without the 5µg of DNA. The 1X DPBS control group injections consisted of just 50µL molecular grade 1X DPBS. Injection solutions were mixed in 1 tube per treatment group and then divided into 2 syringes for injection. Injection solutions were administered within 15 minutes mixing/formulating. Each syringe was used to deliver its treatment to half of the birds within the treatment group. Birds were all injected on the same day with 22-gauge ½ inch needles.

Blood was drawn from the jugular of each bird with a 27-gauge ½ inch needle at a maximum volume of 1mL. Blood was collected every three weeks for 12 weeks. If no blood could be obtained via the jugular, a wing stick was performed instead. After each bleed, the needle was removed from the syringe, and the blood was expelled into a 5mL round bottom

polystyrene test tube with a snap cap (BD Falcon, product number 352054). Tubes with blood samples were set on the counter for approximately 1 hour to allow time for coagulation. Tubes with blood were then centrifuged in a ThermoFisher ST 16R Centrifuge with a 75003181 router at 2200 rpm for 20 minutes to separate out the serum. Serum was then pipetted with sterile 1000 µL tips (USA Scientific, cat 1182-1830) into autoclave-sterilized 1.5mL microcentrifuge tubes (VWR Avantor, cat. No. 89000-044). The serum in the microcentrifuge tubes was then frozen at -30°C until time for use.

3.3.3.2. ELISAs for Antibody Detection

Indirect ELISAs were used for *S.* Javiana-specific antibody detection in the quail serum.

All *Salmonella* proteins used in the following testing were from *S.* Javiana isolate 430 from the LSU Veterinary School. To collect proteins for plate coating, *S.* Javiana was first cultured in 10mL BHI broth (BD, ref 237500) in the New Brunswick Scientific Excella E25 shaker incubator at 100 rpm for 24 hours at 37°C. The CelLytic™ B Plus kit from Sigma-Aldrich (Cat CB0050) was then used to harvest the proteins from these bacteria following the Large-Scale Extraction protocol provided with the kit (Appendix A).

Following protein isolation and testing, the proteins were diluted with endotoxin-free PBS in nonpyrogenic 25mL tubes (Eppendorf, 003012247). The diluted protein was then used to coat 5 NUNC plates. The Indirect ELISA protocol (Appendix A) was then followed with the below modifications. Examples of reagent distributions are in Figure 3.2.

1. Protein samples were diluted to 60ng/µL for the protein coat.
4. Plates 1, 2, and 3 incubated at 4°C for approximately 20 hours, and plates 4 and 5 incubated at 4°C for approximately 40 hours.

10. All primaries were loaded in triplicate. Positive control/standard curve was pooled convalescent horse serum in the stock blocking buffer serially diluted from 1:500 to 1:16,000 formulations. Bird sera were each diluted 1:500 in the stock blocking buffer. The bird sera were randomly assigned to plates and locations on said plates via pulling bird numbers and bleeds from a hat, ensuring that each plate contained at least one bird from each treatment group and all bleeds from selected birds. An additional six (6) wells per plate were coated with 100 μL/well stock blocking buffer.
12. For all the horse-serum coated wells, a 1:25,000 dilution was made of Goat Anti-Equine (Invitrogen PA1-84647) in stock blocking buffer. For all of the bird-serum coated wells, a 1:25,000 dilution was made of Goat Anti-Bird in stock blocking buffer (Abcam, ab112773). For the blocking buffer primary wells, one triplicate received the 1:25000 Goat Anti-Equine dilution and the other triplicate received the 1:25,000 Goat Anti-Bird dilution. These triplicates served as background or blanks for their coordinating serum sample wells.
15. 1-Step Ultra TMB-ELISA incubation was 25 minutes.
17. Temperature inside the spectrophotometer was 19.6℃ to 19.7℃ for all plates.

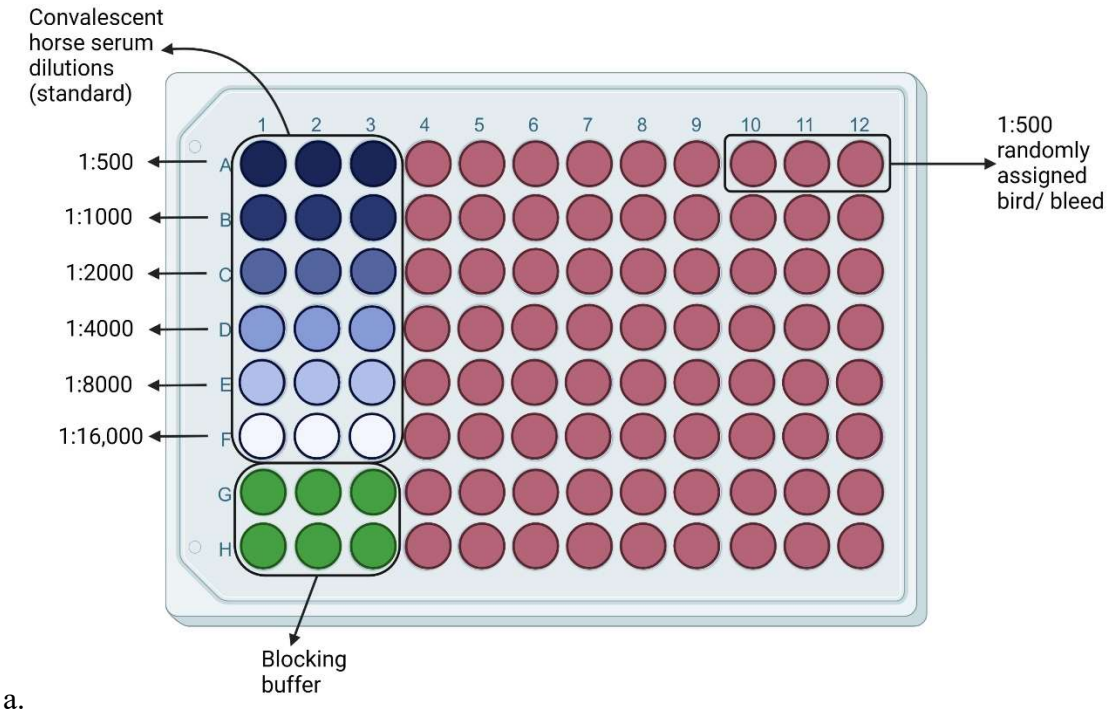

a.

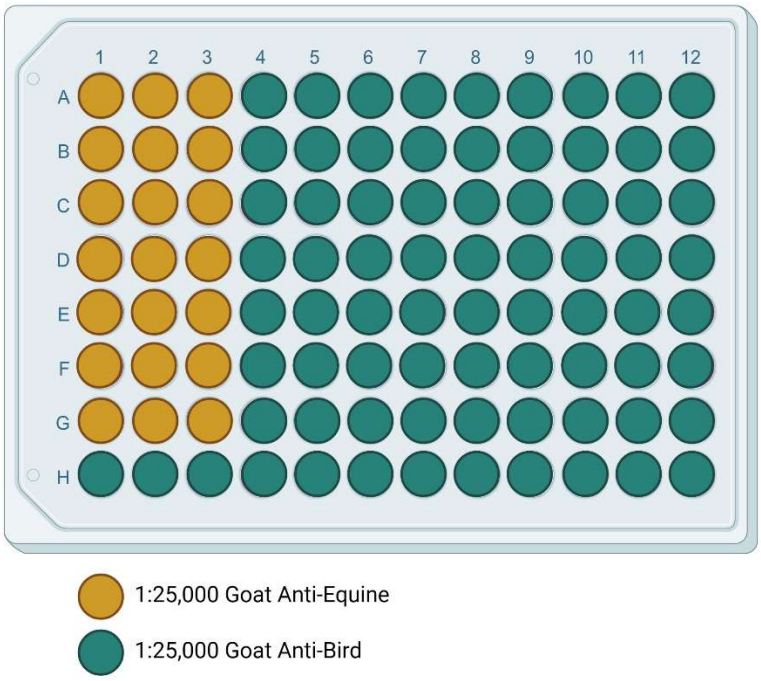

b.

Figure 3.2. Example layouts of primary and secondary antibodies on indirect ELISAs for testing of quail serum. Top (a.) is the primary layout. All treatment groups were represented by at least 1 bird on each plate and all bleeds of that bird. Bottom (b.) is the secondary layout. Created with BioRender.com (Appendix D).

3.3.3.3. Statistics for ELISAs

Interplate CV was calculated in Microsoft Excel. Absorbances for each triplicate were averaged in Microsoft Excel. The absorbances for wells exposed to the blocking buffer at step 10 and Goat Anti-Equine at step 12 were averaged, and this mean was subtracted from each mean absorbance for the standard curve to obtain AMB values for the standard curve. The absorbances for wells exposed to the blocking buffer at step 10 and Goat Anti-Bird at step 12 were averaged, and this mean was subtracted from each mean absorbance for each bird sample to obtain sample AMB values. All AMB values were calculated in Microsoft Excel.

In Graphpad Prism 9.0, a four-parameter logistic regression was used to analyze all data after interpolating the data of each plate to the log transformed standard curve, with Y as the antibody concentration and X as the average AMB. Anti-logs were taken for each interpolated data point to determine an approximate antibody concentration. Two-way mixed-effects analysis with repeated measures was used to analyze the antibody units for the within- and between-groups and bleeds, for all groups that had 3 bleeds (i.e., 1X DPBS, pSCP, pSSCP, and pSECP). An additional, identical analysis was run for just bleed 2 and 3 for all treatment groups. Both mixed-effect analyses also had post hoc Tukey Tests. Both sets of statistics were run to evaluate hypotheses for aims one (H_0: $\mu_C = \mu_{TS} = \mu_{TSS} = \mu_{TSE}$; H_1: Not H_0) and two (H_0: $\mu_1 = \mu_2 = \mu_3 = \mu_4 = \mu_5$; H_1: Not H_0) with adjustments made for attrition that occurred during the experiment..

3.3.3.4. Survival Analysis

A Kaplan-Meier survival analysis was chosen for the aim 3 hypothesis that there would be no difference in survival between the control and vaccine groups at any time (H_0: $S_{C1t} = S_{C2t} = S_{St} = S_{SSt} = S_{SEt}$; H_1: $S_{C1t} \neq S_{C2t} \neq S_{St} \neq S_{SSt} \neq S_{SEt}$). A Gehan-Breslow-Wilcoxon test was run in tandem with the Kaplan-Meier to weight the earlier time points more heavily, as earlier times

could be more indicative of evidence of toxicity from the vaccinations. Survival was analyzed for duration of the bleeds (12 weeks) and at 1-week post-injection.

3.3.4. *In Vitro* Testing of pCP Vaccines

3.3.4.1. Establishing Selection Protocol, Kill Curve

HEK293 cells were acquired from the LSU AgCenter Biotechnology Animal Tissue Culture facility. Cells were used to seed T25 flasks (Corning Incorporated, Corning, NY 14831, 3056) and were cultured to 70-90% in a 10% fetal bovine serum (FBS) media. This 10% FBS media was made by adding 50mL FBS (SAFC Biosciences, cat: 112-300-101) to a 450mL Minimum Essential Medium (MEM) (1X) + Glutamax (Gibco, Ref: 42360-032, New York) bottle.

Four treatment media solutions were mixed as follows. The 10% FBS media was aliquoted into four (4) 150mL sterile polystyrene storage bottles (Corning, product number 431175). Puromycin (InvivoGen, Cat. # ant-pr) was added to three of these bottles so that each had a puromycin concentration of either 0.25 µg/mL, 0.4 µg/mL, or 0.6µg/mL. Puromycin concentrations for testing were selected from a literature review [378, 379]. The remaining bottle of 10% FBS media contained no puromycin. Bottles were gently swirled to mix prior to each use and were stored at 4°C between uses.

Two (2) flasks were used for each treatment group, and this number was determined following the protocol from Mirus [380]. Flasks were each rinsed with 5mL molecular grade 1X DPBS via pipette and then fed with 5mL of its treatment media via pipette every other day for a total of three (3) feeding days. Flasks were visually assessed by use of a Zeiss Axiovert 25 HBO 50 microscope at each feeding and at the 1-week mark from the initial treatment media exposure.

Observations of average confluences were recorded. Analysis of this data followed protocols of Baser and colleagues in 2015 and Mirus, which were reported with simple histograms.

3.3.4.2. Sample Size Selection for pCP Testing

Number of flasks was determined by how many flasks would be necessary for sufficient sample collection for analyses procedures, as outlined by a colleague [273]. This section was treated as a pilot study.

3.3.4.3. Transfection, Selection, and Sample Collection

HEK293 cells were split into 16 T25 flasks by use of 2.5mL of TrypleExpress (ThermoFisher Scientific, Waltham, MA, catalog number 12605010) and gentle tapping. The T25 flasks were transiently transfected 48 hours later. Flasks were 10% to 40% confluent. The transfection reagent for this project was Lipofectamine3000 (Invitrogen, Catalog number L3000001). One transfection mixture was produced for each treatment group of flasks, and the Lipofectamine3000 transfection of HEK293 protocol from a colleague was followed [273] (Appendix A). Groups consisted of 4 flasks for pSCP, 4 flasks for pSSCP, 4 flasks for pSECP, and 4 flasks for Lipofectamine3000 alone. Two T75 flasks of non-transfected HEK293 cells were also among the treatment groups.

Forty-eight (48) hours following transfection, T25 flasks were rinsed with 5mL molecular grade 1X DPBS to remove old media, fed with 5mL fresh 0.4µg/mL puromycin treatment media, and then returned to the incubator. The incubator was set to 37°C with 5% carbon dioxide (CO_2) supplementation. This rinsing, feeding, and incubation process was performed every 48 hours for 26 days, or until new cell growth was subjectively determined to be substantial enough for sample collection: confluency of ~75%. The two T75 flasks containing non-transfected HEK293

cells were rinsed with 10mL molecular grade 1X DPBS, fed with 25mL fresh 10% FBS media, and returned to the incubator every 48 hours, like the T25 flasks. Sample collection for all flasks occurred on the same day.

On sample collection day, spent media was first combined into 50mL nonpyrogenic, polypropolyene conical tubes (CELLSTAR®, Greiner Bio-One, Cat. No. 2270261) for each treatment group, which were then stored at -30°C. Next, lysate collection was performed by first making lysate extraction buffer (LEB) by combining 1083µL of a 200mM phenylmethylsulfonyl fluoride (PMSF) (Life Technologies, cat# 36978) in ethanol with 21mL mammalian protein extraction reagent (M-PER) (ThermoScientific, ref 7850) and 311.1µL Halt Protease Inhibitor Cocktail (100x) (ThermoScientific, Prod # 1862209). LEB, molecular grade 1X DPBS, and flasks were placed on ice until chilled. Flasks were rinsed with 5mL of the chilled molecular grade 1X DPBS to remove any residual waste media, and then, 1.25mL LEB was added to each flask. Cell scrapers (VWR, catalog number 734-2602) were used to detach the cell from the flask and transfer them into the LEB for cell lysis. The LEB and cells were aspirated and transferred to pre-chilled 15mL conical tubes (SpectraTube, VWR catalog number 470224-998), one tube per experimental group. The conical tubes were then vortexed for 3 to 4 seconds and placed back on the ice for a 30-minute incubation for lysis to take place. Following the incubation, the tubes were centrifuged in the Sorvall ST16R Centrifuge equipped with the 75003181 rotor (ThermoScientific) at 1300rpm for 10 minutes to pellet the solid debris from the cells. The supernatant, containing the soluble proteins (referred to henceforth as lysates), was aliquoted to 1.5mL microcentrifuge tubes for storage at -30°C. LEB and lysate harvest protocols were adapted from those of a colleague [273].

Messenger RNA was extracted from the lysate by first passing some of the supernatant through a QIAshredder (Qiagen, ref: 79654) then utilization of the QIAGEN RNEasy® Plus Mini Kit (ref: 74134). QIAhredder and QIAGEN RNEasy® Plus Mini Kit manufacturer protocols were followed (Appendix A).

3.3.4.4. Sample Analyses for Transcription, RT-PCR

RT-PCRs were used to determine if transcription of the vaccines took place following transfection. RNEasy® samples from each treatment group were reverse transcribed utilizing the QIAGEN OneStep *Ahead* RT-PCR Kit (Catalog No. 220213) with specially designed primers for vaccine detection (Table 3.3) and with housekeeping primers for the positive controls (Table 3.4). Every sample was amplified with the vaccine-specific primers (experimental) and positive control primers, the combinations of which are described in Tables 3.3. and 3.4. The mixture for each RT-PCR consisted of 10µL QIAGEN OneStep *Ahead* RT-PCR Master Mix 2.5x, 1µL QIAGEN OneStep *Ahead* RT-Mix 25x, 1µL forward primer, 1µL reverse primer, 3µL mRNA, 4µL RNA/DNA-free water all in a 200µL thin-walled PCR tubes (Bio-Rad, Catalog 223-9473). Tubes were placed in a Bio-Rad T100 Thermal Cycler under the following conditions: reverse transcription at 50°C for 10 minutes, initial PCR activation at 95°C for 5 minutes, 3-step cycling at 95°C for 10 seconds, annealing at approximately 5°C below Tm of the primers for the specific reaction (Tables 3.3 & 3.4) for 10 seconds, extension at 72°C for 10 seconds, and a final extension at 72°C for 2 minutes. The cycling, annealing, and extension steps were repeated 40 times.

Housekeeping genes to serve as positive controls were selected from the Harmonizome Gene Set Database for HEK293 cells [381]. Two proteins with high expression were selected for RT-PCR primer design. The first protein was zinc finger protein 223 (ZNF223) (NCBI Gene ID

7766), and the primers specific to ZNF223 were obtained from OriGene (Cat#: HP210507) (Table 3.4). The second protein was ubiquitin specific peptidase 18 (USP18) (NCBI Gene ID 11274), and the primers specific to USP18 were obtained from OriGene (Cat# HP212347) (Table 3.4).

The RT-PCRs were first evaluated visually via 1% agarose gels dyed with ethidium bromide. Following visual verification, RT-PCRs that appeared to react were rerun on 1% agarose gels dyed with SYBR Safe, excised, and recovered via the Zymoclean DNA Gel Recovery Kit. Each recovered RT-PCR DNA sample and its coordinating primer set was then sent to GeneLab for sequence verification.

Table 3.3. RT-PCR experimental groups and negative control groups by mRNA sample and primer pairing.

RT-PCR Description	**pSCP Experimental**	**pSCP Lipo Control**	**pSCP Negative Control**	**pSSCP Experimental**	**pSSCP Lipofectamine Control**	**pSSCP Negative Control**	**pSECP Experimental**	**pSECP Lipofectamine Control**	**pSECP Negative Control**
mRNA sample	pSCP HEK293	Lipo without DNA HEK293	Non-transfected HEK293	pSSCP HEK293	Lipofectamine without DNA HEK293	Non-transfected HEK293	pSECP HEK293	Lipofectamine without DNA HEK293	Non-transfected HEK293
Forward Primer	SJ1 F: 5’TCGGTCGACAACATGAAGTGGG 3’			SJ1 Short F: 5’GGTCGACAACATGAAGCTCA 3’			SJ1 Ext F: 5'GGTCGACAACATGAAGCTCA 3’		
Reverse Primer	SJ1 R: 5’TTAATTCCCGTCCTTGTTGTACACC 3’			SJ1 Short R: 5’TTAGGTAACATATGCTTGGTGATGT 3’			SJ1 Ext R: 5’TTACCCGTGAACCAACGGAT 3’		
Annealing Temperature	56°C			54°C			55°C		
Product Size (bp)	792	n/a	n/a	937	n/a	n/a	1282	n/a	n/a

Notes: Additionally includes the annealing temperatures used and expected product sizes of each RT-PCR. “Lipo” and “Lipofectamine” refer to Lipofectamine3000.

Table 3.4. RT-PCR positive control groups by mRNA sample and primer pairing.

RT-PCR Description	**USP18 Positive Control**	**USP18 Positive Control2**	**USP18 Positive Control3**	**USP18 Positive Control 4**	**USP18 Positive Control 5**	**ZNF223 Positive Control 1**	**ZNF223 Positive Control 2**	**ZNF223 Positive Control 3**	**ZNF223 Positive Control 4**	**ZNF223 Positive Control 5**
mRNA sample	pSCP HEK293	pSSCP HEK293	pSECP HEK293	Lipo without DNA HEK293	Non-transfected HEK 293	SJ1 CPP HEK 293	SJ1S CPP HEK 293	SJ1E CPP HEK 293	Lipo without DNA HEK293	Non-transfected HEK 293
Forward Primers	USP18 F: 5'TGGACAGACCTGCTGCCTTAAC 3'					ZNF223 F: 5'TTCAGGAACCTGCTGTCAGTGG 3'				
Reverse Primers	USP18 R: 5'CTGTCCTGCATCTTCTCCAGCA 3'					ZNF223 R: 5'GTGGTCCTGCTTCTGGAAAAGTC 3'				
Annealing Temperatures	46°C, 48°C, 50°C, 52°C, 54°C, 56°C, 58°C									
Product Size (bp)	159					163				

Notes: Additionally includes the annealing temperatures used and expected product sizes of each RT-PCR. "Lipo" refers to Lipofectamine3000.

3.3.4.5. Sample Analyses for Translation and Protein Secretion, ELISA

Indirect ELISAs were used for detection of vaccine-specific protein production from the cells.

Positive primary antibodies were from the pooled serum of two *S.* Javiana-infected thoroughbreds from Louisiana. This convalescent serum was obtained, pooled, aliquoted into single use tubes, and frozen at -30°C until ready for use. The protein for the positive control was harvested from *S.* Javiana isolate 430. The *S.* Javiana was isolated from the previously mentioned thoroughbreds by the LSU Veterinary School.

To collect proteins for the standard curve for all plates, *S.* Javiana was first cultured in 10mL BHI broth in the New Brunswick Scientific Excella E25 shaker incubator at 100rpm for 24 hours at 37°C. The CelLytic™ B Plus kit from Sigma-Aldrich (Cat CB0050) was then used to harvest the proteins from these bacteria following the Trial Scale Extraction protocol (Appendix A). Following protein extraction, samples were tested for protein concentration via the Pierce™ BCA Protein Assay Kit. Following protein isolation and testing, *S. enterica* ser. Javiana proteins were diluted with endotoxin-free PBS in nonpyrogenic 25mL tubes.

Before testing the cell culture samples, all cell culture reagents were tested via an indirect ELISA, and a standard curve was established. Reagents tested included the MEM(1X)+Glutamax, FBS, molecular grade 1X DPBS, and LEB. Reagents were all tested undiluted and serially diluted down to 1/32 of its full strength in endotoxin-free 1X DPBS. *S.* Javiana proteins were tested in serial dilution from 60ng/µL down to 0.234ng/µL in endotoxin-free PBS (Figure 3.3). The Indirect ELISA Protocol (Appendix A) was performed with the following modifications:

1. The *S.* Javiana proteins and all the dilutions of the cell culture reagents were used to coat a NUNC plate at 100µL/well in duplicate. Undilute samples coated an additional four wells to check for nonspecific binding– two against the primary and two against the secondary (Figure 3.3).

10. The primary antibody was convalescent serum in the stock blocking buffer at a 1:3000 ratio. Two of the four additional undilute sample wells were coated with this primary dilution and the remaining two were coated with blocking buffer again (Figure 3.3).

12. The secondary antibody, Goat Anti-Equine (Invitrogen PA1-84647), was diluted to a 1:25,000 ratio in the stock blocking buffer. All wells were coated with this secondary– except for those extra wells that received full-strength samples and primary, which were coated with blocking buffer for this step (Figure 3.3).

15. 1-Step Ultra TMB-ELISA incubation was 25 minutes.

17. Temperature inside the spectrophotometer was 19.6℃ to 19.7℃ for all plates.

The extra undilute samples exposed to either just the primary or just secondary wells were visually evaluated for potential source of nonspecific binding via one of the two antibodies.

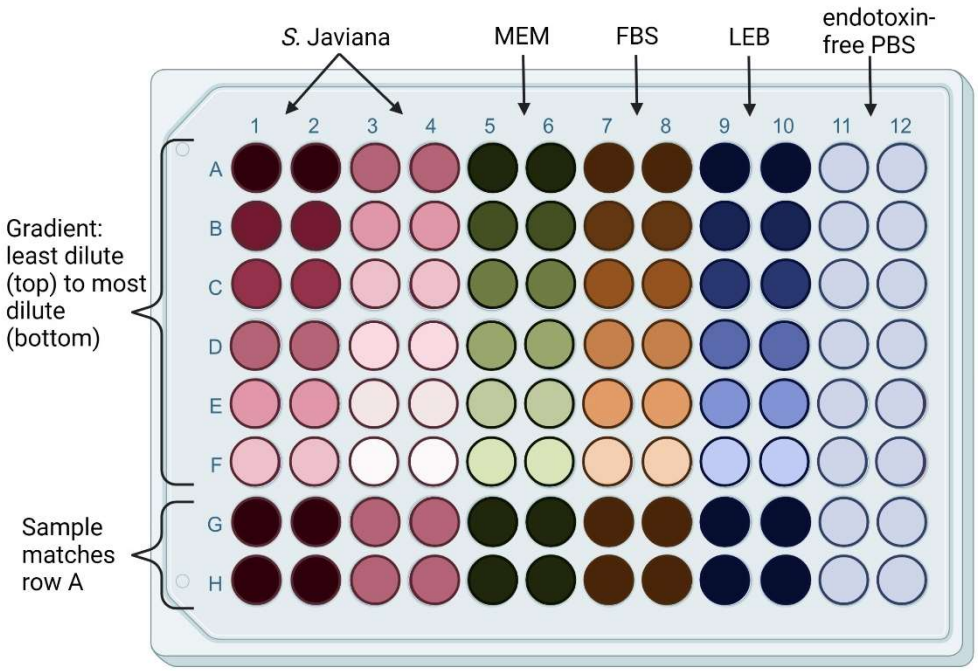

a.

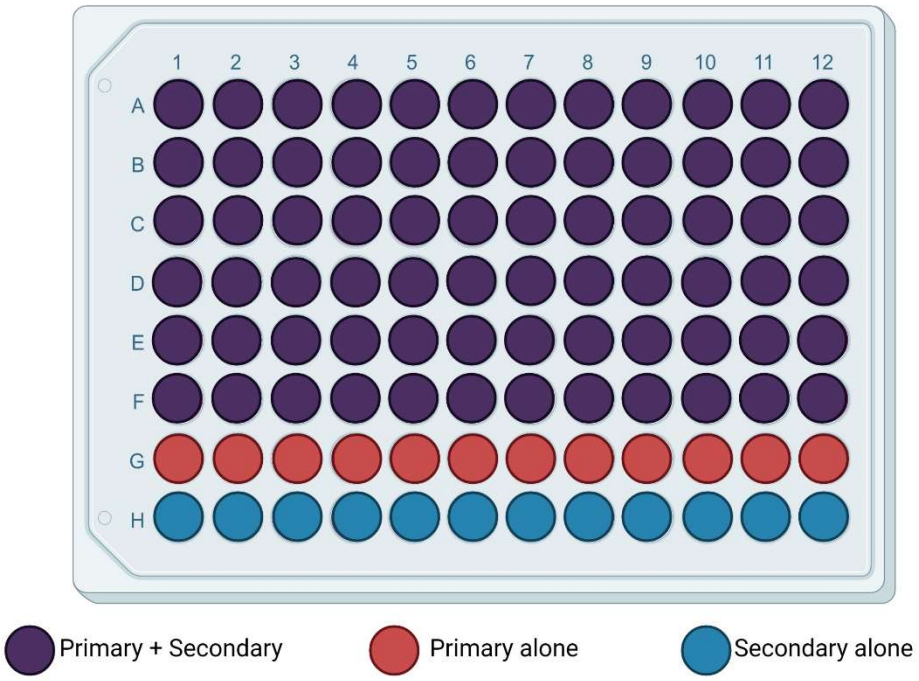

b.

Figure 3.3. Indirect ELISA protein coat and antibody exposure layouts for cell culture reagent testing. Top (a.) is the layout of samples used to coat the plate in step 1 of the indirect ELISA protocol. Rows A, G, and H are undilute samples, except in columns 3 and 4 where those rows are *S.* Javiana proteins diluted to 7.5 ng/µL. Bottom (b.) is the layout of primary and secondary antibodies, with purple representing wells that received both. Created with BioRender.com (Appendix D).

ELISAs for testing detectable protein concentrations in cell culture samples – spent media and lysates for each treatment and control group– were performed following nearly the same protocol used for testing the cell culture reagents' reactivity, which just the following modifications. Cell culture samples were diluted by one half and one fourth with the endotoxin-free PBS, and each sample and its dilutions were randomly assigned a duplicate location on the plate. Two wells coated with endotoxin-free PBS were exposed to the primary and the secondary for a protein concentration of 0ng/μL. The standard curve for this plate was the *S.* Javiana CB harvested proteins diluted to 3.75ng/μL through 0.234375 ng/μL in endotoxin-free PBS.

3.3.4.6. Statistics

No statistical analyses were performed for RT-PCRs because of the combination of all flasks into a single tube for lysate harvest and subsequent mRNA harvest, reducing the sample size for each transfection to 1.

Correlation Tests in Graphpad Prism 9.2.1. were used to evaluate the hypothesis for aim four of this portion of this project (H_0: $\rho=0$; H_1: $\rho>0$) and to determine which range of protein concentrations should be used for the standard curve before the ELISA data interpolations. CVs and mean absorbances for each duplicate exposed to primary and secondary were calculated in Microsoft Excel. The mean absorbance of endotoxin-free PBS wells was subtracted from all standard duplicate means to obtain their AMB values. The AMB values for the nine concentrations of protein from 60ng/μL down to 0.234 ng/μL were tested first. Then, visual inspection of the data was used to reduce the second test to the 5 concentrations of protein from 3.75 ng/μL down to 0.234 ng/μL. Another Correlation Test was also performed on the standard curves on the cell culture sample plate to determine the values to use for interpolation.

Statistics could not be reliably performed on the ELISA data from the *in vitro* vaccine experiment because of the combination of flasks for each treatment group for lysate and spent media collection, making the sample size for each treatment group 1 instead of 6. Therefore, the following was conducted. CVs and mean absorbances for each duplicate were calculated in Microsoft Excel. The mean absorbance of wells with a protein concentration of 0ng/µL were subtracted from all sample and standard means to obtain their AMB values. The mean sample AMB values obtained on the ELISA were interpolated to the standard curve of the ELISA to determine an approximate protein concentration for each sample. Interpolation to the standard curve allowed for evaluation of the hypotheses for aims one and two (H_0: θ_c & θ_t = +/-; H_1: $\theta_c \leq 0$; H_2: $\theta_t > 0$). Interpolation of AMB values to the standard curve was also used for the reagent ELISA test. A combination of an interpolated value greater than zero and a CV of less than 30 was considered a positive result.

3.4. Limitations

3.4.1. pCP Vaccines Construction

Spontaneous mutations that occur through transformation of *E. coli* mean constant screenings and verifications of the sequences after each transformation. This extended the time frame of constructing the full plasmids considerably.

3.4.2. Establishing an ELISA Protocol

The kits tested were expensive. Therefore, the initial tests were treated as a pilot study to reduce costs. Additionally, the amount of convalescent horse serum available was limited. Therefore, the protein detectability portion of this project was not replicated for statistical analysis, but rather continuously monitored across future ELISAs.

The exact time between infection and serum collection for the convalescent horse serum was unknown, so the presence and levels of IgM in the pooled convalescent serum were not definitively known prior to troubleshooting.

3.4.3. *In Vivo* Testing of pCP Vaccines

No pre-bleeds or cloaca swabs were taken because of the birds' small sizes. All birds were housed together for 1 week prior to injection. So, they all were exposed to each other and anything that may lead to a positive antibody result later, which would likely be reflected by the 1X DPBS group. Verbal assurance of no *Salmonella* exposure was received from the quail supplier, but it should be noted that the supplier was suddenly shutdown during the quail portion of this study [234]. Therefore, no additional information about the birds could be obtained, particularly paperwork verifying their *Salmonella*-free status.

No existing ELISA protocol or vaccine for *S.* Javiana existed, so no true positive or negative controls existed for these experiments. The best that could be done for a negative control was ensuring that there was a duplicate of wells exposed to blocking buffer (the primary antibody diluent), which was treated as a blank or background reading. Two years of ELISA development involved the use of a positive control for the secondary antibody, produced in-house, but it was not used in the ELISAs presented here because of sample depletion from ELISA protocol development. Additionally, the exact quantitation of IgM from the *S.* Javiana-specific horse serum was not known prior to experimentation. Therefore, its use as a standard curve could not provide true antibody counts for the bird serum, but rather just if the bird serum antibodies fell within an unknown spectrum of "positive" levels.

Depletion of quail samples occurred as well, impacting the sample size and power of the experiment. Loss of samples was because of a variety of factors: bird fatalities during the

experiment; the birds' small size and fat deposits around the jugular meant some samples weren't large enough to separate out serum; some serum samples were pooled in their entirety for an undergraduate research project which aided in ELISA development for this project; and 2 years of ELISA troubleshooting and protocol refinement led to the depletion of some additional serum samples.

In reference to the fatalities, no necropsies could be performed for toxicity evaluations because the whole bird carcasses were promised and delivered to the raptor unit at the LSU Veterinary School. Therefore, possible causes of death could not be determined beyond a survival analysis.

Considering the novelty of the various aspects of this project, the required dose for administration was not definitively known before starting the experiment, although determination of this initial testing dose was from proprietary research [234].

3.4.4. *In Vitro* Testing of pCP Vaccines

No existing ELISA protocol for *S.* Javiana existed, so no true negative controls existed for these experiments. Therefore, negative controls consisted of a duplicate of wells coated with endotoxin-free PBS (the sample diluent), which were treated as a blank or background reading. Additionally, ELISA troubleshooting was anticipated for this project. Samples for flasks were combined by treatment group in this anticipation to ensure that there was enough sample for all following assays.

The exact time between infection and serum collection for this project was unknown, so the presence and levels of IgM in the pooled convalescent serum were not known prior to troubleshooting. Anti-equine IgM was the available antibody that could be found at the time of this project. Additionally, exact epitopes recognized by the IgM antibodies could not be

determined, meaning that proteins produced by the vaccines may or may not be detectable by this IgM. However, no commercially available antibodies existed for any of the epitopes being investigated.

3.5. Results and Discussion

3.5.1. pCP Vaccines Construction

Miniprepped plasmids for pCP, pSCP, pSECP, and pSSCP appeared to be the expected sizes of 6076 bp, 7162 bp, 7654 bp, and 7309 bp respectively when compared to the Supercoiled DNA ladder (Figures 3.4 and 3.5). The ORF PCRs produced the expected sized bands for each vaccine which were 720 bp for pSCP, 1212 bp for pSECP, and 867 bp for pSSCP when compared to the 1kb ladder (Figure 3.5). In sequencing, all components for each plasmid were matched with 100% sequencing identification and 100% theoretical query cover, as indicated by SnapGene and nBLAST through NCBI (Figures 3.6-3.8). The combination of expected sizes of all bands for the Midipreps and PCRs and the sequencing data indicated that the pCP and ORF ligations were successful. Therefore, the aim of this portion of this project was achieved.

a. 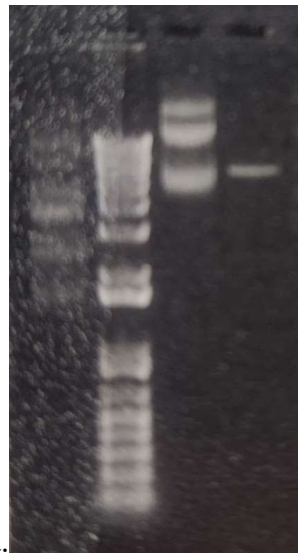 b. 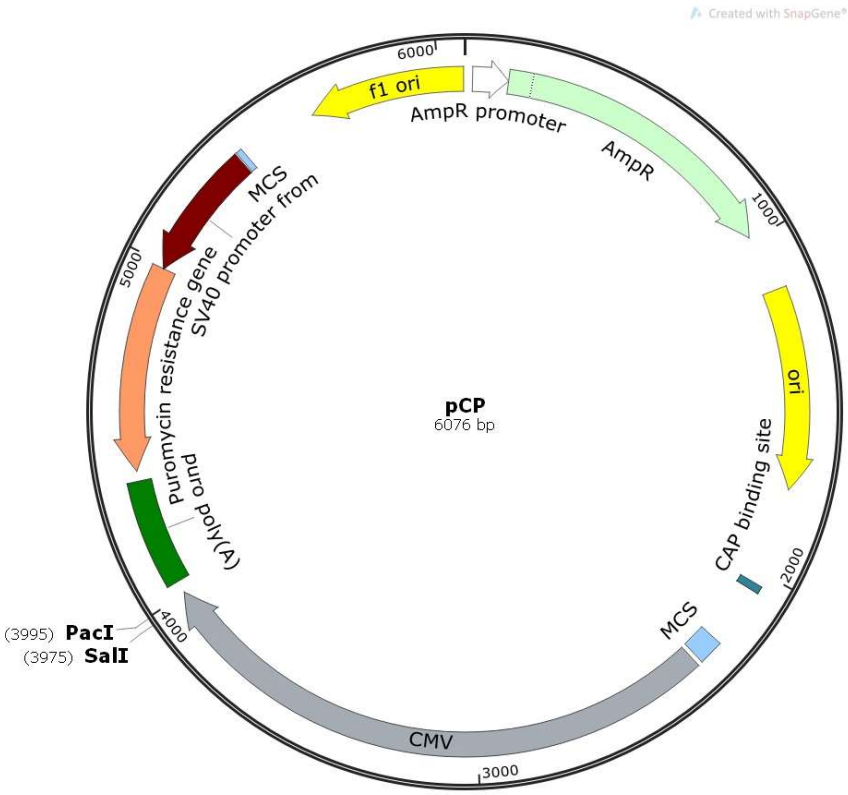

Figure 3.4. Gel confirmation of pCP vector midiprep and SalI test digest showing expected sizes. On left (a.) is a 1% agarose ethidium bromide gel. The order for the gel is lane 1 -Supercoiled ladder, lane 2 - 1kb ladder, lane 3 - pCP midiprep, and lane 4 - pCP SalI test digest. On the right (b.) is the SnapGene circular map of pCP demonstrating the SalI RE location.

a. 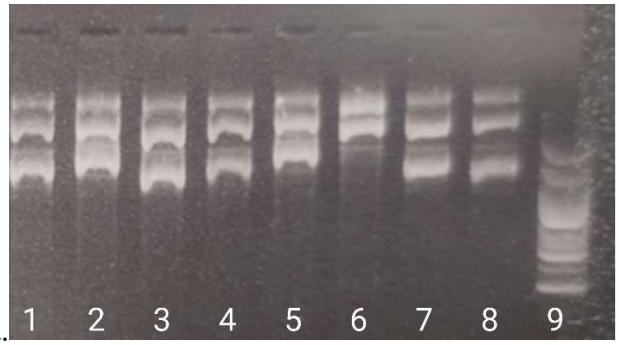

b. 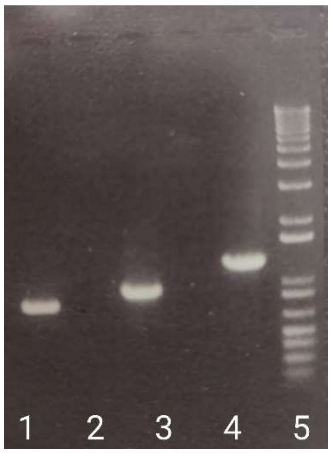

Figure 3.5. Confirmation of pCP and ORFs ligations on a 1% agarose ethidium bromide gels. Left (a.) is the gel visualizing Midipreps of the pCP vaccines. Gel order is lanes 1 and 2 - pSCP minipreps, lanes 3 and 4 - pSSCP minipreps, lanes 5 through 7 - pSECP minipreps, lane 8 - pCP miniprep, and lane 9 - Supercoiled ladder. Ran at 60mA for 2 hours. Right (b.) is the gel confirmation of PCR verification of ORF vaccine inserts in pCP. pSCP, pSSCP, and pSECP. Gel order is lane 1 - pSCP PCR, lane 3 - pSSCP PCR, lane 5 - pSECP PCR, and lane 6 - 1kb ladder.

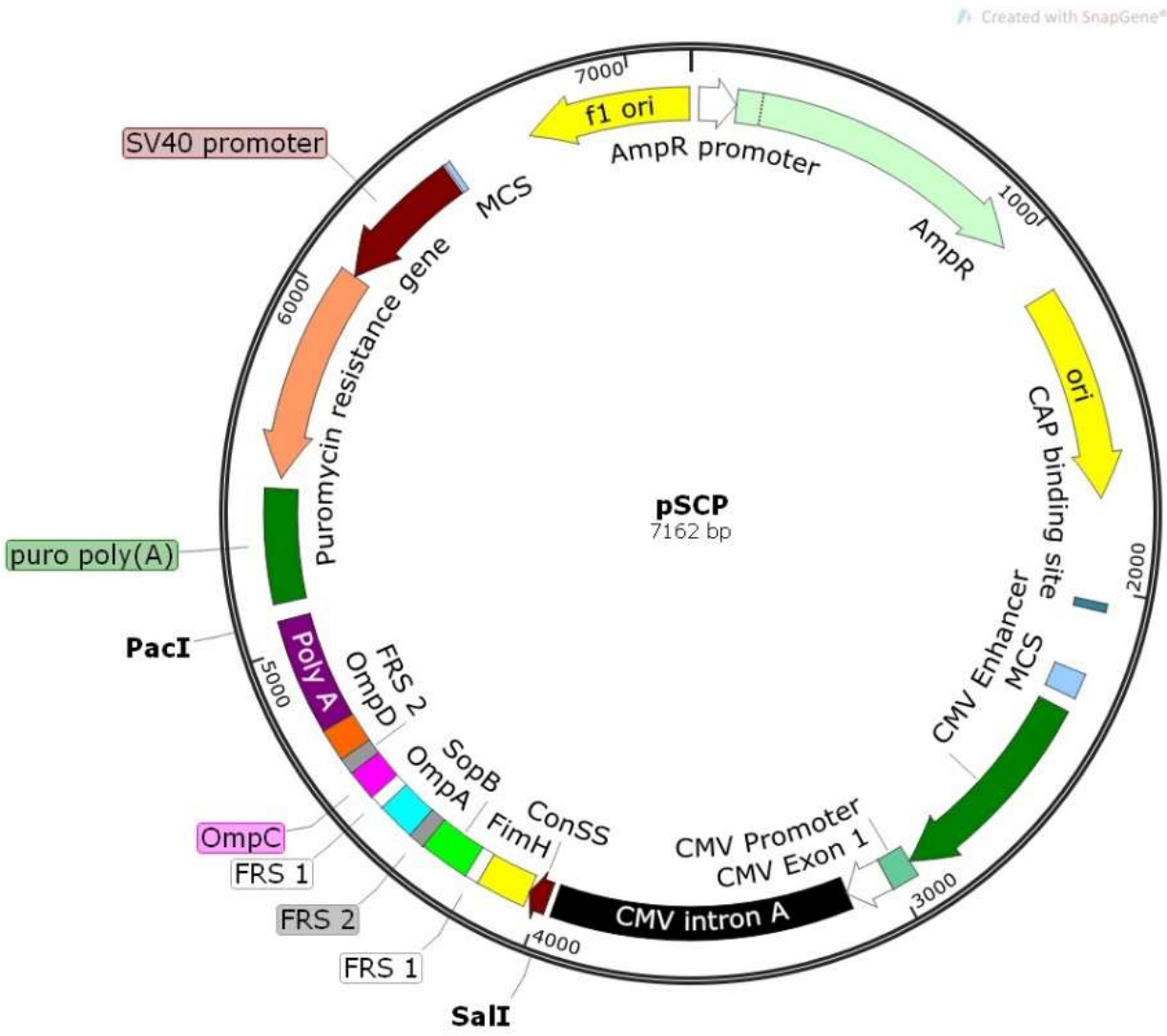

Figure 3.6. SnapGene circular map of pSCP demonstrating the expected size of 7162 bp and orientation of all vaccine components.

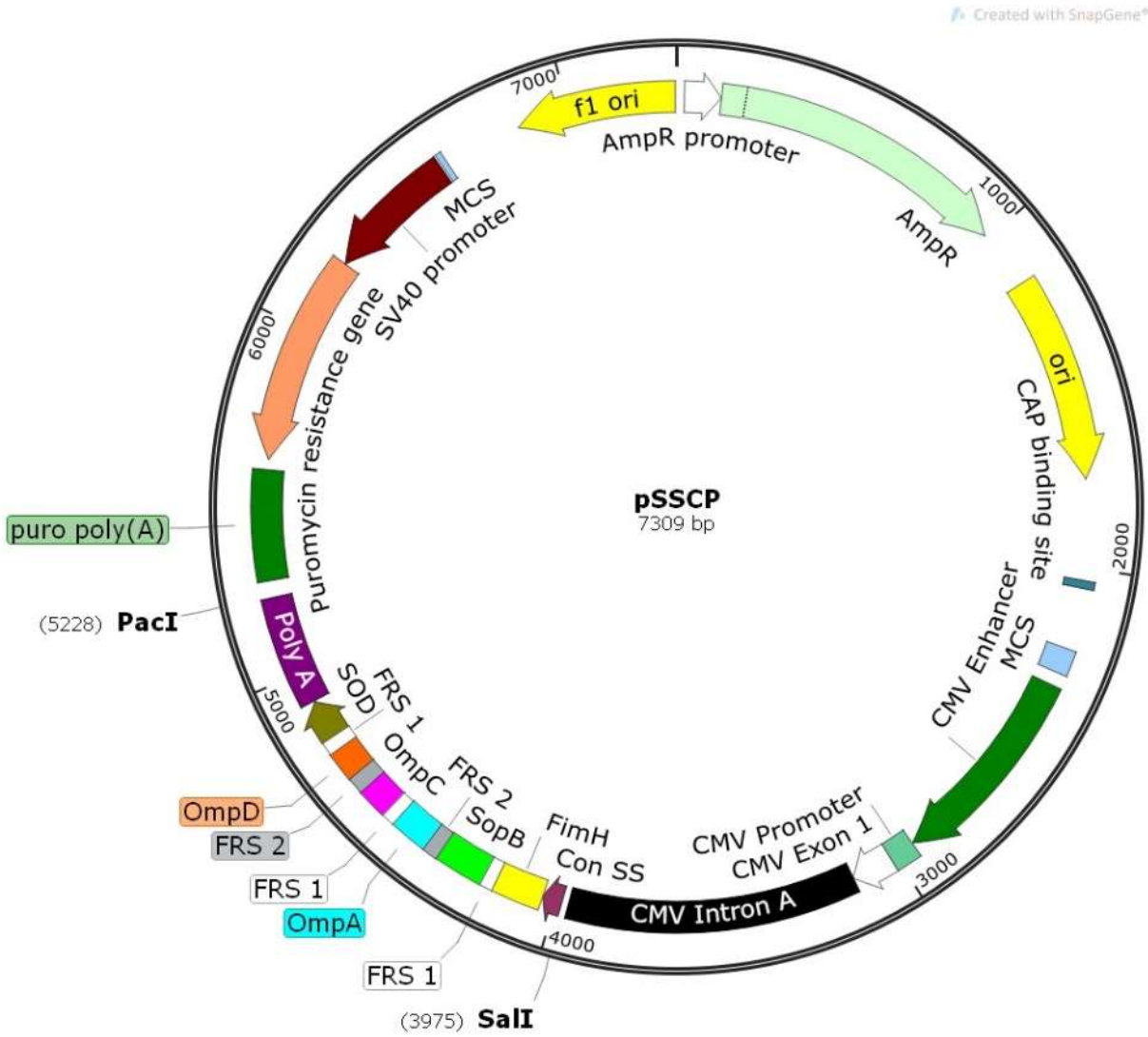

Figure 3.7. SnapGene circular map of pSSCP demonstrating the expected size of 7309 bp and orientation of all vaccine components.

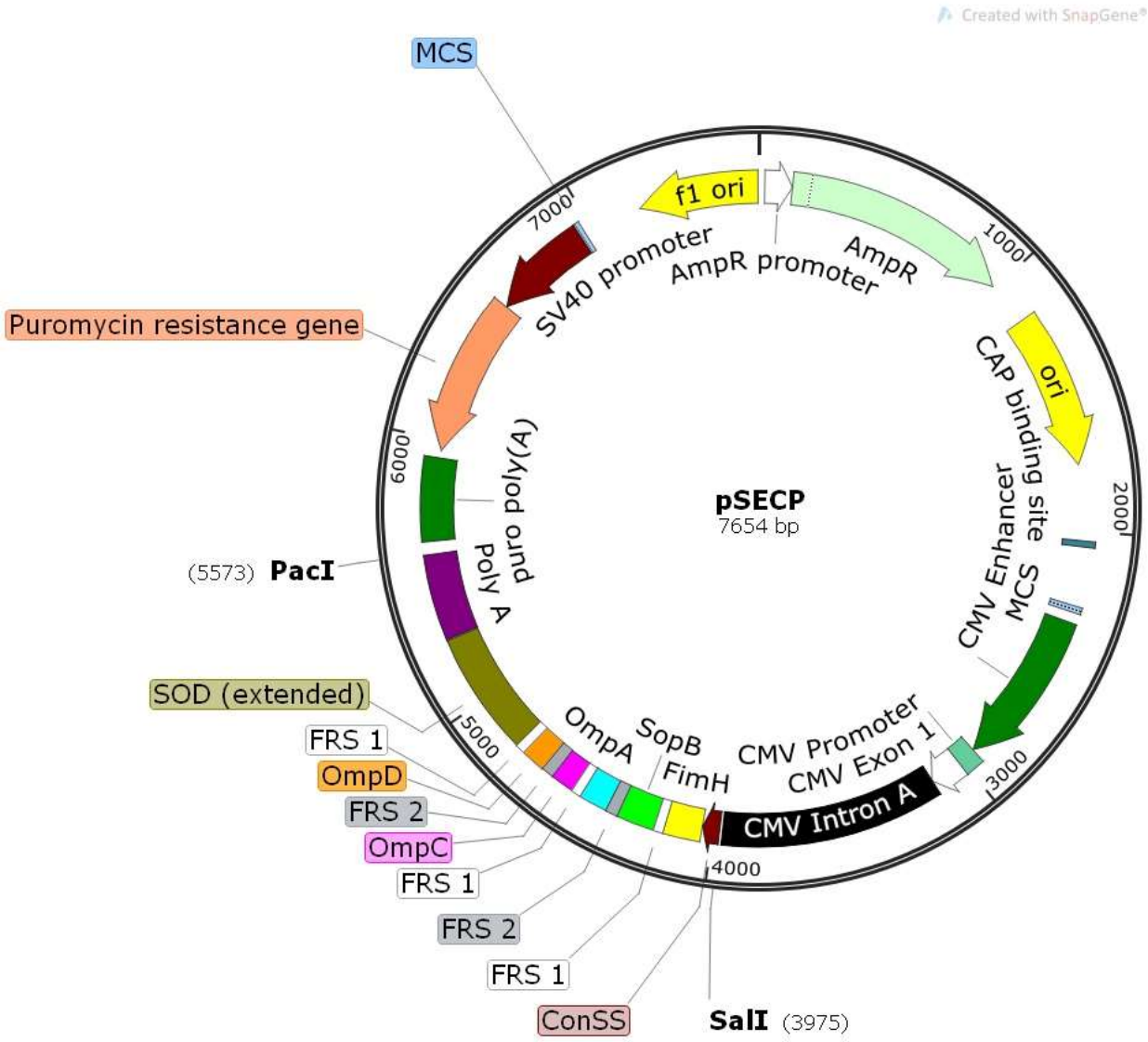

Figure 3.8. SnapGene circular map of pSECP demonstrating the expected size of 7654 bp and orientation of all vaccine components.

3.5.2. Establishing an ELISA Protocol

According to the interpolated data to the standard curve of the pilot study, CB had an endotoxin reading of approximately 0.078 EU/mL and CBE had an endotoxin reading of approximately 0.233 EU/mL. The standard curve is shown in Figure 3.9. The endotoxin-free PBS samples from both overnight ELISA plate incubations were also found to have <0.25

EU/mL. CB and both plates were selected for future protein detection testing based on this pilot information.

The CB samples were not expected to have lower endotoxin levels than CBE in the pilot study. The proposed hypothesis for the difference in outcomes between the two samples is that the CBE sample became cloudy during endotoxin testing, impacting the spectrophotometer reading. This increase in opacity was presumably from a chemical reaction resulting from a combination of some component(s) of the Abcam Endotoxin Removal kit and the LAL ToxinSensor™ Endotoxin Detection System. The color changes of the CBE and CB samples during endotoxin testing were otherwise observed to be similar. The proposed hypothesis for CB having a low endotoxin level despite the lack of an endotoxin removal step is this: the zwitterion detergents in the CelLytic™ B reagent in combination with a final centrifugation step was functionally similar to a two-phase micellar system. Triton X-114 is a two-phase micellar system, and it is a non-ionic detergent that chemically functions similarly to zwitterion detergents [322, 339]. Also, like the two-phase micellar system protocols, the CelLytic™ B Plus kit ends with a centrifugation step which could separate out an endotoxin phase from a protein phase. However, further testing is needed to confirm.

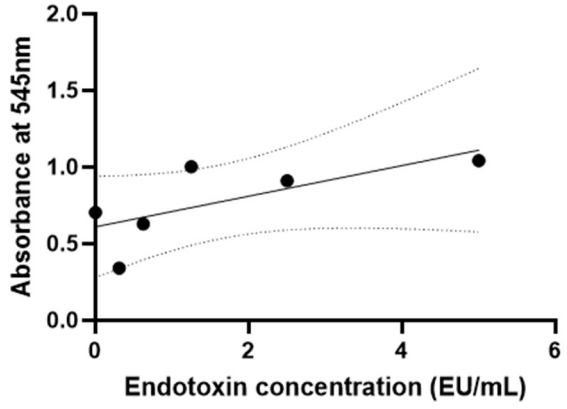

Figure 3.9. The endotoxin standard curve that was used to interpolate the original CB, CBE, and plate PBS sample values.

In the first run of the detectability test, all protein samples, except the one with a concentration of 60ng/µL on the NUNC plate, had a CV of less than 30%. In the repeat for the 60ng/µL sample on the NUNC plate, the CV was 15.1288%. All NUNC samples with CV below 30 had AMB values of over 0 (Table 3.5). All COSTAR samples except the 3.25ng/µL sample had AMB values of below zero, and the 3.25ng/µL AMB value was less than the lowest AMB value on the NUNC plates (Figure 3.10). Sample CVs for the COSTAR plate ranged from 0 to 26.18914 (Table 3.5). Therefore, all protein samples between 3.25ng/µL and 60 ng/µL on the NUNC plates were considered "detectable" proteins suitable for moving forward and aim two of this portion of this project was met. Additionally, this protein detection was used to determine that NUNC plates would be replicated for endotoxin testing and not COSTAR plates.

Hypotheses for the disparity in protein detection between NUNC and COSTAR plates are hard to determine because of the plates' proprietary nature. NUNC plates contain a Maxisorp surface consisting of a charged polystyrene. The charge aids in the affinity between the plate and polar or hydrophilic groups on proteins [382]. COSTAR's description only claims that the polystyrene used has a high-binding surface [383]. It is possible that the Maxisorp surface of the NUNC plates increased protein binding in comparison to the COSTAR plates. Further evaluations would be needed to confirm, however.

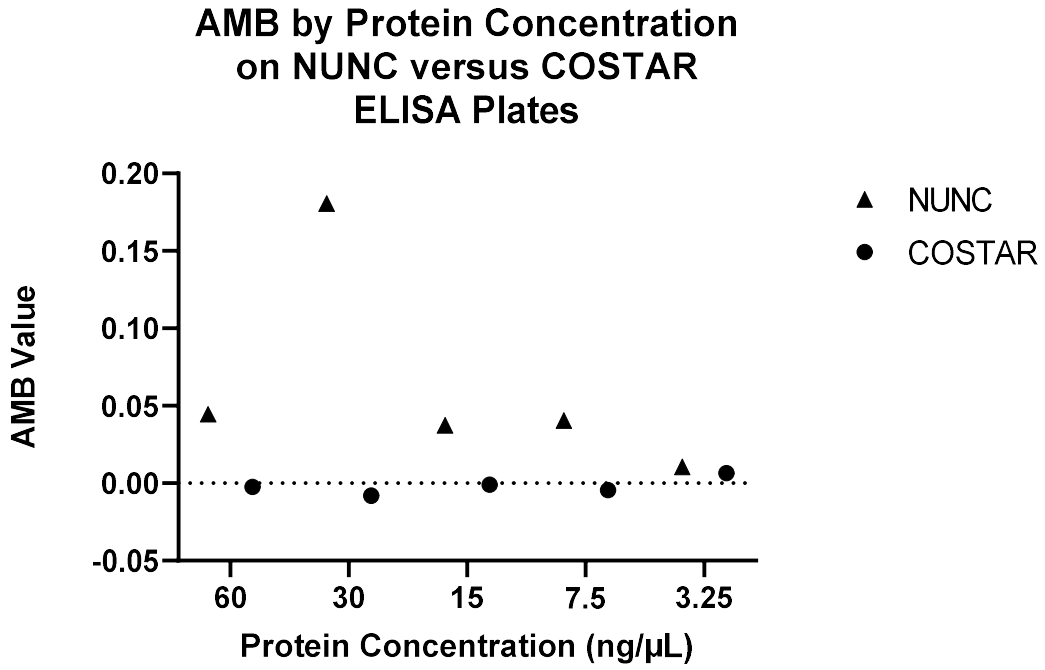

Figure 3.10. AMB by protein concentration on NUNC versus COSTAR ELISA plates for samples with CVs under 30.

Table 3.5. Concentrations of proteins isolated from *S.* Javiana via the CB method on NUNC versus COSTAR plates and their coordinating CV and AMB values.

	NUNC		**COSTAR**	
Protein Concentration (ng/µL)	**CV**	**AMB**	**CV**	**AMB**
60 (first)	48.12254	0.0835	4.351426	-0.0025
60 (second)	15.1288	0.0445	n/a	n/a
30	12.32302	0.1805	10.69573	-0.008
15	17.3169	0.0375	9.569866	-0.001
7.5	5.600846	0.0405	2.244783	-0.0045
3.25	5.97555	0.0105	0	0.0065
0 (first)	8.181401	n/a	26.18914	n/a
0 (second)	4.489567	n/a	n/a	n/a

For the replicates of CB and NUNC DPBS, the Single Sample T tests indicated that CB produced endotoxin readings less than 0.25 EU/mL at 600 ng/µL ($P<0.001$, mean difference -0.24246) and 60 ng/µL ($P=0.001$, mean difference -0.23289) and that the NUNC plate leached less than 0.25 EU/mL ($P<0.001$, mean difference -0.24996). Additionally, the intraplate CV for these analyses was 8.314456. Therefore, null hypotheses for aims one and two of this portion of the project were rejected. CB protein harvest and NUNC plates were therefore determined as the optimal options for moving forward.

Two different goals are pursued in the remainder of this project using Indirect ELISAs: quantifying antibodies and quantifying proteins. For all experiments where serum antibodies or the "primary" is the experimental component of interest, standard curves will be established through serial dilution of the positive primary. Therefore, higher protein concentrations for the protein coat may be the preferred starting point for future ELISA development. For all experiments where the protein coat is the experimental component of interest, standard curves will be established through the serial dilution of the positive protein. In this case, the protein concentration range may need to be determined both by how much protein detection is expected in experimental samples and by where the protein concentration range provides an appropriate linear trend.

Two important hypotheses were not pursued within this project. The first is if the CB kit reduces the amount of endotoxin within the protein sample. The assumption was made that 1.5mL of *Salmonella* culture possessed endotoxins at a concentration greater than 0.25 EU/mL. This assumption should be tested to further explore the impact of the CB protocol. Additionally, it was assumed that endotoxins at <0.25 EU/mL in a 100µL volume would not produce

absorbances on an ELISA that would interfere with the detection of the *S.* Javiana or vaccine proteins. This assumption was tested later (Appendix B).

3.5.3. *In Vivo* Testing of pCP Vaccines

3.5.3.1. ELISA Data for Antibody Quantitation

Standard curves for 3 plates presented linearly and the other 2 presented sigmoidally. The mixed-effect model for those groups that had data for all three bleeds (Saline, pSCP, pSSCP, and pSECP) indicated no differences in antibody concentration between any time and/or treatment (P=0.6292) (Figure 3.11). The mixed-effect model for all groups but at just the 6- and 9-week bleeds indicated a difference (P=0.2677), however the only difference was between 1X DPBS (Saline) and Superfect groups at the 9-week bleed, as indicated by the Tukey Test (P=0.2426). Intraplate CVs ranged from 10.702 to 16.74407, and the interplate CV was 14.434.

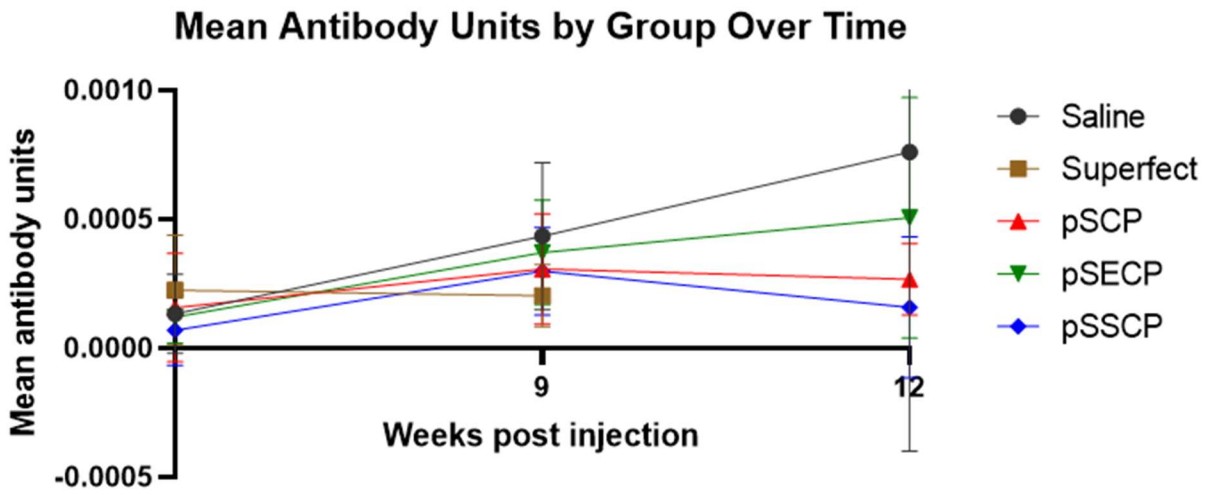

Figure 3.11. Plot of mean antibody units for each quail treatment group over time. Error bars are 95% CI. Antibody units refers to where the sample was interpolated on the standard curve.

All samples were indicated as "positive" when interpolated to the standard curve, but there was a lack of difference between the negative control groups and experimental groups. Therefore, any "positive" values could not be definitively attributed to the vaccine, and the null

hypotheses could not be rejected for aims one or two of this portion of the project. Shared housing, water, and food for the beginning of the study likely exposed all birds to anything that could create this positive reaction, but it is not guaranteed. Additionally, the true *Salmonella*-positive or negative state of the birds was called into question upon closure of quail provider facilities and these results.

True controls were not established for this project, and there were no true positive or negative controls commercially available for this project. For future work, a true positive and true negative control should be created for experimentation. For a true negative control, older birds should be swabbed for any *Salmonella* presence, and serum from *Salmonella*- negative birds (i.e., specific-pathogen free) should be collected. This negative control protocol was not conducted within this project because of the age of the birds obtained for the experiment, but additional older birds could be purchased for future experiments. For a true positive control, *Salmonella*-negative birds should be infected with *S.* Javiana, and serum collected at the same intervals as the vaccinated birds. Additional approvals would need to be obtained, and truly separate housing would need to be established for the infected birds. Clearances for infecting birds were not obtained in the given IACUC protocols, and truly separate housing arrangements were not known to be possible at the time of this experimentation. However, both hurdles for the positive control could be addressed in future testing.

3.5.3.2. Survival Analysis

The Kaplan-Meier survival analysis indicated that there was no significant difference in survival between any of the experimental groups at any time point when analyzed for 1 week or 12 weeks (P=0.7025; P=0.7189) (Figure 3.12). The additional Gehan-Breslow-Wilcoxon test indicated still that there was no significant difference in survival between any of the

experimental groups at any time point, even when survival proportions at the earlier time points were more heavily weighted (1 week P=0.7042; 12 weeks P=0.7336). Therefore, the null hypothesis for aim three of this portion of this project could not be rejected. These data indicate that there was potentially no relationship between the vaccine administration and bird death, which could indicate some degree of safety in the use of these vaccines. However, no necropsies were performed to determine a cause of death. No visual observations evidenced vaccine toxicity, but observations should be considered subjective. Future studies should conduct necropsies upon death to determine the cause, and additional studies should be performed to specifically evaluate the safety of any future vaccines.

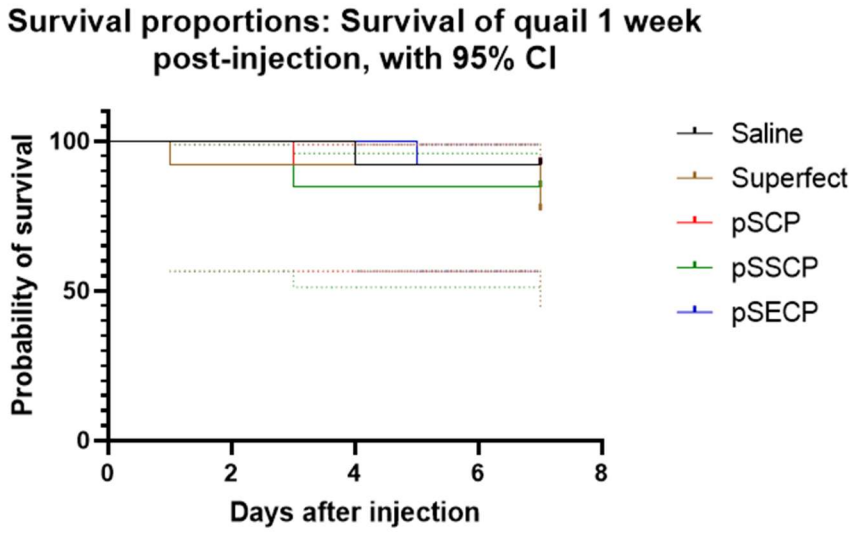

a.

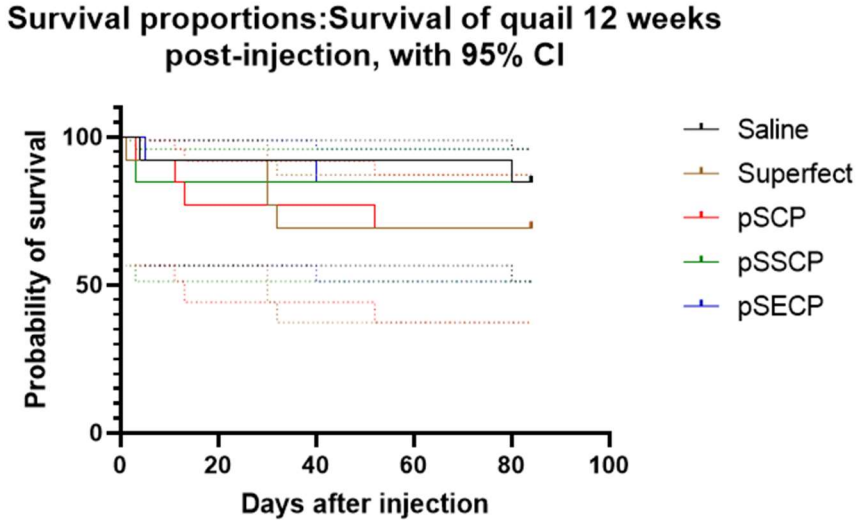

b.

Figure 3.12. Plot of probability of survival by days following injection according to Kaplan-Meier analysis. Top (a.) is the plot for the 1-to-8-week analysis in terms of days. Bottom (b.) is the plot for the 1-to-12-week analysis in terms of days. Error lines (dotted) for both plots are 95% CI.

3.5.4. *In Vitro* Testing of pCP Vaccines

3.5.4.1. Results for the Kill Curve

The flasks fed with 0.25µg/mL puromycin media solution never reached less than 5% confluency. The flasks fed with 0.4µg/mL puromycin media solution reached <5% confluency on the seventh day after initial exposure. The flasks fed with 0.6µg/mL reached <5% confluency at the third feeding day, or four days following initial treatment media exposure (Figure 3.13).

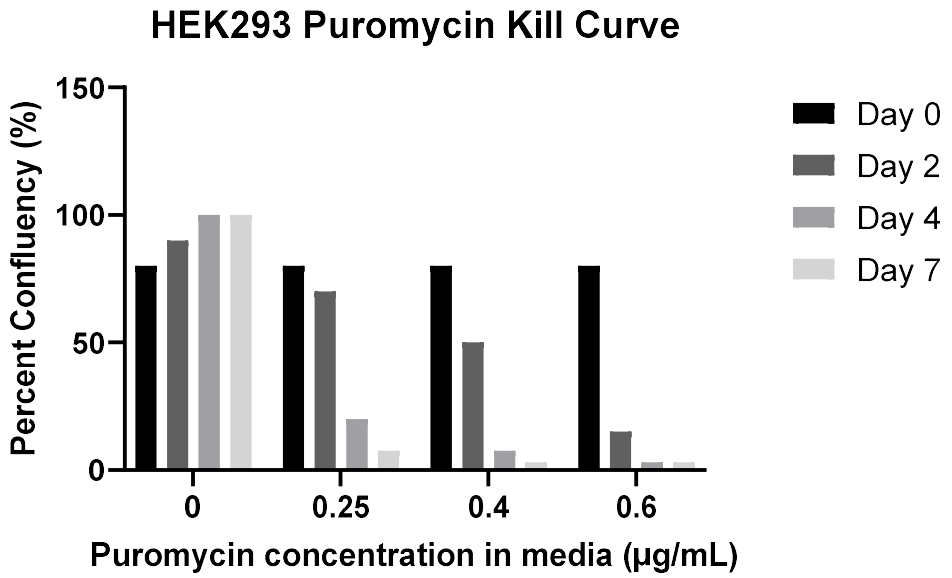

Figure 3.13. HEK293 puromycin kill curve results, visualizing the observed average confluency of remaining cells in flasks under each of the puromycin exposure conditions over time.

The goal of the kill curve was to quickly establish a concentration of puromycin necessary for killing an entire T25 flask of cells in one week, as to keep the selection process short, but not so short that toxicity could potentially overpower even the transfected cells [380]. Given this desired goal, the 0.4 µg/mL puromycin media solution was chosen to move forward in the transfection and sample collection protocol.

Triplicate flasks were later found to be a standard for kill curve analysis, which would likely provide a more reliable interpretation of antibiotics impact on cell persistence [384, 385].

If a kill curve is pursued again, it should be performed in triplicate rather than duplicate, as performed within this research, and perhaps with a wider range of antibiotic concentrations for future studies.

3.5.4.2. Results for the Transfection, Sample Collection, and Sample Analysis of Transcription

The experimental RT-PCRs for pSCP, pSSCP, and pSECP produced bands of the expected sizes as compared to the 1kb Plus ladder (Invitrogen, Ref 10787018): 792, 973, and 1282 bp respectively (Figure 3.14). The negative control RT-PCRs for pSSCP and pSECP did not produce any bands, and the pSCP negative control RT-PCR showed extremely faint bands identical to those in the experimental lane (Figure 3.14). The Lipofectamine control RT-PCRs did not produce any bands, aside from those indicating primer dimer (Figure 3.14). The sequencing for pSCP, pSECP, and pSSCP experimental RT-PCRs had a 100% match to each vaccine's open reading frame. A repeated SYBR safe-dyed gel with just the pSCP negative control did not reproduce the same faint band result as before, indicating that the bands visible in the pSCP negative control column were very likely because of spillover during gel loading. No picture is provided, as the SYBR safe-dyed gel was excised from the gel and used for sequencing purposes.

The initial attempt at the positive control RT-PCRs did not produce bright bands (Figure 3.14). The gradient RT-PCR on the non-transfected HEK293 mRNA samples produced the following results. ZNF223 positive control RT-PCRs were successful with the annealing temperature 46°C, and USP18 positive control RT-PCRs were successful with the annealing temperatures 58°C, 56°C, and 50°C. Success in all cases was indicated by the bright bands at approximately 163bp for ZNF223 (Figure 3.15) and 159bp for USP18 (Figure 3.14 and 3.15).

Additionally, sequencing for all positive control RT-PCRs had 100% matches to their respective housekeeping genes.

It was concluded that mRNA was successfully isolated from all treatment groups as determined by ZNF223 and USP18 primer RT-PCRs and sequencing. It was also concluded that transfection with all three vaccines and transcription of all three vaccines occurred as determined by the experimental RT-PCRs and sequencing. Therefore, aim one for this portion of this project was met.

a.

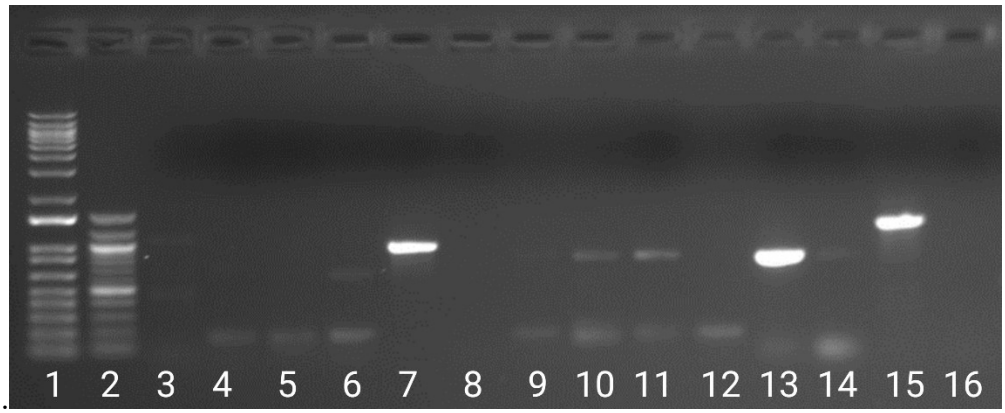

b.

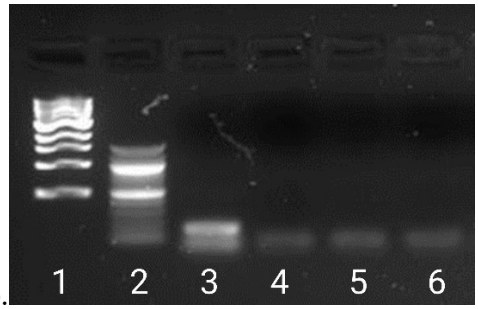

Figure 3.14. Gel confirmation of RT-PCRs showing the expected sizes. On top (a.) is a 1% agarose ethidium bromide gel with the following lane order: lane 1 - 1kb Plus DNA Ladder, lane 2 - 100bp DNA Ladder (New England Biolabs, N0467S), lane 3 - USP18 positive control 3, lane 4 - USP18 positive control 2, lane 5 - USP18 positive control 1, lane 6 - USP18 positive control 5, lane 7 - pSSCP Experimental, lane 8 - pSSCP Negative Control, lane 9 - ZNF223 positive control 3, lane 10 - ZNF223 positive control 2, lane 11 - ZNF223 positive control 1, lane 12 - ZNF223 positive control 5, lane 13 - pSCP Experimental, lane 14 - pSCP Negative Control, lane 15 - pSECP Experimental, lane 16 - pSECP Negative Control. Bottom (b.) is a 1% agarose ethidium bromide gel with the following lane order: lane 1- 1kb Plus DNA ladder, lane 2 - 100bp DNA Ladder, lane 3 - USP18 positive control 4, lane 4 - pSCP Lipofectamine Control, lane -5 pSSCP Lipofectamine Control, lane 6 - pSECP Lipofectamine Control.

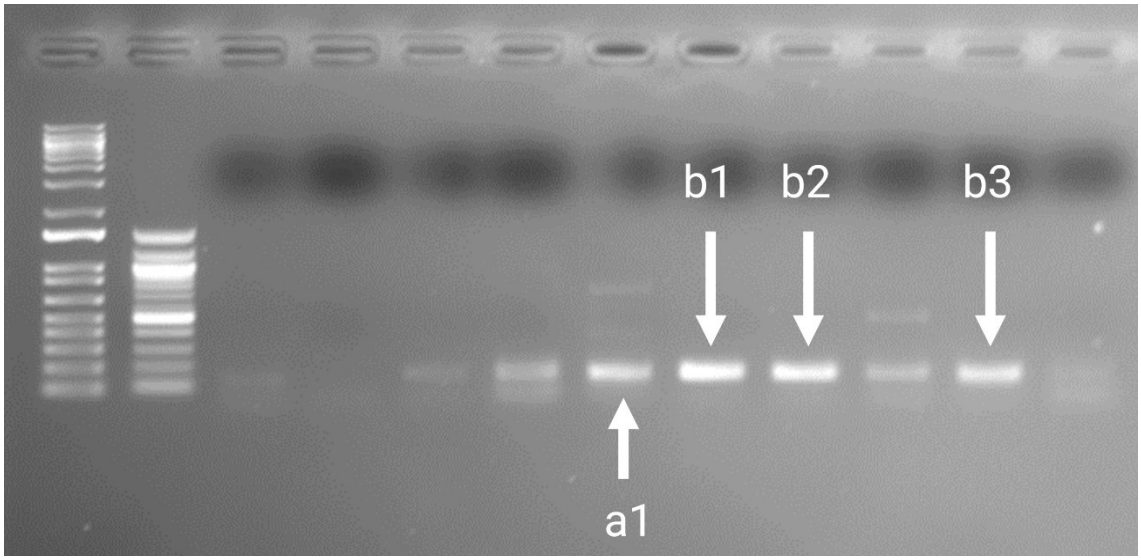

Figure 3.15. The 1% agarose gel dyed with ethidium bromide that allowed for visualization of the housekeeping RT-PCR bands for the non-transfected HEK293 mRNA cells. The first lane is 1kb plus ladder. The second lane is the 100bp ladder. Arrow "a1" is ZNF223 RT-PCR with denaturation temperature of 46°C. Arrows labeled "b" are the RT-PCR's with USP18 primers, and the numbers differentiate the denaturation temperatures: "b1" is 58°C, "b2" is 56°C, and "b3" is 50°C.

3.5.4.3. Results for the Transfection, Sample Collection, and Sample Analysis of Translation

The Correlation Test for the nine concentrations of protein from 60ng/µL down to 0.234 ng/µL produced a Pearson r value of -0.03701 (one-tailed P=0.4908) (Figure 3.16). The Correlation Test for the five concentrations of protein from 3.75 ng/µL down to 0.234 ng/µL produced a Pearson r value of 0.9227 (one-tailed P=0.0128), and the null hypothesis for aim four of this portion of this project was rejected (Figure 3.16). Therefore, it was determined that ELISAs on the cell culture samples should include the five concentrations of protein from 3.75 ng/µL down to 0.234 ng/µL to serve as the standard curve.

The data interpolated to this standard curve for the cell culture reagent test only produced a positive value for the undiluted LEB (0.346 ng/µL) (Figure 3.17). CVs for the entire plate

ranged from 1.168772 to 27.89945 for all samples tested, except for FBS at a dilution factor of 2 (CV=93.94274).

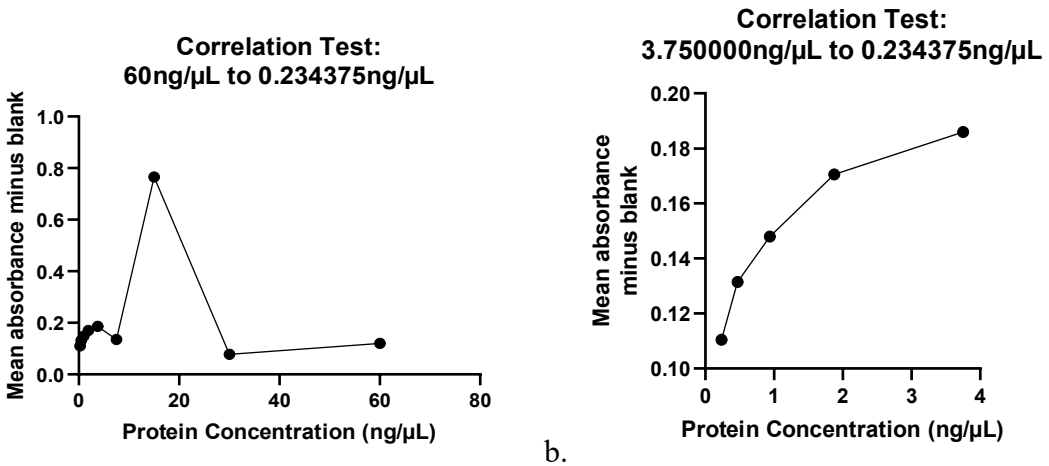

a. b.

Figure 3.16. Correlation test graphs for initial standard curve establishment tests. Left (a.) are the plotted values of absorbances produced for protein concentrations ranging from 0.234 ng/µL to 60 ng/µL. Right (b.) are the plotted values of absorbances produced for protein concentrations ranging from 0.234 ng/µL to 3.75 ng/µL.

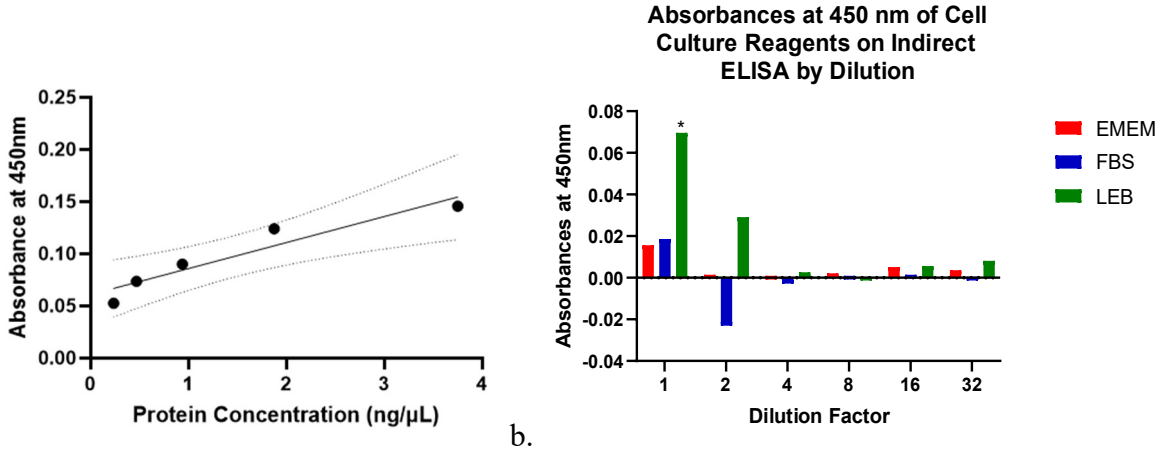

a. b.

Figure 3.17. Cell culture reagent reactivity test results. Left (a.) is the standard curve used for interpolation of absorbance values from cell culture reagents tested on indirect ELISA. Right (b.) are the graphed absorbances of the reagents on the indirect ELISA by dilution factor. The * indicates the only absorbance high enough to be interpolated to the standard curve, which was from undilute LEB.

The interplate CV when looking at the standard curves of the cell culture reagent-ELISA and lysate/media ELISA was 4.656.

The standard curve of 3.75 ng/µL down to 0.234 ng/µL on the cell culture sample ELISA was not positively correlated (r=0.7901; P=0.0559). However, 1.875 ng/µL down to 0.234 ng/µL was positively correlated (r=0.9886; P=0.0057) (Figure 3.18). All cell culture experimental and control lysate samples produced positive values when interpolated to the standard curve when diluted by ½ and ¼ (Figure 3.18). The only media sample to produce a positive value when interpolated to the standard curve was NT diluted to ¼, pSCP diluted to ½, and pSECP undiluted (Figure 3.18). CVs for the entire plate ranged from 0 to 13.5828. Given that the negative control samples produced positive values, it cannot be determined if the vaccines produced proteins. Therefore, the null hypotheses for aims two and three of this portion of this project could not be rejected.

Given the disparity in positive values overall between lysates as compared to media, it is hypothesized that there is something about the HEK293 cells that is reacting with convalescent horse serum. Further investigation would be needed to establish the cause of the reaction. The established lack of reaction to LEB when diluted by at least one half should also be questioned, as the LEB tested was mixed after the LEB for the cell samples. Therefore, future experiments should save a portion of the LEB used within the experiment, store it in the same manner as the samples, and use that LEB as background on future plates. The same should be done for spent media.

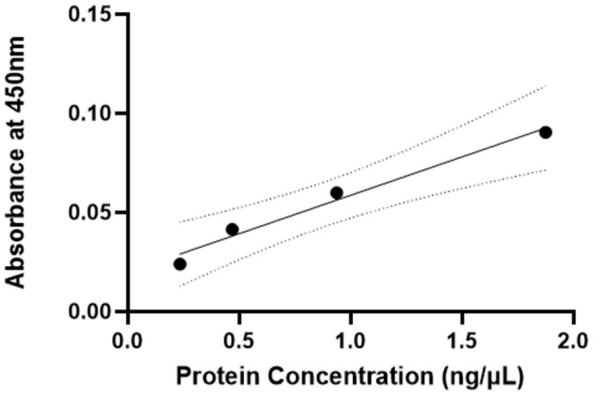

a.

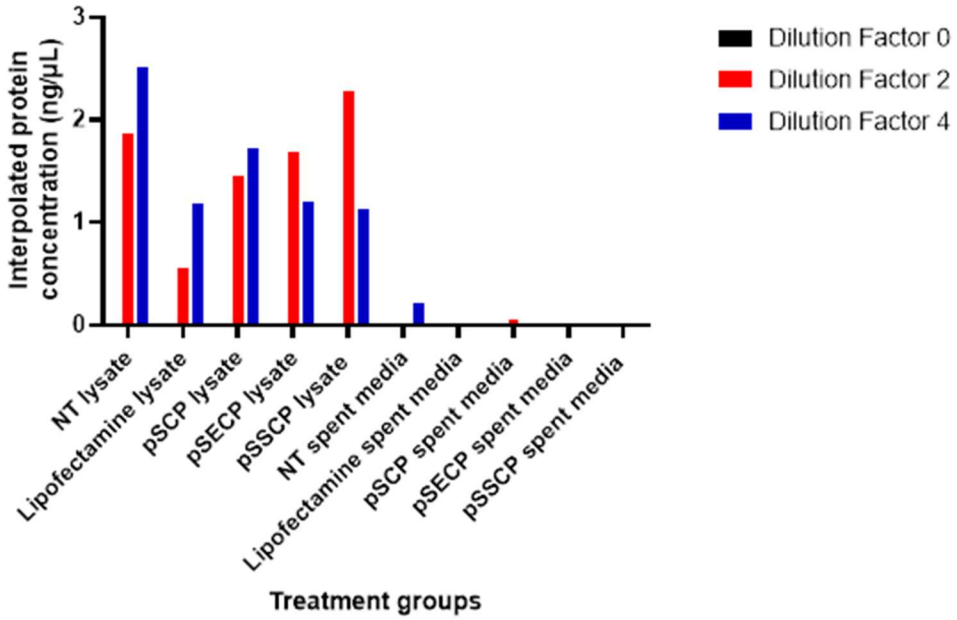

b.

Figure 3.18. Cell culture lysate and spent media sample results. Top (a.) is the standard curve used for interpolation of absorbance values from cell culture samples tested on indirect ELISA. Bottom (b.) is a bar graph of the interpolated detected protein values from indirect ELISAs by samples tested. Samples were HEK293 lysate and spent/waste media from non-transfected (NT) cells, Lipofectamine3000-only exposed cells, and pCP-vaccines-exposed cells.

The entirety of the *in vitro* portion of this project was treated as a pilot trial, and the number of flasks was determined by how much lysate would be needed per group to be able to troubleshoot ELISAs. The combining of lysates into a single tube transitioned the sample size from 6 to 1, and therefore, statistical analysis was not possible. Flasks should be kept separate to allow for statistical analysis in future studies.

Overall, the results were treated as follows: reject the null in favor of the alternative hypothesis for aim one, meaning that transcription of the vaccine did occur within the eukaryotic cells; and no rejection of the null hypotheses of aims two and three, meaning that there was no evidence of detectable translation or secretion of proteins that are definitively from the vaccines.

The culmination of results from this portion of this project and the *in vivo* trial indicates that there is either a design flaw in the vaccines and/or an issue with assay specificity. Regarding the vaccine design, components specific to mRNA stability and translation should be reevaluated because translation was not definitively determined in cell culture. This hypothesis is further supported by the lack of definitive antibody production to the vaccines in the *in vivo* trial as well because proteins would need to be produced for antibodies to be made. Additionally, further optimization of the ELISA protocol or a new assay needs to be established.

Chapter 4. Round Two of Vaccine Design and Testing

4.1. Introduction

As was demonstrated in Chapter 3 of this project, protein or resulting antibodies were not definitively detectable from the pCP versions of the vaccines *in vitro* or *in vivo* differentially from negative controls. The reasons for these outcomes could be multi-faceted. Transcription of the pCP vaccines was confirmed in *in vitro* testing, so those components specific to transcription should not necessarily be altered. The lack of clear evidence for translation could be due to the design/selection of mRNA-stability-specific vaccine components, translation-specific vaccine components, and/or because of the lack of specificity of the assays available. All three of these potential problems are addressed in this chapter.

4.1.1. UTRs

Untranslated regions (UTRs) are sequences that, while not translated themselves, aid in the translation process [386]. They aid in maintaining mRNA stability during translation, they slow down adenylate/uridylate-rich element-mediated decay, and they generally enhance translation [187, 285, 387]. There are two UTRs involved in transcription and translation, the 5' UTR and the 3' UTR. The 5' UTR is the one involved in the actual translation process, typically possessing the Kozak sequence that encompasses the methionine start codon for the ORF. The 3' UTR is the one that maintains mRNA stability and prevents degradation [386].

When researching the functions of UTRs, literature is primarily focused on mRNA vaccines or genes found in nature, with only two articles specifically mentioning 3' UTRs as part of a potential pDNA vaccine design [187, 285, 286, 386-388]. Given that UTRs are known necessities for the translation of mRNA vaccines, translation being among the list of goals of a

pDNA vaccine, it stands to reason that a pDNA vaccine should probably include such components.

The pCP version of the vaccines within this project possessed CMV intron A, which functions as a 5' UTR when downstream of a TATA box and upstream of a Kozak sequence [389, 390]. CMV intron A is found within the CMV promoter and the Kozak sequence partially comprises the start codon of the previous vaccine designs [390]. However, the pCP versions of the vaccines within this project did not possess a 3' UTR, potentially impacting mRNA stability.

There are a wide variety of 3' UTR sequences available. However, among those used in commercial circulation and widely within nucleic acid vaccine research are synthetic versions of *Homo sapiens* hemoglobin subunit alpha 1 gene (*HBA1*) 3' UTR [386]. *HBA1* is located on chromosome 16, and comprises the instructions for making alpha-globin, a subunit of hemoglobin [391]. There are synthetic versions of the *HBA1* 3' UTR sequence that are available and successfully functioning in commercially available mRNA vaccines. However, these sequences are patented and require permission or licensing to use [386]. Therefore, to avoid any conflict with patented sequences, a publicly available and naturally occurring *HBA1* 3' UTR sequence was selected for use in the next phase of the vaccine design.

4.1.2. Polyadenylation

The superiority of SV40 poly(A) signal sequences is explained in Chapter 3 of this project. Hence, its use within this project previously. With a plethora of sequences to choose from, key functional components of the SV40 poly(A) signal in transcription termination and tail addition for stability are a 5'-AATAAA-3' sequence followed by a 5'-CA-3' cleavage site, which is ideally subsequently followed by a GT-rich region [392-398]. The AATAAA sequence is the signal for the addition of the poly(A) tail. The CA cleavage site is where the adenines are

added, and the GT-rich region aids in the poly(A) processing [393]. AATAAA is recognized by the cleavage and polyadenylation specificity factor (CPSF) and the GT-rich region is recognized by the cleavage stimulation factor (CstF). The CstF binds CPSF and the carboxyl-terminal repeat domain (CTD) of the RNA polymerase II large subunit. The CTD is necessary for the CA site cleavage and transcription termination, and this culmination of bonds causes RNA polymerase II to pause, slowing the polymerase enough to begin 3'-end processing [399]. While the pCP versions of the vaccine possessed a poly(A) signal sequence, incorporating a simplified version with easily identifiable AATAAA, CA, and GT-rich regions may be necessary.

4.1.3. Affinity Tagging for Protein Detection

Affinity tags are small amino acid sequences designed in the ORF to be expressed on the N- or C- terminus of a protein that are easily detectable [400, 401]. They are commonly used to help identify protein production for which there are no available antibodies with protein specificity. Common affinity tags include CBP, FLAG, HA, Myc, poly His, S-tag, and V5 [401]. Each possesses its own particular set of specific uses and benefits, but the poly His tag has the particular advantage of rarely impacting protein folding or function even without an FRS to separate it from an upstream or downstream protein [401-403]. However, some evidence indicates that N-terminus 6XHis has an increased likelihood of impacting protein folding, so C-terminus additions were used in this project [402].

Poly His tags consist of 6 to 10 consecutive histidine repeats [404]. The most commonly used poly His tag is the 6XHis tag which is among the smallest available protein tags with a molecular weight of only 0.8kDa [403, 404]. 6XHis tags' lack of influence on adjacent protein folding is attributed to their small size [401-403].There is a wide range of assay applications for 6XHis tags because of their stability in a variety of buffers and detergents, nonimmunogenic

nature, affinity for a wide range of metals, as well as commercial availability of highly specific and sensitive antibodies for this particular tag [403, 405]. Among these assay applications are ELISAs and Western blots [405].

ELISAs within this project, up to this point, were using convalescent serum which is nearly guaranteed to possess antibodies to several other foreign bodies in addition to *S.* Javiana. Cross-reactivity of those antibodies within the assay was not determined beyond the scope of those against endotoxins. Attempting to screen beyond affinity for endotoxins is a task that is inconvenient and expensive at best. The incorporation of a 6XHis tag will allow for continued use of ELISAs as an assay but increase the specificity of the assay within this project.

4.1.4. Horse Antibodies

The benefit of using the convalescent horse serum within this project is that it possibly allows for evaluation of the vaccine epitopes being produced. If the vaccine's protein is recognized by antibodies following a natural infection, then, it stands to reason that antibodies resulting from that vaccine could recognize a natural infection. A major limitation in previous research within this project was the unknown timeline for infection and serum acquisition for the horses from which serum was obtained. Therefore, it may be that a secondary antibody other than, or in addition to, an anti-IgM is necessary for detection of vaccine-encoded proteins.

IgG antibodies, like IgM, are among the classes of antibodies produced following a *Salmonella* infection, but they are known to last longer than IgM after a natural infection and are the predominant antibody found in serum [255, 406-409]. IgG antibodies are monomeric and come in a variety of isotypes or subclasses [410]. Previous research indicates that creation of IgG subclasses IgG1, 3, 4, and 7 from vaccination leads to better protection than other IgG isotypes, especially via complement-mediated pathways. IgG(T) corresponds to IgG3 and IgG5, covering

one of the recommended subclasses for vaccination. A specific IgG(T) secondary, Goat anti horse IgG(T) (Bio-Rad, product code AAI28), can recognize not only IgG3 and 5, but also IgG2, broadening the spectrum for subclass detection [410].

4.1.5. The Cells and Transfection Methodologies

HEK293 cells are commonly used in recombinant protein production. However, they are not an immune cell, which is the cell type that vaccines target in *in vivo* studies. J774A.1 cells are monocyte-macrophages commonly used in *in vitro* immunology research and are more similar to the APCs that will be targeted upon vaccination than HEK293 cells [411]. However, J774A.1 cells are not commonly used in transfection studies for recombinant protein production –the goal of cell culture for vaccine testing– but rather for immune cell motility and deformation studies [412]. This is likely in-part due to difficulties involved in their successful transfection [413].

Methods of transfecting J774A.1 cells used in published research include calcium phosphate methods and electroporation, the latter being the apparently more recently and frequently used methodology [414-417]. Electroporation is a high-voltage electric shock that increases cell permeability and allows DNA to enter. It is considered suitable for most cell types and is a time-efficient process [418]. While electroporation has been used for transfecting HEK293 cells, it is not among the preferred methods [419-421]. Among the more common methods of transfecting HEK293 cells is the use of cationic lipids, such as the Lipofectamine3000 reagent used in Chapter 3 of this project [422]. While Lipofectamine3000 is known to be an effective reagent in HEK293, it is not known to be such for J774A.1 cells [423, 424].

An additional *in vitro* transfection reagent became available at the time of this project that is of the same product line as the intended *in vivo* transfection reagent for future quail studies. The *in vitro* reagent, called jetOPTIMUS®, is a cationic nanotechnology intended for use in a variety of cell lines including HEK293 [425, 426]. While J774A.1 cells are not specified as an intended target cell-line, Polyplus does make the claim that is good for use in "adherent hard-to-transfect mammalian cell(s)," a category that J774A.1 cells arguably fall under [427]. Additionally, there is some evidence that transfection of J774A.1 cells is possible via cationic lipids, but studies comparing electroporation and cationic- or lipid-based transfection methods within J774A.1 could not be found [428].

Each transfection reagent and methodology previously mentioned varies in its recommended cell confluency, DNA amount, and DNA volume. Lipofectamine3000 recommends 70-90% confluency and jetOPTIMUS® recommends 60-80% confluency at the time of transfection [429, 430]. The electroporation protocols recommend anywhere from 33% confluency at the time of transfection to 70-80%, and others recommend a specific cell count [415, 431-433]. The protocol for the machinery available for this project recommends 3×10^6 cells for electroporation [431]. DNA amount recommendations for Lipofectamine3000 and jetOPTIMUS® are 19.53µg per T75 flask and 10µg per T75 flask respectively, and electroporation protocols recommend DNA concentrations ranging from 2ng/µL to 30ng/µL, with quantity range depending on the machinery being used [429-432]. Therefore, there is a need to evaluate these three methodologies under a range of conditions within HEK293 and J774A.1 cells.

4.1.6. Tracking transfection, GFP

Green fluorescent protein (GFP) is a commonly used marker protein within a variety of biological research fields [434, 435]. While the protein originated in jellyfish, synthetic versions exist for specific uses, including pDNA-encoded protein for cell transfection tracking [435, 436]. This GFP-expressing pDNA allows researchers to visually determine the presence of protein production within a given cell line, which is particularly useful when comparing transfection methodologies for pDNA applications [435].

The plasmid selected for this project is the lentiviral pLKO.1-puro plasmid (pGFP) from SigmaAldrich (cat: SHC003). This plasmid was selected for three reasons. The first and foremost reason was because the GFP gene is under control of a CMV promoter, the same promoter that the pDNA vaccines of this project contain [437]. The second reason was that this plasmid is known to lead to visible protein production within at least one of the two cell lines of interest– HEK293 [438]. The third reason is that the pGFP vector is about 2800 bp larger than the new vaccine design within this project, which means that it should theoretically be harder to get into cells than the new vaccine [437]. If pGFP can get into the cells, then transfection with the new vaccine design should be even easier. GFP, including that from the selected vector for this project, are typically harvested 2 days to 5 days post-transfection, and evidence of transfection is visible at day 1 [438-440]. However, no previous research could be found to establish a timeline for this pGFP in HEK293 cells or J774A.1 cells.

4.1.7. Cell Counting with ImageJ by JavaScript and Flow Cytometry

Wayne Rasband developed an automatic cell counter called ImageJ, alternatively known as NIH Image, in 1997 [441-443]. Since its inception, the program has been continuously improved upon as a group effort which included the eventual use of JavaScript as the software

support system [441]. ImageJ has a range of uses, among which is automated cell counting [444-446]. Its use in quantification of fluorescing cells, specifically with GFP, has appeared in several publications [442, 447, 448].

Flow cytometry is a technique for detection and measurement of physical and chemical characteristics of cells. Just within the realm of this project, flow cytometers use lasers to excite fluorescent stains or proteins found within a population of cells and then sort and count those cells based on those excitations [449]. Flow cytometry can also analyze cells based on size and granularity, referred to as "gating." Gating ensures that the data being analyzed is from the cells of interest and not debris. Forward scatter (FSC) is used to gate for size, and side scatter (SSC) is used to gate for complexity [450].

4.1.8. Project Description

This project is in response to the results from Chapter 3. The first portion of this project addresses the potential shortcomings in the cell type and transfection methodologies in Chapter 3's *in vitro* testing. This is done through the comparison of Lipofectamine3000, jetOPTIMUS® and electroporation methodologies in HEK293 versus J774A.1 and comparison of their protein-production timelines. The second portion of this project addresses the potential shortcomings of the pCP design and protein assay specificity, as outlined in the introduction of this chapter. This is done first through the redesign and construction of one of the pCP vaccines. Then, the new vaccine will be tested via use of an affinity tag and newly determined transfection and harvest parameters. Finally, this chapter will also re-explore the immunogenic potential of the originally selected epitopes.

4.2. Aims and Hypotheses

4.2.1. Comparing Transfection Efficiency of Different Methods in Two Cell Types Through GFP

The overall aim of this portion of the project was to determine an optimal protocol for cell culture testing of the pDNA.

4.2.1.1. Aims and Hypotheses for "Equalized" Protocols

Aim 1 was to identify which cell line and transfection method combination(s) are most efficacious for future use with the pDNA vaccines– Lipofectamine3000, jetOPTIMUS®, or electroporation with either HEK293 or J774A.1. There are two hypotheses for aim 1. The first is that there will be a difference in percent fluorescence between at least 2 experimental groups after 24 hours, where "experimental group" refers to the combination of a transfection method, presence or absence of pGFP, and cell type (H_0: $\mu_{NH} = \mu_{LHG} = \mu_{LH} = \mu_{OHG} = \mu_{OH} = \mu_{EHG} = \mu_{EH} = \mu_{NJ} = \mu_{LJG} = \mu_{LJ} = \mu_{OJG} = \mu_{OJ} = \mu_{EJG} = \mu_{EJ}$; H_1: Not H_0). The second hypothesis for aim 1 is that there will be a difference in the total cell counts between at least 2 experimental groups at 24 hours post-transfection.

Aim 2 was to determine when peak protein production will take place within the tested transfection parameters. The hypotheses for aim 2 are that there will be a difference in percent fluorescence between at least 2 time points within or between experimental groups transfected with pGFP (H_0: $\mu_{G1} = \mu_{G2} = \mu_{G3} = \mu_{G4}$; H_1: Not H_0) and there will be a difference in the total cell counts between at least 2 time points within experimental groups transfected with pGFP.

4.2.1.2. Aims and Hypotheses for "Optimized"

The aim of this portion of the project was to identify which cell line and transfection method combination(s) are most efficacious for future use with the pDNA vaccines– Lipofectamine3000, jetOPTIMUS®, or electroporation with either HEK293 or J774A.1. Efficacy

was demonstrated through flow cytometry output ratios of GFP fluorescing and viable cells. There are two hypotheses for the aim. The first is that there will be a difference in the percentages of cells that are both GFP fluorescing and viable between at least 2 experimental groups after 24 hours, where "experimental group" refers to the combination of a transfection method, presence or absence of pGFP, and cell type (H_0: $\mu_{NH75} = \mu_{LHG} = \mu_{LH} = \mu_{OHG} = \mu_{OH} = \mu_{EHG} = \mu_{EH} = \mu_{NJ75} = \mu_{LJG} = \mu_{LJ} = \mu_{OJG} = \mu_{OJ} = \mu_{EJG} = \mu_{EJ}$; H_1: Not H_0).

4.2.2. pSC6 Vaccine Design and Construction

The first aim of this project is to reduce the size of the existing vaccines by removing the puromycin resistance gene. The second aim of this project is to further modify the vaccines by incorporating a non-patented 3'UTR sequence, swapping the poly(A) signal sequence for a simplified version, and adding an affinity tag without altering other sequences within the vector. The hypothesis is that the pSCP vaccine will be modified in accordance with the aims, as evidenced by electrophoresis size verification and sequencing with 100% match to the entirety of the plasmid.

4.2.3. *In Vitro* pSC6 Testing

The first aim of this portion of this project pertains to aims two and three. Aim one is to determine what range of protein concentrations and antibody parameters will produce a positive linear trend (i.e., the standard curve). The hypothesis for aim three is that proteins serially diluted somewhere between 10μg/μL and 0.625ng/μL will produce a positive correlation coefficient that is significantly different from zero on an ELISA when exposed Anti-6X His antibodies diluted to 1:5000, 1:10,000, or 1:20,000 (H_0: $\rho=0$; H_1: $\rho > 0$).

The second aim of this portion of the project is to determine if the pSC6 vaccine will be translated upon transfection. The hypothesis for aim two was that the vaccine would produce

protein concentrations in lysates that are detectable on a direct ELISA when exposed to Anti-6X His— i.e., pSC6 lysate samples will produce higher absorbances or interpolated protein values than the control lysate samples (H_0: $\mu_{C1} = \mu_{C2} = \mu_{SC6}$; H_1: Not H_0).

The third aim of this portion of the project is to determine if the translated proteins are being secreted. The hypothesis for aim three was that the vaccine would produce protein concentrations in spent media that are detectable on a direct ELISA when exposed to Anti-6X His—i.e., pSC6 spent media samples will produce higher absorbances or interpolated protein values than the control spent media samples (H_0: $\mu_{C1} = \mu_{C2} = \mu_{SC6}$; H_1: Not H_0).

4.2.4. Evaluating Immunogenic Potential

The first aim of this portion of the project is contingent on aims two and three of section 4.2.3. This aim is to determine if the translated proteins from pSC6 are detectable via the convalescent horse serum used in Chapter 3 of this project. The hypothesis for this aim is that pSC6 samples will produce higher absorbances or interpolated protein values than the control samples when exposed to the convalescent horse serum in combination with either an anti-horse IgM or anti-horse IgG antibody (H_0: $\mu_{C1} = \mu_{C2} = \mu_{SC6}$; H_1: Not H_0).

The second aim of this portion of the project is to determine if MHC-II binding predictions will be maintained at the time of these experiments as compared to this dissertation's inception. The hypothesis for this aim is that MHC-II binding predictions for the vaccine epitopes from the IEDB Analysis Source software will match the predictions produced in Chapter 2 of this project.

4.3. Materials and Methods

4.3.1. Comparing Transfection Efficiency of Different Methods in Two Cell Types Through GFP

All cells were grown and maintained in a 37℃ incubator with 5% CO_2 supplementation. Flasks were all checked for confluency subjectively by observation under a microscope. All flasks upon transfection had 70-90% confluency and were labeled for their treatment group. Additionally, each flask within each treatment group was labeled A, B, C, D, or E.

NEB 5-alpha F'I^q Competent *E. coli* (Cat C2992) were transformed with 250ng of pGFP and harvested via ZymoPURE™ II Plasmid Midiprep kit. Midiprepped pGFP was quantitated via the Molecular Devices Quick Drop, then stored at 4℃ until ready for use. The harvested pGFP was also sequence verified by GeneLab.

Note that all mentions of PBS refer to molecular grade 1X DPBS without calcium or magnesium (molecular grade 1X DPBS) (Thermofisher Scientific, Massachusetts, Catalog Number 14190144) unless otherwise specified.

4.3.1.1. "Equalized" Protocols

Transfections within each cell were conducted simultaneously to ensure that the cells were in the same condition across all transfections. The goal for confluency was 70% across all flasks- approximately the average recommended confluency between the various protocols. In a further effort to reduce the number of varied variables across all transfection protocols, the DNA amount used for each transfection was 10 µg per flask- again determined by taking the approximate average of the recommendations of the different protocols. DNA volumes were determined by each transfection reagent protocol recommendation, all DNA dilutions were performed in PBS, and all flasks, regardless of treatment group, had a final total content volume of 25mL upon completing each transfection.

All HEK293 treatments were administered on the same day, and all J774A.1 treatments were administered later on the same day. Protocols across the two cell types were nearly identical, and steps that were altered were done so to accommodate the ATCC recommendations for the handling of each cell type (i.e., splitting protocols).

4.3.1.1.1. HEK293 Transfections

HEK293 cells (CRL-1573 batch #70039815 from ATCC) were grown in Eagle's Minimum Essential Medium (EMEM) (ATCC, Cat # 30-2003) supplemented with 10% FBS (SAFC Biosciences, cat: 112-300-101) in T75 flasks (Corning, Ref 431641 U). When cells reached 70% confluency, cells were split after the PBS rinse via exposure to 3mL TrypleExpress and light tapping. Then, the cell suspension was aliquoted into new T75 flasks until there were 35 flasks - 5 flasks per group. Cells were passaged 3 times before transfection.

The flasks assigned to the non-transfected group (NH.1) were rinsed with 10mL of PBS, fed with 25mL of 10% FBS EMEM, and returned to the 37°C incubator.

For flasks assigned to Lipofectamine3000 with pGFP (LHG.1) and Lipofectamine3000 without pGFP (LH.1) groups, the media was removed, cells rinsed with 10mL of PBS, fed with 23mL of 10% FBS EMEM. Flasks were then returned to the 37°C incubator until the transfection mixtures were ready for use - no more than 2 hours. Lipofectamine3000's (Invitrogen, Ref L3000-015) largest surface area protocol was for a six-well plate, or 9.6cm^2. All volumes were therefore multiplied by the quotient of the surface areas of the T75, or 75cm^2, flask to a standard six-well plate to determine the volume of each reagent for use. The calculated quotient was 7.81, and the protocol as recommended by Invitrogen was followed with this quotient applied to each reagent (ThermoFisher Scientific, 2016) (Appendix A). LHG.1 and LH.1 underwent the exact same protocol, but LH.1 received PBS in place of the pGFP.

For the jetOPTIMUS® with pGFP (OHG.1) and without pGFP (OH.1) groups, the jetOPTIMUS® *in vitro* DNA transfection reagent protocol for 100mm/flask 75cm^2 from PolyPlus was followed for utilization of the jetOPTIMUS® kit (PolyPlus, Ref 117-01) (Appendix A). OH.1 received PBS in place of the diluted pGFP. The following modifications were made to the PolyPlus protocol. During the 10-minute incubation of the jetOPTIMUS® reagents, media was removed from the flasks and the attached cells were rinsed with 10mL PBS. The cells of each flask were then released into suspension by using 3mL TrypleExpress and light tapping. Once fully suspended, 7mL of 10% FBS EMEM were added to each flask to bring the volume total to 10mL per flask and deactivate the TrypleExpress.

For the Electroporation with pGFP (EHG.1) group, Survey Number 156 of the Gene Pulser Electroprotocols from BioRad was used as a guide in combination with notes from a colleague who previously performed the protocol [273, 451]. To begin, five 4mm-gap cuvettes (BTX Harvard Apparatus, 45-0126) were loaded with 10µg of midiprepped pGFP each and labeled to match a specific flask. Old media was discarded from all 5 flasks, and the attached cells were rinsed with 10mL PBS. All cells were then released into suspension by using 3mL of TrypleExpress per flask and light tapping. Complete suspension was verified visually by microscope. Once fully suspended, the 3mL of suspended cells were transferred to a 15mL conical tube with a matching label and 4mL 10% FBS EMEM to deactivate the TrypleExpress and reduce toxicity. To further ensure that TrypleExpress toxicity was reduced, tubes were centrifuged at 1300rpm for 10 minutes, and supernatant was gently removed via pipetting to remove as much of the TrypleExpress as possible. Eight hundred microliters (800µL) of fresh 10% FBS EMEM were added to each conical tube to resuspend the cells via pipetting. The 800µL of resuspended cells were then transferred to the pre-loaded cuvette with a matching

label. Cuvettes were then loaded into the Gene Pulse apparatus (Bio-Rad) and received a 0.2kV shock followed by an incubation at 37°C for 20 minutes. During the 20-minute incubation, the original flasks were filled with 24mL 10% FBS EMEM each and returned to the 37°C incubator until the cuvette incubation was complete. After the 20-minute incubation was complete, contents of each cuvette were transferred to the flask with the matching label via aspiration with the pipettes provided with the cuvettes. For the Electroporation without pGFP (EH.1) group, the EHG.1 protocol was followed, but the 10µg of midiprepped pGFP per transfection were not included. All electroporation flasks, with and without DNA, had actual voltages of 0.2kV and capacitances of 960F. Table 4.1 shows the time constants of each individual flask, which ranged from 14.5 to 15.6 msec.

Table 4.1. Time constants for each HEK293 electroporation flask with "equalized" protocols as displayed by the Gene Pulse apparatus following 0.2kV shock.

Flask Label	**Time Constant for "With DNA" flask (msec)**	**Time Constant for "Without DNA" flask (msec)**
A	14.8	14.8
B	14.5	14.8
C	15.0	15.3
D	14.8	15.6
E	14.8	15.4

4.3.1.1.2. J774A.1 Transfections

J774A.1 cells (ATCC, TIB-67 batch #70040953) from *Mus musculus* were grown in Dulbecco's Modified Eagle Medium (DMEM) (cat 30-2002 from ATCC) supplemented with 10% FBS (SAFC Biosciences, cat: 112-300-101) in T75 flasks (Corning, Ref 430720U). Cells

were fed every other day with the 10% FBS DMEM and split via scraping into new T75 flasks until there were 35 flasks total- 5 flasks per group.

The non-transfected J774A.1 cells (NJ.1) group flasks were rinsed with 10 mL PBS and fed with 25mL of 10% FBS DMEM on transfection day.

The flasks assigned to Lipofectamine3000 with pGFP (LJG.1) and Lipofectamine3000 without pGFP (LJ.1) groups followed the same protocols applied to LHG.1 and LH.1 respectively.

For the jetOPTIMUS® with pGFP (OJG.1) group and jetOPTIMUS® without pGFP (OJ.1) group, protocols for OHG.1 and OH.1 were followed respectively. However, instead of using TrypleExpress to suspend the cells and deactivating the TrypleExpress enzyme with complete media, the cells were scraped into 10mL 10% FBS DMEM using cell scrapers.

The Electroporation with pGFP (EJG.1) group and Electroporation without pGFP (EJ.1) group were transfected following protocols for EHG.1 and EG.1 respectively. However, instead of using TrypleExpress and the complete media to deactivate the TrypleExpress, cells were scraped into 3mL 10% FBS DMEM, centrifuged in accordance with EHG.1 and EG.1, supernatant decanted, and pellet resuspended in 800µL 10% FBS DMEM. Time constants for these transfections are outlined in Table 4.2 and ranged from 15.7 to 16.8.

Table 4.2. Time constants for each J774A.1 electroporation flask with "equalized" protocols as displayed by the Gene Pulse apparatus following 0.2kV shock.

Flask Label	Time Constant for "With DNA" flask (msec)	Time Constant for "Without DNA" flask (msec)
A	16.2	16.8
B	16.4	16.0
C	16.2	16.6
D	16.0	16.5
E	15.7	15.7

4.3.1.1.3. Harvesting Lysate and mRNA

HEK Flasks A and B underwent the following lysate collection protocol at 48 hours post transfection. HEK flasks C, D, and E underwent the following lysate collection protocol at 5 days post transfection. J774A.1 flasks all underwent the following lysate collection protocol at 48 hours post-transfection, but no other flasks were harvested beyond that time due to observations of death.

Lysate harvest was performed by first making a new LEB formulation by combining 280µL of a 200mM PMSF in 100% ethanol (Life Technologies, cat 36978) with 55.16mL M-PER (ThermoScientific, Ref 7850) and 560µL Halt Protease Inhibitor Cocktail (100x) (ThermoScientific, Prod # 1862209), achieving final concentrations of 1mM for PMSF and 1% for Halt Protease Inhibitor Cocktail (100x) following Cold Spring Harbor's 2007 protocol, as opposed to the protocol previously used [452-454]. The new LEB formulation will be referred to as LEB2.

The LEB2, PBS, and flasks were placed on ice until chilled. Flasks were rinsed with the chilled PBS to remove any residual waste media, and then, 4mL LEB2 was added to each flask. Cell scrapers were used to detach the cells from the flask and transfer them into the LEB2 for

cell lysis. The LEB2 and cells were aspirated and transferred to pre-chilled 15mL conical tubes, one tube per experimental group. The combination of flasks at this point was to ensure that there was enough lysate per group to perform follow-up analyses as needed. The conical tubes were then vortexed for 3 to 4 seconds and placed back on the ice for a 30-minute incubation for lysis to take place. Following the incubation, the tubes were centrifuged at 1300 rpm for 10 minutes to pellet the solid debris from the cells. The supernatant, containing the lysates, was aliquoted to 1.5mL microcentrifuge tubes for storage at -30°C. Messenger RNA was extracted from the lysate by first passing some of the supernatant through a QIAShredder (Qiagen, ref: 79654) then utilization of the QIAGEN RNEasy® Plus Kit (ref: 74134), both following manufacturer protocols.

4.3.1.1.4. Fluorescence Data Collection and Analysis

All flasks were observed under the Revolve M-107 Microscope by ECHO with an objective 4x lens, a digital zoom setting of 1.0, and "Digital haze reduction" turned off. Images were taken at 24 hours post-transfection in 3 randomly selected spots on each flask under FITC and TRANS channels to obtain images of cells fluorescing green versus the number of cells total within the field. The images were automatically overlaid by the microscope. Additional observations were performed beyond the images taken for personal interest, but data recorded was only for the images taken.

Three HEK293 flasks each were imaged every 24 hours up to 4 days post-transfect with anticipation of using that data. J774A.1 cells were not imaged for that long because of J774A.1 observations during experimentation and resource allocation decisions. Therefore, only the first 24-hour data was used for statistical comparison between all treatment groups– 3 images per flask of each of the groups.

All FITC and TRANS images of the 24-hours post-transfection mark, a total count of 420 pictures, from the Revolve M-107 Microscope by ECHO were processed through ImageJ (NIH) to obtain cell counts [455]. Protocol for counting cells was followed from an instructional video in conjunction with the protocol described by Fassina and colleagues in 2012 [442, 456] (Appendix A). Settings were maintained for all images, except "Threshold" which was manually performed for each image.

All FITC and TRANS images for 24-, 48-, 72-, and 96-hours post-transfection from the OHG.1, LHG.1, and EHG.1 groups were also processed through ImageJ (NIH) to obtain cell counts. 216 pictures in total were analyzed. Protocol for counting cells was followed from an instructional video in conjunction with the protocol described by Fassina and colleagues in 2012 [442, 456] (Appendix A). Settings were maintained for all images, except "Threshold" which was manually performed for each image.

4.3.1.1.5. Sample Analyses, RT-PCR

RT-PCR was used to determine if transcription of the pGFP took place following transfection. Total RNA from cell lysate was harvested using RNEasy® (QIAGEN, Cat. No. / ID: 74104) on samples from each experimental group followed by reverse transcription using the QIAGEN OneStep *Ahead* RT-PCR Kit (Catalog No. 220213), specially designed primers for pGFP detection (Table 4.3), USP18 F and USP18 R primers as the positive controls for all HEK293 samples (Table 3.4), and PON1 F, PON1 R, LRP1 F, and LRP1 R primers as the positive controls for all J774A.1 samples (Table 4.3). The PON1 primers were obtained from OriGene (CAT#HP200426) and LRP1 primers were obtained from OriGene (CAT# HP206040) after selection of the paraoxonase 1 (PON1) and low-density lipoprotein receptor-related protein (LRP1) as highly conserved J774A.1 proteins through MaayanLab [381]. Manufacturer protocol

was followed with some adjustments (QIAGEN OneStep *Ahead* RT-PCR Handbook, 2015). RT-PCR mixtures consisted of 10µL QIAGEN OneStep *Ahead* RT-PCRMaster Mix 2.5x, 1µL QIAGEN OneStep *Ahead* RT-Mix 25x, 1µL forward primer, 1µL reverse primer, 3µL mRNA, 4µL RNA/DNA-free water all in a 500µL PCR tubes. Tubes were placed in a Bio-Rad T100 Thermal Cycler under the following conditions: reverse transcription at 50°C for 10 minutes, initial PCR activation at 95°C for 5 minutes, 3-step cycling at 95°C for 10 seconds, annealing at approximately 5°C below Tm of the primers for the specific reaction for 10 seconds, extension at 72°C for 10 seconds, and a final extension at 72°C for 2 minutes. The 3-step cycling, annealing, and extension steps were repeated 40 times prior to final extension.

Table 4.3. Primers used for GFP and J774A.1 housekeeping RT-PCRs

Primer Name	**Primer Sequence**	**Melting Temperature**	**Expected Product Size**
GFP Fwd	5'- GGCCTGCCCGCCATGGAGATC -3'	65.5℃	672 bp
GFP Rev	5'- ACCGGCATCTGCATCCGGGG -3'	65.2℃	
LRP1 F	5'- CAACGGCATCTCAGTGGACTAC -3'	60℃	122 bp
LRP1 R	5'- TGTTGCTGGACAGAACCACCTC -3'	60℃	
PON1 F	5'- ATGCTCTCCGAGAGGTACAACC -3'	60℃	103 bp
PON1 R	5'- GCCAGTCCATTAGGCAGTATCTC -3'	60℃	

Notes: Primers and their coordinating melting temperatures, annealing temperatures, sequences, and expected product sizes.

4.3.1.2. "Optimized" Protocols

Sample size was determined via a power analysis in MedCalc. Using the results from the "Equalized" protocols portion of this project in combination with an alpha of 0.05 and a beta of 0.2, the sample size was determined to be 5 flasks each.

The same pGFP from "All Things Equal" was used for this portion of this project. The pGFP Midiprep was diluted in PBS to the recommended DNA concentration and volume for each transfection reagent/method.

Each flask was transfected as the ideal confluences or cell counts were reached for each transfection methodology, and all flasks, regardless of treatment group, had a final total content volume of 25mL upon completing each transfection. Flasks were all checked for confluency subjectively by observation under a microscope. Cell confluency for all Lipofectamine3000 flasks, with and without pGFP, were 80-90%. Cell confluency for all jetOPTIMUS® flasks, with and without pGFP, were 60-80%. Electroporation flasks, with and without pGFP, were seeded with 3×10^6 cells. Confluences for non-transfected flasks were 60-90%.

Protocols across the two cell types were nearly identical, and steps altered were done so to accommodate the ATCC recommendations for the handling of each cell type (i.e., splitting protocols).

4.3.1.2.1. HEK293 Transfections

HEK293 cells (CRL-1573 batch #70039815 from ATCC) were grown in EMEM (ATCC, Cat # 30-2003) supplemented with 10% FBS (SAFC Biosciences, cat: 112-300-101) in T75 flasks (Corning, Ref 431641 U). Cells were fed every other day. Feeding consisted of discarding the old media followed by a 5mL PBS rinse, then adding 25mL of fresh 10% FBS EMEM. When cells reached 70% confluency, cells were split after the PBS rinse via exposure to 3mL TrypleExpress and light tapping. Then, the cell suspension was aliquoted into new T75 flasks until there were 35 flasks - 5 flasks per group. Cells were passaged 4 times before transfection.

The non-transfected HEK293 (NH.2) flasks underwent the same protocol as NH.1. The flasks assigned to Lipofectamine3000 with pGFP (LHG.2) and Lipofectamine without pGFP

(LH.2) underwent the same protocols as LHG.1 and LH.1 respectively, with pGFP amount modified for LHG.2. The amount of pGFP used for LHG.2 was 19.53µg per flask. The flasks assigned to jetOPTIMUS® with pGFP (OHG.2) and without pGFP (OH.2) underwent the same protocols as OHG.1 and OH.1 respectively.

The flasks assigned to electroporation with pGFP (EHG.2) and without pGFP (EH.2) underwent a similar protocol as EHG.1 and EH.1 respectively, with pGFP amount modified for EHG.2. The amount of pGFP used for EHG.2 was 4ng in a 2µL volume. An additional modification was that 3×10^6 cells were loaded into the cuvette, and the number of cells was determined by hemocytometer. Time constants for these transfections are outlined in Table 4.4 and ranged from 12.3 to 14.6 msec.

Table 4.4. Time constants for each HEK 293 electroporation flasks with "optimized" protocols as displayed by the Gene Pulse following a 0.2kV.

Flask Label	**Time Constant for "With DNA" flask (msec)**	**Time Constant for "Without DNA" flask (msec)**
A	14.4	13.2
B	13.8	13.2
C	14.2	12.3
D	13.8	14.6
E	13.8	13.4

4.3.1.2.2. J774A.1 Transfections

J774A.1 cells (ATCC, TIB-67 batch #70040953) from *Mus musculus* were grown in DMEM (cat 30-2002 from ATCC) supplemented with 10% FBS (SAFC Biosciences, cat: 112-300-101) in T75 flasks (Corning, Ref 430720U). Cells were fed every other day with the 10% FBS DMEM and split via scraping into new T75 flasks until there were 10 flasks - 5 flasks per

group for a given transfection reagent/method. This was performed a total of 4 times, for a total of 35 flasks– one split was only for the 5 non-transfected flasks.

The non-transfected J774A.1 (NJ.2) underwent the same protocol as NJ.1. The flasks assigned to Lipofectamine3000 with pGFP (LJG.2) and Lipofectamine3000 without pGFP (LJ.2) underwent the same protocols as LJG.1 and LJ.1 respectively, with pGFP amount matching LHG.2 and LH.2 respectively. The flasks assigned to jetOPTIMUS® with pGFP (OJG.2) and without pGFP (OJ.2) underwent the same protocol as OJG.1 and OJ.1 respectively, with pGFP amount matching OHG.2 and OH.2 respectively.

The flasks assigned to electroporation with pGFP (EJG.2) and without pGFP (EJ.2) underwent protocols similar to those of EJG.1 and EJ.1, with pGFP amounts and cell counts matching EHG.2 and EH.2 respectively. Time constants for these transfections are outlined in Table 4.5, and they ranged from 15.6 to 16.6 msec

Table 4.5. Time constants for each J774A.1 electroporation flasks with "optimized" protocols as displayed by the Gene Pulse following a 0.2kV.

Flask Label	**Time Constant for "With DNA" flask (msec)**	**Time Constant for "Without DNA" flask (msec)**
A	15.6	15.8
B	16.5	16.3
C	16.1	16.6
D	16.5	16.5
E	16.4	16.1

4.3.1.2.3. Preparing Samples for Flow Cytometry

Flasks were observed under the Revolve M-107 Microscope by ECHO with an objective 4x lens, a digital zoom setting of 1.0, and "Digital haze reduction" turned off. At least one

picture was taken for each treatment group at 24 hours, and auto-exposures were used. Images were not random, but rather they were used as a quality control measure to determine if any GFP was expressing post-transfection before flow cytometry prep.

For HEK293 cells, the spent media was evenly split between two 15mL conical tubes. Then, 4mL TrypleExpress was used to release the adherent cells into suspension with light tapping. TrypleExpress exposure did not surpass 2 minutes. The suspended cells and TrypleExpress were evenly split between the two 15mL conical tubes already containing the spent media. For J774A.1 cells, adherent cells were released into suspension within the spent media using cell scrapers, and the full volume was evenly distributed between two 15mL conical tubes. The 15mL conical tubes were inverted to mix, then a 1mL sample was taken to determine the concentration of cells. The 1mL sample of cells were pipetted into packed cell volume (PCV) tubes and the MidSci protocol was used to determine the number of cells per milliliter (Appendix A). Volume needed to obtain 1×10^6 cells was kept in one of the 15mL conical tubes. All conical tubes were centrifuged at 300×g for 5 minutes. Supernatant was discarded. Pellets were gently rinsed with 3mL PBS.

For flow cytometry, the pellet with 1×10^6 cells was resuspended in 300µL eBioscience Flow Cytometry Staining Buffer (invitrogen, ref 00-4222-57, Life Technologies Corp. 5781 Van Allen Way, Carlsbad, CA 92008). The resuspended pellet was then pipetted into a BD Falcon sample tube pre-loaded with 15µL eBioscience 7-AAD Viability Staining Solution (BD Falcon, cat 352054; invitrogen, ref 00-6993-50, Life Technologies Corp, 5781 Van Allen Way, Carlsbad, CA 92008). BD Falcon tubes with the samples were immediately transferred to ice. Tubes remained on ice for between 30 minutes to 1 hour.

4.3.1.2.4. Fluorescence Data Analysis

Cells were analyzed for GFP and viability at the Flow Cytometry Facility at the LSU School of Veterinary Medicine. All samples were analyzed in an LSR-Fortessa X-20 flow cytometer (BD Biosciences, San Jose, CA) with a 488nm argon-ion laser. The flow cytometer was additionally configured for GFP and 7-AAD fluorescence measurements using log amplification. Acquisition was set to stop at 50,000 cells on FACS DIVA software (BD Biosciences, San Jose, CA) for an HP computer workstation (Palo Alto, CA). Forward-scatter (FSC) area versus side-scatter (SSC) area plots and FSC height version FSC area plots were used in conjunction with single-dye and no-dye samples for gated removal of aggregates in acquisition.

4.3.1.3. Statistics

4.3.1.3.1. "Equalized" Protocols

For the 24-hours post-transfection data, FITC cells counts across all three images were averaged for each flask and TRANS cell counts across all three images were averaged for each flask. Percent fluorescence for each flask was calculated in Microsoft Excel by dividing the average FITC cell count by the average TRANS cell count. Percentages and average TRANS cell counts were then analyzed in IBM SPSS. To evaluate the hypotheses for aim 1 of this project (H_0: $\mu_{NH} = \mu_{LHG} = \mu_{LH} = \mu_{OHG} = \mu_{OH} = \mu_{EHG} = \mu_{EH} = \mu_{NJ} = \mu_{LJG} = \mu_{LJ} = \mu_{OJG} = \mu_{OJ} = \mu_{EJG} = \mu_{EJ}$; H_1: Not H_0), data was first analyzed via a Multivariate General Linear Model (GLM) with pairwise comparisons and post-hoc Tukey test in SPSS.

For the across-time data from OHG.1, LHG.1, and EHG.1, FITC cells counts across all three images at each time point were averaged for each flask and TRANS cell counts across all three images at each time point were averaged for each flask. Percent fluorescence for each flask

at each time point was calculated in Microsoft Excel by dividing the average FITC cell count by the average TRANS cell count. Percentages and TRANS cell counts were then analyzed in IBM SPSS. To evaluate the hypotheses for aim 2 of this portion of the project (H_0: $\mu_{G1} = \mu_{G2} = \mu_{G3} = \mu_{G4}$; H_1: Not H_0), repeated measures GLM with pairwise comparisons was used to analyze the data with pairwise comparisons to determine which transfection method and which times had the highest GFP fluorescence and highest cell counts.

4.3.1.3.1. "Optimized" Protocols

FlowJo 10.8.1. software (BD Biosciences, Ashland, OR) was used to analyze the dual fluorescence of GFP expression versus 7-AAD viability staining. FlowJo 10.8.1. was also used to equalize samples to 10,000 cells via the "Downsample" feature, then determine the percentages of GFP expressing viable and nonviable cells of each sample. Quadrant 3 data of the FlowJo output, which consisted of the GFP-expressing viable cells, were analyzed using a Univariate General Linear Model with pairwise comparisons in SPSS.

4.3.2. pSC6 Design and Construction

4.3.2.1. The Redesign

A new vaccine was designed including the same portions of the ORF described in Part 1 of this chapter along with the 3' UTR and new poly(A) sequence. Components were combined in SnapGene for the purposes of this project as follows: 5' SalI RE site, ConSS (Genbank X02009.1 basepairs 74-133), FimH, FRS 1, SopB, FRS 2, OmpA, FRS 1, OmpC, FRS 2, OmpD, 6XHis tag, 3' UTR from HBA1 (Genbank MK600513.1, basepairs 862-972), SV40 poly(A) signal sequence (AddGene, Catalog #124537), 3' NheI RE site (Figure 4.1). Orientation and placement of all the components were verified by NEB [457]. This new vaccine, as seen in

Figure 4.1, was ordered from IDT within their pUCIDT(Amp) vector [458]. The new vaccine insert within the IDT pUCIDT(Amp) vector will be referred to as pSIDT.

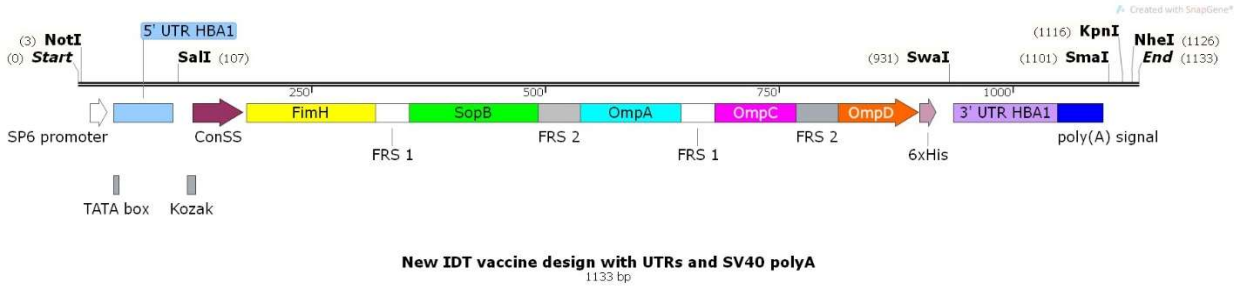

Figure 4.1. pSIDT vaccine design prior to pUCIDT(Amp) vector incorporation. This image demonstrates all included vaccine components and pertinent RE sites.
Notes: The design was such that vaccines and other genes being researched at the time of this construction could easily incorporate desired components. SwaI, SmaI, and KpnI RE sites were added for directional cloning of the 3' UTR from *HBA1* and new SV40 poly(A) signal into the 2 other pDNA vaccines in the Cooper laboratory. The NotI RE site and SalI RE site placements were incorporated for the swapping of the CMV promoter components for an SP6 promoter [459] and incorporating a 5' UTR from *HBA1* that possesses a TATA box (Genbank MK600513.1, basepairs 101-163). The promoter and 5' UTR swap was intended for the conversion of all current vaccines in the Cooper laboratory to mRNA-based vaccines.

4.3.2.2. Modified Vaccine Construction

To remove the puromycin resistance marker from pSCP while maintaining the CMV promoter sequence, pSCP and the pBluescript vector were digested with EcoRI (New England Biolabs, Cat R0652S) following the NEB Restriction Digest protocol (Appendix A). The pSCP 3173bp band was extracted from a 1% agarose SYBR Safe gel and purified via Zymoclean DNA Gel Recovery Kit. The pBluescript vector digest was purified via Clean and Concentrate (Zymo, Catalog Number D4030). Once prepared, both DNA fragments were ligated together by use of the NEB Quick Ligase Kit, and the resulting plasmid, pSC, was used to transform NEB 5-alpha F'I^q Competent *E. coli* (Cat C2992) following the manufacturer instructions (Appendix A).

The 6XHis Tag was added and the poly(A) tail was removed using sequential Q5 mutageneses. All Q5 reactions were performed following the manufacturer protocol with modifications listed in Table 4.6 (Appendix A). The polyhistidine tag was added first to the 3' end of the ORF upstream of the stop codon via the Q5 Mutagenesis Kit and the primers "pSNS 6x Q5 F" and "pSNS 6x Q5 R" (Table 4.6). The pSC with the 6x His tag was confirmed via sequencing with Georgia Reverse 1 and SJ1 6x His F seq (Table 4.7). The SV40 polyA signal was removed from the sequence verified vector via a Q5 Mutagenesis Kit and the primers "SJ1 Q5 poly deletion F" and "SJ16x Q5 poly deletion R" (Table 4.6). The removal of polyA from pSC with the 6x His tag was confirmed via sequencing with Georgia Reverse 1 and M13 fwd (Table 4.7). A ZymoPURE^{TM} II Plasmid Midiprep kit was used on bacterial cultural samples which demonstrated a successful Q5 Mutagenesis via *E. coli* growth. The final product of this series of Q5 Mutagenesis and digests will be referred to as pSQ.

Table 4.6. Q5 primers and parameters for 6X His addition and polyA signal sequence deletion.

Primer Name	**Primer Sequence**	**Melting Temperature**	**Annealing Temperature**	**Extension Time**
pSNS 6x Q5 F	5'- CAC CAC CAC TAA CCT AGA GTA CGA CCT C -3'	60.9℃	62℃	3 min
pSNS 6x Q5 R	5' ATG ATG ATG ATT CCC GTC CTT GTT GTA C -3'	58.6℃		
SJ1 Q5 poly deletion F	5'- TTA ATT AAC AGT GGC GCC -3'	50.4℃	62℃	2 min 30 s
SJ16x Q5 poly deletion R	5'- CTA GGT TAG TGG TGG TGA TG -3'	52.2℃		

Table 4.7. Sequencing primers for pSQ Q5 Mutagenesis series.

Primer Name	**Primer Sequence**	**Melting Temperature (°C)**
Georgia Reverse 1	5'- CTC TGT CGA TAC CCC-3'	49.0
SJ1 6x His F seq	5'- GCT GCC GAG ATT TAC-3'	46.8
M13 fwd	5'- GTA AAA CGA CGG CCA GT -3'	56.0

To create the final pSC6 version of the non-adjuvanted vaccine, pSQ and pSIDT were digested with SalI and NheI (New England Biolabs, Cat). The 4650bp band from pSQ and the 1019bp band from pSIDT were extracted from a 1% agarose SYBR Safe gel and purified via Zymoclean DNA Gel Recovery Kit. The purified gel bands were then ligated by use of the NEB Quick Ligation kit. The resulting pSC6 plasmid was used to transform NEB 5-alpha F'I^q Competent *E. coli* (Cat C2992). The pSC6 was harvested and purified via the use of a ZymoPURE™ II Plasmid Midiprep kit (ZymoResearch, Cat # D4200).

The full pSC6 vector sequence was verified by sequencing with pBXK 4889, CMV SXD orient F, DS Forward, Puro check F, AE Reverse, SK Forward 2, Georgia Reverse 1, and Ippo Reverse 1 (Tables 3.2 & 4.8). SJ1 F and SJ1 R from Table 3.1 were also used in sequencing used to verify the ORF.

Table 4.8. Additional primers used for sequencing of pSC6 that were not included in Tables 3.1 and 3.2.

Primer Name	**Primer Sequence**	**Melting Temperature (°C)**
pBXK 4889	5'- ATA GTC CTG TCG GGT TTC GC -3'	59.0
CMV SXD orient F	5'- ATC GGT CCC GGT GTC TTC TA -3'	58.0
Puro check F	5'- CCA TGG GTC TTT TCT GCA GTC TCG-3'	68.0

All sequencing for this project was ABI 3130 Sanger Sequencing performed by the LSU Veterinary School GeneLab.

4.3.3. *In Vitro* pSC6 Testing

4.3.3.1. Establishing ELISA Standard Curve

E. coli Positive Control Whole Cell Lysate- expressing 6X His tag protein from Abcam (ab2431) was used to coat a NUNC plate in a series of serial dilutions in endotoxin free 1X PBS. A direct ELISA was performed by following the "Indirect ELISA Protocol" (Appendix A) with the following modifications:

1. Plate one was coated with 2.5µg, 5µg, 10µg, and endotoxin-free PBS (Figure 4.2). Plate two was coated with 1µg, 0.2µg, 40ng, 8ng and endotoxin-free PBS. Plate three was coated with 40ng, 20ng, 10ng, 5ng, 2.5ng, 1.25ng, 0.625ng, and endotoxin-free PBS. Each concentration was used to coat 6 wells.

10. Primary antibody used was HRP Anti-6X His tag antibody (Abcam, ab1187). The dilutions for each plate were 1:5000, 1:10,000, and 1:20,000 in blocking buffer. Each dilution was used to coat each protein concentration in duplicate (Figure 4.2).

12. Skipped this step.

13. Skipped this step.

15. Both plates incubated less than 30 seconds.

Plates were analyzed via the Bio-Rad Benchmark Plus microplate spectrophotometer at 450nm.

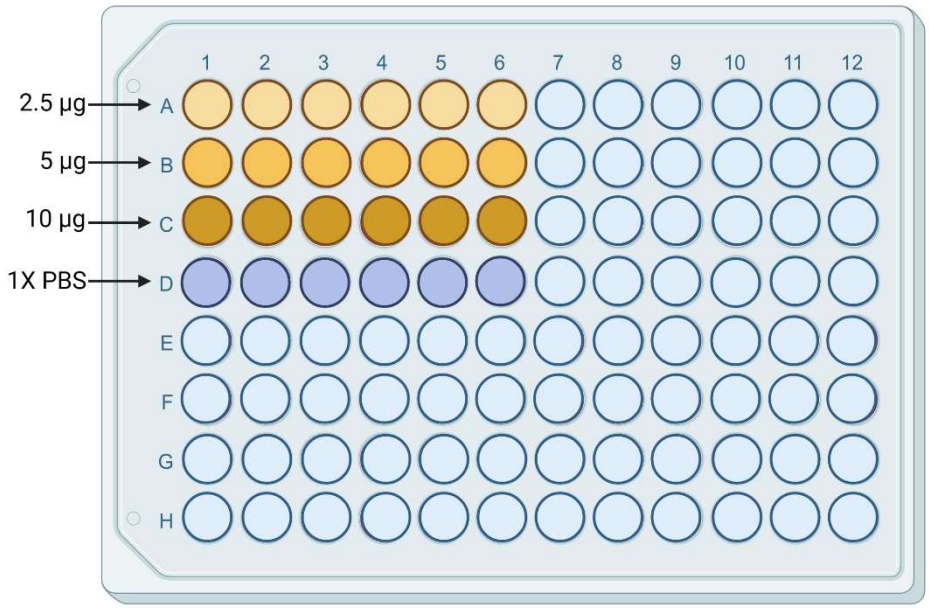

a.

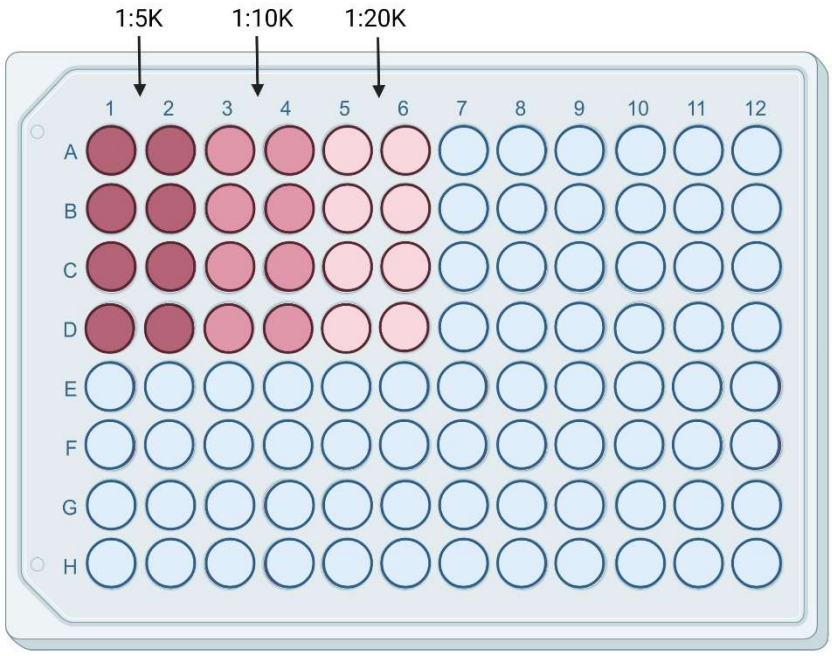

b.

Figure 4.2 Plate one protein coat and antibody dilution layouts as an example image for direct ELISA 6X His troubleshooting. Top (**a**.) is the protein coat layout of the dilutions of the *E. coli* Positive Control Whole Cell Lysate- expressing 6X His tag protein from Abcam. Bottom (**b**.) is the antibody layout for dilutions of the HRP Anti-6X His tag antibody from Abcam. Created with BioRender.com (Appendix D).

4.3.3.2. Transfection and Sample Collection, 24 hours

Number of flasks was determined through the MedCalc Sample Size Calculator for Comparison of Means, using an alpha of 0.05, beta of 0.2, estimated difference of means of 0.2, standard deviations of 0.1, and ratio of sample sizes of 1. Sample size determined was 5 flasks per group.

HEK293 cells were used to seed 1 T75 flask with 20mL 10% FBS EMEM media. The cells were split by adding 5mL of TrypleExpress to the flask and light typing, then aliquoting 0.5mL of suspended cells into 10 new flasks with 25mL of 10% FBS EMEM. Splitting was repeated once more when the original 10 flasks reached 70% confluency to achieve a final count of 15 flasks. All flasks were fed every other day until confluency reached 70-90%. Feeding consisted of discarding the old media followed by a 5mL PBS rinse, then adding 25mL of fresh 10% FBS EMEM. When cells reached 70% confluency, cells were split after the PBS rinse via exposure to 3mL TrypleExpress and light tapping. Then, the cell suspension was aliquoted into new T75 flasks until there were 35 flasks - 5 flasks per group. Cells were passaged 4 times in total before transfection. Five flasks were each transfected with 19.53µg pSC6 that was purified via ZymoPURE^{TM} II Plasmid Midiprep kit following the protocol for LHG.2. Five flasks were transfected in accordance with the protocol used for LH.2. The remaining five flasks were transfected in accordance with the protocol used for NH.2.

Twenty-four hours following transfection, spent media and lysates were harvested from all the flasks. Spent media was first poured into 50mL nonpyrogenic, polypropolyene conical tubes (CELLSTAR®, Greiner Bio-One, Cat. No. 2270261), one per flask. A 20mL aliquot from the bottle of 10% FBS EMEM last used to feed the cells was also transferred to a 20mL nonpyrogenic, polypropylene conical tube to serve as a control. All 50mL conical tubes with the

media samples were stored at -30°C. Next, lysate collection was performed by first making LEB2. Then, LEB2, PBS, and flasks were placed on ice until chilled. Flasks were rinsed with 5mL of the chilled PBS to remove any residual waste media, and then, 1.25mL LEB2 was added to each flask. Cell scrapers (VWR, catalog number 734-2602) were used to detach the cell from the flask and transfer them into the LEB2 for cell lysis. The LEB2 with cells were aspirated and transferred to pre-chilled 15mL conical tubes (SpectraTube, VWR catalog number 470224-998), one tube per experimental group. An additional 15mL conical tube received LEB2 that was not exposed to a flask to serve as a control. The 15mL conical tubes with LEB2 samples were then vortexed for 3 to 4 seconds and placed back on the ice for a 30-minute incubation for lysis to take place. Following the incubation, the LEB2 sample tubes were centrifuged in a Sorvall ST16R Centrifuge equipped with the 75003181 rotor (ThermoScientific) at 1300rpm for 10 minutes to pellet the solid debris from the cells. The supernatant, containing the soluble proteins (referred to henceforth as lysates), was aliquoted to 1.5mL microcentrifuge tubes for storage at -30°C.

4.3.3.3. 24 Hours Post-Transfection Sample Analyses, ELISA

Spent media and lysate samples and controls were thawed and diluted in endotoxin-free PBS to ¼ the original concentration. Undiluted and diluted samples and controls were randomly assigned to duplicate locations on two 96-well NUNC plates. A direct ELISA was performed by following the appended “Indirect ELISA Protocol” (Appendix A) with the following modifications:

1. Both plates were coated with 40ng, 20ng, 10ng, 5ng, 2.5ng, 1.25ng, and 0.625ng of the *E. coli* Positive Control Whole Cell Lysate- expressing 6X His tag protein in duplicate for the standard curve. An additional

duplicate of endotoxin-free PBS was used on each plate to serve as a blank for the standard curve. Plate one was coated with the spent media samples and controls in duplicate. Plate two was coated with the lysate samples and controls in duplicate.

10. Primary antibody used was HRP Anti-6X His tag antibody (Abcam, ab1187). The dilution for both plates was 1:20,000 in blocking buffer, which was used on the entire plate.
12. Skipped this step.
13. Skipped this step.
15. Both plates incubated for 5 minutes.

Plates were analyzed via the Bio-Rad Benchmark Plus microplate spectrophotometer at 450nm.

4.3.3.4. Transfection, Sample Collection, and Sample Analyses for 4-days Post-Transfection

Protocols outlined in sections 4.3.3.2 and 4.3.3.3 were repeated with the following modifications in response to results from 24-hour post-transfection samples. Sample harvest was performed 4 days (96 hours) after the day of transfection. No feedings occurred between transfection and harvest to allow any secreted proteins to accumulate in the media. Direct ELISA analyses were limited to the undilute spent media.

4.3.3.5. Statistics

4.3.3.5.1. Establishing ELISA Standard Curve

CV was calculated for each sample in Microsoft Excel. Absorbances for each duplicate were averaged, and the mean 1X PBS absorbance was subtracted from each mean sample absorbance to obtain AMB values in Microsoft Excel. AMB values were then analyzed in Prism

9.1.2 via a Correlation Test for evaluation of the hypothesis of aim one of this portion of this project (H_0: $\rho=0$; H_1: $\rho>0$).

4.3.3.5.2. 24 Hours Post-Transfection Sample Analyses, ELISA

CV was calculated for each sample duplicate and absorbance values for each duplicate were averaged in Microsoft Excel. AMBs were also calculated in Microsoft Excel. The mean 1X PBS absorbance was subtracted from each mean absorbance of each 6X His duplicate. Mean absorbance for the undilute control media was subtracted from all mean absorbances of undilute spent media samples. Mean absorbance for the control media diluted 1:4 was subtracted from all mean absorbances of spent media samples diluted 1:4. Mean absorbance for the undilute control LEB2 was subtracted from all mean absorbances of undilute lysate samples. Mean absorbance for the control LEB2 diluted 1:4 was subtracted from all mean absorbances of lysate samples diluted 1:4.

AMB values for the standard curves were first analyzed in GraphPad Prism 9.1.2 via a Correlation Test. Then, Graphpad Prism 9.1.2 was used to interpolate the AMB values of the spent media and lysate samples and controls to the standard curves of their given plates. The interpolated values were then analyzed via a Multivariate General Linear Model with pairwise comparisons in SPSS to evaluate the hypotheses for aims two and three of this project (H_0: $\mu_{C1} = \mu_{C2} = \mu_{SC6}$; H_1: Not H_0).

4.3.3.5.2. 4 Days Post-Transfection

Duplicate CVs and absorbance values for each duplicate were averaged in Microsoft Excel. AMBs were also calculated in Microsoft Excel. The mean 1X PBS absorbance was subtracted from each mean absorbance of each 6X His duplicate. Mean absorbance for the undilute control media was subtracted from all mean absorbances of undilute spent media samples. AMB values

for the standard curves were then analyzed in GraphPad Prism 9.1.2 via a Correlation Test. Then, Graphpad Prism 9.1.2 was used to interpolate the AMB values of the spent media samples and controls to the standard curve. Interpolated values were then analyzed via a Univariate GLM with a post hoc Tukey Test to evaluate the hypothesis for aim three of this project (H_0: $\mu_{C1} = \mu_{C2} = \mu_{SC6}$; H_1: Not H_0).

4.3.4. Evaluating Immunogenic Potential

An indirect ELISA was performed on the 4-days post-transfection undilute spent media to evaluate aim 4 of this portion of the project. Samples were thawed and were randomly assigned to two duplicate locations on one NUNC 96-well plate. Newly harvested *S.* Javiana proteins via the CelLytic™ B kit were serially diluted from 3.75ng/µL through 0.234 ng/µL. The indirect ELISA protocol (Appendix A) was performed with the following modifications:

1. The *S.* Javiana proteins and all spent media samples were used to coat a NUNC plate at 100µL/well in duplicate. Two duplicate locations were coated for each sample and standard. Four wells were coated with endotoxin-free PBS to serve as a blank for the standard curves. Two duplicates of cell culture media were coated to serve as blanks for the spent media samples.

10. The primary antibody was convalescent serum in the stock blocking buffer at a 1:3000 ratio. All wells received 100µL/well of the primary.

12. Each standard curve, one duplicate for each sample, and one duplicate of the endotoxin-free PBS were coated with 100µL/well of one of the two secondaries. One secondary was Goat Anti-Equine IgM (anti-IgM) (Invitrogen PA1-84647) diluted to a 1:25,000 ratio in the stock blocking

buffer. The other secondary was Goat anti Horse IgG (T) (anti-IgG) from Bio-Rad (Product Code AAI38) diluted to a 1:1000 ratio in stock blocking buffer.

15. 1-Step Ultra TMB-ELISA incubation was 30 minutes for anti-IgM and 1 hour for anti-IgG.

Plates were analyzed via the Bio-Rad Benchmark Plus microplate spectrophotometer at 450nm.

The IEDB Analysis Resource [271] was used on the epitope region of the pSC6 ORF, matching the analysis parameters used for pSCP in Chapter 2 of this project. Protein sequences were analyzed using the T cell epitope prediction software for predictions of MHC-II binding. Predictions for MHC-II binding were produced for the three available mouse H-2-1 alleles (H2-lAb, H2-lAd, H2-lEd). The output was organized in Microsoft Excel to align alleles and peptides with those of the pSCP analysis for comparison.

4.3.4.1. Statistics

CV was calculated for each duplicate in Microsoft Excel, and duplicates with CV above 30 were excluded from further analysis. Absorbances for each duplicate were averaged in Microsoft Excel.

AMBs were calculated as follows in Microsoft Excel with blanks and samples matched by secondary antibody. The mean endotoxin-free PBS absorbance was subtracted from each mean absorbance of each *S.* Javiana standard duplicate. Mean absorbance for the undilute control media was subtracted from all mean absorbances of undilute spent media samples.

To evaluate the hypothesis for aim 1 of this portion of this project (H_0: $\mu_{C1} = \mu_{C2} = \mu_{SC6}$; H_1: Not H_0), AMB values for each standard curves was first analyzed in GraphPad Prism 9.1.2

via a Correlation Test. Then, sample AMB values were analyzed via a Univariate GLM in IBM SPSS by treatment group and secondary antibody with pairwise comparison.

No statistics were performed for evaluation of the aim 2 hypothesis of this portion of this project. Outputs were visually compared for matches.

4.4. Limitations

4.4.1. Comparing Transfection Efficiency of Different Methods in Two Cell Types Through GFP

The intended "pilot study" nature of the project played a heavy role in "Equalized" protocols. Given the limited funding and time allocated to the first portion of this project, free software (ImageJ) and a readily available microscope (Revolve M-107 Microscope by ECHO) were used. Additionally, RT-PCRs were limited to one flask per treatment group and the across-time image analyses were limited to three groups for the same reasons. ImageJ, the free software, is not capable of differentiating cells by viability. Additionally, use of the ImageJ software is subject to bias by the user. The microscope was not equipped for T75 imaging, and therefore maintaining the same light and depth, and therefore scale, across the flasks was also extremely difficult. The collection of randomized imaging across each flask was intended to account for the shortcomings of the microscope and ImageJ use. The equalization of confluences across flasks was used to account for limitations with determining viability, as the dead cells that detached from the flasks were washed away between feedings.

In the "Optimized" protocols portion of this project, user bias should also be considered. While controls were used for gating, this process still requires the user to set the parameters. An additional limitation is that the data from Flow Cytometry is presented in ratio form and counts the same total number of cells across all samples. Therefore, user interpretation beyond the Flow Cytometry output and statistics is required.

4.4.2. pSC6 Design and Construction

Spontaneous mutations that occur through transformation of *E. coli* mean constant screenings and verifications of the sequences after each transformation. This extended the time frame of constructing the full plasmids considerably.

4.4.3. *In vitro* pSC6 Testing

The positive control protein was whole-cell lysates from *E. coli* that contained a 14kDa recombinant protein with a C-terminal 6X His tag. This, and all other 6X His proteins that could be found commercially, were created for Western Blot use only. The manufacturers do not provide an exact quantitation for the tagged proteins present in the product sample. Therefore, interpolation to the standard curve provides values within an unknown spectrum of "positive" levels and allows for standardization across plates for statistical analysis.

4.4.4. Evaluating Immunogenic Potential

A standard curve for anti-horse IgG (T) could not be established prior to testing because of the limited access to CelLytic™ B Plus kit. The kit is still being produced, but due to unknown reasons, the kit has been backordered for almost 1 year and is still backordered at the time of writing. The laboratory did not have enough kit left for more than one use at the time of this ELISA.

IEDB Analysis Resource analyses of the epitopes were limited to the MHC-II predictions. MHC-I was not included here because MHC-II outputs were prioritized in the original vaccine designs and because of the limited time allotted to this portion of the project.

4.5. Results and Discussion

4.5.1. Comparing Transfection Efficiency of Different Methods in Two Cell Types Through GFP

4.5.1.1. Results and Discussion for "Equalized" Protocols

Data were not normally distributed according to the Kolmogorov-Smirnov and Shapiro-Wilk tests ($P<0.001$), but data could not be transformed due to the presence of values at or below 0. According to the multivariate GLM, transfection method, pGFP presence, and cell type all impacted percent fluorescence individually and together at 24-hours post-transfection ($P<0.001$) (Figure 4.3). Together, the three variables were found to impact cell count as well ($P=0.032$) (Figure 4.4).

The post hoc Tukey test indicated that Lipofectamine3000 had higher percent fluorescence numbers than jetOPTIMUS®, electroporation, and no exposure ($P<0.001$), that jetOPTIMUS® had higher numbers than electroporation and no exposure ($P<0.001$), and that electroporation did not have higher numbers than no exposure ($P=1.000$). No differences in cell counts were found between methods ($P=1.000$). This indicates that Lipofectamine3000, under the transfection conditions used, is likely the best method for protein production one day following transfection.

Pairwise comparisons indicated that the presence of pGFP led to higher percent fluorescence ($P<0.001$) but lower cell count than no pGFP ($P=0.011$). Pairwise comparisons also indicated that HEK293 had higher percent fluorescence ($P<0.001$) but lower cell counts ($P<0.001$) when compared to J774A.1. The higher percent fluorescence and lower cell count is expected because neither cell line naturally produces GFP and GFP expression is toxic in cells [460]. Given that neither cell line produced cell counts of 0 but J774A.1 did produce percent fluorescence values of 0, it was concluded that the lower cell count did not offset the value of the

higher GFP expression in HEK293. Therefore, it was concluded that HEK293 cells were likely the best cell candidate for protein production at 24 hours post-transfection.

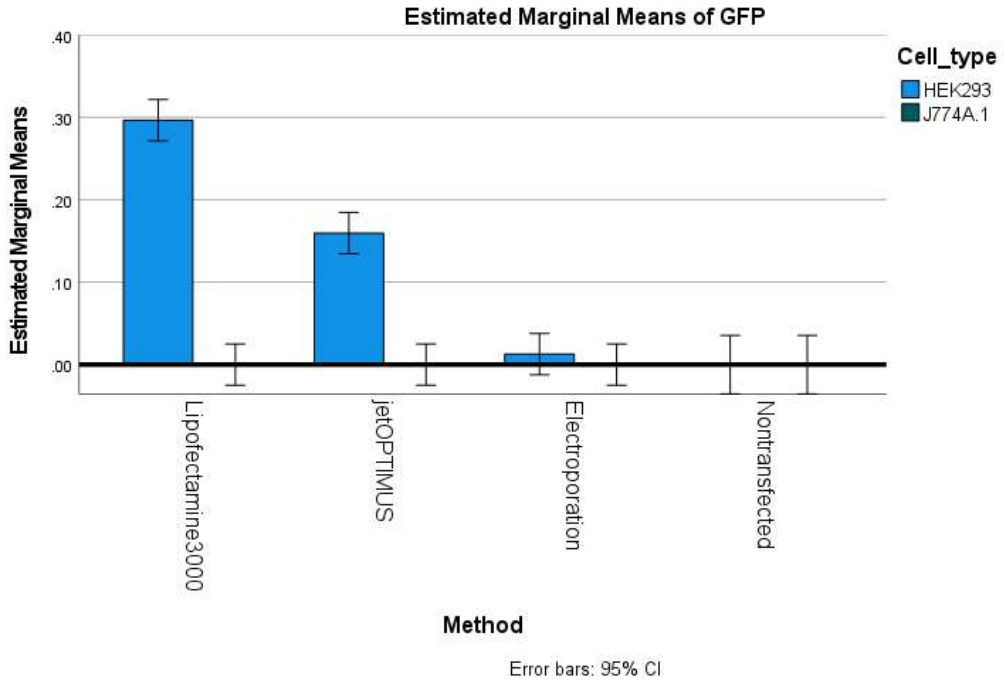

a.

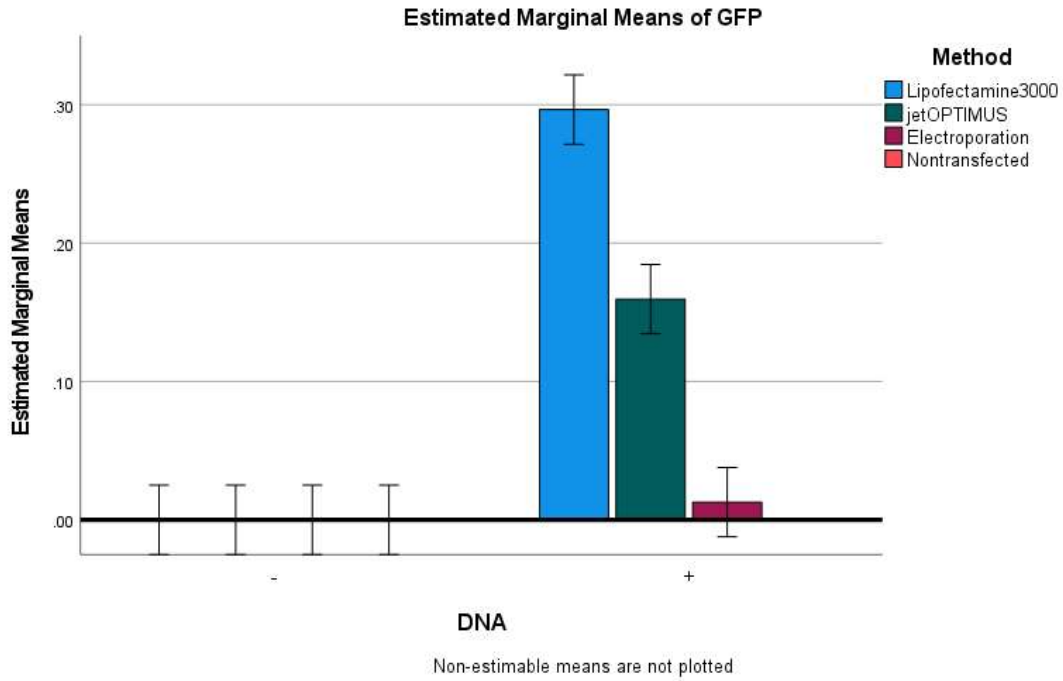

b.

Figure 4.3. SPSS GLM GFP output graphs. Top (a.) is a bar graph of estimated marginal means of percent fluorescence by transfection method and cell type. Bottom (b.) is a bar graph of the estimated marginal means of percent fluorescence by pGFP presence and transfection method.

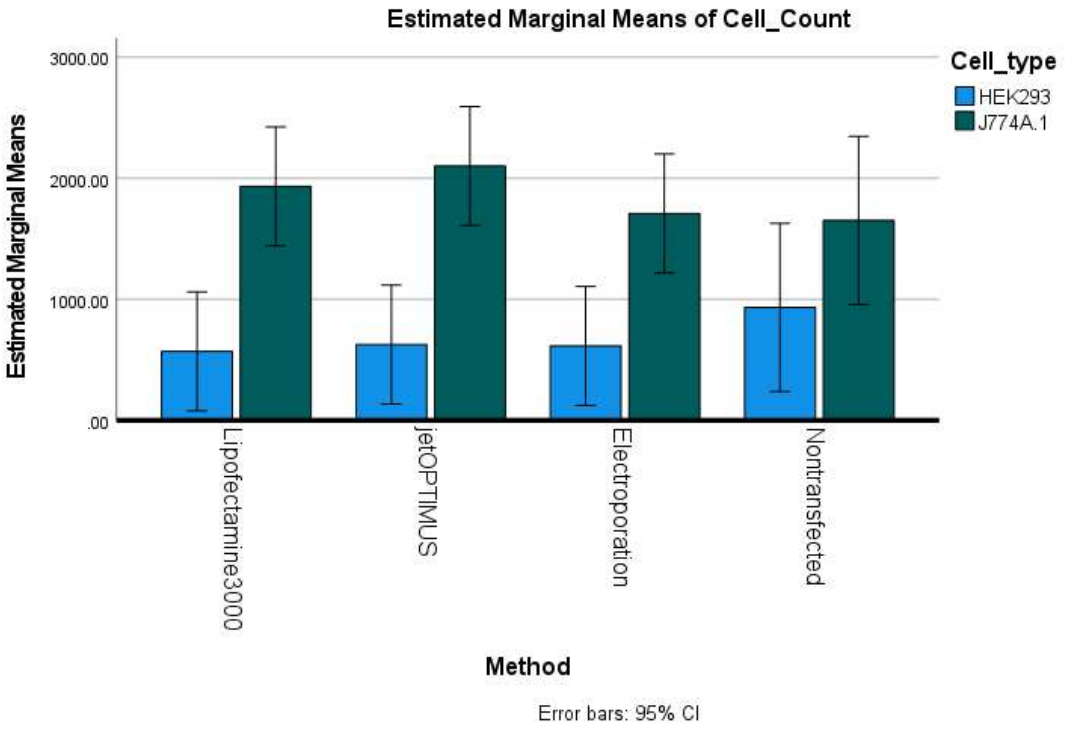

a.

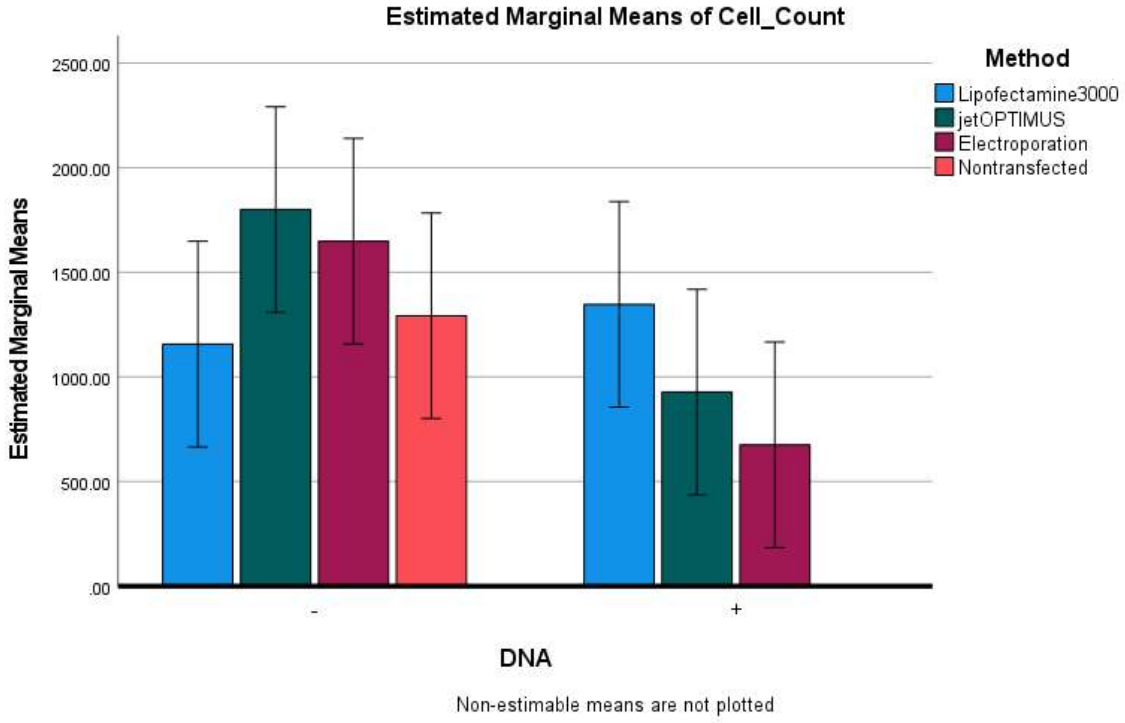

b.

Figure 4.4. SPSS GLM GFP output graphs. Top (a.) is a bar graph of estimated marginal means of cell counts by transfection method and cell type. Bottom (b.) is a bar graph of the estimated marginal means of cell counts by pGFP presence and transfection method.

When looking at OHG.1, LHG.1, and EHG.1 over time, Mauchly's W indicated that sphericity could be assumed for GFP (W=0.06) but Greenhouse-Geisser correction needed to be applied to cell count outputs (W=0.007). The GLM with Repeated Measures indicated that cell counts (P=0.052) and percent fluorescence (P=0.301) were not impacted as a function of time and transfection method (Figure 4.5). Time alone also did not impact cell counts (P=0.270) nor percent fluorescence (P=0.530). Method overall impacted percent fluorescence (P=0.005), as reflected in the 24-hour post-transfection data, and method overall impacted cell count (P<0.001). Pairwise comparisons indicated that Lipofectamine3000 overall had higher percent fluorescence than electroporation (P=0.047) but not higher than jetOPTIMUS® (P=0.292), and jetOPTIMUS and electroporation did not have a difference in percent fluorescence overall (P=0.172). Pairwise comparison also indicated that electroporation had higher cell counts than Lipofectamine3000 (P=0.010) and jetOPTIMUS® (P=0.020). The only within-subject difference found in this GLM was cell count as a function of time (Linear, P=0.028). Pairwise comparison indicated that the difference in cell count was between 24 hours and 72 hours (P=0.006), and the graphed output indicates that this within-subject difference was for EHG.1 (Figure 4.5). While EHG.1 had a higher cell count than LHG.1, LHG.1's higher percent fluorescence indicates that it is likely the best candidate for protein production moving forward, supporting the findings within the Univariate GLM evaluation of all 24-hour data. Additionally, the lack of within-subject difference for percent fluorescence over time as a function of method (P=0.854) indicates that harvest can occur any day between 24- and 96-hours following transfection. Therefore, it was concluded that protein production was sufficient for future studies at 24 hours post-transfection.

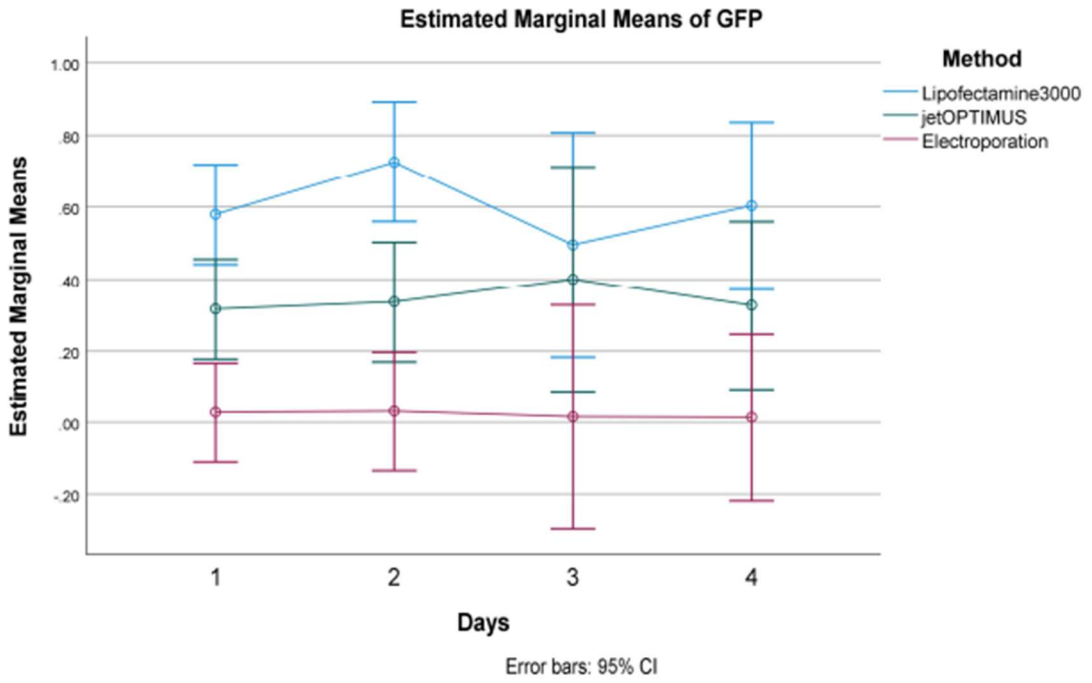

a.

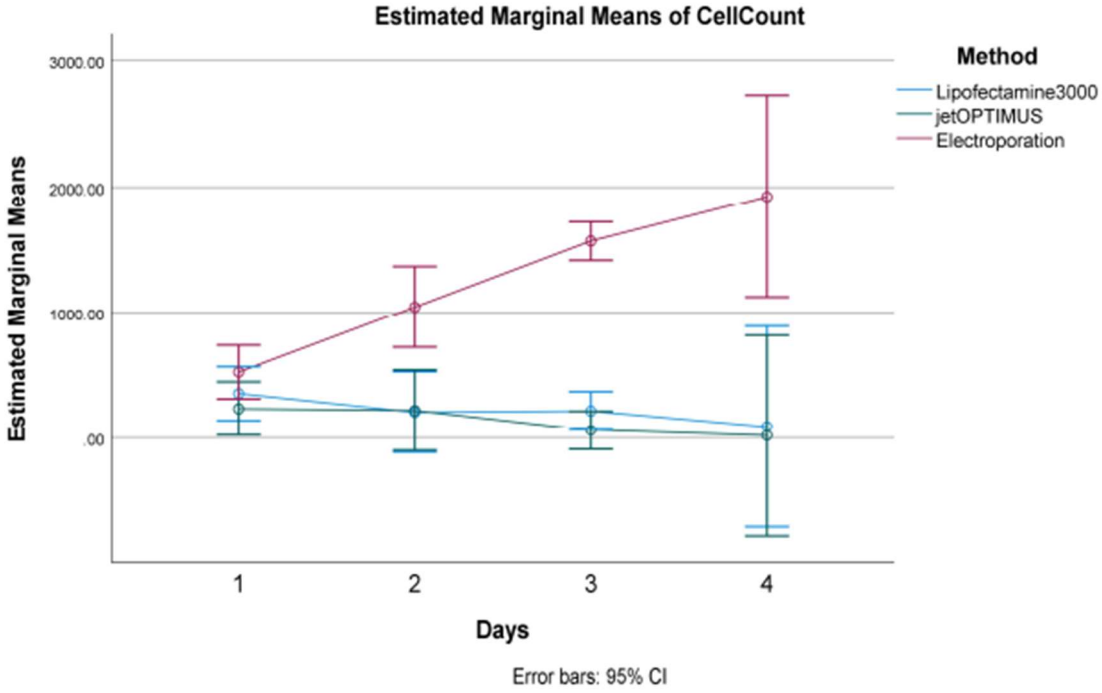

b.

Figure 4.5. Repeated Measures GLM SPSS output graphs. Top (a.) is the estimated marginal means of percent fluorescence for each transfection method by days post-transfection. Bottom (b.) is the estimate marginal means of cell counts for each transfection method by days post-transfection.

All mRNA samples from flasks transfected with pGFP that underwent RT-PCR with the GFP F and R primers and housekeeping primer sets for each cell line resulted in PCR bands of the expected sizes – 672bp for GFP F and R, 159 bp for USP18 F and R, and 122 bp for LRP1 F and R (Figure 4.6). Sequencing verified that the GFP F and R primers amplified the GFP coding sequence, USP18 F and R primers amplified the USP18 housekeeping gene in the HEK293 samples, and LRP1 F and R primers amplified the LRP1 housekeeping gene in the J774A.1 samples. PON1 F and R bands were not bright enough to be considered positive (Figure 4.6).

All mRNA samples from flasks not transfected with pGFP that underwent RT-PCR with the GFP F and R primers resulted in primer-dimer bands, but the housekeeping primers, USP18 F and R for HEK293 and LRP1 F and R for J774A.1, did produce bands of the expected sizes (Figure 4.7). All bands were sequence verified as either primer-dimer or the relevant housekeeping gene.

Some mRNA samples had to be collected twice due to a lack of evidence of successful mRNA harvest, as shown by the lack of housekeeping bands for EHG.1 48 hours, OHG.1 96 hours, OJG.1, LJG.1, and EJG.1 in Figures 4.7a and 4.7b, and then presence of bands in Figures 4.7c and 4.7d. Day 2 NH.1, EH.1, and LH.1 samples produced a faint band with the GFP F and R primers in Figure 4.7a, but sequencing showed no match between what was amplified and the pGFP vector.

Cumulatively, the RT-PCR data indicate that all treatment groups that were intended to be transfected with pGFP were transcribing pGFP, even if translation was not evident in the randomized pictures taken.

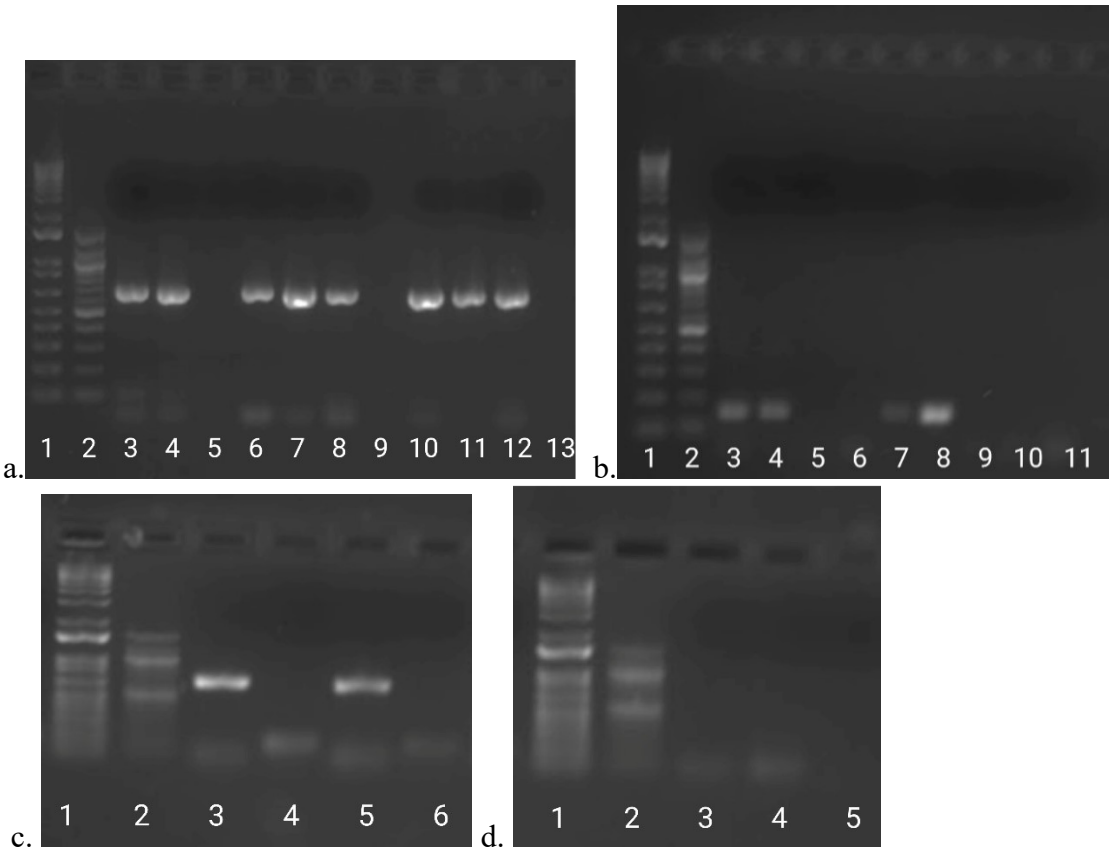

Figure 4.6. Images of 1% agarose gels dyed with ethidium bromide demonstrating RT-PCR results for "Equalized" cell samples that were exposed to pGFP. Top left (a.) are all pGFP-transfected cell mRNA samples amplified with GFP F and R. Lane 1 - 1kb ladder, lane 2 - 100bp ladder, lane 3 - OHG.1 harvested 48 hours post-transfection, lane 4 - LHG.1 harvested 48 hours post-transfection, lane 5 - EHG.1 harvested 48 hours post-transfection, lane 6 - OHG.1 harvested 96 hours post-transfection, lane 7 - LHG.1 harvested 96 hours post-transfection, lane 8 - EHG.1 harvested 96 hours post-transfection, lane 9 - empty, lane 10 - OJG.1, lane 11 - LJG.1, and lane 12 - EJG.1. Top right (b.) are all pGFP-transfected mRNA samples amplified with either USP18 R and F or PON1 R and F. USP18 primer set was used on all HEK293 samples, and PON1 primer set was used on all J774A.1. Lane 1 - 1kb ladder, lane 2 - 100bp ladder, lane 3 - OHG.1 harvested 48 hours post-transfection, lane 4 - LHG.1 harvested 48 hours post-transfection, lane 5 - EHG.1 harvested 48 hours post-transfection, lane 6 - OHG.1 harvested 96 hours post-transfection, lane 7 - LHG.1 harvested 96 hours post-transfection, lane 8 - EHG.1 harvested 96 hours post-transfection, lane 9 - OJG.1, lane 10 - LJG.1, and lane 11 - EJG.1. Bottom left (c.) are the reruns of EHG.1 48 hours post-transfection and OHG.1 96 hours post-transfection. Lane 1 - kb ladder, lane 2 - 100bp ladder, lane 3 - EHG.1 amplified with GFP F and GFP R, lane 4 - EHG.1 amplified with USP18 F and USP18 R, lane 5 - OHG.1 amplified with GFP F and GFP R, and lane 6 - OHG.1 amplified with USP18 F and USP18 R. Bottom right (d.) are the J774A.1 RT-PCRs using LRP1 F and R. Lane 1 - 1kb ladder, lane 2 - 100bp ladder, lane 3 - EJG.1, lane 4 - OJG.1, and lane 5 - LJG.1. Bands were extremely faint, so they were sent for sequencing to confirm.

a. 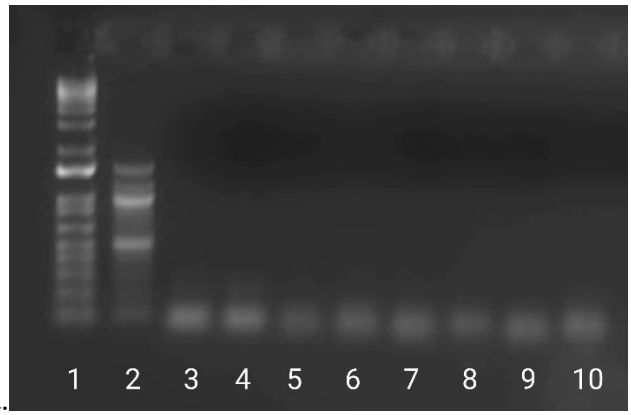

b. 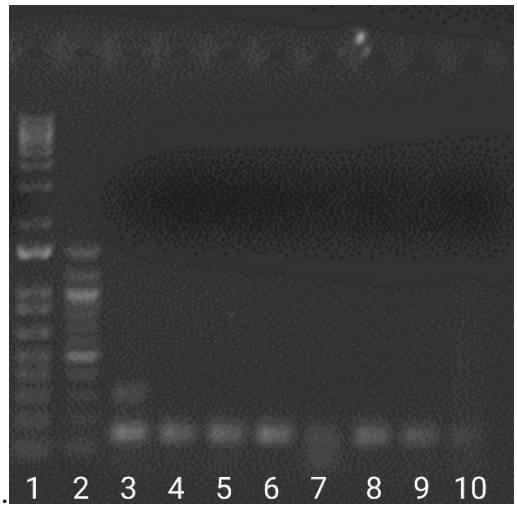

c. 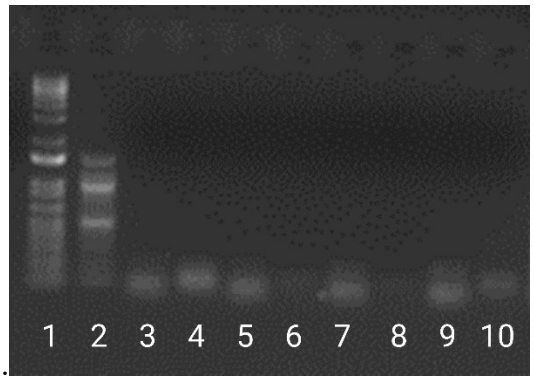

Figure 4.7. Images of 1% agarose gels dyed with ethidium bromide demonstrating RT-PCR results for "Equalized" cell samples that were not exposed to pGFP. Top left (a.) are the HEK293 samples amplified with GFP F and GFP R. Lane 1 - 1kb ladder, and lane 2 - 100bp ladder Lanes 3 through 6 - samples harvested at 48-hours post-transfection. Lane 3 - NH.1, lane 4 - EH.1, lane 5 - OH.1, and lane 6 - LH.1. Lanes 7 through 10 are samples harvested at 96-hours post-transfection. Lane 7 - NH.1, lane 8 - EH.1, lane 9 - OH.1, and lane 10 - LH.1. Top right (b.) has the same loading order as the image to the left (a.), except the samples were amplified with USP18 F and USP18 R. Bottom (c.) are the J774A.1 samples amplified with either GFP F and GFP R or LRP1 F and LRP1 R. Lane 1 - 1kb ladder, lane 2 - 100bp ladder, lane 3 - EJ.1 amplified with GFP primer set, lane 4 - EJ.1 amplified with LRP1 primer set, lane 5 - OJ.1 amplified with GFP primer set, lane 6 - OJ.1 amplified with LRP1 primer set, lane 7 - LJ.1 amplified with GFP primer set, lane 8 - LJ.1 amplified with LRP1 primer set, lane 9 - NJ.1 amplified with GFP primer set, and lane 10 - NJ.1 amplified with LRP1 primer set.

J774A.1 cells overall did not produce significant fluorescence data within this project. However, the production of mRNA was evidenced by the RT-PCR data, indicating that transfection was successful. It is known that J774A.1 cells are capable of producing GFP, so a couple of hypotheses were formed [461]. One hypothesis for the lack of GFP evidence is that the

randomized imaging did not locate regions with larger numbers of fluorescing J774A.1 cells within the flasks, which may have been present in extremely small numbers. The second hypothesis is that translational components within the selected pGFP vector may not be the most compatible with J774A.1 cells. If pursued again, use of a GFP-encoding vector with proven expression in J774A.1 cells may need to be used. However, this hypothesis was not explored within this project because the goal was to determine a cell line, timeline, and transfection method for the pSC6 vaccine protein production, and the pGFP selected for this project has key similarities to pSC6 to allow for this objective to be met.

4.5.1.2. Results and Discussion for "Optimized" Protocols

Data was not normally distributed, as indicated by the Kolmogorov-Smirnov and Shapiro-Wilk tests ($P<0.001$), however, data could not be transformed because of the presence of values at or below 0.

The Univariate General Linear Model determined that there was a significant between-subject effect when looking at each independent variable and their combinations ($P<0.001$) (Figure 4.8). In the pairwise comparisons of the General Linear Model, it was found that Lipofectamine3000 and jetOPTIMUS® methodologies had higher values than Electroporation and Non-transfected methodologies ($P<0.001$) but were not different from each other ($P=0.074$) (Figure 4.8). Additionally, in the pairwise comparison for cell type, HEK293 had higher values than J774A.1 ($P<0.001$), and in the pairwise comparison for DNA presence, pGFP had higher values than no DNA ($P<0.001$) (Figure 4.8). The culmination of GLM results point to either Lipofectamine3000 or jetOPTIMUS® in HEK293 as an ideal combination for protein production at 24 hours with reduced loss in cell viability. It is important to note that the data analyzed are percentages of equally sized samples from larger flasks and that Lipofectamine3000

transfections are performed on a higher cell count than jetOPTIMUS® (Figure 4.9). Therefore, it was determined that Lipofectamine3000 in HEK293 cells was likely the ideal combination for future vaccine testing if harvesting occurs 24-hours after transfection.

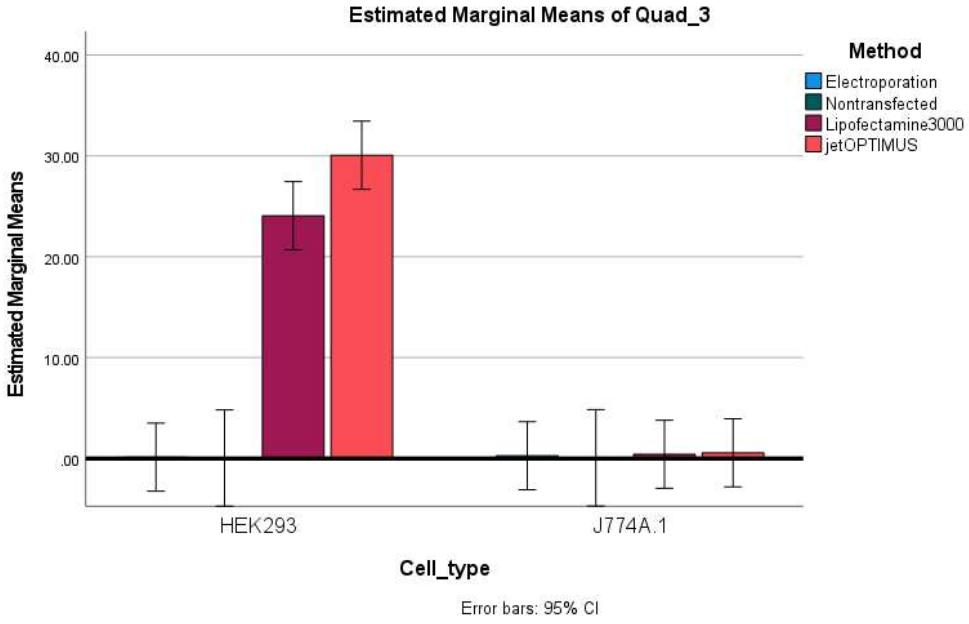

a.

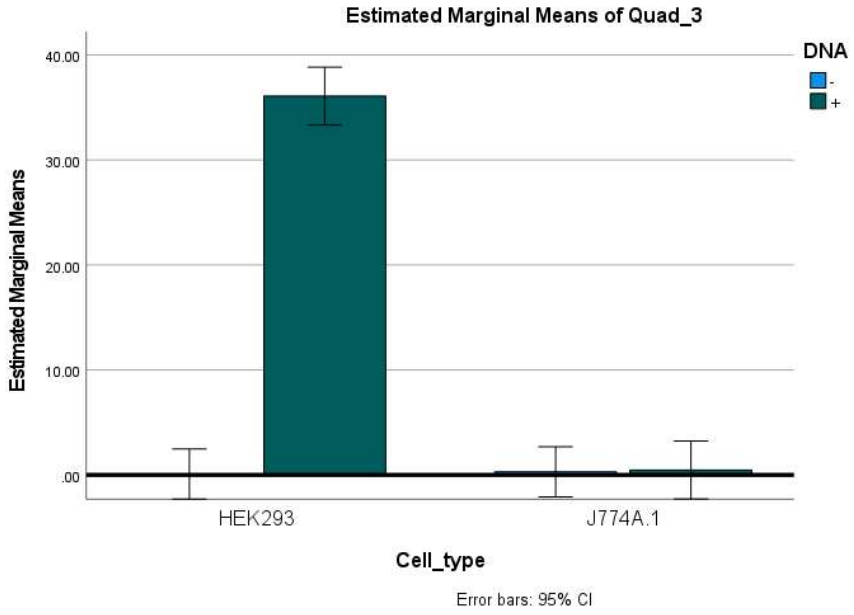

b.

Figure 4.8. SPSS GLM GFP-positive viable cell output graphs. Top (a.) is a bar graph of estimated marginal means of percentages of total cell population that were GFP-positive and viable by transfection method and cell type. Bottom (b.) is a bar graph of the estimated marginal means of percentages of total cell population that were GFP-positive and viable by pGFP presence and cell type.

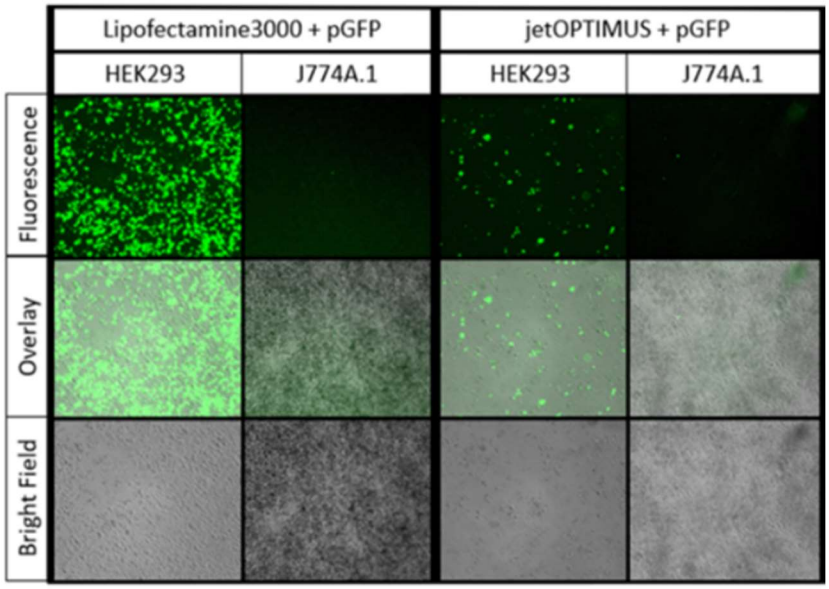

Figure 4.9. Sample images of LHG.2, OHG.2, LJG.2, and OJG.2 before sending for flow cytometry analysis. Demonstrates the differences in fluorescence presence between LHG.2 and OHG.2 despite the lack of statistical differences.

The low GFP values for EHG.1 and EHG.2 could be because of the protocol used. Upon investigation, other electroporation protocols were found with varied recommended voltages [419, 462]. Additionally, some of these protocols mention the inclusion of a buffer reagent which is intended to mimic cytoplasm compositions, aiding in the resealing of pores after the shock and increasing viability [462, 463]. If pursued again, future experiments should evaluate a variety of electroporation protocols, preferably with a protective buffer.

4.5.2. pSC6 Design and Construction

The pSIDT and pSQ double digests with NheI and SalI produced the expected band sizes when compared to the 1kb Plus ladder: 2866 bp and 1608 bp for pSIDT and 4650 bp and 1194 bp for pSQ (Figure 4.10). The pSC6 minipreps were all the expected size of 5669bp (Figure 4.11), which indicated that the ligation of the pSIDT insert and pSQ backbone was

successful. Sequencing data was matched to all components with 100% sequencing identification and 100% query cover, as indicated by SnapGene and nBLAST through NCBI (Figure 4.11).

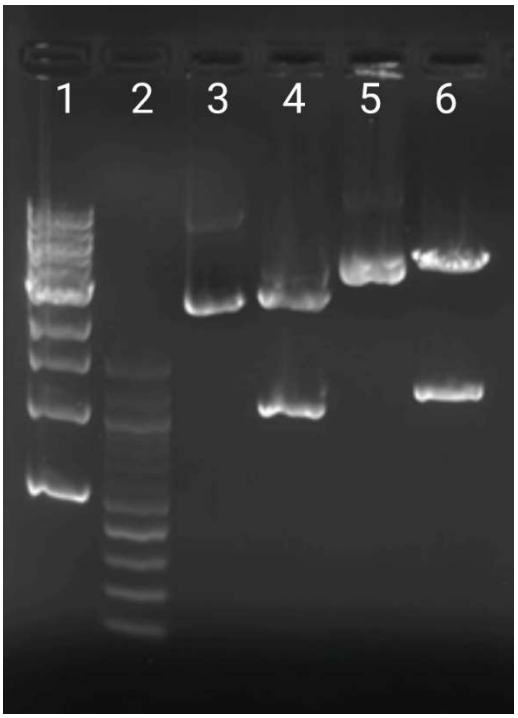

Figure 4.10. Gel confirmation of pSIDT and pSQ sizes and NheI SalI digests on a 1% agarose ethidium bromide gel. Lane 1- 1kb (NEB), lane 2 - 100bp (NEB), lane 3 - pSIDT midiprep, lane 4 - pSIDT NheI SalI digest, lane 5 - pSQ midiprep, and lane 6 - pSQ NheI SalI digest.

a.

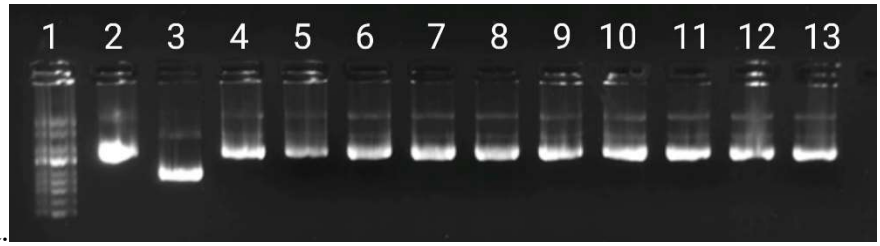

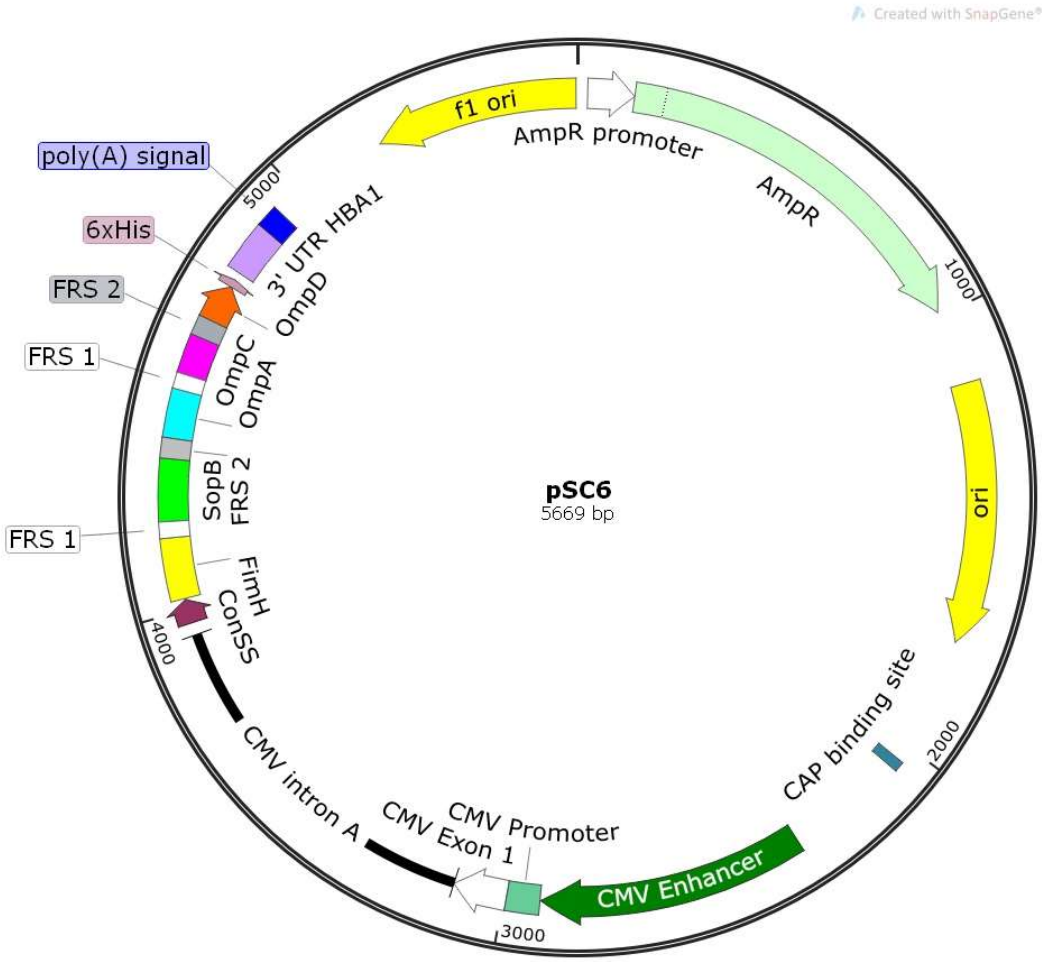

b.

Figure 4.11. Gel confirmation of pSC6. Top (a.) is a 1% agarose ethidium bromide gel with Supercoiled ladder in lane 1, pSQ midiprep in lane 2, pSIDT midiprep in lane 3, pSC6 miniprep 1 in lane 4, miniprep 2 in lane 5, miniprep 3 in lane 6, miniprep 4 in lane 7, miniprep 5 in lane 8, miniprep 6 in lane 9, miniprep 7 in lane 10, miniprep 8 in lane 11, miniprep 9 in lane 12, and miniprep 10 in lane 13. All minipreps ran the expected size of 5669 bp. Bottom (b.) is the SnapGene circular map of pSC6 demonstrating its expected size with confirmed sequencing.

4.5.3. *In Vitro* Testing of pSC6

In the pursuit of establishing a 6X His standard curve, plate one did not produce absorbances that reflected a correlation with protein concentrations, regardless of the antibody dilutions (1:5,000, P=0.1615; 1:10,000, P=0.4307; 1:20,000, P=0.1834) (Figure 4.12). Plate two also did not result in correlations between protein concentration and absorbance regardless of antibody dilutions (1:5000, P=0.2026; 1:10,000, P=0.1689; 1:20,000, P=0.1198) (Figure 4.12). For plate three, all protein dilution series were positively correlated with the absorbance readings in all three antibody dilution conditions (Figure 4.12). The 1:5000 antibody dilution produced an r of 0.9944 (P<0.0001). The 1:10,000 antibody dilution produced an r of 0.9954 (P<0.0001). The 1:20,000 antibody dilution produced an r of 0.9935 (P<0.0001). All within-sample CVs for protein-coated wells ranged from 0 to 19.87543.

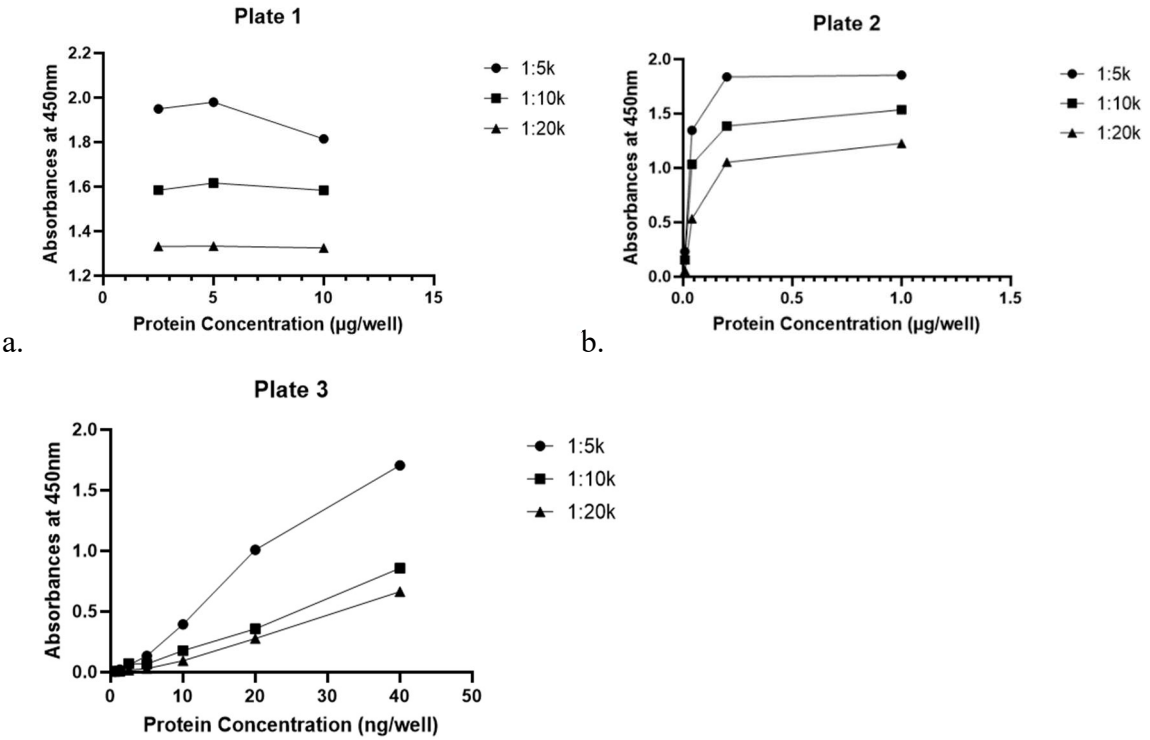

Figure 4.12. Absorbance at 450nm by protein concentration graphs for ELISA plates to establish a 6XHis standard curve. Top left (a.) is the graph of results for plate 1, which tested protein concentrations of 2.5, 5, and 10 µg/well against antibody dilutions of 1:5000, 1:10,000 and 1:20,000. Top right (b.) is the graph of results for plate 2, which tested protein concentrations of 1 µg/well, 0.2 µg/well, 40 ng/well, and 8 ng/well against antibody dilutions of 1:5000, 1:10,000, and 1:20,000. Bottom left (c.) is the graph of results for plate 3, which tested protein concentrations of 0, 20, 10, 5, 2.5, 1.25, and 0.625 ng/well against antibody dilutions of 1:5000, 1:10,000, and 1:20,000.

For the pSC6 24 hours lysate and media plates, intraplate CVs were 6.277 and 6.245 respectively. The Correlation tests for the standard curves produced r values of 0.9984 and 0.9943 respectively both with P values of <0.0001. Sample data was normally distributed as indicated by the Kolmogorov-Smirnov (P=0.200) and Shapiro-Wilk tests (P=0.280).

The Multivariate GLM indicated that 24-hour media interpolated values were impacted by treatment (P<0.001) and dilution factor (P=0.007) and that lysate interpolated values were impacted by treatment (P<0.001) and dilution factor (P<0.001). Pairwise comparisons indicated that, for the lysate samples, pSC6 had higher interpolated values than both non-transfected

(P<0.001) and Lipofectamine3000 samples (P<0.001) (Figure 4.13). The pairwise comparison indicated that pSC6 spent media had higher interpolated values than the non-transfected HEK293 spent media (P=0.005) but not Lipofectamine3000 HEK293 spent media (P=0.240) (Figure 4.13). For lysate and media samples, there were no differences in interpolated values between Lipofectamine3000 and Non-transfected (Lysate P=1.000; Media P=0.321). Therefore, it was concluded that the null hypothesis for aim 2 of this portion of this project could be rejected, and that pSC6 was producing detectable proteins within the cells. However, the null hypothesis for aim 3 for this portion of this project could not be rejected. The lack of evidence for pSC6 secretion could be because of the time of harvest, in that there may not have been enough time for protein secretion between transfection and sample harvest. A repeat of this experiment with harvest times beyond 24 hours could be conducted to determine when secretion will take place.

For the 24-hour lysates, the diluted samples produced higher interpolated values than the undilute samples (P<0.001) (Figure 4.13). For media, the diluted samples produced lower interpolated values than the undilute samples (P<0.001) (Figure 4.13). The dilution of lysates may have created more room for antibody binding in a sample that is dense with other proteins from the HEK293 cells. The dilution of media may have reduced the number of proteins reacting in the direct ELISA. Further investigation would be needed to establish an exact cause.

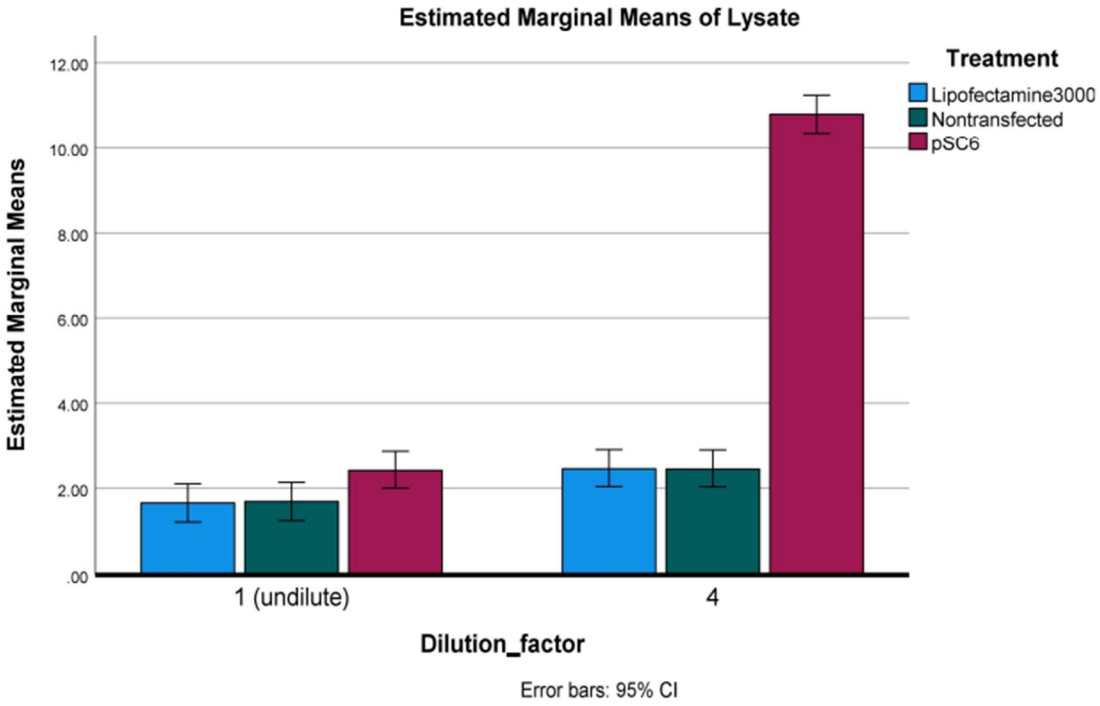

a.

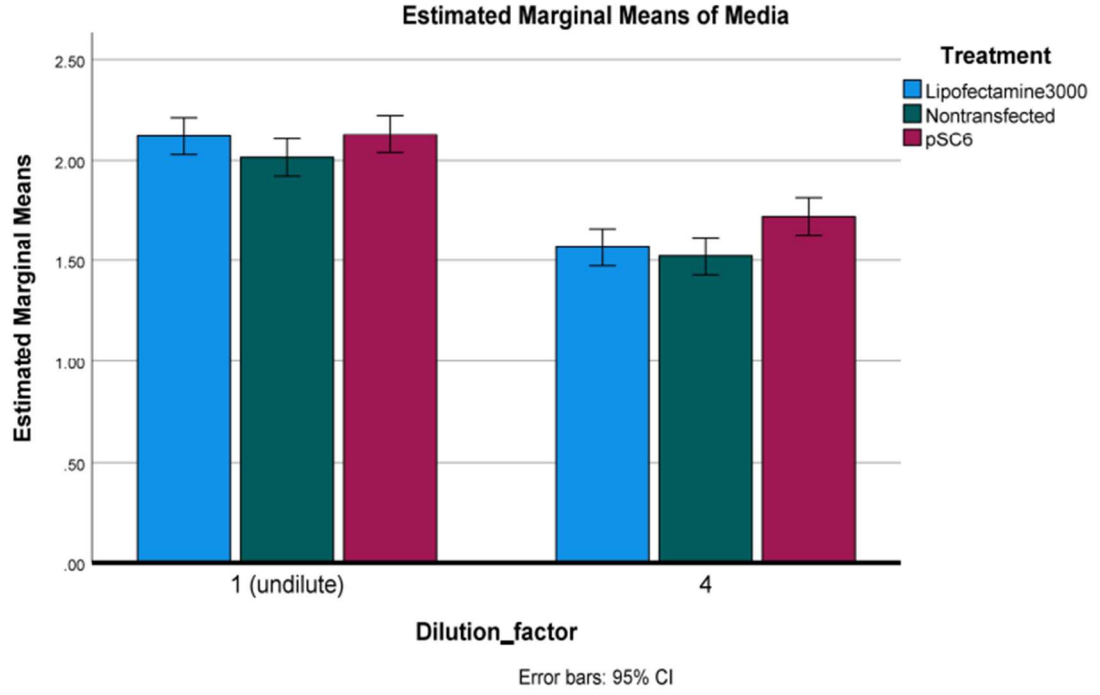

b.

Figure 4.13. SPSS multivariate GLM output graphs for pSC6 cell culture testing. Top (a.) is a bar graph of the estimated marginal means of interpolated values by treatment and dilution factor for lysate samples. Bottom (b.) is a bar graph of the estimated marginal means of interpolated values by treatment and dilution factor for spent media samples.

For the 4-day post-transfection media ELISA plate with anti-6X His, intraplate CV was 4.566. The Correlation test for the standard curve produced an r value of 0.9737 (P<0.0002), but the 40ng reading appeared to be an outlier. Removing the 40ng data from the standard curve produced an r value of 0.9919 (P<0.0001), so the curve without 40ng was used for data interpolation. All data was normally distributed, as evidenced by the Kolmogorov-Smirnov and Shapiro-Wilk tests (P=0.102 to 0.585). The univariate GLM indicated that treatment did impact interpolated protein amount (P<0.001). The post hoc Tukey Test indicated that pSC6 had greater interpolated values than both the Lipofectamine3000 only group (P<0.001) and Non-transfected group (P<0.001) (Figure 4.14). It also indicated that there was no difference between Lipofectamine3000 and Non-transfected (P=0.851) (Figure 4.14). Therefore, it was concluded that the null hypothesis could be rejected for aim three of this portion of the project, and that the pSC6 protein is likely being secreted from the HEK293 cells.

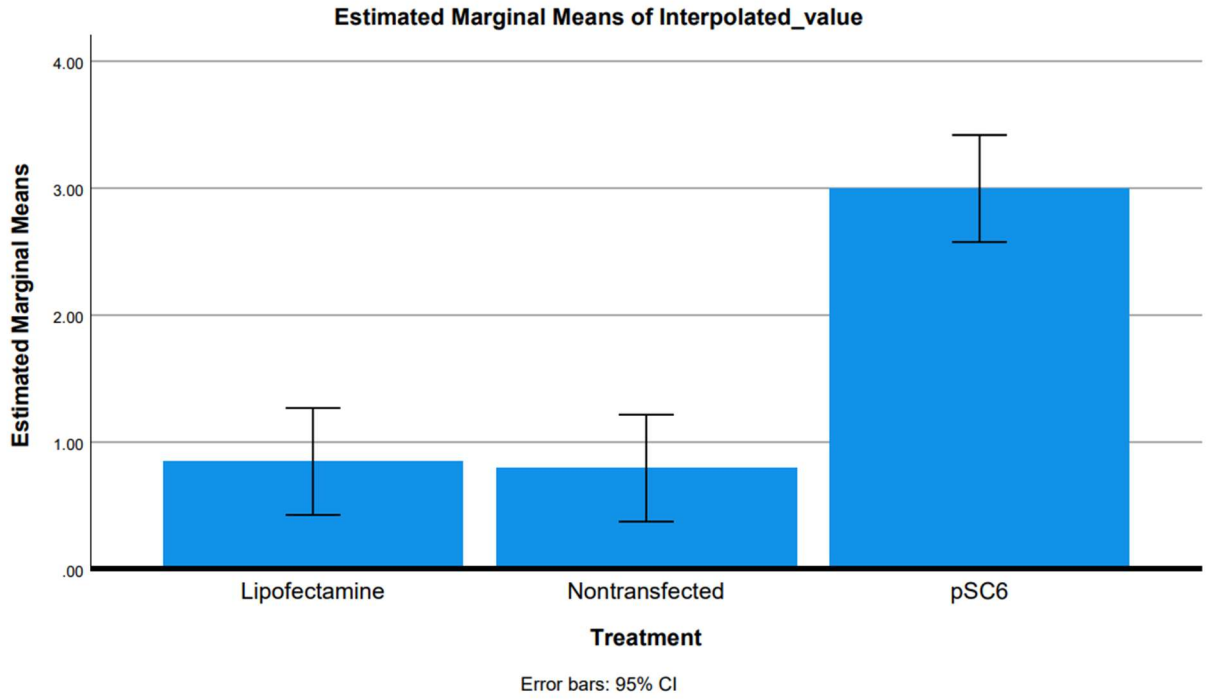

Figure: 4.14. Estimated marginal means of the interpolated values of spent media samples taken 4-days post-transfection by treatment groups.

4.5.4. Evaluating Immunogenic Potential

The 4-day post-transfection media indirect ELISA evaluating reactivity to convalescent horse serum had an intraplate CV of 15.2517. Both standard curves did not produce positive linear trends in the original Correlation Test (anti-IgG P=0.4687; anti-IgM P=0.2765), so the 3.75 ng/µL value was removed from each. The new standard curve Correlation Test with anti-IgM produced a Pearson r value of 0.9959 (P=0.0041) (Figure 4.15). The new standard curve Correlation test with anti-IgG produced a Pearson r value of 0.8802 (P=0.1198) (Figure 4.15). Because the anti-IgG standard curve did not produce a positive linear trend statistically different from 0, AMB values were not interpolated to either standard curve. This was somewhat expected because of the inability to establish a standard curve with the anti-IgG secondary antibody beforehand. If pursued again, efforts towards establishing a full ELISA protocol with anti-IgG should occur first.

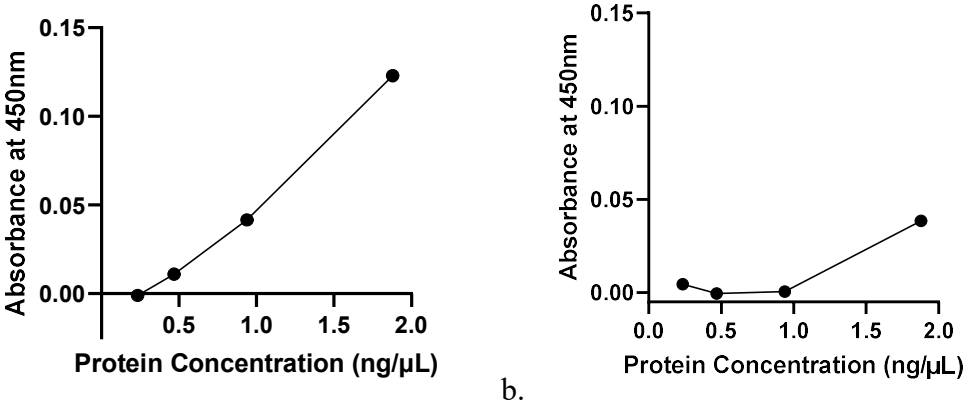

a. b.

Figure 4.15. Standard curve Correlation tests for the secondaries against convalescent horse serum. Left (a.) is the standard curve generated by anti-IgM. Right (b.) is the standard curve generate by anti-IgG.

AMBs for pSC6 flask E, Non-transfected flasks D and E, and Lipofectamine3000 flask A exposed to Goat anti Horse IgG (T) secondary were excluded from analysis because of their high CVs (37.2634 to 47.14045). AMBs for pSC6 flask A and Non-transfected flask E exposed to

Goat Anti-Equine IgM were excluded from analysis because of their high CVs (42.73913 to 51.87819). Data was normally distributed for all independent variables except IgG, as indicated by the Kolmogorov-Smirnov and Shapiro-Wilk tests ($P<0.001$). Data could not be transformed because of values at or less than 0.

The Univariate GLM indicated that there was no interaction between secondary antibody used and treatment group ($P=0.094$) and that there was no difference in means for treatment groups ($P=0.793$) (Figure 4.16). Therefore, it was determined that the null hypothesis for aim 1 of this portion of this project could not be rejected, and that proteins produced by the pSC6 vaccine were not detectable by the available convalescent horse antibody within the used ELISA parameters. If pursued again, serum collected within two months of a natural infection should be used in conjunction with the anti-IgM antibody, as explained in Chapter 3. Additionally, the primary and secondary antibodies used for the anti-IgM portion of this ELISA were 4+ years old, and it is hypothesized that their quality waned. Therefore, it is recommended that future pursuits should use primary and secondary antibodies closer to their acquisition dates.

There was a difference in means for secondary antibody, in which the anti-IgM produced higher AMB values than anti-IgG ($P<0.001$) (Figure 4.16). The establishment of an anti-IgM ELISA protocol beforehand may have contributed to this outcome, even with the potential decline in antibody quality.

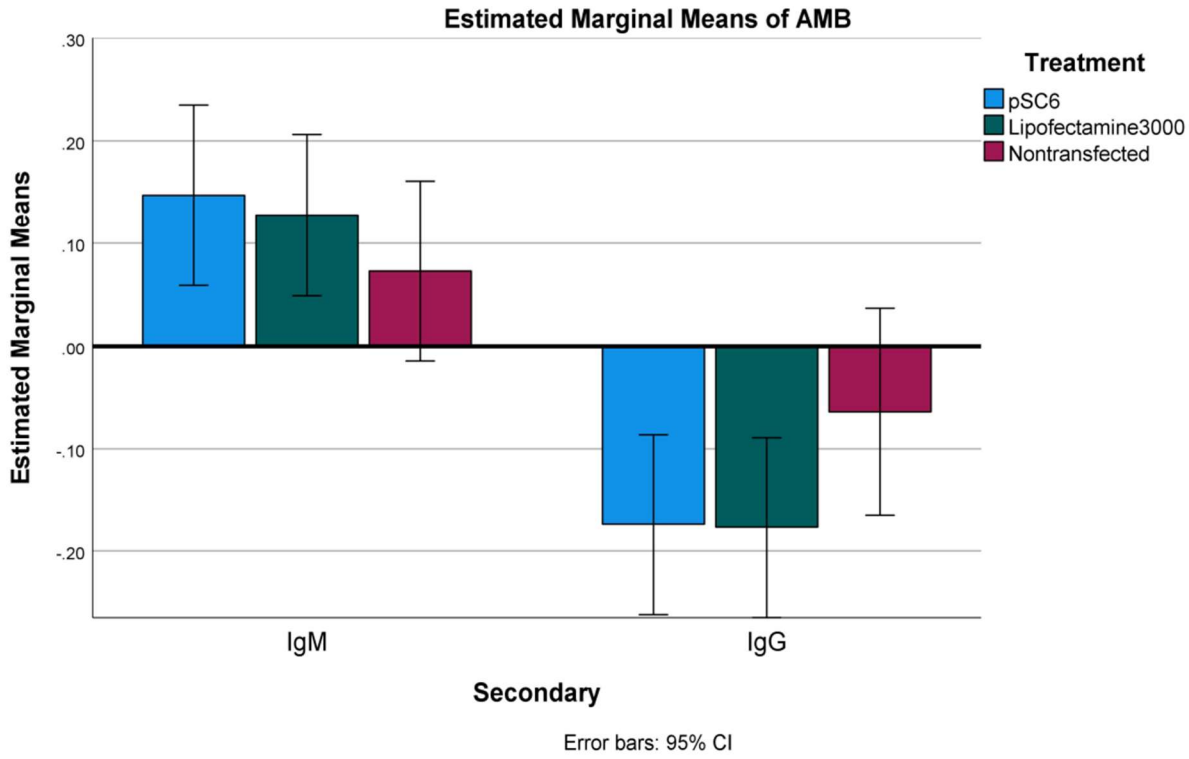

Figure 4.16. Estimated marginal means of AMB values from the 4-days post-transfection spent media samples against convalescent horse serum and anti-IgM or anti-IgG.
6X His protein purification and subsequent SDS-PAGE gels are in progress to confirm that the protein being detected is the expected size of the vaccine product (25.9 kDa) as further verification of protein production and secretion.

Another possibility for why the pSC6 proteins were not detectable by the available convalescent horse antibody is that the epitopes are not recognized by the naturally occurring antibody. This hypothesis is at least partially supported by the MHC-II prediction outputs. The new analysis of the vaccine epitopes for MHC-II binding predictions did not match the predictions produced in Chapter 2 of this project (Appendix C). In the new analysis, FimH and SopB had lower immunogenic peptide counts, and OmpA had a lower immunogenic peptide count and fewer immunogenic peptides across multiple alleles. OmpC had the same immunogenic peptides as before, but the percentile ranks changed. OmpD had the same immunogenic peptides as before along with some additional immunogenic peptides. However,

the OmpD peptides' percentile ranks changed and were not predicted to be immunogenic across all the same alleles.

The changes in predictions are hypothesized to be because of the updates to the IEDB Analysis Resource software. Updates occurred after the original analysis, with new database sources being as recent as 2020 [464, 465]. Therefore, one or both of the following suggestions should likely be pursued before any *in vivo* testing occurs with pSC6. The first suggestion is to conduct additional analyses of the vaccine epitopes, such as the plethora of options for T cell epitope predictions within the IEDB Analysis Resource [271]. The second suggestion is to select new epitopes based on new analyses of the whole-protein sequences using the culmination of outputs from the T cell epitope prediction software within IEDB. If using MHC-I and MHC-II binding predictions again, the updated advisement of IEDB is to make selections based on percentile ranks of less than 1% and less than 10% for MHC-I and MHC-II respectively [466]. Therefore, future analyses should also move away from the arbitrary 5^{th} percentile rank selection method previously used.

Chapter 5. Summary and Conclusion

S. Javiana is among a list of nontyphoidal *Salmonella* serotypes regarded as a serious public health concern. No vaccines currently exist for *S.* Javiana, and vaccines in existence for *Salmonella* have several pitfalls potentially addressed by a nucleic acid-based vaccine design. The experiments within this project were intended to begin the pursuit of a multi-epitope recombinant pDNA-based vaccine for protection against *Salmonella enterica* subspecies *enterica* serovar Javiana and potentially other *Salmonella* serotypes.

The initial vector designs – pSCP, pSECP, and pSSCP – lacked evidence of protein production in HEK293 cells or immune response in quail as determined through indirect ELISA data. However, it was found that the pCP versions of the vaccines were able to enter HEK293 cells and be transcribed as evidenced by RT-PCR. Several hypotheses were formulated for the lack of evidence for protein production, including assay specificity issues and backbone vector design elements.

In the attempts to address the concerns of specificity of convalescent serum antibodies to LPS, some important discoveries were made. It was found that use of CelLytic™ B Plus Kit could lead to protein harvest with endotoxin levels below the FDA threshold. Additionally, an ELISA plate was identified that leaches endotoxin levels below the FDA threshold. However, nonspecific binding in the assays used was still apparently an issue, as evidenced by positive indirect ELISA data from cell culture lysates and from quail serum regardless of treatment groups.

The final vaccine design, pSC6, was constructed in response to all hypothesized issues with the initial pCP vaccine designs without altering the epitope-FRS region encoded within the ORF. The pSC6 vector was the only design in this project to have clear evidence of resulting

protein production and secretion within a mammalian cell line (HEK293), as evidenced by direct ELISA data. Protein production was evidenced at 24 hours post-transfection, and secretion was evidenced at 4 days post-transfection. If continued research is pursued with the pSC6 vector, a longitudinal *in vitro* experiment reflecting Chapter 4 of this experiment should be performed to determine a secretion timeline before pursuing any *in vivo* studies.

Experiments in anticipation of testing pSC6 were conducted using a GFP vector to establish the best materials and methods for optimal protein production and harvest time. It was found that there were no differences in GFP protein production and cell counts between any of the 4 days following transfection, starting at 24 hours, and it was determined that Lipofectamine3000 in HEK293 leads to more protein production than electroporation or jetOPTIMUS in HEK293 cells or J774A.1 at 24 hours post-transfection.

All experiments within this project occurred across approximately a 5-year span. Technology has been improved upon and expanded since the inception of this project. Any future studies seeking to expand on the research within this project should reevaluate the immunogenicity of the epitopes within this vaccine. MHC affinity prediction software have been updated since their initial use within this project, as evidenced in Chapter 4 of this project, and additional prediction software platforms for T cell processing and immunogenicity now exist. Analyzing the selected whole-protein sequences again with the newly available programs could lead to a more efficacious vaccine.

Appendix A. Protocols

Thermo Fisher Restriction Digest Protocol [467]

1. Combined the following at room temperature in a thin-walled microcentrifuge tube:
    a. 5 µL FastDigest Green Buffer
    b. 1 µg DNA
    c. 1 µL each enzyme used
2. Brought total volume in tube to 50 µL with nuclease-free water.
3. Briefly spun down via centrifuge to combine.
4. Incubated at 37°C for specified time of the enzyme.

Zymoclean™ Gel DNA Recovery Kit [468]

1. DNA was excised from gel using a razor blade and transferred to a 1.5mL microcentrifuge tube that was pre-weighed.
2. Tube was weighed again with the DNA fragment inside.
3. Pre-weight was subtracted from the new weight (both in grams) and multiplied by 3000 to determine ADB volume in microliters for use.
4. ADB was added to the tube with the DNA, and the agarose was melted at 55°C for 10 minutes in a water bath.
5. Melted agarose solution was transferred to a Zymo-Spin Column in a Collection Tube, which was then centrifuged at 16000 ×g for 1 minute. Flow-through was discarded.
6. 200 µL DNA Wash Buffer was added to the column and centrifuged at 16000 ×g for 30 seconds. This step was repeated once, but centrifugation was increased to 1 minute on the second spin. Flow-through was discarded both times.
7. 15 µL DNA Elution Buffer was added directly to the Zymo-Spin Column, which was transferred to an Eppendorf DNA LoBind Tube (Sigma Aldrich, Cat EP0030108310) and centrifuged for 1 minute at 16000 ×g.

Zymo DNA Clean & Concentrator®-5 [469]

1. Two to five volumes of DNA Binding Buffer to each volume of DNA sample (Table A.1) were combined in a 1.5mL microcentrifuge tube and vortexed briefly.

Table A.1. DNA Binding Buffer to Sample ratios for Zymo DNA Clean & Concentrator

Application	**DNA Binding Buffer : Sample**
Plasmid, genomic DNA	2 : 1
PCR product, DNA fragement	5 : 1

2. Mixture was transferred to a Zymo-SpinTM Column in a collection tube, which was then centrifuged for 30 seconds at 16,000 ×g. Flow-through was discarded.
3. 200 µL DNA Wash Buffer was added to the column and centrifuged at 16,000 ×g for 30 seconds. This step was repeated once, but centrifugation was increased to 1 minute on the second spin. Flow-through was discarded both times.
4. 15 µL DNA Elution Buffer was added directly to the Zymo-Spin Column, which was transferred to an Eppendorf DNA LoBind Tube (Sigma Aldrich, Cat EP0030108310) and centrifuged for 1 minute at 16,000 ×g.

Quick Ligation Kit Protocol [470]

1. The following reaction was set up on a cold-block:
    a. 10 µL Quick Ligase Reaction Buffer (2X)
    b. 50 ng (0.020 pmol) Vector DNA
    c. 37.5 ng (0.060 pmol) Insert DNA
    d. 1 µL Quick Ligase
    e. QS to 20 µL with Nuclease-free water
2. The mixture was gently combined via pipetting and a pulse in the microcentrifuge.
3. The mixture was incubated at room temperature for 5 minutes.
4. Chilled the mixture on ice and used to transform competent *E. coli.*

NEB C2992 and C2925 Transformation/Transfection Protocols [471, 472]

1. 50 µL tube of cells was thawed on ice.
2. 1-5 µL containing 1pg to 100ng of pDNA was added to the cell mixture. The tube containing the mixture was flicked 4-5 times to mix the pDNA and cells together.
3. Tube with mixture was placed on ice for 30 minutes.
4. Tube with mixture was heat shocked at 42℃ for 30 seconds then placed back on ice for 5 minutes.
5. 950 µL of room temperature SOC media was added to the tube with mixture, and the now final transfection solution was placed in a 37℃ shaker incubator for 1 hour at 100rpm.
6. Agar plates made with appropriate selection media were warmed to 37℃ before spreading 50-100 µL of the transfection solution on each.
7. Plates incubated at 37℃ overnight.

ZymoPURE™ II Plasmid Midiprep [473]

1. 50 mL of bacterial culture, grown in either LB or SB with ampicillin, was centrifuged at 3,400 ×g for 10 minutes. Supernatant was discarded.
2. 8 mL of ZymoPURE P1 was used to resuspend the pellet via vortexing.
3. 8 mL of ZymoPURE P2 was added and immediately mixed by inversion. This mixture incubated at room temperature for 2 minutes.
4. 8mL of ZymoPURE P3 was added and immediately mixed by inversion until solution was fully yellow.
5. Mixture was added to a ZymoPURE Syringe Filter-X and pushed through to a clean 50 mL conical tube via a plunger.
6. 8 mL of ZymoPURE Binding Buffer was added to the flow-through from step 5 and mixed via inversion.
7. Mixture from step 6 was added to the Zymo-Spin V-PS Column Assembly connected to a vacuum manifold. Vacuum was turned on until all solution was passed through the column.
8. 5 mL of ZymoPURE Wash 1 was added to the column assembly and passed through via vacuum suction.
9. 5 mL of ZymoPURE Wash 2 was added to the column assembly and passed through via vacuum suction. This step was repeated once.
10. Reservoirs were removed from the Zymo-Spin V-PS Column

AccuPrime™ *Pfx* DNA Polymerase/ PCR Protocol [474]

1. The following was mixed in a thin-walled microcentrifuge tube:
    a. 5 µL 10X AccuPrime™ *Pfx* Reaction Mix
    b. 1.5 µL (10 µM) of each primer
    c. 10 pg to 200 ng Template DNA
    d. 1 µL AccuPrime™ *Pfx* DNA Polymerase
    e. QS to 50 µL with sterile dH_2O
2. The tube was capped and briefly centrifuged.
3. The tube was transferred to a thermal cycler with the following settings:
    a. Denaturation at 95°C for 2 minutes
    b. 25-35 cycles of the following:
        1. Denature at 95°C for 15 seconds
        2. Anneal at primer-specific temperature for 30 seconds
        3. Extend at 68°C for 1 minute/kb
    c. Maintain at 4°C indefinitely.

Sigma-Aldrich CelLytic™ B Plus kit protocol- Trial Scale Extraction [475]

1. Bacteria were grown in 5 mL of selected culture broth overnight.
2. 1.5mL of culture was placed in each microcentrifuge tube and centrifuged at 17,000 ×g for 2 minutes. Spent media was discarded, preserving the pellet.
3. CelLytic™ B Plus Working Solution was mixed as follows in a sterile 15mL conical tube:
    a. 5mL CelLytic™ B Reagent
    b. 0.1mL Lysozyme
    c. 0.05mL Protease inhibitors
    d. 1µL Benzonase
11. The pelleted bacteria were resuspended in 0.4mL of CelLytic™ B Plus Working Solution by vortexing.
12. The resuspended pellet incubated at room temperature for 15 minutes on the Titer Plate Shaker (Lab Line Instruments, Inc., Melrose Park, ILL) on setting 3.
13. Resuspended pellets were centrifuged at 17,000×g for 5 minutes.
14. Soluble proteins in the aqueous layer were transferred to a nonpyrogenic tube via pipet.

Abcam Endotoxin Removal Kit protocol [476]

1. Snapped the bottom plug off of Rapid Endotoxin Removal Spin Column (RERSC) and removed the cap. Placed the RERSC in an Endotoxin-free Collection Tube and centrifuged them at 15,000×g for 10 seconds in the microcentrifuge. Flow-through was discarded.
2. 0.5 mL of the Endotoxin Removal Equilibration Buffer was added to the RERSC, and the RERSC was centrifuged at 15,000×g for 10 seconds. Flow-through was discarded.
3. 0.5mL of the Rapid Endotoxin Removal Regeneration Buffer was added to the RERSC, and the RERSC was centrifuged at 15,000×g for 10 seconds. Flow-through was discarded.
4. Step three was repeated once.
5. 0.5mL of the Rapid Removal Wash Buffer was added to the RERSC, and the RERSC was centrifuged at 15,000×g for 10 seconds. Flow-through was discarded.

6. Step five was repeated once.
7. 0.5mL of the Endotoxin Removal Equilibration Buffer was added to the RERSC, and the RERSC was centrifuged at 15,000×g for 10 seconds. Flow-through was discarded.
8. Step seven was repeated once.
9. The RERSC was moved to a new Endotoxin-free Collection Tube.
10. Protein Sample was pipetted into the RERSC.
11. Pulsed the RERSC in the centrifuge for 3 seconds to collect the sample.

ThermoFisher Pierce™ BCA Protein Assay Kit [477]

1. Prepared the standards as follows:

Vial	**Volume of endotoxin-free PBS**	**Volume and source of BSA (µL)**	**Final BSA concentration (µg/mL)**
A	0 µL	300 of stock	2000
B	125 µL	375 of stock	1500
C	325 µL	325 of stock	1000
D	175 µL	175 of vial B dilution	750
E	325 µL	325 of vial C dilution	500
F	325 µL	325 of vial E dilution	250
G	325 µL	325 of vial F dilution	125
H	400 µL	100 of vial G dilution	25
I	400 µL	0	0

2. Prepared the working reagent (WR) by combining 50 parts BCA Reagent A with 1 part BCA Reagent B.
3. In duplicate wells on a 96-well plate, 25 µL/well of each standard and unknown sample was pipetted.
4. 200 µL of WR was added to each well, and the wells were mixed by plate shaking for 30 seconds.
5. Plate was covered with a membrane/film and incubated at 37°C for 30 minutes.
6. Absorbances were measured on a spectrophotometer at 562 nm.
7. Standard curve was plotted, and absorbances were interpolated to the line.

GenScript LAL ToxinSensor™ Endotoxin Detection System Protocol [478]

1. All specimens were diluted in LAL Reagent Water.
2. Prepared the standards by serial dilution with LAL Reagent Water, starting at 1 EU/mL down to 0.1 EU/mL.
3. 100 µL of each standard and unknown sample was transferred to its own endotoxin-free vial.
4. 100 µL of LAL (reconstituted) was added to each vial, which was then capped and mixed via gentle swirling.

5. Incubated the tubes at 37°C at the T2 specified time for the kit.
6. 100 µL of chromogenic substrate (reconstituted) was added to each vial, which was then capped and mixed via gentle swirling. This mixture incubated at 37°C for 6 minutes.
7. 500 µL of stop solution (reconstituted) was added to each vial, which was then capped and mixed via gentle swirling.
8. 500 µL of color-stabilizer #2 was added to each vial, which was then capped and mixed via gentle swirling.
9. 500 µL of color-stabilizer #3 was added to each vial, which was then capped and mixed via gentle swirling.
10. Samples were loaded onto a 96-well plate at 100 µL/well, and absorbances were measured on a spectrophotometer at 545 nm.
11. Standard curve was plotted, and absorbances were interpolated to the line.

Indirect ELISA Protocol [479]

1. Proteins were loaded onto the NUNC ELISA plate at 100µL/well
2. Carbonate bicarbonate buffer (made in-house; Table A) was used to coat all protein-loaded wells at 100µL/well.
3. Plate was covered with a membrane and incubated on the Titer Plate Shaker (Barnstead International, Dubuque, Iowa; model no: 4625; Lab Line Instruments, Inc in Melrose Park, IL) on setting "4" for 2-5 minutes.
4. Plate was transferred to a 4°C refrigeration for 20-24 hours to incubate.
5. Plate was warmed to room temperature through stationary incubation.
6. Contents of plate were discarded, and wells were blocked with 200µL/well freshly made (in-house) blocking buffer (Table A). Plate was covered with a membrane.
7. Plate incubated on the Titer Plate Shaker on setting "4" for 2 hours.
8. Contents of the plate were discarded.
9. Wells were washed with a freshly made (in-house) wash buffer (Table A.2) using the BioRad Immunowash (Model 1575; Catalog Number 170-7009) set to a 5-wash cycle. Plate was tapped dry.
10. Wells were loaded with primary – as specified within each chapter – at 100µL/well. Primary was room temperature and inverted to mix prior to plating. Plate was covered with a membrane.
11. Steps 7-9 were repeated.
12. Wells were loaded with secondary – as specified within each chapter – at 100µL/well. Secondary was room temperature and inverted to mix prior to plating. Plate was covered with a membrane.
13. Steps 7-9 were repeated.
14. Wells were each loaded with 100µL of 1-Step Ultra TMB-ELISA (ThermoScientific, Rockford, IL; Ref: 34028) in the dark. Plate was covered with a membrane.
15. Plate incubated for the amount of time specified within each chapter in the dark on the Titer Plate Shaker on setting "4".
16. TMB-Secondary reaction was stopped with 100µL/well 2M sulfuric acid (made in-house).
17. Reactions were read on the BioRad Benchmark Plus Microplate Spectrophotometer with a wavelength of 450nm.

Table A.2. Indirect ELISA Protocol reagent recipes.

Reagent	**10X PBS**	**Carbonate-bicarbonate buffer**	**Blocking buffer**	**Wash buffer**
Recipe	160g 140mM NaCl; 4.0g 1.5mM KH2PO4; 43.4g 8.0mM Na2HPO-7H2O; 4.0g 2.7mM KCl; 2.0L dH2O	1.59g Na2CO3 (or 1.86 g Na2CO3-H2O); 2.93g NaHCO3; QS to 1 liter with deionized water	1-gram Bovine Serum Albumin (Sigm, A9647); 10mL 10x PBS; QS to 100mL with ultra-filtered deionized water	25mL 20% Tween20 (Amresco, Ohio, 0777-1L) in deionized water; 100mL 10x DPBS; QS to 1 liter with ultra-filtered deionized water

Sigma-Aldrich CelLytic™ B Plus kit protocol- Large Scale Extraction [475]

1. Bacteria were grown in 250mL of selected culture broth overnight.
2. A 50mL conical tube was weighed prior to use.
3. The 250mL of bacterial culture were pelleted by centrifuging 50mL at a time at 5000×g for 10 minutes, discarding supernatant between spins. Pellet was weighed.
4. The following CelLytic™ B Plus Working Solution was mixed:
    a. 18mL CelLytic™ B Reagent
    b. 0.36mL Lysozyme
    c. 0.18mL Protease inhibitors
    d. 3.6µL Benzonase
5. The CelLytic™ B Plus Working Solution was added to the pellet at 10mL/gram and used to resuspend the pellet via gentle mixing.
6. The resuspended pellet incubated at room temperature for 15 minutes on the plate shaker on setting 3.
7. The resuspended pellet was aliquoted to 1.5mL microcentrifuge tubes, which were centrifuged at 16,000×g for 10 minutes.
8. Supernatant was transferred to nonpyrogenic microcentrifuge tubes.

Korle Lipofectamine3000 Protocol (T25) [273]

"Six T-25 flasks were seeded with approximately $0.7x10^6$ HEK 293 cells which were dissociated using TrypLE Express Enzyme (ThermoFisher Scientific, Waltham, MA). The T-25 flasks were incubated at 37°C supplemented with 5%CO2 for 48 hours until they were approximately 50% confluent containing ~$1.4x10^6$ cells. A 2.25 mL aliquot of serum-free Minimum Essential Medium +Earle's Salts+ 25mM HEPES + GlutaMAX media was added to a 15 mL conical tube supplemented with 67.5 µl of lipofectamine 3000 reagent. This mixture was vortexed briefly. Then 2.25 mL of serum free media containing 13.5 µl of SDB3 midi prep DNA (~2.5 µg of DNA/ T-25 flask) and 90 µl of P3000 reagent was added to the mixture followed by brief vortexing and incubation at room temperature for 15 minutes. Approximately 700 µl of the transfection complex was added to each of the six T-25 flasks."

QIAGEN QIAshredder & QIAGEN RNEasy® Plus Mini Kit [480]

1. 1 mL of lysate was passed through a QIAshredder via centrifugation at 1300 rpm for 1 minute. Centrifuge used was the Thermo Electron Corporation Heraeus Pic 17 Centrifuge.
2. Flow through was transferred to a gDNA Eliminator Spin Column placed in a 2 mL collection tube.
3. Centrifuged for 30 seconds at 10,000 ×g. Column was discarded.
4. Flow-through from step 3 was mixed with 350 µL of 70% ethanol via pipetting.
5. 350 µL of step 4 solution was transferred to an RNEasy® Spin Column placed in a 2 mL collection tube.
6. Centrifuged the tube from step 5 at 10,000 ×g for 15 seconds. Flow-through was discarded.
7. 700 µL of buffer RW1 was added to the column and centrifuged at 10,000 ×g for 15 seconds. Flow-through was discarded.
8. 500 µL Buffer RPE was added to the column and centrifuged at 10,000 ×g for 15 seconds. Flow-through was discarded.
9. Repeated step 8 but centrifuged 2 minutes. Flow-through was discarded.
10. Centrifuged at 13,000 ×g for 1 minutes to dry the membrane.
11. RNEasy® Spin Column was placed in a new 1.5 mL microcentrifuge tube (provided) and loaded with 50 µL RNase-free water directly to the spin column membrane.
12. Centrifuged the tube from step 11 at 10,000 ×g for 1 minutes to elute RNA.
13. Stored RNA at -30°C.

Life Technologies Lipofectamine3000 Protocol (T75) [429]

1. In a 15 mL conical tube labelled “Tube 1,” the following were combined:
    1. 975 µL serum free media. Media refers to the type used for feeding the cell line that will be transfected.
    2. 58.575 µL Lipofectamine reagent
2. In a separate 15 mL conical tube labelled “Tube 2,” the following were combined:
    1. 975 µL serum-free media. Media refers to the type used for feeding the cell line that will be transfected.
    2. DNA at the desired concentration.
    3. 39 µL P3000
3. Vortexed Tube 1 and Tube 2 briefly to mix. Pulse centrifuged to bring contents to the bottom of the tube.
4. Combined Tube 1 and Tube 2 by pipetting. Aspirated Tube 2 and dispensed into Tube 1.
5. Vortexed the product of step 4, still labelled Tube 1, to mix. Pulse centrifuged to bring contents to the bottom of the tube.
6. Incubated the Tube 1 from step 5 at room temperature for 15 minutes.
7. Transferred the contents of Tube 1 from step 6 to the flask of cells via pipetting. Contents were always approximately 2 mL.
8. Returned flask to the incubator.

jetOPTIMUS® Polyplus Protocol (T75) [430]

1. Diluted desired DNA amount into 1 mL jetOPTIMUS® buffer in a 15 mL conical tube.
2. Vortexed for 5 seconds and pulse centrifuged to get solution into the bottom of the tube.

3. Added jetOPTIMUS® Reagent into the DNA solution at a 1 : 1 ratio corresponding to the µg of DNA (1 µg DNA : 1 µL jetOPTIMUS® Reagent).
4. Vortexed step 3 product for 1 second and pulse centrifuged to bring solution into the bottom of the tube.
5. Incubated at room temperature for 10 minutes.
6. Transferred full jetOPTIMUS® transfection mixture to the flask via pipetting.
7. Returned flask to the incubator.
8. Visually inspected flask 4 hours later for signs of toxicity.

ImageJ Protocol [442, 456]

1. Open image in ImageJ software.
2. Process→ subtract background (12 pixels, no additional settings selected)
3. (If green) image → color → split channels
    a. Proceed only with the green channel
4. Image→ adjust → threshold
5. Process→ binary → fill holes
6. Process → binary → convert to mask
7. Analyze → analyze particles (size=120-infinity; circularity=0.00-1.00; show nothing; select "display results," "clear results," "summarize," and "exclude edges."

MidSci PCV (or TPP) Cell Counting Protocol [481]

1. Performed a hemocytometer count with 10 µL of cell sample.
2. Loaded 100 µL to 1 mL into the PCV tube and centrifuged at 2,500 ×g for 1 minute. Centrifugation was performed in a Thermo Electron Corporation Heraeus Pico17 Centrifuge.
3. Determined which number line in the PCV capillary was reached by the cell pellet.
4. Extrapolated the hemocytometer count to the PCV reading using the following formula series:
    a. V ÷ 10 µL = Y
        1. V = volume in PCV tube in µL
    b. Y × H = C
        1. Hemocytometer cell count from 10 µL sample = H
        2. C= cell count in PCV
    c. Extrapolate findings: If C at PCV line 1 is 1×10^6, then C at PCV line 2 is 2×10^6, C at PCV line 3 is 3×10^6, and so-on.
    d. 1000 µL/mL ÷ V × C = X
        1. X = cells per mL
5. Steps 1-4 were replicated 3 times to verify precision. Once precision was determined to be acceptable, only steps 2, 3, 4c, and 4d were followed.

NEB Restriction Digest Protocol [482]

1. Determined appropriate incubation temperature and NEBuffer through NEBcloner [483]
2. Combined the following in a thin-walled microcentrifuge tube:
    a. 1 µg DNA
    b. 5 µL 10X NEBuffer, as determined in step one
    c. 1 µL of each enzyme used

3. Brought total volume in tube to 50 µL with nuclease-free water.
4. Incubation time varied by enzyme, but was typically 1 to 2 hours.

NEB Q5 Site-Directed Mutagenesis Kit Quick Protocol (E0554) [484]

1. In a thin-walled microcentrifuge tube, the following were combined:
    a. 12.5 µL Q5 Hot Start High-Fidelity 2X Master Mix
    b. 1.25 µL of 10µM forward primer
    c. 1.25 µL of 10µM reverse primer
    d. 1 µL DNA (1-25ng/µL
    e. 9.0 µL nuclease-free water
2. Cycling conditions were set as follows:

Step	**Temperature (°C)**	**Time**
Initial Denaturation	98	30 seconds
25 Cycles	98	10 seconds
	Determined by primers	20 seconds
	72	30 seconds/kb
Final Extension	72	2 minutes
Hold	4	Until retrieved

3. KLD Reaction was set up as follows:
    a. 1 µL PCR product from step 2
    b. 5 µL 2X KLD Reaction Buffer
    c. 1 µL 10X KLD Enzyme Mix
    d. 3 µL nuclease-free water
4. KLD Reaction mix incubated at room temperature for 10 minutes.
5. 5 µL of the step 4 product was used to transfect 50 µL chemically-competent cells following manufacturer protocol.

Appendix B. Testing Endotoxin Reactivity

B.1. Introduction

The CelLytic B Plus kit produces *S.* Javiana proteins with endotoxin levels below 0.25EU/mL when diluted to 600 ng/µL or 60ng/µL, as explained in Chapter 3 of this project. What Chapter 3 did not definitively explore is the assumption that endotoxins <0.25 EU/mL would produce absorbance or AMB values lower than those produced by the *S.* Javiana proteins when exposed to the available antibodies. The experiment within this Appendix explores this assumption.

B.2. Aim and Hypothesis

The aim of this portion of the project is to determine if the *S.* Javiana proteins isolated via the CB method produce indirect ELISA absorbances differentially from their coordinating endotoxin levels. The hypothesis is that *S.* Javiana proteins will lead to higher absorbances than their coordinating endotoxin concentrations when exposed to the convalescent horse serum and anti-IgM antibody (H_0:$\mu_{60SJ} = \mu_{15SJ} = \mu_{3.25SJ} = \mu_{60EU} = \mu_{15EU} = \mu_{3.25EU}$; H_1: Not H_0).

B.3. Materials and Methods

Sample size was determined by use of an online sample size calculator for ANOVA [485]. AMB values from Table 3.5 were used as estimates for the means produced from the *S.* Javiana proteins. Zero was the estimated mean for the endotoxin samples. Standard deviation was estimated to be 0.05, alpha was 0.05, and power was 0.8. Sample size calculated was 3.

S. Javiana proteins were the same as those harvested for use in Chapter 4 of this project, which were stored at -20°C overnight before use. Proteins were serially diluted to 60 ng/µL, 15 ng/µL, and 3.25 ng/µL in endotoxin-free PBS. The endotoxin standard from the LAL

ToxinSensor™ Endotoxin Detection System (GenScript, cat L00350) was diluted to 0.02 EU/mL in endotoxin-free PBS. This was the approximate endotoxin concentration determined for the 60 ng/µL *S.* Javiana CB sample in Chapter 4 of this project. The 0.02 EU/mL were then serially diluted in endotoxin-free PBS to 0.004 EU/mL and 0.001 EU/mL, matching the dilution factors of the *S.* Javiana protein samples.

The indirect ELISA protocol (Appendix A) was performed with the following modifications:

1. The *S.* Javiana proteins and all spent media samples were used to coat 3 NUNC plates at 100µL/well in duplicate. Two wells were coated with endotoxin-free PBS to serve as a blank.

10. The primary antibody was convalescent serum in the stock blocking buffer at a 1:3000 ratio. All wells received 100µL/well of the primary.

12. All wells were coated with 100µL/well of Goat Anti-Equine IgM (anti-IgM) (Invitrogen PA1-84647) diluted to a 1:25,000 ratio in the stock blocking buffer.

15. 1-Step Ultra TMB-ELISA incubation was 30 minutes.

Plates were analyzed via the Bio-Rad Benchmark Plus microplate spectrophotometer at 450nm.

Within each plate, endotoxin-free PBS average absorbance was subtracted from each sample average of absorbances to obtain AMB values in Microsoft Excel. CVs for each sample were also calculated in Microsoft Excel. AMB values were statistically analyzed via a Univariate GLM in SPSS with a post hoc Tukey Test.

B.4. Limitations

The CelLytic B Plus kit was still on backorder at the time of this experiment, and therefore, this experiment could only be conducted once and just within the parameters set by the sample size calculator. No accounts could be made for any attrition.

B.5. Results and Discussion

Sample CVs ranged from 0.8 to 16.2. The only exception was for one of the 0.02EU/mL samples which had a CV of 41.03, and it was excluded from analysis for that reason.

Data was normally distributed according to the Shapiro-Wilk (P=0.496) and Kolmogorov-Smirnov (P=0.200) tests. There was no difference in means as a function of sample type and concentration (P=0.363). There was a difference in means as a function of just sample type (P=0.030) or of just concentration (P=0.009), however. The post hoc Tukey test could only compare concentrations because of the removal of one of the endotoxin samples from analysis, and the only difference indicated was between the highest and lowest concentrations (P=0.011). Additionally, the graphed output indicated that there were no differences between the *S.* Javiana protein and the endotoxins when comparing within a single concentration pairing (Figure B). Therefore, it was concluded that the null hypothesis could not be rejected, and that *S.* Javiana proteins do not lead to higher absorbances than their coordinating endotoxin concentrations when exposed to the convalescent horse serum and anti-IgM antibody.

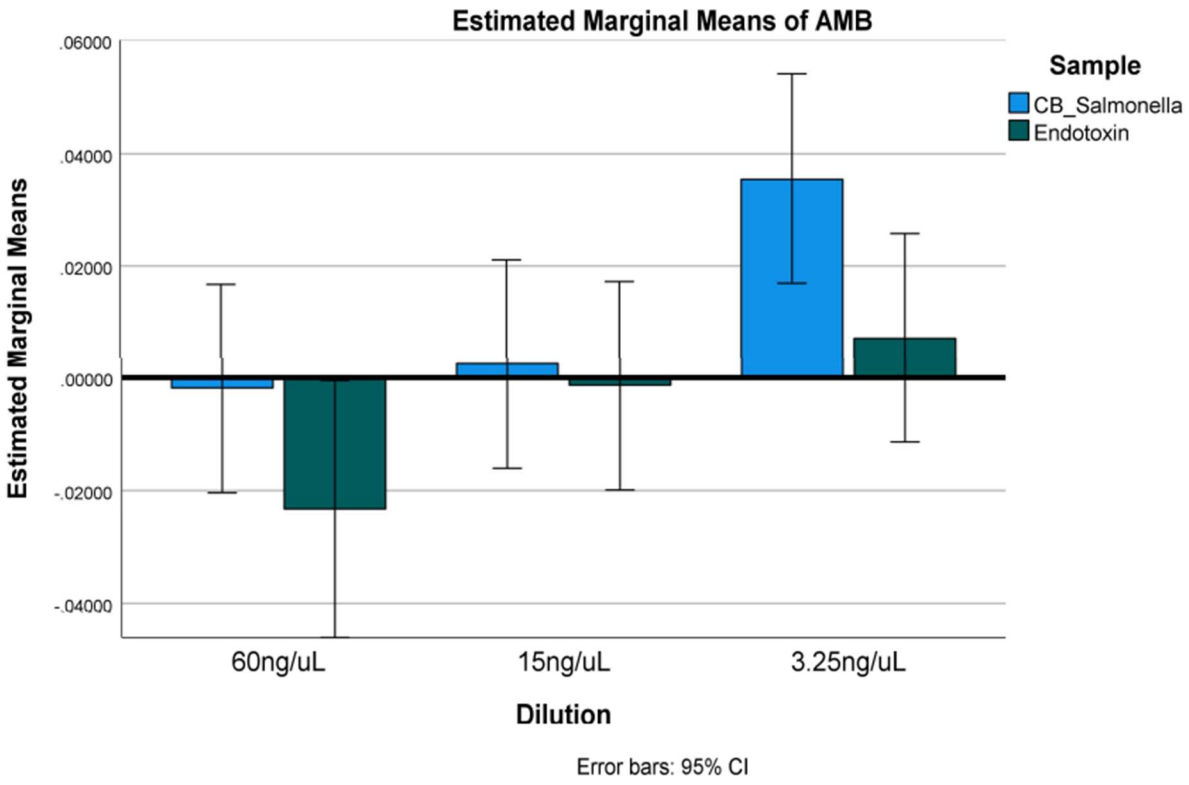

Figure B. Estimated marginal means of AMB values for *S.* Javiana protein samples harvested via the CelLytic B Plus kit and the endotoxin standard by coordinating concentrations. Concentrations within this figure only reflect those of the *S.* Javiana protein samples.

Overall, *S.* Javiana proteins had higher AMB values than the endotoxin samples, which is reflected in the graphed output (Figure B). The removal of one endotoxin sample because of the high CV likely impacted this outcome, and this experiment should be repeated with at least one extra plate to account for attrition such as this. Additionally, conducting multiple, fresh protein harvests instead of just one that was 24-hours old and using endotoxin samples specifically from *S.* Javiana should be considered. The CelLytic B Plus kit recommends immediate use of proteins, and a freeze-thaw cycle can impact protein structure and therefore antibody recognition [486]. Endotoxin structure varying could also impact antibody recognition for the same reason.

The graphed output does indicate an overall upward trend with increasing dilution, which could be because of the layout of samples. If layout did impact AMB values, randomizing the sample placement could also impact outcomes when comparing sample types within coordinating concentrations. Randomized placement of samples should be incorporated in future projects.

It should be noted that this experiment occurred several years following the endotoxin analyses presented in Chapter 3 of this project. Also, the same antibodies used in Chapter 3 were used within this experiment, meaning that the antibodies were several years old. The quality of the antibodies is hypothesized to have decreased, and newly acquired antibodies should be used in future experiments.

Appendix C. MHC-II Binding Prediction Outputs

Table C.1. All MHC-II binding predictions for the FimH epitope used within all vaccine designs in this project.

Allele	Peptide	Percentile Rank within *S.* Javiana	Percentile Rank within pSCP	Percentile Rank within pSSCP	Percentile Rank within pSECP	Percentile Rank within pSCP/pSC6 2023
H2-IAb	GNRPQGVTPQTKTIA	16.94	16.94	16.94	16.94	13.7
H2-IAd	GNRPQGVTPQTKTIA	46.52	46.52	46.52	46.52	66
H2-IEd	GNRPQGVTPQTKTIA	69.75	69.75	69.75	69.75	66
H2-IAb	NRPQGVTPQTKTIAI	17.24	17.24	17.24	17.24	13.15
H2-IAd	NRPQGVTPQTKTIAI	39.65	39.65	39.65	39.65	43
H2-IEd	NRPQGVTPQTKTIAI	66.88	66.88	66.88	66.88	60
H2-IAb	RPQGVTPQTKTIAIK	23.98	23.98	23.98	23.98	22
H2-IAd	RPQGVTPQTKTIAIK	49.09	49.09	49.09	49.09	38.5
H2-IEd	RPQGVTPQTKTIAIK	61.3	61.3	61.3	61.3	50
H2-IAb	PQGVTPQTKTIAIKC	26.35	26.35	26.35	26.35	24
H2-IAd	PQGVTPQTKTIAIKC	33.85	33.85	33.85	33.85	25
H2-IEd	PQGVTPQTKTIAIKC	60.73	60.73	60.73	60.73	48
H2-IAb	QGVTPQTKTIAIKCT	31.01	31.01	31.01	31.01	28
H2-IAd	QGVTPQTKTIAIKCT	11.13	11.13	11.13	11.13	14.95
H2-IEd	QGVTPQTKTIAIKCT	57.1	57.1	57.1	57.1	43
H2-IAb	GVTPQTKTIAIKCTN	39.43	39.43	39.43	39.43	38.5
H2-IAd	GVTPQTKTIAIKCTN	6.86	6.86	6.86	6.86	14.3
H2-IEd	GVTPQTKTIAIKCTN	56.85	56.85	56.85	56.85	43
H2-IAb	VTPQTKTIAIKCTNV	50.05	50.05	50.05	50.05	48.5
H2-IAd	VTPQTKTIAIKCTNV	4.98	4.98	4.98	4.98	12.7
H2-IEd	VTPQTKTIAIKCTNV	59.09	59.09	59.09	59.09	46
H2-IAb	TPQTKTIAIKCTNVA	39.8	39.8	39.8	39.8	53
H2-IAd	TPQTKTIAIKCTNVA	2.99	2.99	2.99	2.99	9.2
H2-IEd	TPQTKTIAIKCTNVA	65.65	65.65	65.65	65.65	60
H2-IAb	PQTKTIAIKCTNVAA	37.72	37.72	37.72	37.72	48
H2-IAd	PQTKTIAIKCTNVAA	2.88	2.88	2.88	2.88	10.05
H2-IEd	PQTKTIAIKCTNVAA	55.77	55.77	55.77	55.77	48.5
H2-IAb	QTKTIAIKCTNVAAQ	34.34	34.34	34.34	34.34	42
H2-IAd	QTKTIAIKCTNVAAQ	3.2	3.2	3.2	3.2	11.3
H2-IEd	QTKTIAIKCTNVAAQ	60.36	60.36	60.36	60.36	61
H2-IAb	TKTIAIKCTNVAAQA	32.64	32.64	32.64	32.64	38
H2-IAd	TKTIAIKCTNVAAQA	2.96	2.96	2.96	2.96	10.6

(Table cont'd.)

Allele	Peptide	Percentile Rank within *S.* Javiana	Percentile Rank within pSCP	Percentile Rank within pSSCP	Percentile Rank within pSECP	Percentile Rank within pSCP/pSC6 2023
H2-IEd	TKTIAIKCTNVAAQA	59.18	59.18	59.18	59.18	60.5
H2-IAb	KTIAIKCTNVAAQAY	31.3	31.3	31.3	31.3	37
H2-IAd	KTIAIKCTNVAAQAY	2.5	2.5	2.5	2.5	8.65
H2-IEd	KTIAIKCTNVAAQAY	64.45	64.45	64.45	64.45	69
H2-IAb	TIAIKCTNVAAQAYL	35.44	35.44	35.44	35.44	41
H2-IAd	TIAIKCTNVAAQAYL	3.08	3.08	3.08	3.08	11.55
H2-IEd	TIAIKCTNVAAQAYL	64.66	64.66	64.66	64.66	71
H2-IAb	IAIKCTNVAAQAYLS	15.96	15.96	15.96	15.96	22.5
H2-IAd	IAIKCTNVAAQAYLS	1.18	1.18	1.18	1.18	5.05
H2-IEd	IAIKCTNVAAQAYLS	72.72	72.72	72.72	72.72	77.5
H2-IAb	AIKCTNVAAQAYLSM	17.03	17.03	17.03	17.03	23.5
H2-IAd	AIKCTNVAAQAYLSM	0.57	0.57	0.57	0.57	2.8
H2-IEd	AIKCTNVAAQAYLSM	75.78	75.78	75.78	75.78	78
H2-IAb	IKCTNVAAQAYLSMR	17.09	17.09	17.09	17.09	26
H2-IAd	IKCTNVAAQAYLSMR	0.25	0.25	0.25	0.25	2.1
H2-IEd	IKCTNVAAQAYLSMR	65.93	65.93	65.93	65.93	67.5
H2-IAb	KCTNVAAQAYLSMRL	17.2	17.2	17.2	17.2	25.5
H2-IAd	KCTNVAAQAYLSMRL	0.2	0.2	0.2	0.2	1.55
H2-IEd	KCTNVAAQAYLSMRL	41.92	41.92	41.92	41.92	41
H2-IAb	CTNVAAQAYLSMRLE	18.82	18.82	18.82	18.82	24.5
H2-IAd	CTNVAAQAYLSMRLE	0.34	0.34	0.34	0.34	1.45
H2-IEd	CTNVAAQAYLSMRLE	31.59	31.59	31.59	31.59	27
H2-IAb	TNVAAQAYLSMRLEA	24.4	24.4	24.4	24.4	30.5
H2-IAd	TNVAAQAYLSMRLEA	3.84	3.84	3.84	3.84	3.8
H2-IEd	TNVAAQAYLSMRLEA	29.86	29.86	29.86	29.86	16.95
H2-IAb	NVAAQAYLSMRLEAE	21.13	21.13	21.13	21.13	26.5
H2-IAd	NVAAQAYLSMRLEAE	2.57	2.57	2.57	2.57	5.6
H2-IEd	NVAAQAYLSMRLEAE	26.68	26.68	26.68	26.68	12.15
H2-IAb	VAAQAYLSMRLEAEK	35.43	35.43	35.43	35.43	32
H2-IAd	VAAQAYLSMRLEAEK	6.55	6.55	6.55	6.55	18.15
H2-IEd	VAAQAYLSMRLEAEK	26.69	26.69	26.69	26.69	11.15
H2-IAb	AAQAYLSMRLEAEKA	37.44	37.44	37.44	37.44	34
H2-IAd	AAQAYLSMRLEAEKA	1.96	1.96	1.96	1.96	6.2
H2-IEd	AAQAYLSMRLEAEKA	29.84	29.84	29.84	29.84	11.95
H2-IAb	AQAYLSMRLEAEKAS	37.82	37.82	37.82	37.82	32
H2-IAd	AQAYLSMRLEAEKAS	1.36	1.36	1.36	1.36	3.85

(Table cont'd.)

Allele	Peptide	Percentile Rank within *S.* Javiana	Percentile Rank within pSCP	Percentile Rank within pSSCP	Percentile Rank within pSECP	Percentile Rank within pSCP/pSC6 2023
H2-IEd	AQAYLSMRLEAEKAS	35.72	35.72	35.72	35.72	14.5
H2-IAb	QAYLSMRLEAEKASG	40.83	40.83	40.83	40.83	38
H2-IAd	QAYLSMRLEAEKASG	1.61	1.61	1.61	1.61	6.1
H2-IEd	QAYLSMRLEAEKASG	43.4	43.4	43.4	43.4	21
H2-IAb	AYLSMRLEAEKASGQ	45.49	45.49	45.49	45.49	47
H2-IAd	AYLSMRLEAEKASGQ	1.61	1.61	1.61	1.61	6.47
H2-IEd	AYLSMRLEAEKASGQ	51.08	51.08	51.08	51.08	29
H2-IAb	YLSMRLEAEKASGQA	46.39	46.39	46.39	46.39	49.5
H2-IAd	YLSMRLEAEKASGQA	2.85	2.85	2.85	2.85	8.91
H2-IEd	YLSMRLEAEKASGQA	59.14	59.14	59.14	59.14	47
H2-IAb	LSMRLEAEKASGQAM	43.91	43.91	43.91	43.91	39
H2-IAd	LSMRLEAEKASGQAM	2.27	2.27	2.27	2.27	11.8
H2-IEd	LSMRLEAEKASGQAM	61.7	61.7	61.7	61.7	55.5
H2-IAb	SMRLEAEKASGQAMV	39.16	39.16	39.16	39.16	36
H2-IAd	SMRLEAEKASGQAMV	2.15	2.15	2.15	2.15	16.45
H2-IEd	SMRLEAEKASGQAMV	68.43	68.43	68.43	68.43	71.5
H2-IAb	MRLEAEKASGQAMVS	19.76	19.76	19.76	19.76	26
H2-IAd	MRLEAEKASGQAMVS	7.52	7.52	7.52	7.52	21.3
H2-IEd	MRLEAEKASGQAMVS	72.18	72.18	72.18	72.18	77.5
H2-IAb	RLEAEKASGQAMVSD	20.61	20.61	20.61	20.61	27.5
H2-IAd	RLEAEKASGQAMVSD	10.36	10.36	10.36	10.36	25.5
H2-IEd	RLEAEKASGQAMVSD	75.78	75.78	75.78	75.78	86
H2-IAb	LEAEKASGQAMVSDN	20.84	20.84	20.84	20.84	27
H2-IAd	LEAEKASGQAMVSDN	11.57	11.57	11.57	11.57	25
H2-IEd	LEAEKASGQAMVSDN	75.78	75.78	75.78	75.78	89
H2-IAb	EAEKASGQAMVSDNP	23.8	23.8	23.8	23.8	30.5
H2-IAd	EAEKASGQAMVSDNP	16.61	16.61	16.61	16.61	31.5
H2-IEd	EAEKASGQAMVSDNP	75.78	75.78	75.78	75.78	89.5

Table C.2. All MHC-II binding predictions for the SopB epitope used within all vaccine designs in this project.

Allele	Peptide	Percentile Rank within *S.* Javiana	Percentile Rank within pSCP	Percentile Rank within pSSCP	Percentile Rank within pSECP	Percentile Rank within pSCP/pSC6 2023
H2-IAb	VLGKQDPVLTSMANQ	29.16	29.16	29.16	29.16	23.5
H2-IAd	VLGKQDPVLTSMANQ	17.19	17.19	17.19	17.19	22.5
H2-IEd	VLGKQDPVLTSMANQ	71.31	71.31	71.31	71.31	71.5
H2-IAb	LGKQDPVLTSMANQM	15.82	15.82	15.82	15.82	16.5
H2-IAd	LGKQDPVLTSMANQM	14.36	14.36	14.36	14.36	20.5
H2-IEd	LGKQDPVLTSMANQM	73.98	73.98	73.98	73.98	83
H2-IAb	GKQDPVLTSMANQME	15.72	15.72	15.72	15.72	17
H2-IAd	GKQDPVLTSMANQME	15.74	15.74	15.74	15.74	21
H2-IEd	GKQDPVLTSMANQME	75.78	75.78	75.78	75.78	87
H2-IAb	KQDPVLTSMANQMEL	16.4	16.4	16.4	16.4	17.5
H2-IAd	KQDPVLTSMANQMEL	27.91	27.91	27.91	27.91	24
H2-IEd	KQDPVLTSMANQMEL	75.78	75.78	75.78	75.78	85.5
H2-IAb	QDPVLTSMANQMELA	17.36	17.36	17.36	17.36	20
H2-IAd	QDPVLTSMANQMELA	19.89	19.89	19.89	19.89	16
H2-IEd	QDPVLTSMANQMELA	75.78	75.78	75.78	75.78	85
H2-IAb	DPVLTSMANQMELAK	19.54	19.54	19.54	19.54	22.5
H2-IAd	DPVLTSMANQMELAK	21.36	21.36	21.36	21.36	21.15
H2-IEd	DPVLTSMANQMELAK	75.78	75.78	75.78	75.78	82
H2-IAb	PVLTSMANQMELAKV	27.9	27.9	27.9	27.9	33
H2-IAd	PVLTSMANQMELAKV	5.42	5.42	5.42	5.42	22.75
H2-IEd	PVLTSMANQMELAKV	75.78	75.78	75.78	75.78	79.5
H2-IAb	VLTSMANQMELAKVK	31.82	31.82	31.82	31.82	38
H2-IAd	VLTSMANQMELAKVK	2.12	2.12	2.12	2.12	20.2
H2-IEd	VLTSMANQMELAKVK	51.57	51.57	51.57	51.57	56
H2-IAb	LTSMANQMELAKVKA	52.93	52.93	52.93	52.93	52
H2-IAd	LTSMANQMELAKVKA	0.47	0.47	0.47	0.47	11.19
H2-IEd	LTSMANQMELAKVKA	47.24	47.24	47.24	47.24	49.5
H2-IAb	TSMANQMELAKVKAD	49.09	49.09	49.09	49.09	59
H2-IAd	TSMANQMELAKVKAD	0.39	0.39	0.39	0.39	6.55
H2-IEd	TSMANQMELAKVKAD	45.77	45.77	45.77	45.77	43
H2-IAb	SMANQMELAKVKADR	50.04	50.04	50.04	50.04	60.5
H2-IAd	SMANQMELAKVKADR	0.31	0.31	0.31	0.31	4.45
H2-IEd	SMANQMELAKVKADR	35.23	35.23	35.23	35.23	27.5

(Table cont'd.)

Allele	Peptide	Percentile Rank within *S.* Javiana	Percentile Rank within pSCP	Percentile Rank within pSSCP	Percentile Rank within pSECP	Percentile Rank within pSCP/pSC6 2023
H2-IAb	MANQMELAKVKADRP	56.33	56.33	56.33	56.33	70.5
H2-IAd	MANQMELAKVKADRP	0.21	0.21	0.21	0.21	3.8
H2-IEd	MANQMELAKVKADRP	31.73	31.73	31.73	31.73	19
H2-IAb	ANQMELAKVKADRPA	48.96	48.96	48.96	48.96	58
H2-IAd	ANQMELAKVKADRPA	0.2	0.2	0.2	0.2	3.4
H2-IEd	ANQMELAKVKADRPA	28.19	28.19	28.19	28.19	13.3
H2-IAb	NQMELAKVKADRPAT	42.72	42.72	42.72	42.72	39.5
H2-IAd	NQMELAKVKADRPAT	1.59	1.59	1.59	1.59	5.3
H2-IEd	NQMELAKVKADRPAT	27.97	27.97	27.97	27.97	12.25
H2-IAb	QMELAKVKADRPATK	35.55	35.55	35.55	35.55	24.5
H2-IAd	QMELAKVKADRPATK	2	2	2	2	7.5
H2-IEd	QMELAKVKADRPATK	17.5	17.5	17.5	17.5	8.2
H2-IAb	MELAKVKADRPATKQ	35.29	35.29	35.29	35.29	24
H2-IAd	MELAKVKADRPATKQ	4.75	4.75	4.75	4.75	18
H2-IEd	MELAKVKADRPATKQ	20.04	20.04	20.04	20.04	8.65
H2-IAb	ELAKVKADRPATKQE	35.55	35.55	35.55	35.55	24.5
H2-IAd	ELAKVKADRPATKQE	11.07	11.07	11.07	11.07	34
H2-IEd	ELAKVKADRPATKQE	21.2	21.2	21.2	21.2	9.95
H2-IAb	LAKVKADRPATKQEE	34.64	34.64	34.64	34.64	25.5
H2-IAd	LAKVKADRPATKQEE	15.77	15.77	15.77	15.77	46.5
H2-IEd	LAKVKADRPATKQEE	27.41	27.41	27.41	27.41	20
H2-IAb	AKVKADRPATKQEEA	37.05	37.05	37.05	37.05	30.5
H2-IAd	AKVKADRPATKQEEA	20.56	20.56	20.56	20.56	46
H2-IEd	AKVKADRPATKQEEA	28.06	28.06	28.06	28.06	24.75
H2-IAb	KVKADRPATKQEEAA	40.96	40.96	40.96	40.96	39
H2-IAd	KVKADRPATKQEEAA	37.37	37.37	37.37	37.37	50.5
H2-IEd	KVKADRPATKQEEAA	43.52	43.52	43.52	43.52	38
H2-IAb	VKADRPATKQEEAAA	46.38	46.38	46.38	46.38	53
H2-IAd	VKADRPATKQEEAAA	47.05	47.05	47.05	47.05	52
H2-IEd	VKADRPATKQEEAAA	45.71	45.71	45.71	45.71	41.5
H2-IAb	KADRPATKQEEAAAK	58.11	58.11	58.11	58.11	64
H2-IAd	KADRPATKQEEAAAK	42.93	42.93	42.93	42.93	55.5

(Table cont'd.)

Allele	Peptide	Percentile Rank within *S.* Javiana	Percentile Rank within pSCP	Percentile Rank within pSSCP	Percentile Rank within pSECP	Percentile Rank within pSCP/pSC6 2023
H2-IEd	KADRPATKQEEAAAK	68.59	68.59	68.59	68.59	67.5
H2-IAb	ADRPATKQEEAAAKA	50.76	50.76	50.76	50.76	54.5
H2-IAd	ADRPATKQEEAAAKA	28.55	28.55	28.55	28.55	43
H2-IEd	ADRPATKQEEAAAKA	68.11	68.11	68.11	68.11	68
H2-IAb	DRPATKQEEAAAKAL	23.03	23.03	23.03	23.03	21
H2-IAd	DRPATKQEEAAAKAL	9.87	9.87	9.87	9.87	23.1
H2-IEd	DRPATKQEEAAAKAL	70.47	70.47	70.47	70.47	74
H2-IAb	RPATKQEEAAAKALK	21.88	21.88	21.88	21.88	20.5
H2-IAd	RPATKQEEAAAKALK	4.56	4.56	4.56	4.56	15.2
H2-IEd	RPATKQEEAAAKALK	64.09	64.09	64.09	64.09	67
H2-IAb	PATKQEEAAAKALKK	20.84	20.84	20.84	20.84	19.5
H2-IAd	PATKQEEAAAKALKK	2.49	2.49	2.49	2.49	9.25
H2-IEd	PATKQEEAAAKALKK	52.41	52.41	52.41	52.41	55.5
H2-IAb	ATKQEEAAAKALKKN	20.51	20.51	20.51	20.51	19.5
H2-IAd	ATKQEEAAAKALKKN	1.71	1.71	1.71	1.71	7.6
H2-IEd	ATKQEEAAAKALKKN	46.9	46.9	46.9	46.9	51.5
H2-IAb	TKQEEAAAKALKKNL	22.26	22.26	22.26	22.26	20
H2-IAd	TKQEEAAAKALKKNL	2.29	2.29	2.29	2.29	10
H2-IEd	TKQEEAAAKALKKNL	43.54	43.54	43.54	43.54	45
H2-IAb	KQEEAAAKALKKNLI	28.6	28.6	28.6	28.6	26
H2-IAd	KQEEAAAKALKKNLI	3.04	3.04	3.04	3.04	10.4
H2-IEd	KQEEAAAKALKKNLI	40.06	40.06	40.06	40.06	39.5
H2-IAb	QEEAAAKALKKNLIE	32.15	32.15	32.15	32.15	31
H2-IAd	QEEAAAKALKKNLIE	5.46	5.46	5.46	5.46	16
H2-IEd	QEEAAAKALKKNLIE	39.83	39.83	39.83	39.83	31.5
H2-IAb	EEAAAKALKKNLIEL	46.59	46.59	46.59	46.59	48
H2-IAd	EEAAAKALKKNLIEL	15.95	15.95	15.95	15.95	33
H2-IEd	EEAAAKALKKNLIEL	39.22	39.22	39.22	39.22	23
H2-IAb	EAAAKALKKNLIELI	53.25	53.25	53.25	53.25	58
H2-IAd	EAAAKALKKNLIELI	14.5	14.5	14.5	14.5	36
H2-IEd	EAAAKALKKNLIELI	40.75	40.75	40.75	40.75	23

Table C.3. All MHC-II binding predictions for the OmpA epitope used within all vaccine designs in this project.

Allele	Peptide	Percentile Rank within *S.* Javiana	Percentile Rank within pSCP	Percentile Rank within pSSCP	Percentile Rank within pSECP	Percentile Rank within pSCP/pSC6 2023
H2-IAb	GLLSVGVSYRFGQQE	74.94	74.94	74.94	74.94	81
H2-IAd	GLLSVGVSYRFGQQE	62.71	62.71	62.71	62.71	79.5
H2-IEd	GLLSVGVSYRFGQQE	60.9	60.9	60.9	60.9	47.5
H2-IAb	LLSVGVSYRFGQQEA	69.41	69.41	69.41	69.41	72.5
H2-IAd	LLSVGVSYRFGQQEA	68.63	68.63	68.63	68.63	85
H2-IEd	LLSVGVSYRFGQQEA	58.83	58.83	58.83	58.83	44
H2-IAb	LSVGVSYRFGQQEAA	5.93	5.93	5.93	5.93	11.35
H2-IAd	LSVGVSYRFGQQEAA	49.05	49.05	49.05	49.05	68
H2-IEd	LSVGVSYRFGQQEAA	58.34	58.34	58.34	58.34	43
H2-IAb	SVGVSYRFGQQEAAP	5.35	5.35	5.35	5.35	10.85
H2-IAd	SVGVSYRFGQQEAAP	50.78	50.78	50.78	50.78	64.5
H2-IEd	SVGVSYRFGQQEAAP	57.92	57.92	57.92	57.92	43
H2-IAb	VGVSYRFGQQEAAPV	4.13	4.13	4.13	4.13	8.95
H2-IAd	VGVSYRFGQQEAAPV	32.85	32.85	32.85	32.85	53
H2-IEd	VGVSYRFGQQEAAPV	65.42	65.42	65.42	65.42	45
H2-IAb	GVSYRFGQQEAAPVV	3.63	3.63	3.63	3.63	5.7
H2-IAd	GVSYRFGQQEAAPVV	15.95	15.95	15.95	15.95	47
H2-IEd	GVSYRFGQQEAAPVV	68.62	68.62	68.62	68.62	51
H2-IAb	VSYRFGQQEAAPVVA	3.5	3.5	3.5	3.5	1.7
H2-IAd	VSYRFGQQEAAPVVA	4.79	4.79	4.79	4.79	20.1
H2-IEd	VSYRFGQQEAAPVVA	73.84	73.84	73.84	73.84	55.5
H2-IAb	SYRFGQQEAAPVVAP	4.55	4.55	4.55	4.55	2.55
H2-IAd	SYRFGQQEAAPVVAP	2.67	2.67	2.67	2.67	11.05
H2-IEd	SYRFGQQEAAPVVAP	75.78	75.78	75.78	75.78	60.5
H2-IAb	YRFGQQEAAPVVAPA	4.07	4.07	4.07	4.07	2.11
H2-IAd	YRFGQQEAAPVVAPA	1.64	1.64	1.64	1.64	6.6
H2-IEd	YRFGQQEAAPVVAPA	75.78	75.78	75.78	75.78	64.5
H2-IAb	RFGQQEAAPVVAPAP	3.8	3.8	3.8	3.8	1.77
H2-IAd	RFGQQEAAPVVAPAP	1.51	1.51	1.51	1.51	6.1
H2-IEd	RFGQQEAAPVVAPAP	75.78	75.78	75.78	75.78	67.5
H2-IAb	FGQQEAAPVVAPAPA	3.33	3.33	3.33	3.33	1.65
H2-IAd	FGQQEAAPVVAPAPA	1.25	1.25	1.25	1.25	5.6
H2-IEd	FGQQEAAPVVAPAPA	75.78	75.78	75.78	75.78	78
H2-IAb	GQQEAAPVVAPAPAP	2.46	2.46	2.46	2.46	1.45

(Table cont'd.)

Allele	Peptide	Percentile Rank within *S.* Javiana	Percentile Rank within pSCP	Percentile Rank within pSSCP	Percentile Rank within pSECP	Percentile Rank within pSCP/pSC6 2023
H2-IAd	GQQEAAPVVAPAPAP	3.62	3.62	3.62	3.62	9.9
H2-IEd	GQQEAAPVVAPAPAP	75.78	75.78	75.78	75.78	81.5
H2-IAb	QQEAAPVVAPAPAPA	0.55	0.55	0.55	0.55	0.75
H2-IAd	QQEAAPVVAPAPAPA	7.33	7.33	7.33	7.33	11.7
H2-IEd	QQEAAPVVAPAPAPA	75.78	75.78	75.78	75.78	77
H2-IAb	QEAAPVVAPAPAPAP	0.26	0.26	0.26	0.26	1.38
H2-IAd	QEAAPVVAPAPAPAP	12.6	12.6	12.6	12.6	19
H2-IEd	QEAAPVVAPAPAPAP	75.78	75.78	75.78	75.78	75.5
H2-IAb	EAAPVVAPAPAPAPE	0.24	0.24	0.24	0.24	1.58
H2-IAd	EAAPVVAPAPAPAPE	17.87	17.87	17.87	17.87	25.9
H2-IEd	EAAPVVAPAPAPAPE	75.78	75.78	75.78	75.78	75
H2-IAb	AAPVVAPAPAPAPEV	0.21	0.21	0.21	0.21	1.67
H2-IAd	AAPVVAPAPAPAPEV	23.02	23.02	23.02	23.02	29.7
H2-IEd	AAPVVAPAPAPAPEV	75.78	75.78	75.78	75.78	75
H2-IAb	APVVAPAPAPAPEVQ	0.22	0.22	0.22	0.22	1.88
H2-IAd	APVVAPAPAPAPEVQ	30.44	30.44	30.44	30.44	30.05
H2-IEd	APVVAPAPAPAPEVQ	75.78	75.78	75.78	75.78	75
H2-IAb	PVVAPAPAPAPEVQT	0.38	0.38	0.38	0.38	2.75
H2-IAd	PVVAPAPAPAPEVQT	37.68	37.68	37.68	37.68	38.5
H2-IEd	PVVAPAPAPAPEVQT	75.78	75.78	75.78	75.78	74
H2-IAb	VVAPAPAPAPEVQTK	0.76	0.76	0.76	0.76	3.76
H2-IAd	VVAPAPAPAPEVQTK	37.78	37.78	37.78	37.78	43
H2-IEd	VVAPAPAPAPEVQTK	63.76	63.76	63.76	63.76	68
H2-IAb	VAPAPAPAPEVQTKH	2.02	2.02	2.02	2.02	7.96
H2-IAd	VAPAPAPAPEVQTKH	57.58	57.58	57.58	57.58	65
H2-IEd	VAPAPAPAPEVQTKH	56.95	56.95	56.95	56.95	63.5
H2-IAb	APAPAPAPEVQTKHF	12.04	12.04	12.04	12.04	16.25
H2-IAd	APAPAPAPEVQTKHF	67.8	67.8	67.8	67.8	74
H2-IEd	APAPAPAPEVQTKHF	50.71	50.71	50.71	50.71	53.5
H2-IAb	PAPAPAPEVQTKHFT	15.88	15.88	15.88	15.88	21.65
H2-IAd	PAPAPAPEVQTKHFT	70.15	70.15	70.15	70.15	82
H2-IEd	PAPAPAPEVQTKHFT	48.42	48.42	48.42	48.42	44

Table C.4. All MHC-II binding predictions for the OmpC epitope used within all vaccine designs in this project.

Allele	Peptide	Percentile Rank within *S.* Javiana	Percentile Rank within pSCP	Percentile Rank within pSSCP	Percentile Rank within pSECP	Percentile Rank within pSCP/pSC6 2023
H2-IAb	KVKVLSLLVPALLVA	18.41	18.41	18.41	18.41	16.5
H2-IAd	KVKVLSLLVPALLVA	11.44	11.44	11.44	11.44	15
H2-IEd	KVKVLSLLVPALLVA	67.73	67.73	67.73	67.73	70
H2-IAb	VKVLSLLVPALLVAG	16.02	16.02	16.02	16.02	16
H2-IAd	VKVLSLLVPALLVAG	12.92	12.92	12.92	12.92	22.5
H2-IEd	VKVLSLLVPALLVAG	70.52	70.52	70.52	70.52	75.5
H2-IAb	KVLSLLVPALLVAGA	19.81	19.81	19.81	19.81	20
H2-IAd	KVLSLLVPALLVAGA	9.55	9.55	9.55	9.55	19.5
H2-IEd	KVLSLLVPALLVAGA	66.25	66.25	66.25	66.25	73.5
H2-IAb	VLSLLVPALLVAGAA	19.14	19.14	19.14	19.14	19.5
H2-IAd	VLSLLVPALLVAGAA	10.9	10.9	10.9	10.9	19
H2-IEd	VLSLLVPALLVAGAA	70.48	70.48	70.48	70.48	78
H2-IAb	LSLLVPALLVAGAAN	21.98	21.98	21.98	21.98	20
H2-IAd	LSLLVPALLVAGAAN	24.07	24.07	24.07	24.07	23
H2-IEd	LSLLVPALLVAGAAN	67.88	67.88	67.88	67.88	75.5
H2-IAb	SLLVPALLVAGAANA	10.88	10.88	10.88	10.88	9.8
H2-IAd	SLLVPALLVAGAANA	19.21	19.21	19.21	19.21	20.5
H2-IEd	SLLVPALLVAGAANA	70.43	70.43	70.43	70.43	78
H2-IAb	LLVPALLVAGAANAA	1.02	1.02	1.02	1.02	1.11
H2-IAd	LLVPALLVAGAANAA	13.19	13.19	13.19	13.19	11
H2-IEd	LLVPALLVAGAANAA	69.22	69.22	69.22	69.22	78
H2-IAb	LVPALLVAGAANAAE	0.95	0.95	0.95	0.95	0.9
H2-IAd	LVPALLVAGAANAAE	12.55	12.55	12.55	12.55	11.5
H2-IEd	LVPALLVAGAANAAE	72.85	72.85	72.85	72.85	82.5
H2-IAb	VPALLVAGAANAAEI	0.91	0.91	0.91	0.91	0.71
H2-IAd	VPALLVAGAANAAEI	12.55	12.55	12.55	12.55	12.5
H2-IEd	VPALLVAGAANAAEI	74.85	74.85	74.85	74.85	84.5
H2-IAb	PALLVAGAANAAEIY	0.94	0.94	0.94	0.94	0.69
H2-IAd	PALLVAGAANAAEIY	13.34	13.34	13.34	13.34	13
H2-IEd	PALLVAGAANAAEIY	75.78	75.78	75.78	75.78	86
H2-IAb	ALLVAGAANAAEIYN	0.96	0.96	0.96	0.96	0.7
H2-IAd	ALLVAGAANAAEIYN	17.16	17.16	17.16	17.16	14.5
H2-IEd	ALLVAGAANAAEIYN	75.78	75.78	75.78	75.78	85.5
H2-IAb	LLVAGAANAAEIYNK	2.52	2.52	2.52	2.52	2.25

(Table cont'd.)

Allele	Peptide	Percentile Rank within *S.* Javiana	Percentile Rank within pSCP	Percentile Rank within pSSCP	Percentile Rank within pSECP	Percentile Rank within pSCP/pSC6 2023
H2-IAd	LLVAGAANAAEIYNK	14.86	14.86	14.86	14.86	24.5
H2-IEd	LLVAGAANAAEIYNK	75.78	75.78	75.78	75.78	86.5
H2-IAb	LVAGAANAAEIYNKD	3.01	3.01	3.01	3.01	3.85
H2-IAd	LVAGAANAAEIYNKD	12.82	12.82	12.82	12.82	33.5
H2-IEd	LVAGAANAAEIYNKD	75.78	75.78	75.78	75.78	87.5
H2-IAb	VAGAANAAEIYNKDG	34.42	34.42	34.42	34.42	28.5
H2-IAd	VAGAANAAEIYNKDG	22.29	22.29	22.29	22.29	58.5
H2-IEd	VAGAANAAEIYNKDG	70.55	70.55	70.55	70.55	82.5
H2-IAb	AGAANAAEIYNKDGN	45.88	45.88	45.88	45.88	45.5
H2-IAd	AGAANAAEIYNKDGN	26.99	26.99	26.99	26.99	66.5
H2-IEd	AGAANAAEIYNKDGN	62	62	62	62	74

Table C.5. All MHC-II binding predictions for the OmpD epitope used within all vaccine designs in this project.

Allele	Peptide	Percentile Rank within *S.* Javiana	Percentile Rank within pSCP	Percentile Rank within pSSCP	Percentile Rank within pSECP	Percentile Rank within pSCP/pSC6 2023
H2-IAb	KLKLVAVAVTSLLAA	17.52	17.52	17.52	17.52	19
H2-IAd	KLKLVAVAVTSLLAA	2.79	2.79	2.79	2.79	0.86
H2-IEd	KLKLVAVAVTSLLAA	67.46	67.46	67.46	67.46	66.5
H2-IAb	LKLVAVAVTSLLAAG	18.96	18.96	18.96	18.96	19.5
H2-IAd	LKLVAVAVTSLLAAG	4.08	4.08	4.08	4.08	1.04
H2-IEd	LKLVAVAVTSLLAAG	64.82	64.82	64.82	64.82	64.5
H2-IAb	KLVAVAVTSLLAAGV	18.91	18.91	18.91	18.91	20
H2-IAd	KLVAVAVTSLLAAGV	9.52	9.52	9.52	9.52	1.23
H2-IEd	KLVAVAVTSLLAAGV	66.9	66.9	66.9	66.9	69
H2-IAb	LVAVAVTSLLAAGVV	21.18	21.18	21.18	21.18	19
H2-IAd	LVAVAVTSLLAAGVV	6.39	6.39	6.39	6.39	1.75
H2-IEd	LVAVAVTSLLAAGVV	67.64	67.64	67.64	67.64	72
H2-IAb	VAVAVTSLLAAGVVN	23.43	23.43	23.43	23.43	16
H2-IAd	VAVAVTSLLAAGVVN	4.66	4.66	4.66	4.66	3.3
H2-IEd	VAVAVTSLLAAGVVN	68.54	68.54	68.54	68.54	71.5
H2-IAb	AVAVTSLLAAGVVNA	13.11	13.11	13.11	13.11	10.7
H2-IAd	AVAVTSLLAAGVVNA	2.12	2.12	2.12	2.12	3.2

(Table cont'd.)

Allele	Peptide	Percentile Rank within *S.* Javiana	Percentile Rank within pSCP	Percentile Rank within pSSCP	Percentile Rank within pSECP	Percentile Rank within pSCP/pSC6 2023
H2-IEd	AVAVTSLLAAGVVNA	69.21	69.21	69.21	69.21	75.5
H2-IAb	VAVTSLLAAGVVNAA	4.31	4.31	4.31	4.31	4
H2-IAd	VAVTSLLAAGVVNAA	1.33	1.33	1.33	1.33	5.15
H2-IEd	VAVTSLLAAGVVNAA	72.14	72.14	72.14	72.14	81
H2-IAb	AVTSLLAAGVVNAAE	4.29	4.29	4.29	4.29	4.05
H2-IAd	AVTSLLAAGVVNAAE	1.89	1.89	1.89	1.89	7.15
H2-IEd	AVTSLLAAGVVNAAE	70.1	70.1	70.1	70.1	79
H2-IAb	VTSLLAAGVVNAAEV	4.25	4.25	4.25	4.25	3.9
H2-IAd	VTSLLAAGVVNAAEV	2.25	2.25	2.25	2.25	8.3
H2-IEd	VTSLLAAGVVNAAEV	73.24	73.24	73.24	73.24	82
H2-IAb	TSLLAAGVVNAAEVY	4.64	4.64	4.64	4.64	4.15
H2-IAd	TSLLAAGVVNAAEVY	2.82	2.82	2.82	2.82	9.7
H2-IEd	TSLLAAGVVNAAEVY	72.97	72.97	72.97	72.97	80.5
H2-IAb	SLLAAGVVNAAEVYN	5.07	5.07	5.07	5.07	4.7
H2-IAd	SLLAAGVVNAAEVYN	12.89	12.89	12.89	12.89	15.7
H2-IEd	SLLAAGVVNAAEVYN	75.04	75.04	75.04	75.04	80.5
H2-IAb	LLAAGVVNAAEVYNK	9.92	9.92	9.92	9.92	12.2
H2-IAd	LLAAGVVNAAEVYNK	16.38	16.38	16.38	16.38	23.5
H2-IEd	LLAAGVVNAAEVYNK	75.78	75.78	75.78	75.78	82.5
H2-IAb	LAAGVVNAAEVYNKD	11.37	11.37	11.37	11.37	16.5
H2-IAd	LAAGVVNAAEVYNKD	28.33	28.33	28.33	28.33	40.5
H2-IEd	LAAGVVNAAEVYNKD	75.78	75.78	75.78	75.78	83
H2-IAb	AAGVVNAAEVYNKDG	49.22	49.22	49.22	49.22	37
H2-IAd	AAGVVNAAEVYNKDG	43.76	43.76	43.76	43.76	53
H2-IEd	AAGVVNAAEVYNKDG	69.71	69.71	69.71	69.71	76.5
H2-IAb	AGVVNAAEVYNKDGN	55.21	55.21	55.21	55.21	44
H2-IAd	AGVVNAAEVYNKDGN	46.92	46.92	46.92	46.92	58
H2-IEd	AGVVNAAEVYNKDGN	62.53	62.53	62.53	62.53	69

Appendix D. BioRender Figure Licenses

49 Spadina Ave. Suite 200
Toronto ON M5V 2J1 Canada
www.biorender.com

Confirmation of Publication and Licensing Rights

April 19th, 2023
Science Suite Inc.

Subscription:	*Lab*
Agreement number:	*BW259LCOKI*
Journal name:	*LSU Digital Commons*

To whom this may concern,

This document is to confirm that Ashley Edwards has been granted a license to use the BioRender content, including icons, templates and other original artwork, appearing in the attached completed graphic pursuant to BioRender's Academic License Terms. This license permits BioRender content to be sublicensed for use in journal publications.

All rights and ownership of BioRender content are reserved by BioRender. All completed graphics must be accompanied by the following citation: "Created with BioRender.com".

BioRender content included in the completed graphic is not licensed for any commercial uses beyond publication in a journal. For any commercial use of this figure, users may, if allowed, recreate it in BioRender under an Industry BioRender Plan.

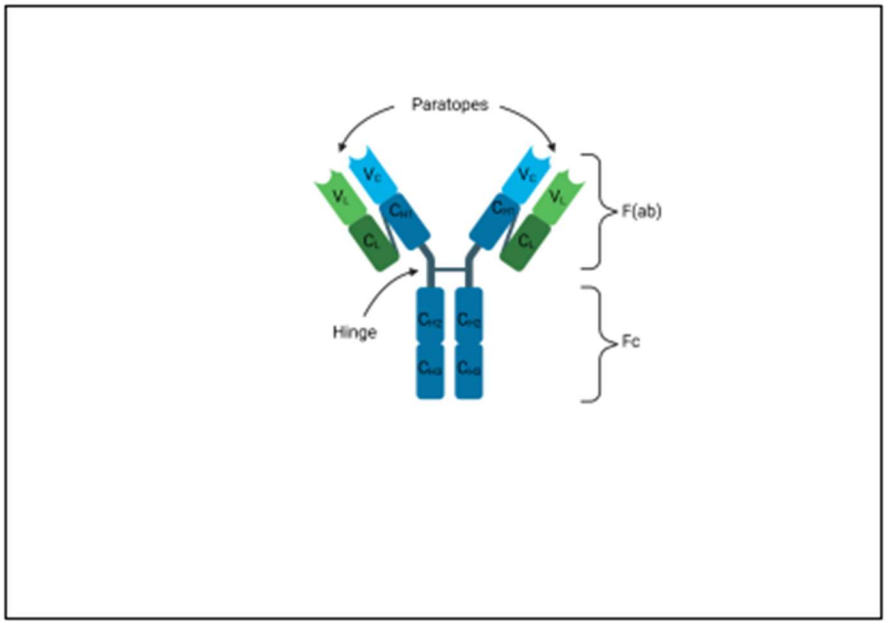

For any questions regarding this document, or other questions about publishing with BioRender refer to our BioRender Publication Guide, or contact BioRender Support at support@biorender.com.

49 Spadina Ave. Suite 200
Toronto ON M5V 2J1 Canada
www.biorender.com

Confirmation of Publication and Licensing Rights

April 19th, 2023
Science Suite Inc.

Subscription:	*Lab*
Agreement number:	*BD259LC7RN*
Journal name:	*LSU Digital Commons*

To whom this may concern,

This document is to confirm that Ashley Edwards has been granted a license to use the BioRender content, including icons, templates and other original artwork, appearing in the attached completed graphic pursuant to BioRender's Academic License Terms. This license permits BioRender content to be sublicensed for use in journal publications.

All rights and ownership of BioRender content are reserved by BioRender. All completed graphics must be accompanied by the following citation: "Created with BioRender.com".

BioRender content included in the completed graphic is not licensed for any commercial uses beyond publication in a journal. For any commercial use of this figure, users may, if allowed, recreate it in BioRender under an Industry BioRender Plan.

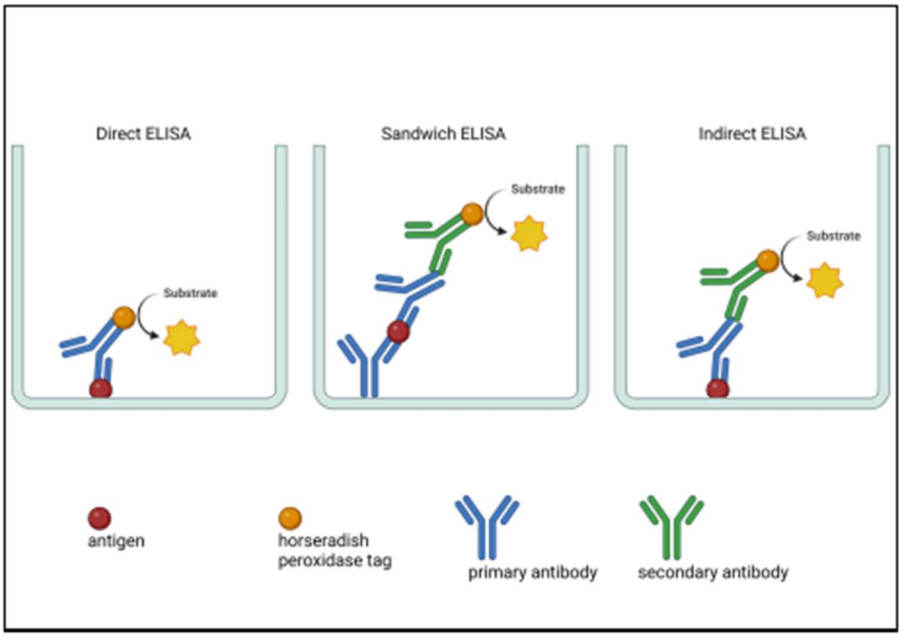

For any questions regarding this document, or other questions about publishing with BioRender refer to our BioRender Publication Guide, or contact BioRender Support at support@biorender.com.

49 Spadina Ave. Suite 200
Toronto ON M5V 2J1 Canada
www.biorender.com

Confirmation of Publication and Licensing Rights

April 19th, 2023
Science Suite Inc.

Subscription:	*Lab*
Agreement number:	*PW259LD566*
Journal name:	*LSU Digital Commons*

To whom this may concern,

This document is to confirm that Ashley Edwards has been granted a license to use the BioRender content, including icons, templates and other original artwork, appearing in the attached completed graphic pursuant to BioRender's Academic License Terms. This license permits BioRender content to be sublicensed for use in journal publications.

All rights and ownership of BioRender content are reserved by BioRender. All completed graphics must be accompanied by the following citation: "Created with BioRender.com".

BioRender content included in the completed graphic is not licensed for any commercial uses beyond publication in a journal. For any commercial use of this figure, users may, if allowed, recreate it in BioRender under an Industry BioRender Plan.

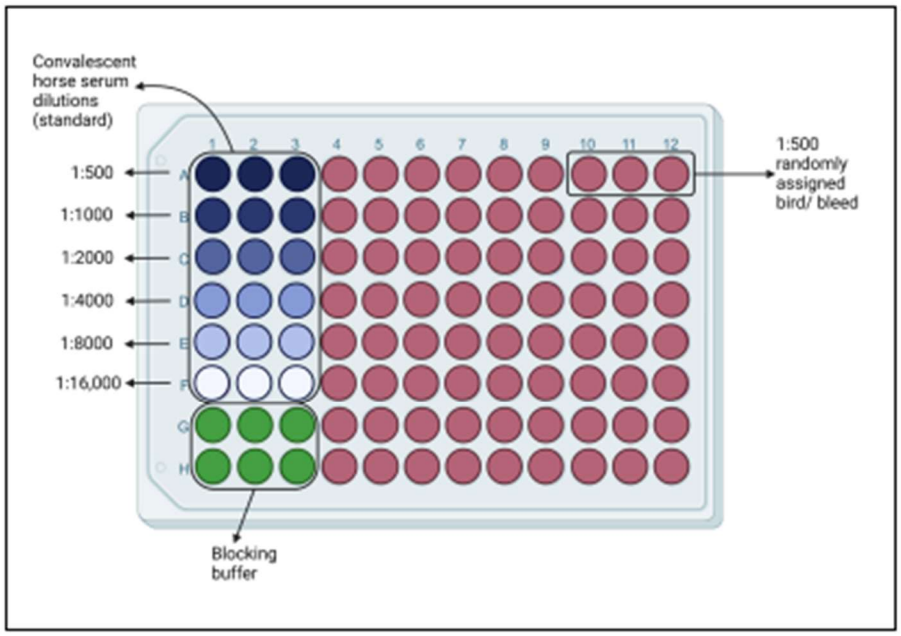

For any questions regarding this document, or other questions about publishing with BioRender refer to our BioRender Publication Guide, or contact BioRender Support at support@biorender.com.

49 Spadina Ave. Suite 200
Toronto ON M5V 2J1 Canada
www.biorender.com

Confirmation of Publication and Licensing Rights

April 19th, 2023
Science Suite Inc.

Subscription: *Lab*
Agreement number: *YV259LCVCL*
Journal name: *LSU Digital Commons*

To whom this may concern,

This document is to confirm that Ashley Edwards has been granted a license to use the BioRender content, including icons, templates and other original artwork, appearing in the attached completed graphic pursuant to BioRender's Academic License Terms. This license permits BioRender content to be sublicensed for use in journal publications.

All rights and ownership of BioRender content are reserved by BioRender. All completed graphics must be accompanied by the following citation: "Created with BioRender.com".

BioRender content included in the completed graphic is not licensed for any commercial uses beyond publication in a journal. For any commercial use of this figure, users may, if allowed, recreate it in BioRender under an Industry BioRender Plan.

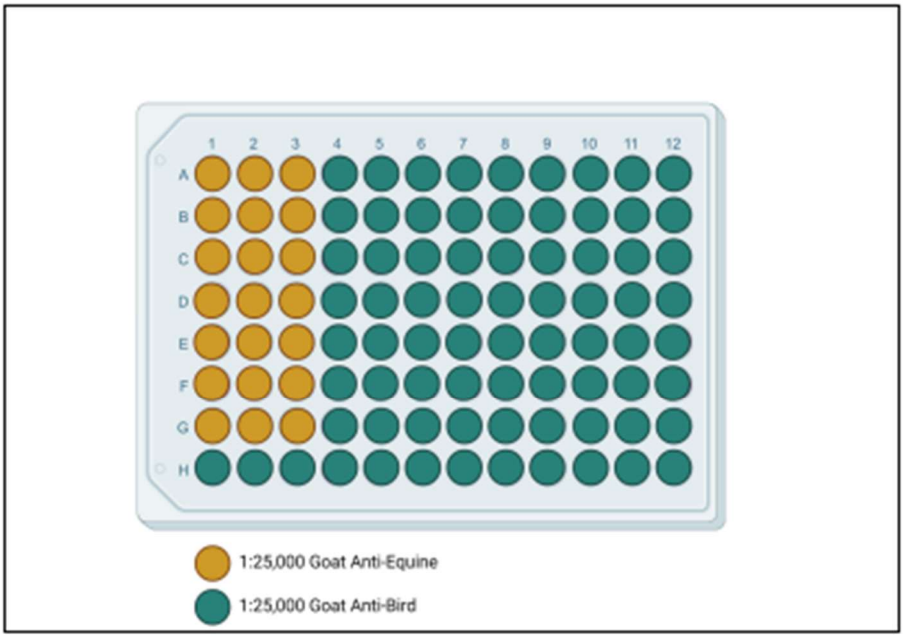

For any questions regarding this document, or other questions about publishing with BioRender refer to our BioRender Publication Guide, or contact BioRender Support at support@biorender.com.

49 Spadina Ave. Suite 200
Toronto ON M5V 2J1 Canada
www.biorender.com

Confirmation of Publication and Licensing Rights

April 19th, 2023
Science Suite Inc.

Subscription:	*Lab*
Agreement number:	*XY259LCXTV*
Journal name:	*LSU Digital Commons*

To whom this may concern,

This document is to confirm that Ashley Edwards has been granted a license to use the BioRender content, including icons, templates and other original artwork, appearing in the attached completed graphic pursuant to BioRender's Academic License Terms. This license permits BioRender content to be sublicensed for use in journal publications.

All rights and ownership of BioRender content are reserved by BioRender. All completed graphics must be accompanied by the following citation: "Created with BioRender.com".

BioRender content included in the completed graphic is not licensed for any commercial uses beyond publication in a journal. For any commercial use of this figure, users may, if allowed, recreate it in BioRender under an Industry BioRender Plan.

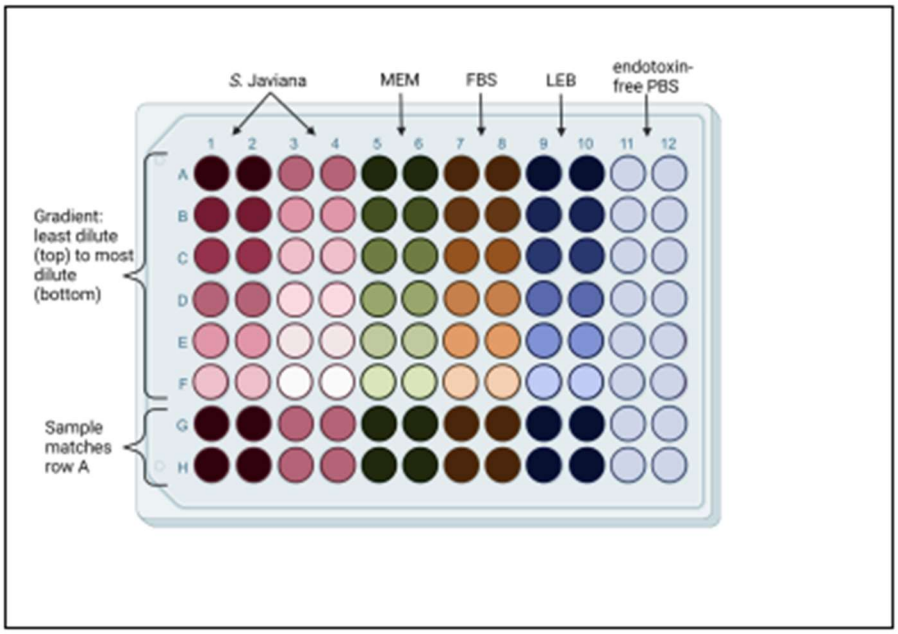

For any questions regarding this document, or other questions about publishing with BioRender refer to our BioRender Publication Guide, or contact BioRender Support at support@biorender.com.

49 Spadina Ave. Suite 200
Toronto ON M5V 2J1 Canada
www.biorender.com

Confirmation of Publication and Licensing Rights

April 19th, 2023
Science Suite Inc.

Subscription: *Lab*
Agreement number: *UX259LCROR*
Journal name: *LSU Digital Commons*

To whom this may concern,

This document is to confirm that Ashley Edwards has been granted a license to use the BioRender content, including icons, templates and other original artwork, appearing in the attached completed graphic pursuant to BioRender's Academic License Terms. This license permits BioRender content to be sublicensed for use in journal publications.

All rights and ownership of BioRender content are reserved by BioRender. All completed graphics must be accompanied by the following citation: "Created with BioRender.com".

BioRender content included in the completed graphic is not licensed for any commercial uses beyond publication in a journal. For any commercial use of this figure, users may, if allowed, recreate it in BioRender under an Industry BioRender Plan.

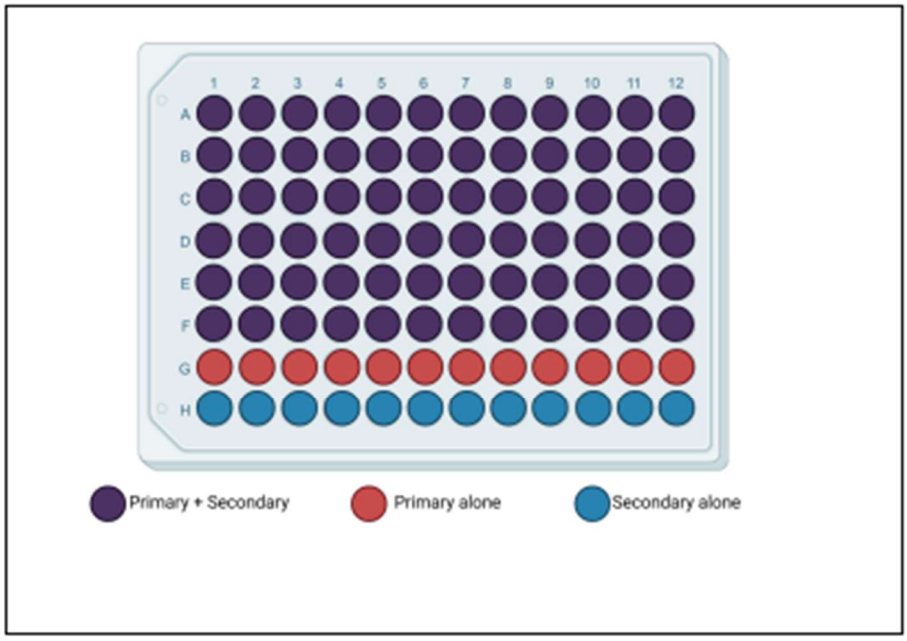

For any questions regarding this document, or other questions about publishing with BioRender refer to our BioRender Publication Guide, or contact BioRender Support at support@biorender.com.

49 Spadina Ave. Suite 200
Toronto ON M5V 2J1 Canada
www.biorender.com

Confirmation of Publication and Licensing Rights

April 19th, 2023
Science Suite Inc.

Subscription:	*Lab*
Agreement number:	*BT259LD2VS*
Journal name:	*LSU Digital Commons*

To whom this may concern,

This document is to confirm that Ashley Edwards has been granted a license to use the BioRender content, including icons, templates and other original artwork, appearing in the attached completed graphic pursuant to BioRender's Academic License Terms. This license permits BioRender content to be sublicensed for use in journal publications.

All rights and ownership of BioRender content are reserved by BioRender. All completed graphics must be accompanied by the following citation: "Created with BioRender.com".

BioRender content included in the completed graphic is not licensed for any commercial uses beyond publication in a journal. For any commercial use of this figure, users may, if allowed, recreate it in BioRender under an Industry BioRender Plan.

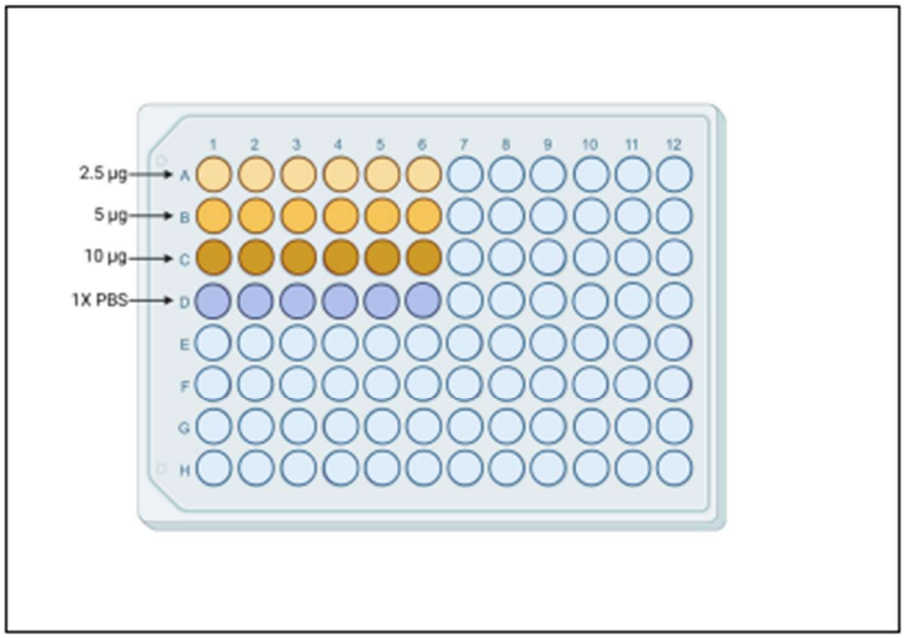

For any questions regarding this document, or other questions about publishing with BioRender refer to our BioRender Publication Guide, or contact BioRender Support at support@biorender.com.

49 Spadina Ave. Suite 200
Toronto ON M5V 2J1 Canada
www.biorender.com

Confirmation of Publication and Licensing Rights

April 19th, 2023
Science Suite Inc.

Subscription:	*Lab*
Agreement number:	*ZW259LD075*
Journal name:	*LSU Digital Commons*

To whom this may concern,

This document is to confirm that Ashley Edwards has been granted a license to use the BioRender content, including icons, templates and other original artwork, appearing in the attached completed graphic pursuant to BioRender's Academic License Terms. This license permits BioRender content to be sublicensed for use in journal publications.

All rights and ownership of BioRender content are reserved by BioRender. All completed graphics must be accompanied by the following citation: "Created with BioRender.com".

BioRender content included in the completed graphic is not licensed for any commercial uses beyond publication in a journal. For any commercial use of this figure, users may, if allowed, recreate it in BioRender under an Industry BioRender Plan.

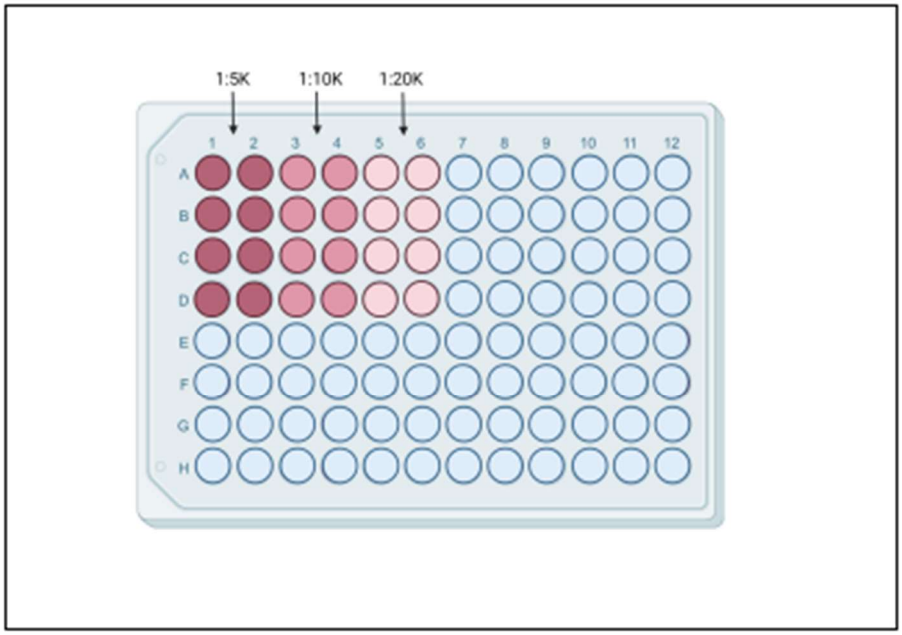

For any questions regarding this document, or other questions about publishing with BioRender refer to our BioRender Publication Guide, or contact BioRender Support at support@biorender.com.

References

1. Hurley, D., et al., Salmonella - Host Interactions - Modulation of the Host Innate Immune System. Frontiers in Immunology, 2014. **5**(481).

2. MacKenzie, K.D., et al., Examining the link between biofilm formation and the ability of pathogenic salmonella strains to colonize multiple host species. Frontiers in Veterinary Science, 2017. **4**.

3. Gal-Mor, O., E.C. Boyle, and G.A. Grassi, Same species, different diseases: how and why typhoidal Salmonella enterica serovars differ. Frontiers in Microbiology, 2014. **5**: p. 391.

4. McClure, E.E., et al., Engineering of obligate intracellular bacteria: progress, challenges and paradigms. . Nature Review Microbiology 2017. **15**(2017): p. 544-558.

5. Hentges, D.J., Anaerobes: General Characteristics, in Medical Microbiology, S. Baron, Editor. 1996, University of Texas Medical Branch at Galveston.

6. Brenner, F.W., et al., Salmonella Nomenclature. Journal of Clinical Microbiology, 2000. **38**(7): p. 2465-2467.

7. Hudson, L.K., et al., Genomic characterization and phylogenetic analysis of Salmonella enterica serovar Javiana. The Journal of Life and Environmental Sciences 2020. **8**: p. e010256.

8. Mukherjee, N., et al., Sources of human infection by Salmonella enterica serotype Javiana: A systematic review. PLoS One, 2019. **14**(9).

9. Switt, A.I.M. and R.A. Cheng. Salmonella Javiana 2021 [cited 2022 May 5]; Available from: https://confluence.cornell.edu/display/FOODSAFETY/Salmonella+Javiana

10. Williams, K., et al., Cytotoxic mechanism of cytolethal distending toxin in nontyphoidal salmonella serovar (salmonella javiana) during macrophage infection. DNA and Cell Biology 2015. **34**(2): p. 113-124.

11. Clarkson, L.S., et al., Sporadic Salmonella enterica serotype Javiana infections in Georgia and Tennessee: a hypothesis-generating study. Epidemiology & Infection, 2010. **138**(3): p. 340-346.

12. Srikantiah, P., et al., Salmonella enterica serotype Javiana infections associated with amphibian contact, Mississippi, 2001. Epidemiology & Infection, 2004. **132**: p. 273-281.

13. Dione, M., et al., Antimicrobial resistance and virulence genes of non-typhoidal Salmonella isolates in the Gambia and Senegal. The Journal of Infection in Developing Countries, 2016. **5**(11).

14. Miller, R. and M. Wiedmann, Dynamic duo- The Salmonella cytolethal distending toxin combines ADP-ribosyltransferase and nuclease activities in a novel form of the cytolethal distending toxin. Toxins 2016. **8**(5): p. 121.

15. Wemyss, M.A. and J.S. Pearson, Host cell death responses to non-typhoidal salmonella infection. Frontiers in Immunology, 2019. **10**: p. 1758.

16. Santos, R.L. and A.J. Bäumler, Cell tropism of Salmonella enterica. International Journal of Medical Microbiology 2004. **294**(2004): p. 225-233.

17. Johnson, R., E. Mylona, and G. Frankel, Typhoidal Salmonella: distinctive virulence factors and pathogenesis. Cellular Microbiology 2018. **20**(9): p. e12939.

18. Lou, L., et al., Salmonella pathogenicity island 1 (SPI-1) and its complex regulatory network. Frontiers in Cellular and Infection Microbiology 2019. **9**.

19. Lorkowski, M., et al., Salmonella enterica invasion of polarized epithelial cells is a highly cooperative effort. Infection and Immunity, 2014. **82**(6): p. 2657-2667.

20. Zhang, S., et al., Molecular pathogenesis of Salmonella enterica serotype Typhimurium-induced diarrhea. Infectious Immunology 2003. **71**(1): p. 1-12.

21. Salamoh, H., et al., The role of O-polysaccharide chain and complement resistance of Escherichia coli in mammary virulence. Veterinary Research 2020. **51**(77).

22. Azimi, T., et al., Molecular mechanisms of Salmonella effector proteins: a comprehensive review. Infection and Drug Resistance, 2020. **13**: p. 11-26.

23. Griffin, A.J. and S.J. McSorley, Development of protective immunity to Salmonella, a mucosal pathogen with a systemic agenda. Mucosal Immunology 2011. **4**(4): p. 371-382.

24. Uribe-Querol, E. and C. Rosales, Phagocytosis: our current understanding of a universal biological process. Frontiers in Immunology, 2020. **11**.

25. Gallois, A., et al., Salmonella pathogenicity island 2-encoded type III secretion system mediates exclusion of NADPH oxidase assembly from the phagosomal membrane. The Journal of Immunology, 2001. **166**(9): p. 5741-5748.

26. Vazquez-Torres, A., et al., Salmonella pathogenicity island 1-dependent evasion of the phagocyte NADPH oxidase Science, 2000. **287**(5458): p. 1655-1658.

27. Wang, M., et al., Salmonella virulence and immune escape. Microorganisms 2020. **8**(3): p. 407.

28. Fenlon, L.A. and J.M. Slauch, Phagocyte roulette in salmonella killing. Cell Host & Microbe, 2015. **15**(1): p. 7-8.

29. van der Velden, A.W.M., M. Velasquez, and M.N. Starnbach, Salmonella rapidly kill dendritic cells via a caspase-1-dependent mechanism Journal of Immunology 2003. **171**(12): p. 6742-6749.

30. Du Toit, A., A metabolic trigger for Salmonella. Nature Reviews Microbiology, 2021. **19**: p. 222-223.

31. Fink, S.L. and B.T. Cookson, Pyroptosis and host cell death responses during Salmonella infection. Cell Microbiology 2007. **9**(11): p. 2562-2570.

32. Brusch, J.L. What is the difference between nontyphoidal Salmonellae and S Typhi or S paratyphi? Latest Medical News. Clinical Trials, Guidelines - Today on Medscape 2021 [cited 2021 November 30]; Available from: https://www.medscape.com/answers/231135-10569/what-is-the-difference-between-nontyphoidal-salmonellae-and-s-typhi-or-s-paratyphi#:~:text=Nontyphoidal%20salmonellae%20are%20phagocytized%20throughout%20the%20distal%20ileum,molecular%20patterns%20%28PAMPs%29%20such%20as%20flagella%20and%20lipopolysaccharides

33. Dougan, G., et al., Immunity to salmonellosis. Immunological Reviews, 2011. **240**(1): p. 192-210.

34. Miller, R.A., et al., The typhoid toxin produced by the nontyphoidal Salmonella enterica serotype Javiana is required for induction of DNA damage response in vitro and systemic spread in vivo. mBio, 2018. **9**(2): p. e00467-18.

35. den Bakker, H.C., et al., Genome sequencing reveals diversification of virulence factor content and possible host adaptation in distinct subpopulations of Salmonella enterica. BMC Genomics, 2011. **12**(425).

36. Wallach, D. and A. Kovalenko, Apoptosis: keeping inflammation at bay. eLife, 2014. **3**: p. e02583.

37. Mezal, E.H., D. Bae, and A.A. Khan, Detection and functionality of the CdtB, PltA, and PltB from Salmonella enterica serovar Javiana. Pathogens and Disease 2014. **72**(2): p. 95-103.

38. Brawn, L.C., R.D. Hayward, and V. Koronakis, Salmonella SPI1 effector SipA persists after entry and cooperates with SPI2 effector to regulate phagosome maturation and intracellular replication. Cell Host & Microbe, 2007. **1**(1): p. 63-75.

39. Kolodziejek, A.M. and S.I. Miller, Salmonella modulation of the phagosome membrane, role of SseJ. Cellular Microbiology, 2015. **7**(3): p. 333-341.

40. Mallo, G.V., et al., SopB Promotes Phosphatidylinositol 3-Phosphate Formation on Salmonella Vacuoles by Recruiting Rab5 and Vps34. Journal of Cell Biology, 2008. **182**(4): p. 741-752.

41. Kim, J., et al., Oxidative stress activates transcription of Salmonella pathogenicity island-2 genes in macrophages. Journal of Biological Chemistry, 2022. **298**(7): p. 102130.

42. Bayer-Santos, E., et al., The Salmonella effector SteD mediates MARCH8-dependent ubiquitination of MHCII molecules and inhibits T cell activation. Cell Host & Microbe, 2016. **20**(5): p. 584-595.

43. Jechalke, S., et al., Salmonella establishment in agricultural soil and colonization of crop plants depend on soil type and plant species. Frontiers in Microbiology, 2019. **10**.

44. Bondo, K.J., et al., Impact of season, demographic and environmental factors on salmonella occurrence in raccoons (Procyon lotor) from swine farms and conservation areas in Southern Ontario. PLoS One, 2016. **11**(9).

45. Mathew, E.N., et al., Attachment of salmonella enterica on mangoes and survival under conditions simulating commercial mango packing house and importer facility. Frontiers in Microbiology, 2018. **9**.

46. Weidemann, A., et al., Interactions of Salmonella with animals and plants. Frontiers in Microbiology, 2014. **5**: p. 791.

47. Salmonellosis: Background, management and Control. 2019 [cited 2022 April 5]; Available from: https://www.vet.cornell.edu/animal-health-diagnostic-center/programs/nyschap/modules-documents/salmonellosis-background-management-and-control#:~:text=Unfortunately%2C%20when%20salmonellosis%20occurs%20on,acute%20signs%20of%20the%20infection

48. CDC. CDC Vital signs - making food safer to eat: Prevention from farm to table infographic. 2011 June 07 [cited 2021; Available from: https://www.cdc.gov/vitalsigns/foodsafety/infographic.html#:~:text=Employ%20pre%2Dharvest%20food%20safety,steps%20to%20reduce%20contamination%20work. .

49. Liu, H., C.A. Whitehouse, and B. Li, Presence and persistence of Salmonella in water: The impact on microbial quality of water and food safety. Frontiers in Public Health 2018. **6**: p. 159.

50. Haley, B.J., D.J. Cole, and E.K. Lipp, Distribution, diversity, and seasonality of waterborne Salmonellae in a rural watershed. Applied and Environmental Microbiology, 2009. **75**(5): p. 1248-1255.

51. Underthun, K., et al., Survival of Salmonella and Escherichia coli in two different soil types at various moisture levels and temperatures. Journal of Food Protection, 2017. **81**(1): p. 150-157.

52. Jacobsen, C.S. and T.B. Bech, Soil survival of Salmonella and transfer to freshwater and fresh produce. Food Research International 2012. **45**(2): p. 557-566.

53. Bardsley, C.A., et al., Strain, soil-type, irrigation regimen, and poultry litter influence salmonella survival and die-off in agricultural soils. Frontiers in Microbiology, 2021. **12**.

54. Collignon, S. and L. Korsten, Attachment and colonization by escherichia coli O157:H7, listeria monocytogenes, salmonella enterica subsp. enterica serovar typhimurium, and Staphylococcus aureus on stone fruit surfaces and survival through a simulated commercial export chain. Journal of Food Protection 2010. **73**(7): p. 1247-1256.

55. Carstens, C.K., J.K. Salazar, and C. Darkoh, Multistate outbreaks of foodborne illness in the United States associated with fresh produce from 2010 to 2017. Frontiers in Microbiology, 2019. **10**.

56. Hedberg, C.W., et al., Outbreaks of salmonellosis associated with eating uncooked tomatoes: implications for public health. The Investigation Team. Epidemiology & Infection, 1999. **122**(3): p. 385-393.

57. Hirneisen, K.A., M. Sharma, and K.E. Kneil, Human enteric pathogen internalization by root uptake into food crops. Foodborne Pathogens and Disease, 2012. **9**(5).

58. Walia, K., et al., The efficacy of different cleaning and disinfection procedures to reduce Salmonella and Enterobacteriaceae in the lairage environment of a pig abattoir. International Journal of Food Microbiology, 2017. **246**: p. 64-71.

59. Corcoran, M., et al., Commonly used disinfectants fail to eradicate Salmonella enterica biofilms from food contact surface materials. Applied and Environmental Microbiology, 2014. **80**(4): p. 1507-1514.

60. Demirbilek, S.K., Salmonellosis in Animals, in Salmonella A Re-emerging Pathogen 2018, InTech Open. p. 19-37.

61. Grünberg, W. Salmonellosis in animals- digestive system. 2020 [cited 2021 June 1]; Available from: https://www.merckvetmanual.com/digestive-system/salmonellosis/salmonellosis-in-animals.

62. McGuirk, S. and P. S. Salmonellosis in Cattle: A Review [Review of the preconvention seminar Dairy Herd Problem Investigation Strategies]. in Dairy Herd Problem Investigation StrategiesL American Association of Bovine Practitioners, 36th Annual Conference. 2003. Columbus, OH: American Association of Bovine Practitioners.

63. Beaudoin, A. and S. Valberg. Salmonella in Horses. 2021 [cited 2022 August 09]; Available from: https://extension.umn.edu/horse-health/salmonella-horses#:~:text=Salmonella%20can%20upset%20the%20gut,if%20your%20horse%20is%20infected.

64. Mallicote, M., DACVIM. Salmonella FAQs 2019 [cited 2019 July 22]; Available from: https://largeanimal.vethospitals.ufl.edu/hospital-services/internal-medicine/salmonellafaqs/.

65. Seepersadsingh, N., A. Adesiyun, and R. Seebaransingh, Prevalence and Antimicrobial Resistance of Salmonella spp. in Non-diarrhoeic Dogs in Trinidad. Zoonosis and Public Health, 2007. **51**(7).

66. Salmonella infection in horses: Equine GI disease library. 2016 [cited 2022 April 5]; Available from: https://www.succeed-vet.com/equine-gi-disease-library/colitis/salmonella/

67. Cummings, K.J., et al., Sequence analysis of Salmonella enterica isolates obtained from shelter dogs throughout Texas. Veterinary Medicine and Science, 2020. **6**(4): p. 975-979.

68. Amadi, V.A., et al., Serovars and antimicrobial resistance of non-typhoidal Salmonella isolated from non-diarrhoeic dogs in Grenada, West Indies. Veterinary Medicine and Science, 2017. **4**(1): p. 26-34.

69. Gutema, F.D., et al., Prevalence and serotype diversity of salmonella in apparently healthy cattle: Systematic review and meta-analysis of published studies, 2000–2017. Frontiers in Veterinary Science, 2019. **6**(102).

70. CDC. Salmonella infection. 2015 September 24 [cited 2021 June 1]; Available from: https://www.cdc.gov/healthypets/diseases/salmonella.html#:~:text=Many%20animals%20with%20Salmonella%20have.vomit%20or%20have%20a%20fever.

71. Biomin. Salmonellosis in Poultry. [cited 2022 May 1]; Available from: https://www.biomin.net/us/species/poultry/salmonellosis-in-poultry/

72. Rosario, I., et al., Salmonella enterica subsp. Enterica serotypes isolated for the first time in feral cats: the impact on public health. Comparative Immunology, Microbiology and Infectious Diseases 2022. **84**: p. 101792.

73. Rothers, K.L., et al., Atypical salmonellosis in a horse: Implications for hospital safety. Case Reports in Veterinary Medicine, 2020. **2020**(7062408): p. 1-5.

74. USDA. USDA launches new effort to reduce salmonella illnesses linked to poultry. 2021 [cited 2022 June 6]; Available from: https://www.usda.gov/media/press-releases/2021/10/19/usda-launches-new-effort-reduce-salmonella-illnesses-linked-poultry

75. Scharff, R.L., Food Attribution and Economic Cost Estimates for Meat- and Poultry-Related Illnesses. Journal of Food Protection, 2020. **83**(6): p. 959-967.

76. El-Saadony, M.T., et al., The control of poultry salmonellosis using organic agents: an updated review Poultry Science 2022. **101**(4).

77. CDC. Salmonella outbreaks linked to Backyard Poultry 2021 November 18 [cited 2022 May 1]; Available from: https://www.cdc.gov/salmonella/backyardpoultry-05-21/index.html

78. CDC. Outbreaks involving Salmonella 2022 May 21 [cited 2022 May 26]; Available from: https://www.cdc.gov/salmonella/outbreaks.html

79. Get the facts about Salmonella [cited 2022 June 9]; Available from: https://www.fda.gov/animal-veterinary/animal-health-literacy/get-facts-about-salmonella#:~:text=Salmonellosis%20is%20uncommon%20in%20dogs,other%20pets%20in%20the%20household

80. Chomel, B.B., Zoonoses of house pets other than dogs, cats, and birds. The Pediatric Infectious Disease Journal, 1992. **11**(6): p. 479-487.

81. The human-animal bond throughout time. 2018 [cited 2022 June 9]; Available from: https://cvm.msu.edu/news/perspectives-magazine/perspectives-fall-2018/the-human-animal-bond-throughout-time

82. PetfoodIndustry.com. Infographic: Most of world owns parts; Dogs are tops 2016 [cited 2022 June 9]; Available from: https://www.petfoodindustry.com/articles/5845-infographic-most-of-world-owns-pets-dogs-are-tops#:~:text=Dogs%20are%20the%20most%20popular,%25)%20all%20rank%20significantly%20lower.

83. Pets, pets everywhere: The world's most popular pets. 2017 [cited 2022 August 1]; Available from: https://www.lonetreevet.com/blog/most-popular-pets/

84. Bradshaw, J. Dogs we understand; cats are mysterious, even though they are the most popular pet. 2013 [cited 2022 August 1]; Available from: https://www.washingtonpost.com/national/health-science/dogs-we-understand-cats-are-mysterious-even-though-they-are-the-most-popular-pet/2013/10/14/2c59c6b0-26ca-11e3-ad0d-b7c8d2a594b9_story.html

85. New research suggests Cat and Dog 'moms' and 'Dads' really are parenting their pets – here's the evolutionary explanation why. 2022 [cited 2022 August 1]; Available from: https://www.boisestate.edu/news/2021/11/01/new-research-suggests-cat-and-dog-moms-and-dads-really-are-parenting-their-pets-heres-the-evolutionary-explanation-why/

86. DePolo, J. The ties that bind: How the human-animal bond is Changing Veterinary Medicine. 2018 [cited 2022 August 1]; Available from: https://cvm.msu.edu/news/perspectives-magazine/perspectives-fall-2018/the-ties-that-bind-how-the-human-animal-bond-is-changing-veterinary-medicine

87. Rost, D.H. and A.H. Hartmann, Children and their pets Anthrozoös, 2015. **7**(4): p. 242-254.

88. McConnell, A.R., E.P. Lloyd, and B.T. Humphrey, We are family: viewing pets as family members improves wellbeing. Anthrozoös, 2019. **32**(4): p. 459-470.

89. ASPCA. Species Suitable to be Companion Animals. [cited 2022; Available from: https://www.aspca.org/about-us/aspca-policy-and-position-statements/species-suitable-

be-companion-animals#:~:text=Species%20suitable%20to%20be%20companion%20animals%20include%20dogs%2C%20cats%2C%20horses,also%20be%20maintained%20as%20companions.

90. Stewart, A.J. Salmonellosis in horses - digestive system. 2016 [cited 2022 April 5]; Available from: https://www.merckvetmanual.com/digestive-system/intestinal-diseases-in-horses-and-foals/salmonellosis-in-horses

91. CDC. Reptile-associated salmonellosis --- Selected States, 1998--2002. 2003 [cited 2020; Available from: https://www.cdc.gov/mmwr/preview/mmwrhtml/mm5249a3.htm

92. Roos , R. USDA estimates E coli, salmonella costs at $3.1 billion. 2010 [cited 2022 April 4]; Available from: https://www.cidrap.umn.edu/news-perspective/2010/05/usda-estimates-e-coli-salmonella-costs-31-billion#:~:text=The%20USDA%27s%20Economic%20Research%20Service,all%20sources%2C%20with%20415%20deaths.

93. ERS. Cost of foodborne illness estimates for Salmonella (nontyphoidal) 2013. Available from: http://ers.usda.gov/data-products/cost-estimates-of-foodborne-illnesses.aspx, https://view.officeapps.live.com/op/view.aspx?src=https%3A%2F%2Fwww.ers.usda.gov%2Fwebdocs%2FDataFiles%2F48464%2FSalmonella_2013.xlsx%3Fv%3D343.9&wdOrigin=BROWSELINK

94. Hoffmann, S. Quantifying the impacts of foodborne illnesses. USDA ERS - Quantifying the Impacts of Foodborne Illnesses 2015 [cited 2022 May 4]; Available from: https://www.ers.usda.gov/amber-waves/2015/september/quantifying-the-impacts-of-foodborne-illnesses/

95. ERS. Total cost of foodborne illness estimates for 15 leading foodborne pathogens 2018. 2021; Available from: https://view.officeapps.live.com/op/view.aspx?src=https%3A%2F%2Fwww.ers.usda.gov%2Fwebdocs%2FDataFiles%2F48464%2FTotal_cost_for_top_15_pathogens_2018.xlsx%3Fv%3D4295&wdOrigin=BROWSELINK.

96. ERS. Cost estimates of foodborne illnesses. USDA ERS - Cost Estimates of Foodborne Illnesses 2022 [cited 2022 May 4]; Available from: https://www.ers.usda.gov/data-products/cost-estimates-of-foodborne-illnesses/

97. ERS. Cost of foodborne illness estimates for Salmonella (nontyphoidal) 2018. 2021; Available from: http://ers.usda.gov/data-products/cost-estimates-of-foodborne-illnesses.aspx, https://view.officeapps.live.com/op/view.aspx?src=https%3A%2F%2Fwww.ers.usda.gov%2Fwebdocs%2FDataFiles%2F48464%2FSalmonella_2018.xlsx%3Fv%3D4295&wdOrigin=BROWSELINK .

98. Robinson, S. The Big Five: Most Common Salmonella Strains in Foodborne Illness Outbreaks. 2013 [cited 2019 May 22]; Available from: https://www.foodsafetynews.com/2013/08/the-five-most-common-salmonella-strains/.

99. ASPA. Bacteria and viruses 2022 [cited 2022.

100. Salmonellosis- Salmonella Annual Report, L.D.o. Health, Editor. 2017, Louisiana Department of Health Louisiana

101. Annual Report, Salmonella, General, Louisiana, 2019. [cited 2022 May 4]; Available from: https://www.americashealthrankings.org/explore/annual/measure/salmonella/state/LA?edition-year=2019

102. CDC. Outbreaks of salmonella infections associated with eating Roma tomatoes ---united states and Canada, 2004. . Morbidity and Mortality Weekly Report 2005 April 08 [cited 2022 May 4]; Available from: https://www.cdc.gov/mmwr/preview/mmwrhtml/mm5413a1.htm

103. Iveson, J.B. and S.D. Bradshaw, Salmonella javiana infection in an infant associated with a marsupial, the quokka, Setonix brachyurus, in Western Australia. Journal of Hygiene 1973. **71**(3): p. 423-432.

104. Gordon, M.A., et al., Non-typhoidal salmonella bacteraemia among HIV-infected Malawian adults: high mortality and frequent recrudescence. AIDS, 2002. **16**(12): p. 1633-1641.

105. Walsh, A.L., et al., Bacteremia in febrile Malawian children: clinical and microbiologic features. The Pediatric Infectious Disease Journal, 2000. **19**(4): p. 312-318.

106. Beach, C. Salmonella outbreak case count grows as FDA begins traceback; no food specified. 2021 [cited 2022 May 3];].

107. Outbreak investigation of Salmonella Javiana: Fruit Mix, December 2019. 2020 [cited 2022 May 3]; Available from: https://www.fda.gov/food/outbreaks-foodborne-illness/outbreak-investigation-salmonella-javiana-fruit-mix-december-2019

108. 2018 Outbreak of Salmonella Javiana at La Luz Restaurant, Fort Collins, Colorado. Foodborne Illness Outbreak Database [cited 2022 May 3]; Available from: http://outbreakdatabase.com/details/2018-outbreak-of-salmonella-javiana-at-la-luz-restaurant-fort-collins-colorado/?outbreak=javiana

109. 2017-2018 Multistate Outbreak of Salmonella Infections Linked to Kratom. Foodborne Illness Outbreak Database [cited 2022 May 3]; Available from: http://outbreakdatabase.com/details/2017-2018-multisate-outbreak-of-salmonella-infections-liked-to-kratom/?outbreak=javiana&year=2017.

110. 2017 Outbreak of Salmonella Javiana, Chincoteague Chili and Chowder Cook Off. Foodborne Illness Outbreak Database [cited 2022 May 3]; Available from: http://outbreakdatabase.com/details/2017-outbreak-of-salmonella-javiana-chincoteague-chili-and-chowder-cook-off/?outbreak=javiana&year=2017.

111. 2017-2018 Multistate Outbreak of Salmonella Linked to Coconut Tree Brand Frozen Shredded Coconut. Foodborne Illness Outbreak Database [cited 2022 May 3]; Available from: http://outbreakdatabase.com/details/2017-2018-multistate-outbreak-of-salmonella-linked-to-coconut-tree-brand-frozen-shredded-coconut/?

112. 2016 Outbreak of Salmonella Javiana in Maricopa County, AZ. Foodborne Illness Outbreak Database [cited 2022 May 3]; Available from: http://outbreakdatabase.com/details/2016-outbreak-of-salmonella-javiana-in-maricopa-county-az/?

113. 2008 Outbreak of Salmonella Javiana at a Multi-Site Day Care Center, California. Foodborne Illness Outbreak Database [cited 2022 May 3]; Available from: http://outbreakdatabase.com/details/2008-outbreak-of-salmonella-javiana-at-a-multi-site-day-care-center-california/?outbreak=javiana&year=2008.

114. North Carolina Picnic Pork Barbeque 2008. Foodborne Illness Outbreak Database [cited 2022 May 3]; Available from: http://outbreakdatabase.com/details/north-carolina-picnic-pork-barbeque-2008/?outbreak=javiana&year=2008.

115. 2008 Outbreak of Salmonella at a Wedding Reception, Virginia. Foodborne Illness Outbreak Database [cited 2022 May 3]; Available from: http://outbreakdatabase.com/details/2008-outbreak-of-salmonella-at-a-wedding-reception-virginia/?outbreak=javiana&year=2008.

116. Tennessee Restaurant Iceberg Lettuce 2006. Foodborne Illness Outbreak Database [cited 2022 May 3]; Available from: http://outbreakdatabase.com/details/tennessee-restaurant-iceberg-lettuce-2006/?outbreak=javiana&year=2006.

117. CDC. Outbreaks of salmonella infections associated with eating Roma tomatoes - United States and Canada, 2004. Morbidity and Mortality Weekly Report 2005 [cited 2022 May 4]; Available from: https://www.cdc.gov/mmwr/preview/mmwrhtml/mm5413a1.htm

118. Elward, A., et al., Outbreak of Salmonella Javiana infection at a children's hospital. Infection Control & Hospital Epidemiology, 2006. **27**(6): p. 586-592.

119. Children's Hospital Cafeteria Food Worker 2003. Foodborne Illness Outbreak Database [cited 2022 May 3]; Available from: http://outbreakdatabase.com/details/childrens-hospital-cafeteria-food-worker-2003/?outbreak=javiana.

120. Disney World U.S. Transplant Games Roma Tomatoes 2002. Foodborne Illness Outbreak Database [cited 2022 May 3]; Available from: http://outbreakdatabase.com/details/disney-world-u.-s.-transplant-games-roma-tomatoes-2002/?outbreak=javiana&year=2002.

121. CDC. Outbreak of salmonella serotype Javiana infections - Orlando, Florida, June 2002. 2002 August 09 [cited 2022 May 4]; Available from: https://www.cdc.gov/mmwr/preview/mmwrhtml/mm5131a2.htm

122. 1993 Outbreak of Salmonella Linked to Contaminated Paprika and Paprika-Powdered Potato Chips, Germany. Foodborne Illness Outbreak Database [cited 2022 May 3]; Available from: http://outbreakdatabase.com/details/1993-outbreak-of-salmonella-linked-to-contaminated-paprika-and-paprika-powdered-potato-chips-germany/?outbreak=javiana&year=1993.

123. Bolstein, J., An Outbreak of Salmonella Javiana Associated with Consumption of Watermelon. Environmental Health, 2013. **56**(1): p. 29-31.

124. 1991 Outbreak of Salmonella Javiana Linked to Watermelon, Michigan. Foodborne Illness Outbreak Database [cited 2022 May 3]; Available from: http://outbreakdatabase.com/details/1991-outbreak-of-salmonella-javiana-linked-to-watermelon-michigan/?outbreak=javiana&year=1991.

125. Commercially Produced Mozzarella Cheese and Shredded Cheeses 1989. Foodborne Illness Outbreak Database [cited 2022 May 3]; Available from: http://outbreakdatabase.com/details/commercially-produced-mozzarella-cheese-and-shredded-cheeses-1989/?outbreak=javiana&year=1989

126. Feasey, N.A., et al., Invasive non-typhoidal salmonella disease: An emerging and neglected tropical disease in Africa. The Lancet, 2012. **379**(9835): p. 2489-2499.

127. Tennant, S.M., et al., Nontyphoidal salmonella disease: Current status of vaccine research and development. Vaccine, 2016. **34**(26): p. 2907-2910.

128. Haselbeck, A.H., et al., Current perspectives on invasive nontyphoidal Salmonella disease. Gastrointestinal infections, 2017. **30**(5): p. 498-503.

129. Gordon, M.A., Invasive nontyphoidal Salmonella disease. Current Opinion in Infectious Diseases, 2012. **24**(5): p. 484-489.

130. Sirinavin, S. and P. Garner, Antibiotics for treating salmonella gut infections. Cochrane Database of Systematic Reviews, 1999.

131. Onwuezobe, I.A., P.O. Oshun, and C.C. Odigwe, Antimicrobials for treating symptomatic non-typhoidalsalmonellainfection. Cochrane Database of Systemic Reviews, 2012.

132. Christenson, J.C., Salmonella infections. Pediatrics in Review, 2013. **34**(9): p. 375-383.

133. WHO. Salmonella (non-typhoidal). [cited 2021 June 1]; Available from: https://www.who.int/news-room/fact-sheets/detail/salmonella-(non-typhoidal).

134. Majowicz, S.E., et al., The global burden of nontyphoidal Salmonella gastroenteritis. Clinical Infectious Diseases 2010. **50**(6): p. 882-889.

135. Ao, T.T., et al., Global Burden of Invasive Nontyphoidal Salmonella Disease, 2010. Emerging Infectious Diseases, 2015. **21**(6): p. 941-949.

136. Poorest countries in Africa 2022. 2022 [cited 2022; Available from: https://worldpopulationreview.com/country-rankings/poorest-countries-in-africa

137. Heritage. Malawi Economy: Population, GDP, Inflation, Business, Trade, FDI, Corruption. 2022 Index of Economic Freedom 2022 [cited 2022; Available from: https://www.heritage.org/index/country/malawi

138. HHS. Vaccine Types 2019 [cited 2022 May 12]; Available from: https://www.niaid.nih.gov/research/vaccine-types.

139. OIDP. Vaccine Types Immunization 2021 [cited 2022 May 12]; Available from: https://www.hhs.gov/immunization/basics/types/index.html#:~:text=Inactivated%20vaccines%20use%20the%20killed,get%20ongoing%20immunity%20against%20diseases.

140. Zhou, B., et al., Reversion of cold-adapted live attenuated influenza vaccine into a pathogenic virus. Journal of Virology, 2016. **90**(19): p. 8454-8463.

141. Burrell, C.J., C.R. Howard, and F.A. Murphy, Vaccines and Vaccination, in Fenner and White's Medical Virology. 2017, Academic Press. p. 155–167.

142. McWhorter, A.R. and K.K. Chousalkar, A long-term efficacy trial of a live, attenuated salmonella typhimurium vaccine in Layer Hens. Frontiers in Microbiology, 2018. **9**.

143. Vaxxinova. SRP® Technology. Epitopix a part of Vaxxinova 2022 [cited 2022 May 12]; Available from: https://vaxxinova.us.com/srp-technology/

144. Thomson, D.U., et al., Use of a siderophore receptor and porin proteins-based vaccine to control the burden of escherichia coliO157:H7 in Feedlot Cattle. Foodborne Pathogens and Disease, 2009. **6**(7): p. 871-877.

145. DailyMed. TYPHIM VI- salmonella typhi ty2 vi polysaccharide antigen injection, solution [cited 2022 October 31]; Available from: https://dailymed.nlm.nih.gov/dailymed/drugInfo.cfm?setid=ad1fbe7f-2995-45dd-92f3-7baccaab85d9.

146. Mandell, L.A., Streptococcus Pneumoniae Infections, in Goldman's Cecil Medicine L.G.A.I. Schafer, Editor. 2012, Elsevier Inc. p. 1820-1823.

147. Spickler, A.R. and J.A. Roth, Adjuvants in veterinary vaccines: Modes of action and adverse effects. Journal of Veterinary Internal Medicine, 2003. **17**(3): p. 273-281.

148. CDC. Adjuvants and vaccines. 2020 August 14 [cited 2022 May 12]; Available from: https://www.cdc.gov/vaccinesafety/concerns/adjuvants.html#:~:text=Adjuvants%20help%20the%20body%20to,she%20is%20being%20vaccinated%20against

149. ValleyVet. Salmonella Newport bacterial extract SRP cattle vaccine. Salmonella Newport Bacterial Extract SRP Cattle Vaccine Zoetis Animal Health - Salmonella | Miscella. [cited 2022 May 12]; Available from: https://www.valleyvet.com/ct_detail.html?pgguid=9f3cb950-c4e4-4e89-91c1-9b7d109475b9&itemguid=5b97bc9b-f16e-405b-bd96-720f768d08c7&sfb=1&grp=1000&grpc=1100&grpsc=1170&sp=f&utm_content=33999&ccd=IFF003&gclid=Cj0KCQjwmPSSBhCNARIsAH3cYgaepHdAr9lpSK2_v6GRhHSO5v83sGXcmVJnEjbSu-qGiCur8j4PyUsaAgZHEALw_wcB

150. ValleyVet. Endovac-Beef with ImmunePlus Cattle Vaccine. [cited 2022; Available from: https://www.cdc.gov/salmonella/reportspubs/salmonella-atlas/serotype-snapshots.html.

151. ValleyVet. Endovac-Dairy with ImmunePlus Cattle Vaccine [cited 2022; Available from: https://www.valleyvet.com/ct_detail.html?pgguid=30E0791E-7B6A-11D5-A192-00B0D0204AE5.

152. ValleyVet. Endovac-Porci with ImmunePlus Swine Vaccine. [cited 2022; Available from: https://www.valleyvet.com/ct_detail.html?pgguid=33588F84-F155-4CC4-B1C9-9E837731606B.

153. ValleyVet. Vaxxon SRP Salmonella Cattle Vaccine [cited 2022; Available from: https://www.valleyvet.com/ct_detail.html?pgguid=D6242CEA-932D-4B4C-9E98-C9448B73094F.

154. EnterVene-d. [cited 2022 May 12]; Available from: https://www.bi-vetmedica.com/species/cattle/products/EnterVene-d.html#:~:text=ENTERVENE%2DD%20is%20indicated%20for,(2%20weeks%20or%20older).&text=ENTERVENE%2DD%20is%20USDA%20approved,dose%20and%2050%2Ddose%20bottles

155. Safety Data Sheet for Entervene® D, B. Ingelheim, Editor. 2015, Boehringer Ingelheim: 2621 North Belt HWY St. Joseph, MO 64506-2002.

156. AlliVet. Endovac-dairy with immune plus. [cited 2022 May 12]; Available from: https://www.allivet.com/product/endovac-dairy-with-immune-plus/50886.html?sku=50886-1&gclid=Cj0KCQjwmPSSBhCNARIsAH3cYgakn0GnBaeyYzuZyXTAhTVIrCWB6RTKM_Srwk95gdfL4A34fMakWPoaAmNpEALw_wcB.

157. AlliVet. Enterisol Salmonella T/C oral swine vaccine, 100 DS/200 ML [cited 2022 May 12]; Available from: https://www.allivet.com/product/enterisol-salmonella-t-c-oral-swine-vaccine-100-ds-200-ml/50894.html?gclid=Cj0KCQjwmPSSBhCNARIsAH3cYgZ4L2g9F50__lmsDVs1aAp9lNsHrROFzAzW9XArs-uUlrvhbRksekUaArVfEALw_wcB

158. AlliVet. Endovac-Beef with Immune Plus [cited 2022; Available from: https://www.allivet.com/product/endovac-beef-with-immune-plus/50243.html.

159. AlliVet. Endovac-Dairy with Immune Plus [cited 2022; Available from: https://www.allivet.com/product/endovac-dairy-with-immune-plus/50886.html?sku=50886-1&gclid=Cj0KCQjwmPSSBhCNARIsAH3cYgakn0GnBaeyYzuZyXTAhTVIrCWB6RTKM_Srwk95gdfL4A34fMakWPoaAmNpEALw_wcB.

160. AlliVet. Enterisol Salmonella T/C Oral Swine Vaccine, 100 ds/200 ml. [cited 2022; Available from: https://www.allivet.com/product/enterisol-salmonella-t-c-oral-swine-vaccine-100-ds-200-ml/50894.html?gclid=Cj0KCQjwmPSSBhCNARIsAH3cYgZ4L2g9F50__lmsDVs1aAp9lNsHrROFzAzW9XArs-uUlrvhbRksekUaArVfEALw_wcB.

161. Salmonella. 2020 [cited 2022 May 12]; Available from: https://www.merck-animal-health-usa.com/condition/salmonella

162. Benoun, J.M., et al., Optimal protection against Salmonella infection requires noncirculating memory. Proceedings of the National Academy of Sciences. 2018. **201808339**.

163. UC-Davis. Breakthrough in designing a better Salmonella vaccine. 2018 [cited 2020 August 17]; Available from: https://www.sciencedaily.com/releases/2018/09/180924160933.htm.

164. Jones, M.K., et al., Evaluation of a modified live Salmonella typhimurium vaccination efficacy against Salmonella enterica serovar Infantis in broiler chickens at processing age. Journal of Applied Poultry Research 2021. **30**(2): p. 100156.

165. Jia, S., et al., Challenges in vaccinating layer hens against Salmonella Typhimurium. Vaccines, 2020. **8**(4): p. 696.

166. Neustroev, M.P. and S.G. Petrova, Developmental results of a vaccine against Salmonella-induced equine abortion. Russian Agricultural Science, 2020. **46**(5): p. 530-533.

167. CDC. Vaccine Storage and Handling Toolkit. 2022 [cited 2022 May 12]; Available from: https://www.cdc.gov/vaccines/hcp/admin/storage/toolkit/storage-handling-toolkit.pdf

168. MacLennan, C.A., L.B. Martin, and F. Micoli, Vaccines against invasive Salmonella disease: current status and future directions. Human Vaccines & Immunotherapeutics 2014. **10**(6): p. 1478-1493.

169. CDC. Snapshots of Serotypes An Atlas of Salmonella in the United States, 1968-2011 2022 [cited 2022 August 08]; Available from: https://www.cdc.gov/salmonella/reportspubs/salmonella-atlas/serotype-snapshots.html.

170. FDA, Vivotif Package Insert USA, FDA, Editor. 2013, FDA.

171. Aliouche, H. Could there be a Salmonella Vaccine? 2022 [cited 2022; Available from: https://www.news-medical.net/life-sciences/Could-there-be-a-Salmonella-Vaccine.aspx#:~:text=At%20present%2C%20the%20only%20licensed,generating%20mutants%20using%20random%20mutagenesis.

172. Galen, J.E., et al., Live attenuated human Salmonella vaccine candidates: tracking the pathogen in natural infection and stimulation of host immunity. EcoSal Plus 2016. **7**(1).

173. Zoetis. Salmonella [cited 2022; Available from: https://www.health4horses.com.au/health-care/conditions/salmonella/salmonella.aspx?ReturnUrl=/index.aspx.

174. Zoetis, Safety Data Sheet for Equivac EST Vaccine Zoetis, Editor. 2021, Zoetis

175. Zoetis. Poulvac® ST. [cited 2022; Available from: https://www2.zoetisus.com/products/poultry/poulvac-st#:~:text=Poulvac%20%C2%AE%20ST%20is%20a,including%20the%20intestines%20and%20ceca.

176. Multi-drug resistant Salmonella in Horses 2019 [cited 2022 August 10]; Available from: https://www.vet.cornell.edu/animal-health-diagnostic-center/news/multi-drug-resistant-salmonella-horses.

177. Callaway, T.R., et al., Novel methods for pathogen control in livestock pre-harvest: an update, in Advances in Microbial Food Safety. 2013, USDA-ARS, USA.

178. Collado, M.C., M. Gueimonde, and S. Salminen, Probiotics in Adhesion of Pathogens: Mechanisms of Action, in Bioactive Foods in Promoting Health. 2010. p. 353-370.

179. Duffy, G., Pathogen control in primary production: meat, dairy and eggs, in Foodborne Pathogens 2009. p. 182-204.

180. Swaggerty, C.L., et al., The First 30 Years of Shiga Toxin- Producing Escherichia coli in Cattle Production: Preharvest Intervention Strategies, in Food and Feed Safety Systems and Analysis. 2018. p. 133-151.

181. Callaway, T.R., Edrington, T. S., Byrd, J. A., Nisbet, D. J., Ricke, S. C. , Use of Direct-Fed Microbials in Layer Hen Production - Performance Response and Salmonella Control, in Producing Safe Eggs. 2017. p. 301-322.

182. Buttaccio, J.L. How salmonella is treated. Salmonella Guide 2022 [cited 2022 May 12]; Available from: https://www.verywellhealth.com/salmonella-treatment-4164292

183. CDC. Diagnosis and treatment. Salmonella 2019 April 08 [cited 2022 May 12]; Available from: https://www.cdc.gov/salmonella/general/diag-testing-

salmonella.html#:~:text=Most%20people%20recover%20without%20specific,person%20needs%20to%20be%20hospitalized.

184. Leitner, W.W., H. Ying, and N.P. Restifo, DNA and RNA-based vaccines: principles, progress and prospects. Vaccine, 1999. **18**(9-10): p. 765-777.

185. Gazaille, B. Exciting Starts for New Players and Platforms: Nucleic-Acid Vaccines Prepare for Their Commercial Debut. 2021; Available from: https://bioprocessintl.com/manufacturing/vaccines/new-players-and-platforms-dna-vaccines-prepare-for-their-commercial-debut/.

186. Suri, R. COVID-19: US researchers develop new cheap, DNA vaccine which may offer protection from deadly virus. 2021; Available from: https://www.indiatvnews.com/health/covid-19-us-researchers-develop-new-cheap-dna-vaccine-which-may-offer-protection-from-deadly-virus-699165.

187. Schlake, T., et al., Developing mRNA-vaccine technologies. RNA Biology, 2012. **9**(11): p. 1319-1330.

188. Nagarajan, A.G., et al., SopB of Salmonella enterica serovar Typhimurium is a potential DNA vaccine candidate in conjugation with live attenuated bacteria. Vaccine, 2009. **27**(21): p. 2804-2811.

189. CDC. Myths & Facts. COVID-19 2022 [cited 2022; Available from: https://www.cdc.gov/coronavirus/2019-ncov/vaccines/facts.html.

190. Martin, J.E., et al., A SARS DNA vaccine induces neutralizing antibody and cellular immune responses in healthy adults in a Phase I clinical trial. Vaccine, 2008. **26**(50): p. 6338-6343.

191. Redding, L. and D.B. Werner, DNA vaccines in veterinary use. Expert Review of Vaccines, 2009. **8**(9): p. 1251-1276.

192. Muhar, B.K., et al., The race for covid-19 vaccines: The various types and their strengths and weaknesses. Journal of Pharmacy Practice 2022.

193. Flingai, S., et al., Synthetic DNA vaccines: improved vaccine potency by electroporation and co-delivered genetic adjuvants. Frontiers in Immunology, 2013. **4**.

194. Scheerlinck, J.Y., Genetics adjuvants for DNA vaccines Vaccine, 2001. **19**(17-19).

195. CDC. Covid-19 vaccine training modules. 2021 [cited 2022 August 11]; Available from: https://www2.cdc.gov/vaccines/ed/covid19/janssen/20030.asp

196. Douoguih, M. Overview of Janssen's Single-Dose COVID-19 Vaccine, Ad26.COV2.S, Janssen Pharmaceutical Companies of Johnson & Johnson. ACIP meeting COVID-19 Vaccines 2021; Available from: https://stacks.cdc.gov/view/cdc/105728.

197. Aida, V., et al., Novel vaccine technologies in veterinary medicine: a herald to human medicine vaccines Frontiers in Veterinary Science, 2021. **8**: p. 8654289.

198. Schmidt, C. New COVID Vaccines Need Absurd Amounts of Material and Labor. 2021; Available from: https://www.scientificamerican.com/article/new-covid-vaccines-need-absurd-amounts-of-material-and-labor1/. .

199. GenScript. Gene Synthesis Handbook. [cited 2022 July 15]; Available from: https://www.genscript.com/gsfiles/gene_synthesis_handbook.pdf. .

200. Miyaji, E.N., et al., Analysis of serum cross-reactivity and cross-protection elicited by immunization with DNA vaccines against Streptococcus pneumoniae expressing PspA fragments from different clades. Infection and Immunity, 2002. **70**(9): p. 5086-5090.

201. Vemula, S.V., et al., Vaccine approaches conferring cross-protection against influenza viruses. Expert Review of Vaccines, 2017. **16**(11): p. 1141-1154.

202. Koday, M.T., et al., Multigenic DNA vaccine induces protective cross-reactive T cell responses against heterologous influenza virus in nonhuman primates. PLoS One, 2017. **12**(12): p. e0189780.

203. Gómez, L. and A. Oñate. Plasmid-Based DNA Vaccines. 2018 [cited 2020 August 17]; Available from: https://www.intechopen.com/books/plasmid/plasmid-based-dna-vaccines.

204. Abbas, A.K., A.H. Lichtman, and S. Pillai, Basic Immunology: Functions and Disorders of the Immune System 5th ed. 2015: Elsevier.

205. Bolhassani, A. and S.R. Yazdi, DNA immunization as an efficient strategy for vaccination. Avicenna Journal of Medical Biotechnology, 2009. **1**(2): p. 71-88.

206. Khan, K.H., DNA vaccines: roles against diseases. Germs, 2013. **3**(1): p. 26-35.

207. Coban, C., et al., Novel strategies to improve vaccine immunogenicity. Current Gene Therapy, 2011. **11**(6): p. 479-484.

208. Paludan, S.R. and A.G. Bowie, Immune sensing of DNA Immunity, 2013. **38**(5): p. 870-880.

209. Janeway, C.A., et al., T Cell-Mediated Immunity, in Immunobiology: The Immune System in Health and Disease. 2001, Garland Science New York.

210. Kawasaki, T. and T. Kawai, Toll-like receptor signaling pathways. Frontiers in Immunology, 2014. **5**(461).

211. Lee, A.J. and A.A. Ashkar, The dual nature of type I and type II interferons. Frontiers in Immunology, 2018. **9**.

212. Krieg, A.M., AIMing 2 detect foreign DNA. Science Signaling 2009. **2**(7): p. e39.

213. Rider, P., et al., IL-1α and IL-1β Recruit Different Myeloid Cells and Promote Different Stages of Sterile Inflammation. Journal of Immunology, 2011. **187**(9): p. 4835-4843.

214. Ahn, J. and G.N. Barber, STING signaling and host defense against microbial infection. . Experimental & Molecular Medicine, 2019. **51**: p. 1-10.

215. Alam, M., G.M. Hasan, and M.I. Hassan, A review on the role of TANK-binding kinase 1 signaling in cancer. Int. J. Biol. Macromol.

, 2021. **31**(183): p. 2364-2375.

216. Daniels, M.A., et al., CD8 binding to MHC class I molecules is influenced by T cell maturation and glycosylation. Immunity 2001. **15**(6): p. 1051-1061.

217. Wherry, E.J. and D. Masopust, Adaptive Immunity: Neutralizing, Eliminating, and Remembering for the Next Time in Viral Pathogenesis M.G. Katze, et al., Editors. 2016, Academic Press p. 57-69.

218. Luckerheeram, R.V., et al., CD4+T Cells: Differentiation and Functions. Clinical & Developmental Immunology, 2012. **2012**: p. 925135.

219. Alberts, B., A. Johnson, and J. Lewis, Helper T Cells and Lymphocytes in Molecular Biology of the Cell 2002, Garland Science New York.

220. Abcam. Antibody structure and isotypes 2022 [cited 2023 February 1]; Available from: https://www.abcam.com/protocols/antibody-structure-and-isotypes.

221. van Erp, E.A., et al., Fc-mediated antibody effector functions during respiratory syncytial virus infection and disease Frontiers in Immunology, 2019. **10**(548).

222. NIH. Open Reading Frame 2022 [cited 2022; Available from: https://www.genome.gov/genetics-glossary/Open-Reading-Frame.

223. Ingolotti, M., et al., DNA vaccines for targeting bacterial infections. Expert Review of Vaccines, 2010. **9**(7): p. 747-763.

224. Campeau, P., et al., Transfection of large plasmids in primary human myoblasts. Gene Therapy, 2001. **8**: p. 1387-1394.

225. Hornstein, B.D., et al., Effects of circular DNA length on transfection efficiency by electroporation into HeLa cells. PLoS One, 2016. **11**(12): p. e0167537.

226. Yin, W., P. Xiang, and Q. Li, Investigations of the effect of DNA size in transient transfection assay using dual luciferase system. Analytical Biochemistry, 2005. **346**(2): p. 289-294.

227. Kreiss, P., et al., Plasmid DNA size does not affect the physicochemical properties of lipoplexes but modulates gene transfer efficiency. Nucleic Acids Research, 1999. **27**(19): p. 3792-3798.

228. Tuller, T., et al., Translation efficiency is determined by both codon bias and folding energy. Proceedings of the National Academy of Sciences, 2010. **107**(8): p. 3645-3650.

229. Racaniello, V. The lost picorbavirus ORF. 2018; Available from: http://www.virology.ws/2018/11/29/the-lost-orf/.

230. IDT. Using a codon optimization tool-how it works and advantages [cited 2020; Available from: https://www.idtdna.com/pages/education/decoded/article/using-a-codon-optimization-tool-how-it-works-and-advantages-it-provides.

231. Chung, Y.H., et al., COVID-19 vaccine Frontrunners and their nanotechnology design. ACS Nano, 2020. **14**(10): p. 12522-12537.

232. Wang, Z. and J. Xu, Better adjuvants for better vaccines: progress in adjuvant delivery systems, modifications, and adjuvant-antigen codelivery. Vaccines, 2020. **8**(1): p. 128.

233. Van Lint, S., et al., The Renaissance of mrna-based cancer therapy. Expert Review of Vaccines, 2014. **14**(2): p. 235-251.

234. Cooper, R.K., A. Edwards, Editor. 2018: School of Animal Sciences, Molecular Biology Laboratory

235. Watt, S.A., et al., Identification of the bacterial superoxide dismutase (SodM) as plant-inducible elicitor of an oxidative burst reaction in tobacco cell suspension cultures. Journal of Biotechnology, 2006. **126**(1): p. 78-86.

236. Huang, Q., W. Yu, and T. Hu, Potent antigen-adjuvant delivery system by conjugation of Mycobacterium tuberculosis Ag85B-HspX fusion protein with arabinogalactan-poly(I:C) conjugate. Bioconjugate Chemistry, 2016. **27**(4): p. 1165-1174.

237. Nosrati, M., et al., Designing a multi-epitope vaccine for cross-protection against Shigella spp: An immunoinformatics and structural vaccinology study. Molecular Immunology, 2019. **116**: p. 106-116.

238. Kaushik, V., et al., Immunoinformatics aided design and in-vivo validation of a cross-reactive peptide based multi-epitope vaccine targeting multiple serotypes of Dengue virus. Frontiers in Immunology, 2022. **13**: p. 865180.

239. Zhang, Y., et al., Development and evaluation of a multi-epitope subunit vaccine against group B Streptococcus infection. Emerging Microbes & Infections, 2022. **11**(1): p. 2371-2382.

240. IEDB. Epitope Prediction and Analysis Tools [cited 2022; Available from: http://tools.iedb.org/main/.

241. Bonsack, M., et al., Performance evaluation of MHC class-I binding prediction tools based on an experimentally validated MHC-peptide binding data set. Cancer Immunology Research, 2019. **7**(5): p. 719-736.

242. Wang, P., et al., A systematic assessment of MHC class II peptide binding predictions and evaluation of a consensus approach. PloS Computational Biology, 2008. **4**(4).

243. Wang, P., et al., Peptide binding predictions for HLA DR, DP and DQ molecules. BMC Bioinformatics 2010. **11**: p. 568.

244. Chichili, V.P.R., V. Kumar, and J. Sivaraman, Linkers in the structural biology of protein-protein interactions. Protein Science, 2013. **22**(2): p. 153-167.

245. Pepscan. Linkers & Spacers 2015 [cited 2022; Available from: https://www.pepscan.com/custom-peptide-synthesis/peptide-modifications/linkers-spacers/.

246. Taraballi, F., et al., Glycine-spacers influence functional motifs exposure and self-assembling propensity of functionalized substrates tailored for neural stem cell cultures. Frontiers in Neuroengineering, 2010. **3**(1): p. eCollection2010.

247. Van Rosmalen, M., M. Krom, and M. Merkx, Tuning the flexibility of Glycine-Serine linkers to allow rational design of multidomain proteins. Biochemistry 2017. **56**(50): p. 6565-6574.

248. Raza, S., et al., In silico analysis of four structural proteins of aphthovirus serotypes revealed significant B and T cell epitopes. Microbial Pathogenesis 2019. **128**: p. 254-262.

249. Livingston, B., et al., A rational strategy to design multiepitope immunogens based on multiple Th lymphocyte epitopes. Journal of Immunology, 2002. **168**(11): p. 5499-5506.

250. T Helper 17 Cells Overview [cited 2022; Available from: https://www.thermofisher.com/us/en/home/life-science/cell-analysis/cell-analysis-learning-center/immunology-at-work/t-helper-17-cell-overview.html#:~:text=References-,Th17%20cell%20activation%20and%20differentiation,%2Dpresenting%20cells%20%5B6%5D.

251. InvivoGen. Vaccine Adjuvants Review 2011 [cited 2022; Available from: https://www.invivogen.com/review-vaccine-adjuvants.

252. Janeway, C.A., et al., Macrophage activation by armed CD4 Th1 cells, in Immunobiology: The Immune System in Health and Disease. 2001, Garland Science New York.

253. MacLennan, C.A., Antibodies and protection against invasive Salmonella disease. Frontiers in Immunology, Sec. Microbial Immunology, 2014. **5**.

254. Mantis, N.J., Role of B Cells and Antibodies in Controlling Bacterial Pathogens, in Encyclopedia of Microbiology, T.M. Schmidt, Editor. 2019, Academic Press. p. 194-200.

255. Mastroeni, P. and O. Rossi, Antibodies and Protection in Systemic Salmonella Infections: Do We Still Have More Questions than Answers? Infection and Immunity, 2020. **88**(10): p. e00219-20.

256. Firestein, G.S., Mechanisms of Inflammation and Tissue Repair, in Goldman's Cecil Medicine, L. Goldman and A.I. Schafer, Editors. 2012, W. B. Saunders. p. 230-235.

257. Doorduijn, D.J., et al., Polymerization of C9 enhances bacterial cell envelope damage and killing by membrane attack complex. PLoS Pathogens, 2021. **17**(11): p. e1010051.

258. Thorns, C.J., Salmonella fimbriae: Novel antigens in the detection and control of Salmonella infections British Veterinary Journal 1995. **151**(6): p. 643-658.

259. UniProtKB - A0A0A7CRC2 (A0A0A7CRC2_SALET). [cited 2016 September 29]; Available from: http://www.uniprot.org/uniprot/A0A0A7CRC2

260. Langermann, S., et al., Prevention of Mucosal Escherichia coli Infection by FimH-Adhesin-Based Systemic Vaccination. Science 1997. **276**(5312): p. 607-611.

261. Uchiya, K., et al., Salmonella fimbrial protein FimH is involved in expression of proinflammatory cytokines in a toll-like receptor 4-dependent manner. Infection and Immunity, 2019. **87**(3).

262. Zeiner, S.A., B.E. Dwyer, and S. Clegg, FimA, FimF, and FimH are necessary for assembly of Type 1 fimbriae on Salmonella enterica serovar Typhimurium. Infection and Immunity, 2012. **80**(9): p. 3289-3296.

263. Li, Y., et al., A sopB Deletion Mutation Enhances the Immunogenicity and Protective Efficacy of a Heterologous Antigen Delivered by Live Attenuated Salmonella enterica Vaccines. Infection and Immunity 2008. **76**(11): p. 5238-5246.

264. Chowdhury, A.R., Sah, S., Varshney, U., & Chakravortty, D. , Salmonella Typhimurium outer membrane protein A (OmpA) renders protection from nitrosative stress of macrophages by maintaining the stability of bacterial outer membrane. PLoS Pathogens, 2022. **18**(8): p. e1010708.

265. UniProtKB - A5JP12 (A5JP12_SALTM). [cited 2016 September 30]; Available from: http://www.uniprot.org/uniprot/A5JP12.

266. Okamura, M., et al., Immunization with outer membrane protein A from Salmonella enterica serovar Enteritidis induces humoral immune response but no protection against homologous challenge in chickens. Poultry Science, 2012. **9**(10): p. 2444-2449.

267. UniProtKB - A0A0A7CW61 (A0A0A7CW61_SALTM). [cited 2016 October 10]; Available from: http://www.uniprot.org/uniprot/A0A0A7CW61

268. Prejit, et al., Evaluation of recombinant outer membrane protein based vaccine against Salmonella Typhimurium in birds. Biologicals 2013. **41**(3): p. 162-168.

269. Gil-Cruz, C., et al., The porin OmpD from nontyphoidal Salmonella is a key target for a protective B1b cell antibody response. Proceedings of the National Academy of Sciences, 2009. **106**(24): p. 9803-9808.

270. National Center for Biotechnology Information [cited 2018; Available from: https://www.ncbi.nlm.nih.gov/.

271. IEDB. T Cell Epitope Prediction Tools [cited 2022; Available from: http://tools.iedb.org/main/tcell/.

272. McGee, M., Design and Humoral Analysis of Two Epitope-Based Brucella abortus DNA Vaccines. 2017, Louisiana State University and Agricultural and Mechanical College Animal Sciences Commons

273. Korle, S.L., The Design, Construction, and Testing of a Recombinant DNA Vaccine for Brucella abortus and Brucella melitensis, in Animal Science 2022, Louisiana State University

274. IDT. Codon Optimization Tool. [cited 2018; Available from: https://www.idtdna.com/pages/tools/codon-optimization-tool.

275. NIH. BlastP Suite [cited 2022; Available from: https://blast.ncbi.nlm.nih.gov/Blast.cgi?PROGRAM=blastp&PAGE_TYPE=BlastSearch&LINK_LOC=blasthome.

276. Egan, M.A., et al., Rational design of a plasmid DNA vaccine capable of eliciting cell-mediated immune responses to multiple HIV antigens in mice. Vaccine 2016. **24**(21): p. 4510-4523.

277. Lara, A.R. and O.T. Ramírez, Plasmid DNA Production for Therapeutic Applications. Recombinant Gene Expression 2011: p. 271-303.

278. Smith, R.L., et al., Characterization of promoter function and cell-type-specific expression from viral vectors in the nervous system. Journal of Virology, 2000. **74**(23): p. 11254-11261.

279. Zheng, C. and B.J. Baum, Evaluation of viral and mammalian promoters for use in gene delivery to salivary glands. Molecular Therapy, 2005. **12**(3): p. 528-536.

280. Barrow, K.M., F.M. Perez-Campo, and C.M. Ward, Use of the cytomegalovirus promoter for transient and stable transgene expression in mouse embryonic stem cells. . Turksen K. (eds) Embryonic Stem Cell Protocols. Methods in Molecular Biology. Vol. 329. 2006: Humana Press.

281. Damdindorj, L., et al., A comparative analysis of constitutive promoters located in adeno-associated viral vectors PLoS One, 2014. **9**(8).

282. Paton, D.J., S. Gubbins, and D.P. King, Understanding the transmission of foot-and-mouth disease virus at different scales. Current Opinion in Virology 2018. **28**(85-91).

283. Gao, Y., S. Sun, and H. Guo, Biological function of Foot-and-mouth disease virus non-structural proteins and non-coding elements. Virology 2016. **13**: p. 107.

284. Moulin, V., et al., Targeting dendritic cells with antigen via dendritic cell-associated promoters. Cancer Gene Therapy 2012. **19**(5): p. 303-311.

285. Priess, T., The End in Sight: Poly(A), Translation and mRNA Stability in Eukaryotes, in Translation mechanisms, J. Lapointe, & Brakier-Gingras, L. , Editor. 2003, Landes Bioscience; Eurekah.com: Georgetown, TX.

286. Williams, J.A., A.E. Carnes, and C.P. Hodgson, Plasmid DNA vaccine vector design: Impact on efficacy, safety and upstream production. Biotechnology Advances 2009. **27**(4): p. 353-370.

287. Taylor-Parker, J., Plasmids 101: Terminators and PolyA signals 2016, AddGene: AddGene Blog.

288. Schek, N., C. Cooke, and J.C. Alwine, Definition of the upstream efficiency element of the simian virus 40 late polyadenylation signal by using in vitro analyses. Molecular Cell Biology 1992. **12**(12): p. 5386-5393.

289. Gil, A. and N.J. Proudfoot, Position-dependent sequence elements downstream of AAUAAA are required for efficient rabbit beta-globin mRNA 3' end formation. Cell, 1987. **49**(3): p. 399-406.

290. Meek, R.L., K.A. Walsh, and R.D. Palmiter, The Signal Sequence of Ovalbumin is Located Near the NH2 Terminus The Journal of Biological Chemistry 1982. **257**(20): p. 12245-12251.

291. Cohrt, K.O. pUC18-Probably the Best High-Copy plasmid in the World 2014; Available from: https://blog.addgene.org/plasmids-101-terminators-and-polya-signals.

292. Kutzler, M.A. and D.B. Weiner, DNA vaccines: ready for prime time? . Nature Reviews Genetics, 2008. **9**(2008): p. 776-788.

293. Eun, H., Marker/Reporter Enzymes in Enzymology Primer for Recombinant DNA Technology. 1996, Academic Press p. 567-645.

294. Stratagene. pBluescript SK(+). 2018]; Available from: https://www.snapgene.com/resources/plasmid-files/?set=basic_cloning_vectors&plasmid=pBluescript_SK(+).

295. Alting-Mees, M.A., J.A. Sorge, and J.M. Short, pBluescriptII: Multifunctional Cloning and Mapping Vectors, in Selected Methods in Enzymology, Recombinant DNA Methodology II R. Wu, Editor. 1995, Academic Press. p. 171-183.

296. ThermoFisher. Reverse Transcription- A Brief Introduction. [cited 2020; Available from: https://www.thermofisher.com/us/en/home/life-science/cloning/cloning-learning-center/invitrogen-school-of-molecular-biology/rt-education/reverse-transcription-basics.html.

297. Thomas, P. and T.G. Smart, Hek293 cell line: A vehicle for the expression of recombinant proteins. Journal of Pharmacological and Toxicological Methods, 2005. **51**(3): p. 187-200.

298. Simmons, H. HEK293 Cells: Applications and Advantages. Available from: https://www.news-medical.net/life-sciences/HEK293-Cells-Applications-and-Advantages.aspx.

299. ThermoFisher. Stable Transfection. [cited 2020; Available from: https://www.thermofisher.com/us/en/home/references/gibco-cell-culture-basics/transfection-basics/applications/stable-transfection.html.

300. ThermoFisher. Transient Transfection. [cited 2020; Available from: https://www.thermofisher.com/us/en/home/references/gibco-cell-culture-basics/transfection-basics/applications/transient-transfection.html.

301. Chong, Z.X., S.K. Yeap, and W.Y. Ho, Transfection types, methods and strategies: a technical review. PeerJ, 2021. **9**: p. e11165.

302. Lipofectamine 3000 reagent. [cited 2020 January 19]; Available from: https://www.thermofisher.com/us/en/home/brands/product-brand/lipofectamine/lipofectamine-3000.html

303. How cationic lipid mediated transfection works. [cited 2020 January 19]; Available from: https://www.thermofisher.com/us/en/home/references/gibco-cell-culture-basics/transfection-basics/gene-delivery-technologies/cationic-lipid-mediated-delivery/how-cationic-lipid-mediated-transfection-works.html

304. Maugeri, M., et al., Linkage between endosomal escape of LNP-mrna and loading into evs for transport to other cells. Nature Communications 2019. **10**(1): p. 4333.

305. Conway, A., et al., Non-viral Delivery of Zinc Finger Nuclease mRNA Enables Highly Efficient In Vivo Genome Editing of Multiple Therapeutic Gene Targets. Molecular Therapy, 2019. **27**(4): p. 866-877.

306. Durymanov, M. and J. Reineke, Non-viral delivery of nucleic acids: insight into mechanisms of overcoming intracellular barriers. Frontiers in Pharmacology, 2018. **9**.

307. OneStep Ahead RT-PCR Kit Handbook. 2015, QIAGEN.

308. Farrell, R.E., RNA Methodologies: Laboratory Guide for Isolation and Characterization fourth ed. 2010: Elsevier Inc.

309. NIH. Western Blot. 2023; Available from: https://www.genome.gov/genetics-glossary/Western-Blot.

310. Overview of ELISA Overview of ELISA [cited 2022; Available from: https://www.thermofisher.com/us/en/home/life-science/protein-biology/protein-biology-learning-center/protein-biology-resource-library/pierce-protein-methods/overview-elisa.html#:~:text=The%20enzyme%20linked%20immunosorbent%20assay,microplate%20wells%20using%20specific%20antibodies.

311. GraceBio. Immunoassays: Protein Arrays vs. ELISA and Westerns 2013 [cited 2022; Available from: https://gracebio.com/immunoassays-protein-arrays-vs-elisa-and-westerns/.

312. HRP Linked Secondary Antibodies. HRP Linked Secondary Antibodies [cited 2022; Available from: https://www.thermofisher.com/us/en/home/life-science/antibodies/secondary-antibodies/hrp-secondary-antibodies.html

313. Bio-Rad. Secondary antibody specific binding locations: Bio-Rad. [cited 2022; Available from: https://www.bio-rad-antibodies.com/secondary-antibody-binding-locations-benefits.html

314. Invitrogen. Goat anti-equine IgM secondary antibody, HRP. [cited 2022; Available from: https://www.thermofisher.com/antibody/product/Goat-anti-Equine-IgM-Secondary-Antibody-Polyclonal/PA1-84647

315. Sathe, A. and J.K. Cusick, Biochemistry, Immunoglobulin M in StatPearls [Internet]. 2021, StatPearls Publishing Treasure Island, FL.

316. Ostlund, E.N., et al., Equine West Nile encephalitis, United States Emerging Infectious Diseases, 2001. **7**(4): p. 665-669.

317. Perkins, G.A., et al., Serum IgM concentrations in normal, fit horses and horses with lymphoma or other medical conditions Journal of Veterinary Internal Medicine, 2003. **17**(3): p. 337-342.

318. MilliporeSigma. CelLytic™ B Plus Kit. [cited 2022; Available from: https://www.sigmaaldrich.com/US/en/product/sigma/cb0050.

319. MilliporeSigma. CelLytic™ B Cell Lysis Reagent. [cited 2022; Available from: https://www.sigmaaldrich.com/US/en/product/sigma/b7435.

320. Blackman, L.D., et al., An introduction to zwitterionic polymer behavior and applications in solution and at surfaces. Chemical Society Reviews 2019. **2019**(48): p. 757-770.

321. Gunawardena, G. Zwitterion. 2022 [cited 2022; Available from: https://chem.libretexts.org/Ancillary_Materials/Reference/Organic_Chemistry_Glossary/Zwitterion.

322. Islam, M.S., A. Aryasomayajula, and P.R. Selvaganapathy, A review on macroscale and microscale cell lysis methods Micromachines (Baseline) 2017. **8**(3): p. 83.

323. MilliporeSigma. Lysozyme from chicken egg white [cited 2022; Available from: https://www.sigmaaldrich.com/US/en/product/sigma/l3790.

324. Aryal, S. Cell Disruption- Definition, Methods, Types, Significance 2021 [cited 2023 January 19]; Available from: https://microbenotes.com/cell-disruption-methods/.

325. Delves-Broughton, J., The use of EDTA to enhance the efficacy of nisin towards gram-negative bacteria International Biodeterioration & Biodegradation 1993. **32**(1-3): p. 87-97.

326. Bruslind, L., Bacteria: Cell Walls, in General Microbiology 2020, Oregon State University

327. Ramos, O.L. and F.X. Malcata, Food-Grade Enzymes in Comprehensive Biotechnology 2017. p. 587-603.

328. MilliporeSigma. Benzonase® Nuclease for Microbiome Workflows. [cited 2022; Available from: https://www.sigmaaldrich.com/US/en/technical-documents/technical-article/genomics/dna-and-rna-purification/benzonase-nuclease-microbiome-workflows.

329. MilliporeSigma. Benzonase® Nuclease. [cited 2022; Available from: https://www.sigmaaldrich.com/US/en/product/sigma/e1014.

330. Yang, W., Nucleases: Diversity of structure, function and mechanism Quarterly Reviews of Biophysics, 2010. **44**(1): p. 1-93.

331. Raetz, C.R.H. and C. Whitfield, Lipopolysaccharide endotoxins. Annual Review of Biochemistry, 2008. **2002**(71): p. 635-700.

332. Zivot, J.B. and W.D. Hoffman, Pathogenic effects of endotoxin. New Horizons, Baltimore, MD 1995. **3**(2): p. 267-275.

333. FDA, Bacterial Endotoxins/Pyrogens. 1985, FDA.

334. Chong, K. and M. Huston, Implications of endotoxin contamination in the evaluation of antibodies to lipopolysaccharides in a murine model of gram-negative sepsis. The Journal of Infectious Diseases, 1987. **156**(5): p. 713-719.

335. Gorbet, M.B. and M.V. Sefton, Review: Biomaterial-associated thrombosis: roles of coagulation factors, complement, platelets and leukocytes, in The Biomaterials Silver

Jubilee Compendium: The Best Papers Published in Biomaterials, 1980-2004 2006, Elsevier. p. 219–241.

336. Traditional LAL Kinetic Chromogenic Assay. [cited 2022 June]; Available from: https://www.criver.com/products-services/qc-microbial-solutions/endotoxin-testing/lal-reagents-accessories/kinetic-chromogenic-lal#:~:text=The%20LAL%20kinetic%20chromogenic%20assay%20works%20in%20the%20presence%20of,liberation%20can%20be%20measured%20spectrophotometrically.

337. Ahamad, N. and D.S. Katti, A two-step method for extraction of lipopolysaccharide from Shigella dysenteriae serotype 1 and Salmonella typhimurium: An improved method for enhanced yield and purity Journal of Microbiological Methods 2016. **127**: p. 41-50.

338. Farooqui, R., B. Antharavally, and A. Alegria-Schaffer. A highly specific affinity resin enables endotoxin removal from various protein sources, sizes and charges. Eliminate Endotoxins from Protein and Antibody Samples 2012 [cited 2023 January 19]; Available from: https://www.thermofisher.com/us/en/home/life-science/protein-biology/protein-biology-learning-center/protein-biology-resource-library/protein-biology-application-notes/eliminate-endotoxins-protein-antibody-samples.html.

339. Magalhães, P., et al., Methods of endotoxin removal from biological preparations: a review Journal of Pharmacy & Pharmaceutical Sciences 2007. **10**(3): p. 388-404.

340. Sandle, T., Removal of Endotoxin from Protein in Pharmaceutical Processes. American Pharmaceutical Review, 2016. **19**(8): p. 1-5.

341. Aida, Y. and M.J. Pabst, Removal of endotoxin from protein solutions by phase separation using Triton X-114. Journal of Immunological Methods, 1990. **132**(1990): p. 191-195.

342. Abcam. Endotoxin Removal Kit (Rapid) (ab239707). [cited 2022 August 30]; Available from: https://www.abcam.com/endotoxin-removal-kit-rapid-ab239707.html.

343. De Rosa, S., et al., Endotoxin removal therapy with Polymyxin B immobilized fiber column as a COVID-19-bedside strategy protocol for endotoxic shock. Frontiers in Nephrology, 2022. **2**: p. 847305.

344. Vesentini, S., et al., Mechanisms of polymyxin B endotoxin removal from extracorporeal blood flow: molecular interactions Contributions to Nephrology 2010. **167**: p. 45-54.

345. Babu, U., et al., Effects of live attenuated and killed Salmonella vaccine on T-lymphocyte mediated immunity in laying hens. Veterinary Immunology and Immunopathology, 2003. **91**(2003): p. 39-44.

346. CDC. Salmonella Outbreaks Linked to Backyard Poultry. 2022 [cited 2023 February 13]; Available from: https://www.cdc.gov/salmonella/backyardpoultry-06-22/index.html.

347. CDC. Investigation Details. Salmonella 2022 [cited 2023 February 13]; Available from: https://www.cdc.gov/salmonella/backyardpoultry-06-22/details.html.

348. Jackson, B.R., et al., Outbreak-associated Salmonella enterica serotypes and food Commodities, United States, 1998-2008. Emerging Infectious Diseases, 2013. **19**(8): p. 1239-1244.

349. Revolledo, L. and A.J.P. Ferreira, Current perspectives in Avian Salmonellosis: Vaccines and immune mechanisms of protection. Journal of Applied Poultry Research, 2012. **21**(2): p. 418-431.

350. Huss, D., G. Poynter, and R. Lansford, Japanese quail (Coturnix japonica) as a laboratory animal model Lab Animal 2008. **37**: p. 513-519.

351. Poynter, G., D. Huss, and R. Lansford, Japanese quail: an efficient animal model for the production of transgenic avians. Cold Spring Harbor Protocols 2009. **2009**(1): p. pdb.emo122.

352. Morris, K.M., et al., The quail genome: insights into social behavior, seasonal biology and infectious disease response. BMC Biology, 2020. **18**(14).

353. Lansford, R. Quail as a model system. [cited 2022; Available from: https://dnalc.cshl.edu/view/2039-Quail-as-a-model-system.html#:~:text=Keywords%20Info%20Professor%20Rusty%20Lansford%20explains%20that%20quail,to%20grow%20in%20a%20laboratory%2C%20and%20develop%20quickly.

354. Pavlidis, H. Avian immunity 101: The basics Health/Nutrition 2019 [cited 2022; Available from: https://www.poultryworld.net/health-nutrition/avian-immunity-101-the-basics/.

355. Genovese, K.J., et al., The avian heterophil Developmental and Comparative Immunology 2013. **41**(3): p. 334-340.

356. Braukmann, M., U. Methner, and A. Berndt, Immune Reaction and Survivability of Salmonella Typhimurium and Salmonella Infantis after Infection of Primary Avian Macrophages. PLoS One, 2015. **10**(3): p. e0122540.

357. Lee, L., et al., Immunoglobulin Y for potential diagnostic and therapeutic applications in infectious diseases. Frontiers in Immunology, 2021. **12**: p. 696003.

358. Pereira, E.P.V., et al., Egg yolk antibodies (IgY) and their applications in human and veterinary health: A review. International Immunopharmacology, 2019. **73**: p. 293-303.

359. Dias da Silva, W. and D. Tambourgi, IgY: A promising antibody for use in immunodiagnostic and in immunotherapy Veterinary Immunology and Immunopathology, 2010. **135**(3): p. 173-180.

360. Taylor, A.I., et al., Avian IgY binds to a monocyte receptor with IgG-like kinetics despite an IgE-like structure. Journal of Biological Chemistry, 2008. **283**(24): p. 16384-90.

361. Diseases of Poultry. Available from: http://extension.msstate.edu/agriculture/livestock/poultry/diseases-poultry.

362. Piteskey, M. Vaccinating Strategies for Chicks Healthy Flock, Pitesky's Poultry; Available from: https://www.chickenwhisperermagazine.com/health-and-wellness/vaccinating-strategies-for-chicks.

363. Contributor, C. How To Administer the Marek's Disease Vaccine to Poultry Chicks Backyard Poultry 2021; Available from: https://backyardpoultry.iamcountryside.com/feed-health/how-to-administer-the-mareks-vaccine-to-poultry-chicks/.

364. When Do Quails Start Laying Eggs/. [cited 2022; Available from: https://learnpoultry.com/when-quails-start-laying-eggs/.

365. Stuttgen, S. Life Cycle of a Laying Hen. [cited 2022; Available from: https://livestock.extension.wisc.edu/articles/life-cycle-of-a-laying-hen/#:~:text=When%20do%20hens%20begin%20to,they%20are18%2D%2022%20weeks%20old.

366. Oshop, G.L., et al., In ovo delivery of DNA to the avian embryo. Vaccine, 2003. **7**(21): p. 11-12.

367. Firouzamandi, M., et al., Preparation, characterization, and in ovo vaccination of dextranspermine nanoparticle DNA vaccine coexpressing the fusion and hemagglutinin genes against Newcastle disease. International Journal of Nanomedicine, 2016. **11**: p. 259-267.

368. Fynan, E.F., et al., DNA vaccines: Protective immunizations by parenteral, mucosal, and gene-gun inoculations. Proceedings of the National Academy of Sciences, 1993. **90**(24): p. 11478-114820.

369. Lindsay, K.E., et al., Visualization of early events in mRNA vaccine delivery in non-human primates via PET–CT and near-infrared imaging. Nat Biomed Eng 2019. **3**: p. 371-380.

370. Oberländer, B., et al., Evaluation of Newcastle Disease antibody titers in backyard poultry in Germany with a vaccination interval of twelve weeks. PLoS One, 2020. **15**(8): p. e0238068.

371. USDA. How olf are chickens used for meat? . Ask USDA 2019 [cited 2020; Available from: https://ask.usda.gov/s/article/How-old-are-chickens-used-for-meat.

372. Average slaughter age of coturnix quail. 2015, Backyard Chickens.

373. QIAGEN, SuperFect® Transfection Reagent Handbook, QIAGEN, Editor. 2002, QIAGEN.

374. Hudde, T., et al., Activated polyamidoamine dendrimers, a non-viral vector for gene transfer to the corneal endothelium. Gene Therapy, 1999. **6**: p. 939-943.

375. Hu, J., K. Hu, and Y. Cheng, Tailoring the dendrimer core for efficient gene delivery. Acta Biomaterialia, 2016. **35**: p. 1-11.

376. Tang, M.X., C.T. Redemann, and F.C. Szoka, In vitro gene delivery by degraded polyamidoamine dendrimers. Bioconjugate Chemistry, 1996. **7**(6): p. 703-714.

377. Camassola, M., et al., Nonviral in vivo gene transfer in mucopolysaccharidosis I murine model. Journal of Inherited Metabolic Disease, 2005. **28**(6): p. 1035-1043.

378. Bell, S. Are you familiar with the puromycin concentration in HEK 293 Cells for shRNA? 2015 [cited 2020]; Available from: https://www.researchgate.net/post/Are_you_familiar_with_the_puromycin_concentration_in_HEK_293_Cells_for_shRNA.

379. TOKU-E, HEK-293-Munc18b, in Cell-culture Database. TOKU-E.

380. Mirus. Determining the Optimal Selection Antibiotic Concentration. Available from: https://www.mirusbio.com/applications/stable-cell-line-generation/antibiotic-kill-curve#:~:text=A%20kill%20curve%20is%20a,the%20course%20of%20one%20week.

381. Rouillard, A., et al., The harmonizome: a collection of processed datasets gathered to serve and mine knowledge about genes and proteins. 2016.

382. ThermoFisher. Adsorption Immunoassay Plates. [cited 2023; Available from: https://www.thermofisher.com/us/en/home/life-science/protein-biology/protein-assays-analysis/elisa/elisa-microplates-plasticware/adsorption-immunoassay-plates.html#:~:text=The%20MaxiSorp%20surface%20is%20a%20modified%2C%20highly%20charged,very%20high%20sensitivity%20in%20double%20antibody%20%E2%80%9Csandwich%E2%80%9D%20tests.

383. MilliporeSigma. Corning® 96 Well EIA/RIA Assay Microplate CLSs590. [cited 2023; Available from: https://www.sigmaaldrich.com/US/en/product/sigma/cls3590.

384. MilliporeSigma. Antibiotic Kill Curve. Mammalian Cell Culture [cited 2022.

385. Promega. Transfection. Product Gudies and Selectors [cited 2022; Available from: https://www.promega.com/resources/guides/cell-biology/transfection/.

386. Fang, E., et al., Advances in COVID-19 mRNA vaccine development. Signal Transduction and Targeted Therapy, 2022. **7**(94).

387. Grzybowska, E.A., A. Wilczynska, and J.A. Siedlecki, Regulatory Functions of 3′UTRs. Biochemical and Biophysical Research Communications, 2001. **288**(2): p. 291-295.

388. Zinckgraf, J.W. and L.K. Silbart, Modulating gene expression using DNA vaccines with different 3'-UTRs influences antibody titer, seroconversion and cytokine profiles. Vaccine, 2003. **21**(15): p. 1640-1649.

389. Quilici, L.S., et al., A minimal cytomegalovirus intron A variant can improve transgene expression in different mammalian cell lines. Biotechnology Letters 2013. **35**(1): p. 21-27.

390. Chapman, B.S., et al., Effect of intron A from human cytomegalovirus (Towne) immediate-early gene on heterologous expression in mammalian cells. Nucleic Acids Research, 1991. **19**(4): p. 3979-3986.

391. HBA1 gene. Genes [cited 2022; Available from: https://medlineplus.gov/genetics/gene/hba1/.

392. Addgene search results for sv40 poly. [cited 2022 August 1]; Available from: https://www.addgene.org/search/catalog/plasmids/?q=sv40+poly.

393. Marie-Paule. Polyadenylation (or Poly(A)) signal, site and tail. 2020; Available from: https://www.imgt.org/IMGTeducation/Aide-memoire/_UK/poly/.

394. Li, S., et al., The effects of SV40 PolyA sequence and its aataaa signal on upstream GFP gene expression and transcription termination. Yi Chuan, 2012. **34**(1): p. 113-119.

395. Connelly, S. and J.L. Manley, A functional mRNA polyadenylation signal is required for transcription termination by RNA polymerase II. Genes & Development, 1988. **2**: p. 440-452.

396. Salem, T.Z., et al., The influence of SV40 polyA on gene expression of Baculovirus expression vector systems. PLoS One, 2015. **10**(12): p. e0145019.

397. Gimmi, E.R., et al., Deletions in the SV40 late polyadenylation region downstream of the AATAAA mediate similar effects on expression in various mammalian cell lines. Nucleic Acids Research, 1988. **16**(18): p. 8977-8997.

398. Zarkower, D., et al., The AUAAA sequence is required both for cleavage and for polyadenylation of Simian virus 40 pre-mRNA in vitro. Molecular and Cellular Biology, 1986. **6**(7): p. 2317-2323.

399. Nag, A., et al., The conserved AAUAAA hexamer of the poly(A) signal can act alone to trigger a stable decrease in RNA polymerase II transcription velocity. RNA, 2006. **12**(8): p. 1534-1544.

400. Aslantas, Y. and N.B. Surmeli, Effects of N-terminal and C-terminal polyhistidine tag on the stability and function of the thermophilic P450 CYP119. Bioinorganic Chemistry and Applications, 2016. **2019**: p. 1–8.

401. Perkins, E.J., Plasmids 101: Protein Tags. AddGene: AddGene Blog.

402. Booth, W.T., et al., Impact of an N-terminal Polyhistidine Tag on Protein Thermal Stability. ACS Omega,, 2018. **3**(1): p. 760-768.

403. Klink, S. Protein Tagging: How to Choose a Tag for Your Protein. 2019 [cited 2022 August 1]; Available from: https://www.promega.com/resources/pubhub/2019/choosing-a-tag-for-your-protein/.

404. Abcam. His-tag. [cited 2022 August 1]; Available from: https://www.abcam.com/content/his-tag.

405. TheProteinMan, A Look into the 6XHis Tag and its Uses, in The Protein Man's Blog: A Discussion of Protein Research. 2014, G-Biosciences: G-Biosciences.

406. Humoral Immunodeficiencies. Immunodeficiencies in Horses [cited 2023; Available from: https://www.vet.cornell.edu/research/labs/equine-immunology/immunodeficiencies/humoral-immunodeficiencies.

407. ThermoFisher. Immunoglobulin Structure and Classes. [cited 2023; Available from: https://www.thermofisher.com/us/en/home/life-science/antibodies/antibodies-learning-center/antibodies-resource-library/antibody-methods/immunoglobulin-structure-classes.html.

408. Horse IgG. [cited 2023; Available from: https://www.lsbio.com/targets/horse-igg/b459#:~:text=Horse%20IgG%20Representing%20approximately%2075%25%20of%20serum%20antibodies%2C,about%20150%20kDa%20made%20of%20four%20peptide%20chains.

409. Rouse, B.T. and D.G. Ingram, The total protein and immunoglobulin profile of equine colostrum and milk. Immunology, 1970. **19**(6): p. 901-907.

410. Lewis, M.J., B. Wagner, and J.M. Woof, The different effector function capabilities of the seven equine IgG subclasses have implications for vaccine strategies. Molecular Immunology, 2008. **45**(3): p. 818-827.

411. ATCC. J774A.1. [cited 2021 July 10]; Available from: https://www.atcc.org/products/tib-67

412. Lam, J., et al., Baseline Mechanical Characterization of J774 macrophages. Biophysical Journal, 2009. **96**(1): p. 248-254.

413. Dassano, A. What is the best reagent and protocol to transfect J774A.1 macrophage cells with DNA plasmid. 2017 [cited 2021 July 10]; Available from:

https://www.researchgate.net/post/What-is-the-best-reagent-and-protocol-to-transfect-J774A1-macrophage-cells-with-DNA-plasmid.

414. Huang, Z.H., et al., Expression of scavenger receptor BI facilitates sterol movement between the plasma membrane and the endoplasmic reticulum in macrophages. Biochemistry, 2003. **42**(13): p. 3949-3955.

415. Ferrauto, G., et al., In vivo MRI visualization of different cell populations labeled with PARACEST agents. Magnetic Resonance in Medicine 2012. **69**(6): p. 1703-1711.

416. Dolat, E., et al., Silver nanoparticles and electroporation: their combinational effect on Leishmania major. Bioelectromagnetics 2015. **36**(8): p. 586-596.

417. Smits, E., et al., The human omologue of Caenorhabditis elegans CED-6 specifically promotes phagocytosis of apoptotic cells. Current Biology, 1999. **9**(22): p. 1351-1354.

418. Potter, H. and R. Heller, Transfection by Electroporation Current Protocols in Molecular Biology 2010. **62**(1): p. 9.3.1-9.3.6.

419. Protean, Electroporation protocol for HEK293 cells, GTporator®, Protean, Editor., Protean.

420. IrvineScientific. HEK293 System FAQ. [cited 2022; Available from: https://www.irvinesci.com/resources/hek293-system-faq.html#:~:text=What%20is%20the%20preferred%20transfection%20method%20to%20be,other%20transfection%20methods%20using%20cationic%20liposomes%20or%20electroporation.

421. Arena, T.A., P.D. Harms, and A.W. Wong, High throughput transfection of HEK293 cells for transient protein production, in Recombinant Protein Expression in Mammalian Cells 2018. p. 179-187.

422. Wright, J.F., Transient Transfection Methods for Clinical Adeno-Associated Viral Vector Production. Human Gene Therapy, 2009. **20**(7): p. 698-706.

423. Cell-specific transfection protocols. [cited 2021 July 10]; Available from: https://www.thermofisher.com/us/en/home/life-science/cell-culture/transfection/transfection-support/transfection-selection-tool.html

424. Arkusz, J., et al., Assessment of usefulness of J774A.1 macrophages for the assay of IL-1β promoter activity. Toxicology in Vitro, 2006. **20**(1): p. 109-116.

425. Polyplus. JetOPTIMUS - DNA transfection reagent - polyplus-transfection. 2022 [cited 2022 July 10]; Available from: https://www.polyplus-transfection.com/products/jetoptimus/#:~:text=jetOPTIMUS%C2%AE%20is%20a%20powerful,resulting%20in%20higher%20transfection%20efficiency

426. Polyplus, jetOPTIMUS for hard-to-transfect cells Polyplus.

427. Polyplus. jetOPTIMUS. Life science research [cited 2022; Available from: https://www.polyplus-transfection.com/blog/hard-to-transfect-cells/.

428. Putze, S., et al., Cationic lipid/pDNA complex formation as potential generic method to generate specific IRF pathway stimulators European Journal of Pharmaceutics and Biopharmaceutics 2020. **155**: p. 112-121.

429. Lipofectamine 3000 Reagent 2016, Thermo Fisher Scientific - US.

430. Polyplus, jetOPTIMUS® in vitro DNA transfection reagent PROTOCOL, Polyplus, Editor. 2020.

431. Gene Pulser®Electroprotocols. UTHSC-DB: Houston, TX.

432. Deora, A.A., et al., Efficient electroporation of DNA and protein into confluent and differentiated epithelial cells in culture. Traffic (Copenhagen, Denmark) 2007. **8**(10): p. 1304-1312.

433. Electroporation. The ES Cell Targeting Core Laboratory [cited 2022; Available from: https://www.hopkinsmedicine.org/core/ES_Targeting/Protocol_Pages/electroporation.html.

434. Chalfie, M. and S.R. Kain, Green fluorescent protein: Properties, applications and protocols. 2 ed. 2005: John Wiley and Sons.

435. Zou, Y. The Embryo Project Encyclopedia. Green Fluorescent Protein | The Embryo Project Encyclopedia 2014 [cited 2021 July 10].

436. Ward, T.H. and J. Lippincott-Schwartz, The uses of green fluorescent protein in mammalian cells. Methods of Biochemical Analysis 2006. **47**: p. 305-337.

437. MilliporeSigma. MISSION® pLKO.1-puro-CMV-TurboGFP™ Positive Control Plasmid DNA. [cited 2021; Available from: https://www.sigmaaldrich.com/US/en/product/sigma/shc003.

438. Mahmoudian, R.A., et al., MEIS1 knockdown may promote differentiation of esophageal squamous carcinoma cell line KYSE-30. Molecular Genetics & Genomic Medicine 2019. **7**(7): p. e00746.

439. Gruben, A.N., et al., Stable expression of green fluorescent protein after liposomal transfection of K562 cells without selective growth conditions. Biotechniques 1999. **27**(6): p. 1162-1164; 1166-1170.

440. Porosk, L., et al., Expressed therapeutic protein yields are predicted by transiently transfected mammalian cell population. Pharmaceutics 2022. **14**(9): p. 1949.

441. Schneider, C.A., W.S. Rasband, and K.W. Eliceiri, NIH Image to ImageJ: 25 years of image analysis. Nature Methods 2012. **9**(7): p. 671-675.

442. Fassina, L., et al., AUTOCOUNTER, an ImageJ JavaScript to analyze LC3B-GFP expression dynamics in autophagy-induced astrocytoma calls. European Journal of Histochemistry, 2012. **56**(4): p. e44.

443. Schneider, C.A., W.S. Rasband, and K.W. Eliceiri. ImageJ. Available from: https://imagej.net/software/imagej/.

444. Week 2: Analyzing Change Over Time. Eyes in the Sky II, GIT Web Course [cited 2022; Available from: https://serc.carleton.edu/eyesinthesky2/week2/intro_imagej.html#:~:text=You%20can%20use%20ImageJ%20to,format%2C%20such%20as%20from%20spreadsheets.

445. Bankhead, P., Analyzing fluorescence microscopy images with ImageJ. 2014: Nikon Imaging Center, Heidelberg University.

446. Fitzpatrick, M., Measuring cell fluorescence using ImageJ, in The Open Lab Book. 2014, Github Repository.

447. Brazill, J.M., et al., Quantitative cell biology of neurodegeneration in drosophila through unbiased analysis of fluorescently tagged proteins using imagej. Journal of Visualized Experiments, 2018. **138**.

448. Mesquita, A., J. Pereira, and A. Jenny, Streamlined particle quantification (SParQ) plug-in is an automated fluorescent vesicle quantification plug-in for particle quantification in Fiji/ImageJ. Autophagy, 2020. **16**(9): p. 1711-1717.

449. McKinnon, K.M., Flow Cytometry: An Overview. Current Protocols in Immunology 2019. **120**(1): p. 5.1.1-5.1.11.

450. Bio-Rad. A guide to gating in flow cytometry. [cited 2022 December 1]; Available from: https://www.bio-rad-antibodies.com/blog/a-guide-to-gating-in-flow-cytometry.html.

451. Cachiares, G., Gene Pulser Electroprotocols, Bio-Rad, Editor.

452. Lysis buffer for purification of interacting proteins. Cold Spring Harbor Protocols, 2007. **2007**(2): p. pdb.rec10729.

453. Borker, C.D. How can I dissolve PMSF (Protease inhibitor) in lysis buffer? Question 2015; Available from: https://www.researchgate.net/post/How_can_I_dissolve_PMSF_Protease_inhibitor_in_lysis_buffer#:~:text=because%20pmsf%20is%20instable%20don,volume%20of%20your%20lysis%20buffer%20.

454. GoldBio, 1M PMSF Stock Solution. 2019, GoldBio.

455. Arena, E.T., et al., Quantitating the cell: turning images into numbers with ImageJ. WIRES Developmental Biology, 2016. **6**(2): p. e260.

456. Foley, K., Counting Cells with ImageJ 2014: YouTube.

457. NEB_Technical_Support, DNA/mRNA component orientation and selection verification, A. Edwards and A. Nguyen, Editors. 2022.

458. IDT. IDT cloning vectors. Gene Synthesis; Available from: https://www.idtdna.com/pages/products/genes-and-gene-fragments/custom-gene-synthesis.

459. NEB. FAQ: What is the promoter sequence for SP6 RNA Polymerase. [cited 2022 August 1]; Available from: https://www.neb.com/faqs/2016/12/21/what-is-the-promoter-sequence-for-sp6-rna-polymerase#:~:text=The%20SP6%20promoter%20sequence%20is,%C2%B4%20to%203%C2%B4%20direction.

460. Liu, H.S., et al., Is green fluorescent protein toxic to the living cells? Biochemical and Biophysical Research Communications, 1999. **260**(3): p. 712-717.

461. Lonza 4D-Nucleofector Protocol for J774A.1 Cells For 4D-Nucleofector X Unit-Transfection in Suspension. 2017.

462. Bio-Rad, Gene Pulser Electroprotocols, Bio-Rad, Editor.

463. AltogenBiosystems. What is the benefit of using an electroporation buffer. 2017 August 12 [cited May 1, 2023]; Available from: https://altogen.com/benefit-using-electroporation-buffer/#:~:text=Electroporation%20buffers%20are%20formulations%20that%20mimic%20cellular%20cytoplasm,in%20single%20cuvettes%20or%20in%20multiwell%20electroporation%20plates.

464. IEDB. MHC-II binding predictions - Example data. [cited 2023; Available from: http://tools.iedb.org/mhcii/example/.

465. IEDB. IEDB Analysis Resource - References. [cited 2023; Available from: http://tools.iedb.org/mhci/reference/.

466. Fleri, W. What thresholds (cut-offs) should I use for MHC class I and II binding predictions. Frequently Asked Questions 2017 [cited 2023; Available from: https://help.iedb.org/hc/en-us/articles/114094152371-What-thresholds-cut-offs-should-I-use-for-MHC-class-I-and-II-binding-predictions#:~:text=For%20MHC%20class%20II%20T%20cell%20epitope%20predictions%2C,a%20consensus%20percentile%20rank%20of%20the%20top%2010%25.

467. ThermoScientific, Fast Digestion of DNA, T.F. Scientific, Editor. 2012, Thermo Fisher Scientific.

468. Zymo, Zymoclean™ Gel DNA Recovery Kit, Z. Research, Editor. 2021, Zymo Research.

469. Zymo, DNA Clean & Concentrator®-5 Z. Research, Editor. 2022, Zymo Research.

470. NEB. Quick Ligation Protocol. [cited 2018; Available from: https://www.neb.com/protocols/0001/01/01/quick-ligation-protocol.

471. NEB. High efficiency transformation protocol (C2992). [cited 2019 July 12]; Available from: https://www.neb.com/protocols/0001/01/01/high-efficiency-transformation-protocol-c2992

472. NEB. Transformation Protocol (C2925). [cited 2018; Available from: https://www.neb.com/protocols/2012/11/20/transformation-protocol-c2925.

473. Zymo, ZymoPURE™ II Plasmid Midiprep Kit. 2022, Zymo Research.

474. Invitrogen, AccuPrime™ Pfx DNA Polymerase Product Information 2016, ThermoFisher Scientific.

475. Sigma-Aldrich, CelLytic B Plus Kit Product Information. 2019, Sigma-Aldrich: Saint Louis, Missouri, 63103 USA.

476. Abcam, ab239707 Endotoxin Removal Kit (Rapid). 2020, Abcam.

477. ThermoScientific, Pierce™ BCA Protein Assay Kit User Guide. 2020, ThermoFisher Scientific.

478. GenScript, ToxinSensorTM Endotoxin Detection System User Manual. GenScript.

479. Dudly, B., A. Edwards, Editor. 2018.

480. QIAGEN, QuickStart Protocol RNeasy® Plus Mini Kit, QIAGEN, Editor. 2016, QIAGEN.

481. MIDSCIBiotech, TPP Cell Counter (*www.midsci.com*). 2009, MidSci: YouTube.

482. NEB. Optimizing Restriction Endonuclease Reactions. Protocols [cited 2018-2023; Available from: https://www.youtube.com/watch?v=LHOtMGVJiME.

483. NEB. Restriction Enzyme Single/Double Digestion. NEBcloner; Available from: https://nebcloner.neb.com/#!/redigest.

484. NEB. Q5® Site-directed mutagenesis Kit quick protocol (E0554). [cited 2022 July 12]; Available from: https://www.neb.com/protocols/2013/01/26/q5-site-directed-mutagenesis-kit-quick-protocol-e0554

485. Ristl, R. Sample size for one-way analysis of variance. Sample Size Calculator version 1.060; Available from: https://homepage.univie.ac.at/robin.ristl/samplesize.php?test=anova.

486. Cao, E., et al., Effect of freezing and thawing rates on denaturation of proteins in aqueous solutions. Biotechnology and Bioengineering, 2003. **82**(6): p. 684-690.

Vita

Ashley Reneé Edwards graduated from St. Joseph's Academy in Baton Rouge with Honors. She received her Bachelor of Arts degree with *Magna Cum Laude* in Sociology with a concentration in Criminology, a minor in Psychology, and a minor in Women's and Gender Studies from Louisiana State University (LSU), Baton Rouge in December 2017. During her undergraduate studies, she discovered her love of medicine and passion for helping under-resourced populations. In her pursuit to find a way to combine her two passions, she began a pre-medical school course load while working for the Public Defender's Office of Baton Rouge and the Animal Sciences Laboratories at LSU. She was then accepted into the Graduate program at Louisiana State University in May 2018, where she continued and expanded upon her undergraduate research in the Animal Sciences Laboratories and where she has completed the requirements for the degree of Doctor of Philosophy. She hopes that this work contributes to a knowledge base that current and future scientists will use to leave the world a better place than they found it.